

Experimental setup for RC car suspensions

Giancarlo De Giuseppe¹

¹ Politecnico di Torino, Department of Mechanical and Aerospace Engineering
Corso Duca degli Abruzzi, 24 – 10129 Torino, Italy

Index

Index.....	1
Abstract	3
Introduction.....	4
1. Experiment knowledge	5
1.1 Project context.....	5
1.2 Theoretical bases of the experiments	8
1.3 Analysis of available equipment	11
1.4 Basic ideas.....	17
1.5 The vehicle	19
2. Construction of experimental setups.....	24
2.1 Elementary CAD components	24
2.2 Setup design	26
2.2.1 Damper dimensions.....	26
2.2.2 Upper frame	30
2.2.3 Lower frame.....	31
2.2.4 Shaker position.....	34
2.2.5 Lower plate	34
2.2.6 Clamping systems	36
2.2.7 Laser position.....	42
3. Simulation of data acquiring	50
3.1 Single case.....	50
3.2 State space and linear regression	56
3.3 State space and polynomial regression	62
4. Real experiment	79
4.1 Data acquisition system	79
4.2 Experiment procedure	81
4.2.1 Possible damper configurations	81
4.2.2 Damper assembly procedure	82
4.2.3 Acquisition settings and procedure	88
4.3 Preliminary acquisition and model correction	94
4.3.1 First acquisition and comparison with the supposed models	94
4.3.2 Model correction	98
4.3.3 Mass effect	100
4.3.4 Air effect	106
4.4 Postprocessing and results	112
4.4.1 Signal filtering.....	112

4.4.2 Regression	118
4.4.3 Overall damper regression	125
4.4.4 Front–rear comparison	131
4.4.5 Temperature effect	133
4.4.6 Friction effect	135
4.4.7 Compression or extension effect	141
Conclusions	142
Appendix	143
Reference	144

Abstract

The aim is to design the steps for experimental measures of suspension components characteristics in laboratory setups. The objective of the tests is to characterise dampers properties for linear and nonlinear behaviour, deriving in the case of a 1:5 scale radio commanded car model: Losi 5ive-T 2.0^[2]. The resultant characteristic data acquired during this project of thesis will be used to model possible lumped parameters car models to extract numerical syntheses, where the stiffness and viscosity variations of the suspensions will be explored. This solutions can ultimately be used as a basis for comparison with the data of experiments on the entire vehicle.

Introduction

This thesis aims to characterize the damping parameter for the suspensions of a radio controlled car, on a 1:5 scale model. The car will be studied in all its various parts in a series of theses and projects that will focus on different characteristics and that will require different experimental setups. The final objective of the mentioned path is to compare the behaviour of the vehicle between what will emerge from an analytical model with 7 degrees of freedom and how much will be experimentally measured on the vehicle itself, the result sought is a coincidence between what happens in the two cases varying stiffness and damping. For this reason the choice of the 1: 5 model is quite appropriate, this type of vehicle has all the functional characteristics normally mounted on a real vehicle: a complete damper composed of interchangeable parts, which can be disassembled and therefore can be customized with various oil grades and springs. different stiffness, quadrilateral suspension system, anti-roll bar, wheels with interchangeable tires, etc.

For the comparison the model and the vehicle will obviously have to share the same database, it will therefore be necessary to characterize not only the dampers, the subject of this thesis, but also the stiffness of the springs, the stiffness and damping provided by the tires, the frequencies resonance of the body and the system, etc. It is therefore important that the data obtained here are as precise as possible since they will not only be ends in themselves but will constitute an essential information for future users who will work on this project.

To do this it will be necessary to divide the procedure into two phases: a preliminary one where the experimental set will be imagined via CAD based on estimates of the components' measurements, since they are not yet available, and it will be also possible to imagine data acquisitions to start taking confidence with the regression processes that will have to be included in algorithms (to do this, Simulink and Matlab will be used). The second phase is instead the purely experimental one where the test rig will be physically built and the car, together with all the other spare parts to be analysed, will be available. This division between the two phases is sometimes carried out in parallel (chapters 1 & 2) by showing together the design and implementation phases, while at other times it is clearly separated as it happens for the data acquisition phases where the design/forecasting (chapter 3) will be totally unrelated to true experimentation (chapter 4). Temporarily, however, the two phases have always been well divided by the arrival of the purchased components, which required a high timing, but the long time available for the design phases has certainly shortened the experimental ones, leaving the requested total time interval almost unchanged.

The strength of this thesis is to have a predominantly experimental character, confining the analytical part to the essential. The manual component assembly and test procedure alone took more than 100 hours. As it will be possible to see the results obtained will constitute a first important confirmation that the 1:5 model used is coherent and well done. It paves the way, drastically reducing costs, to the construction of analytical automotive models that will be able to quickly find confirmation through the use of this scale model. The object of the thesis is not of particular originality if taken in its own right, but the function it occupies and will occupy in the aforementioned and larger project instead is; in addition it being able to demonstrate that even with relatively inexpensive objects such as those used is possible to capture even subtle nuances of the damping behaviour.

1. Experiment knowledge

1.1 Project context

As mentioned in the introduction this thesis project has to be inserted in a larger context whose ultimate goal is to obtain a validation of analytical results in a rapid and economic manner. To give an example, a quick reference will be made here to the most important automotive analytical model, the same that led to undertake this experimental project. It is a classic lumped parameter model with 7 degrees of freedom:

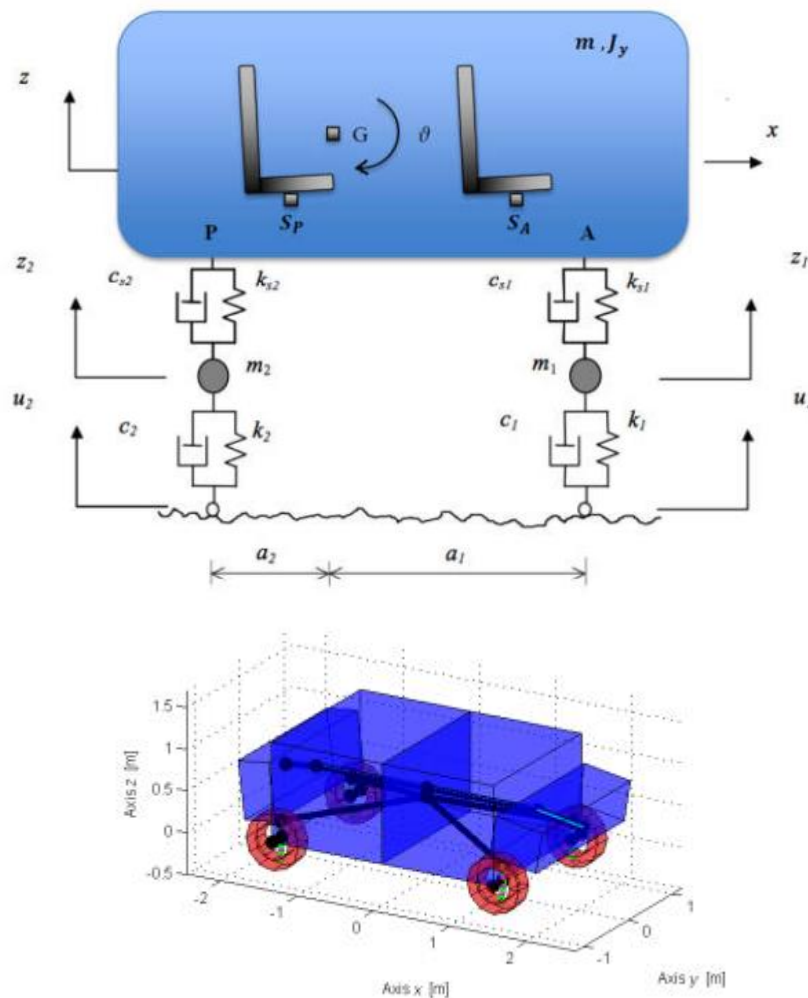


Figure 1.1.1 – 7 dofs lumped parameter car model (up) and equivalent graphic model obtained in Lupos (down).

If a parametric analysis of eigenvalues modifications in Complex Modal Analysis is analysed, with a proportional coefficient of the suspension dashpot that, with respect to the nominal value, is changed in the range 0.01%÷200% and where the nominal value corresponds to unitary parameter (100%), quite interesting results can be obtained (in Figure 1.1.2 eigenvalues moduli, damping coefficients and root loci are shown):

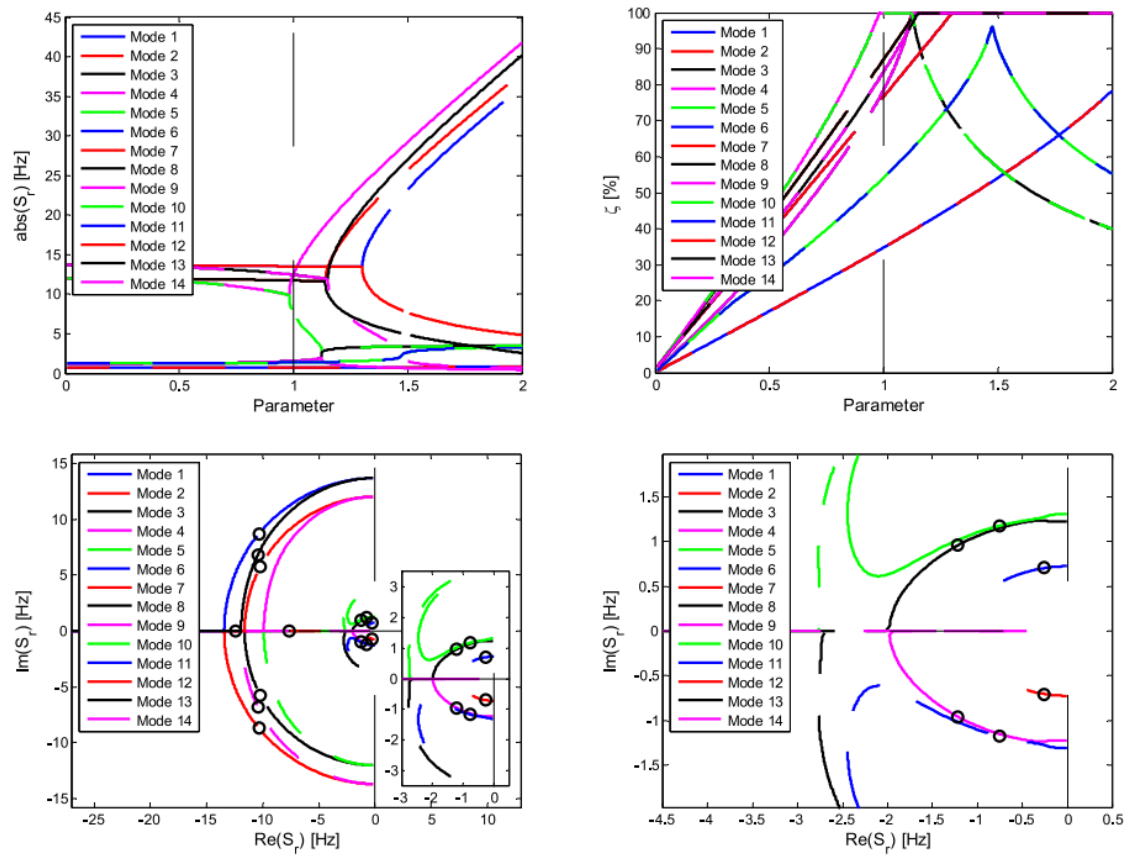


Figure 1.1.2 – Parametric Complex Modal Analysis results obtained varying suspension damping, nominal model has ball symbols.

Also others Parametric Complex Modal Analysis could be done, for example by exploring the springs stiffness variation or the tyres stiffness one. By superposing in an unique graph all these three cases the most interesting deduction can be done:

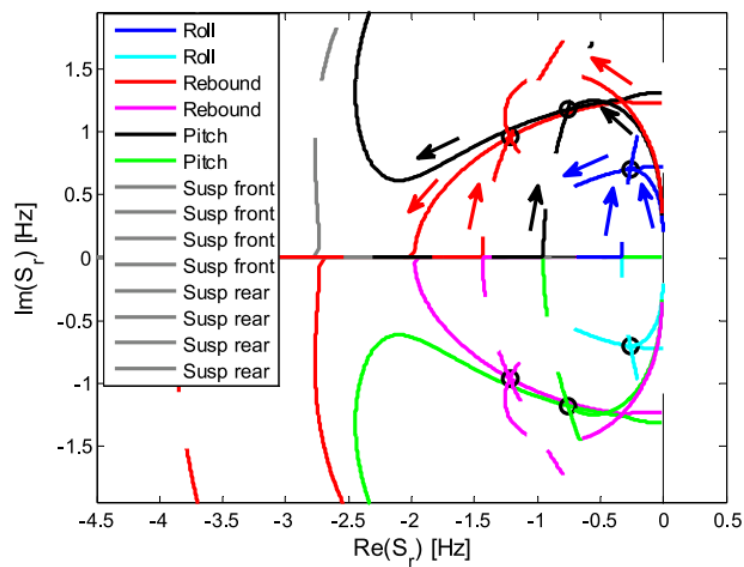


Figure 1.1.3 – Parametric Complex Modal Analysis of the damped system eigenvalues: detail of chassis body eigenvalues varying suspension damping (solid lines), tyre stiffness (dashed lines), suspension stiffness (dotted lines), nominal model has ball symbols.

The analytic result obtained suggest, for example, that is not possible to null the pitch motion by simply varying the damping suspension, in fact the black solid line real part (but also the immaginary one) never gone to zero with a quite strange shape that firstly would tend to lower values (follow black arrow direction) but at a certain poit return to rise.

The only way to validate such a result is an experimental test, but this test must share the same data base with the model, and the present thesis aims precisely to characterize a part of them, the already mentioned dampers.

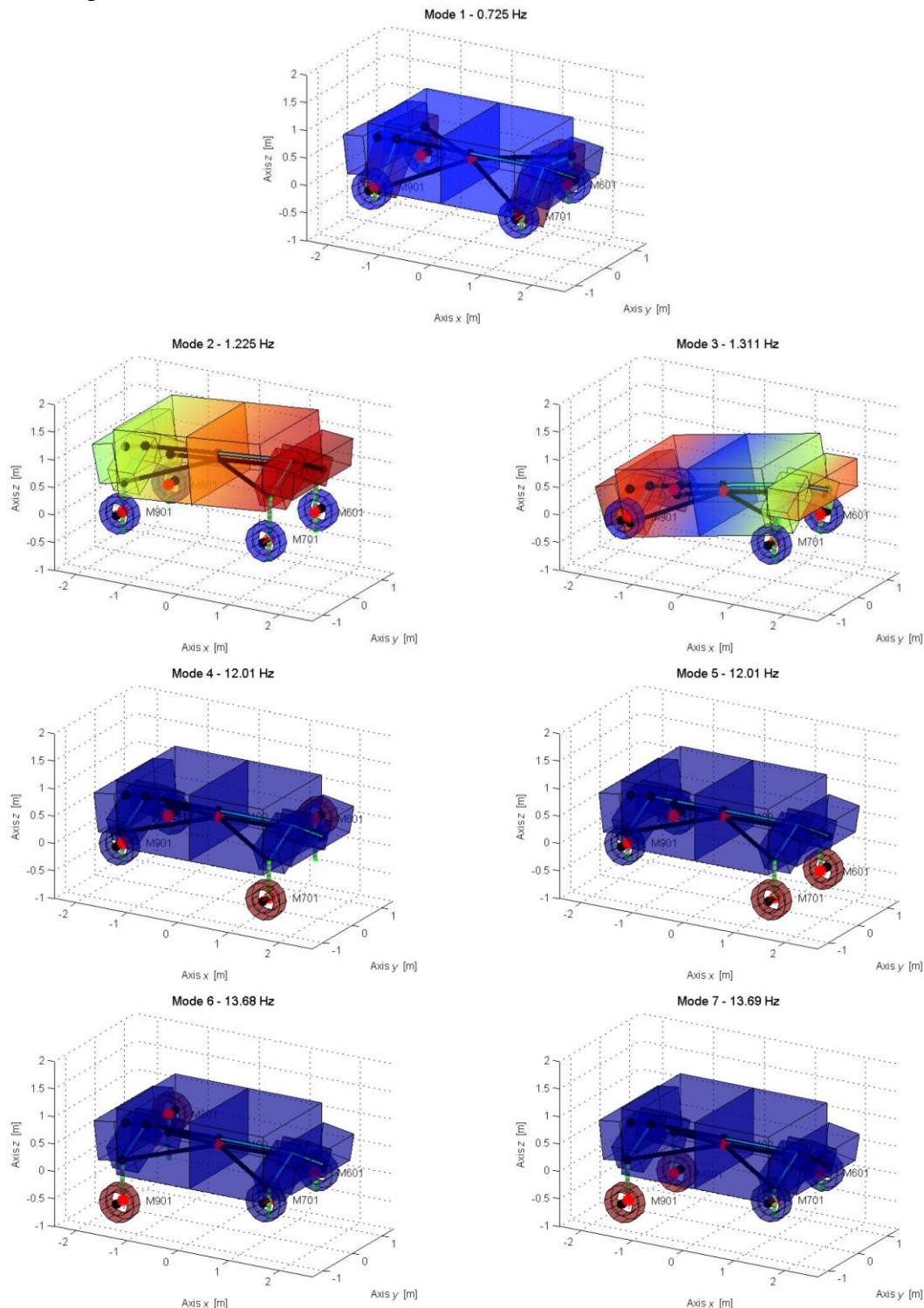


Figure 1.1.4 – Graphic visualization of chassis and suspension modes in Real Modal Analysis.

1.2 Theoretical bases of the experiments

As mentioned the objective is to characterize elementary dampers. These elements work essentially along the axial direction responding, as known, proportionally to the speed:

$$c \cdot \dot{x} = F_{damper}(t) \quad (1.2.1)$$

where:

- c : viscous coefficient of the damper, the unknown;
- \dot{x} : speed;
- $F_{damper}(t)$: the force applied or the produced response.

Therefore a deformation along a single direction is necessary. In the case of a damper analysis the resultant velocity will be considered:

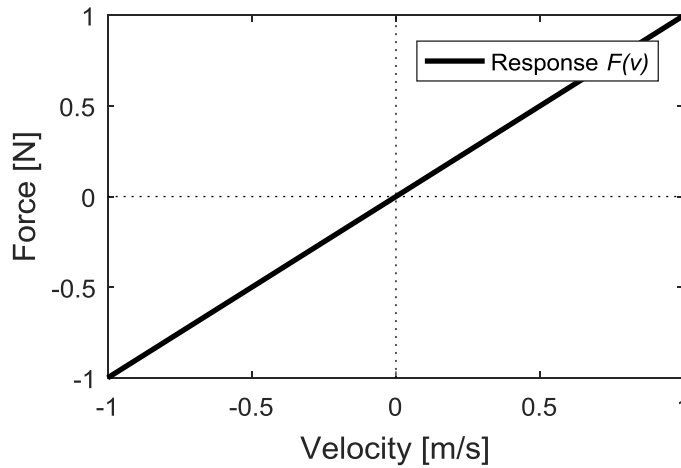


Figure 1.2.2 – A trivial linear response in a damper.

With some sensors the produced force and a motion variable will be registered. The motion variable could be: displacement, velocity or acceleration.

The idea is to take out a series of point, united by the time factor, and from this “*cloud of points*” draw the most realistic linear or nonlinear trend possible. So later a vector notation will become necessary.

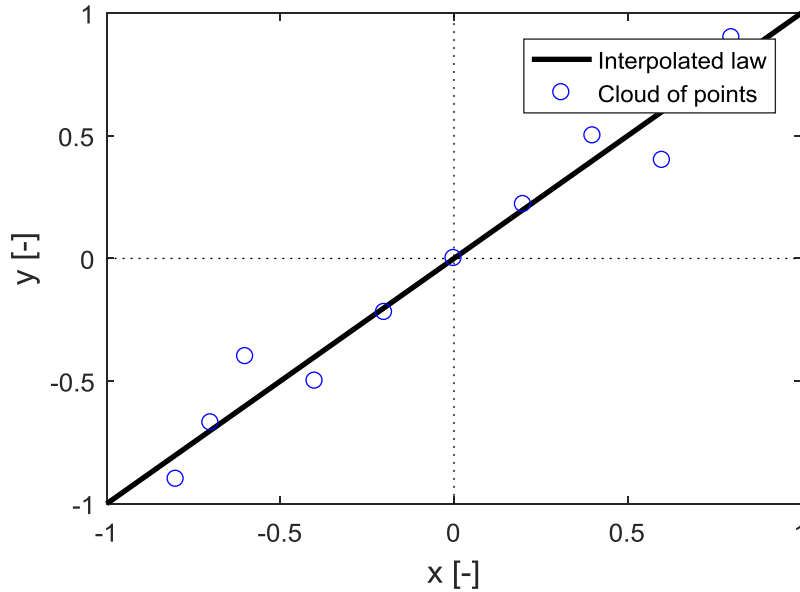


Figure 1.2.3 – Linear regression of a generic parameter.

The number of the points will depends by the sampling rate of data acquisition system, furthermore there will certainly be the need to process the data acquired in order to get a clear reading, so an algorithm must be will written. Beyond precision, obviously, as higher will be the number of point as reliable will be the deduced data.

It is also necessary to consider that will not be strictly true the solution goes not to depend on a previous state of pre-compression or pre-extension. So will be more realistic to consider not only the dependence by speed but also by current displacement or, maybe, acceleration. In this case it will therefore be convenient to use the state space in the analytical procedures, while from an experimental point of view it will mean to imagine a system of easy adjustment of the relative distance between the engagement fixed point and the point of excitation.

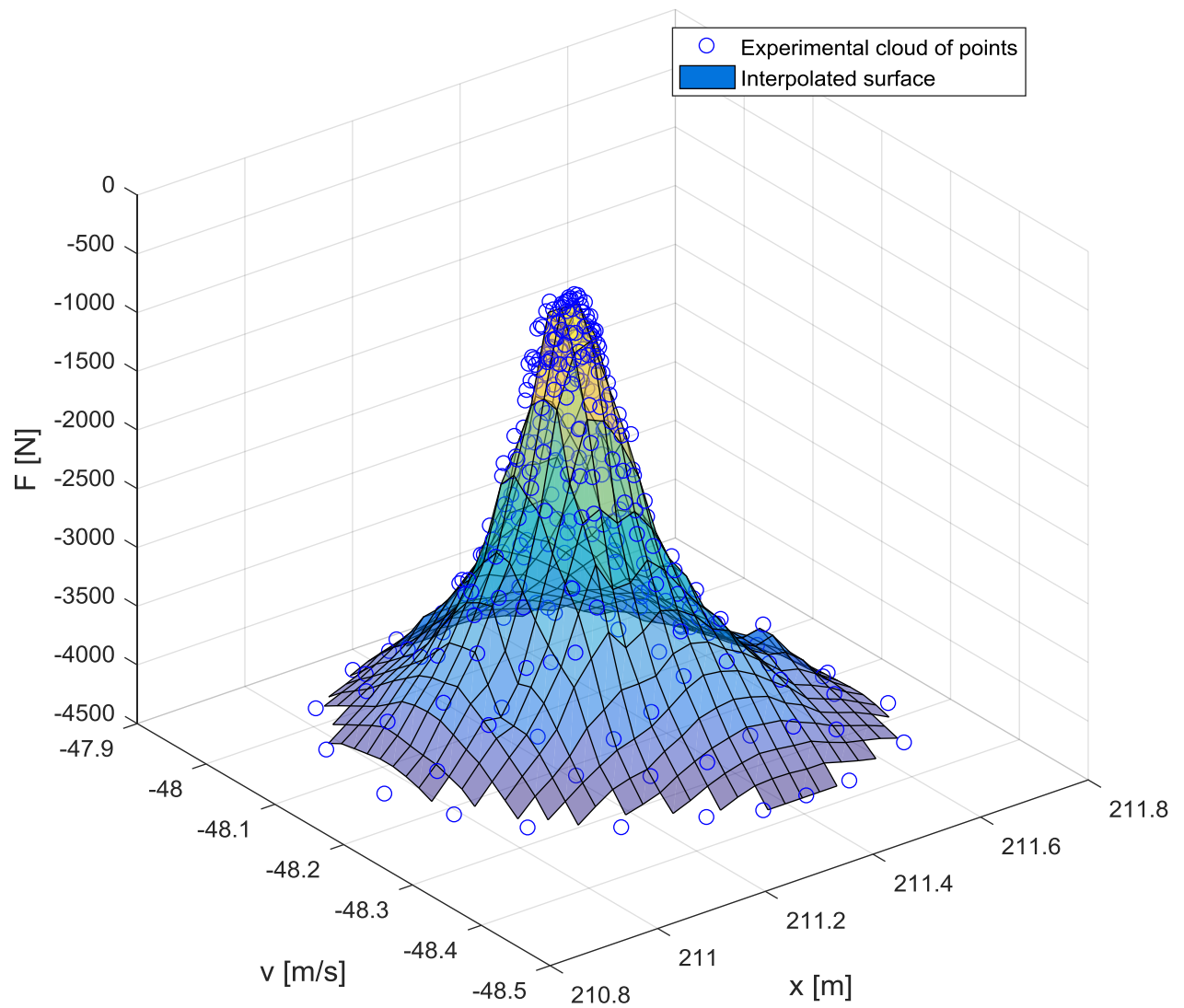


Figure 1.2.4 – Example of a 3D interpolation through a surface, not representative of a damper or a spring.

1.3 Analysis of available equipment

The starting point is to consider the equipment that may be available or, in any case, the one that would be used. The goal of using a CAD design tool is precisely to minimize the use of materials and the types of equipment, trying to avoid possible waste of time and money. A direct manual attempt would inevitably result in an expensive trial and error procedure.

Therefore a visit to the laboratory is necessary, where in particular it's been observed that were available:

- An electro-mechanical shaker: a tool whose sole function is to repeatedly exercise a force in a single direction with a certain frequency and amplitude, therefore perfect for the purpose intended (shown in Figure 1.3.1). The shaker is produced by Dongling-Italy and is a ESD-045 able to produce forces up to about 450 N in the frequency range from 5 Hz to 3000 Hz.



Figure 1.3.1 – The electro-mechanical shaker. A support plate from a previous experiment was already mounted on the main shaft.

The shaker needs its own amplifier whose task is to transform a low voltage signal (emitted by the control system) into the voltage suitable for excitation. The white wire visible in Figure 1.3.1 is exactly the one comes from the amplifier. The other block pipe union is for the air cooling system that become necessary when the shaker bears a large effort (will be possible to see no air cooling will be necessary in this case of study).

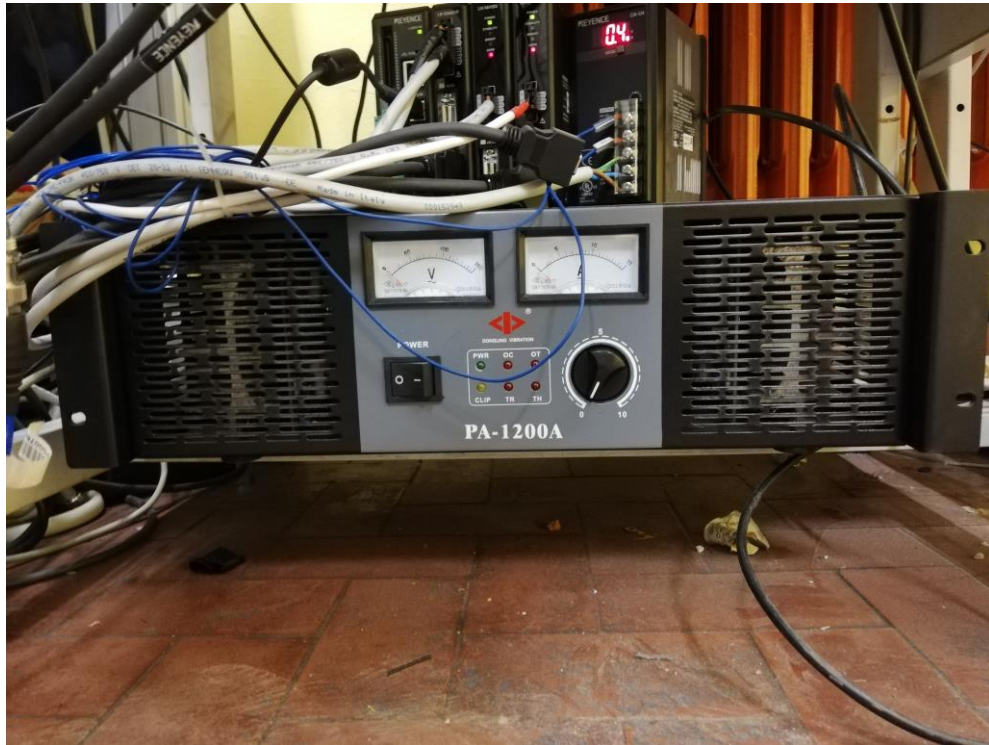


Figure 1.3.2 – Shaker amplifier.

- A series of aluminium bars for the creation of a support frame for the various equipment. Other whole bars were available to create other frame segments if needed. The cost of these bars is very low and allows a simple composition and a different suitability. They can be easily assembled with corner elements, which can be fixed with bolts. So no welding will ever be necessary. The frame element is visible at Figure 1.3.3 while a sketch with exact measures in Figure 1.3.4.

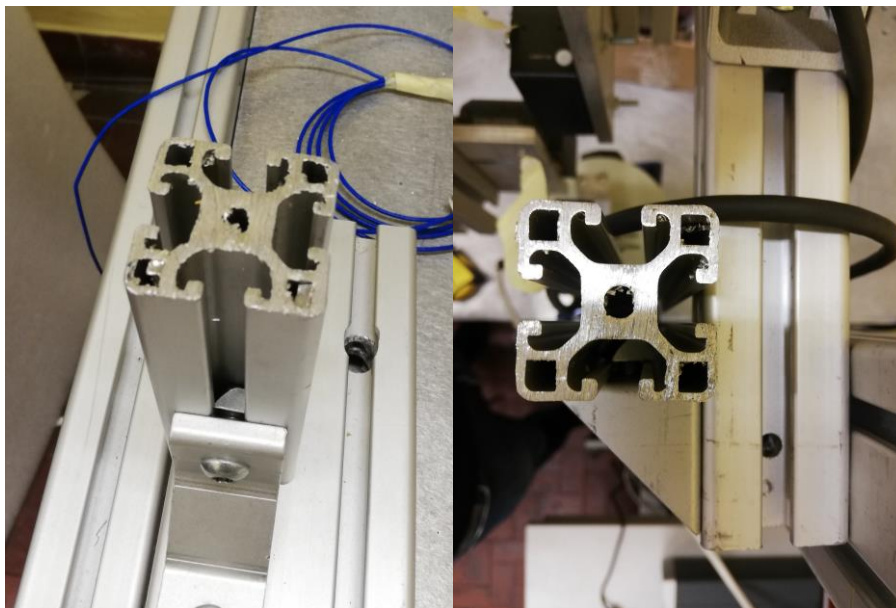


Figure 1.3.3 – Two photos of a frame element.

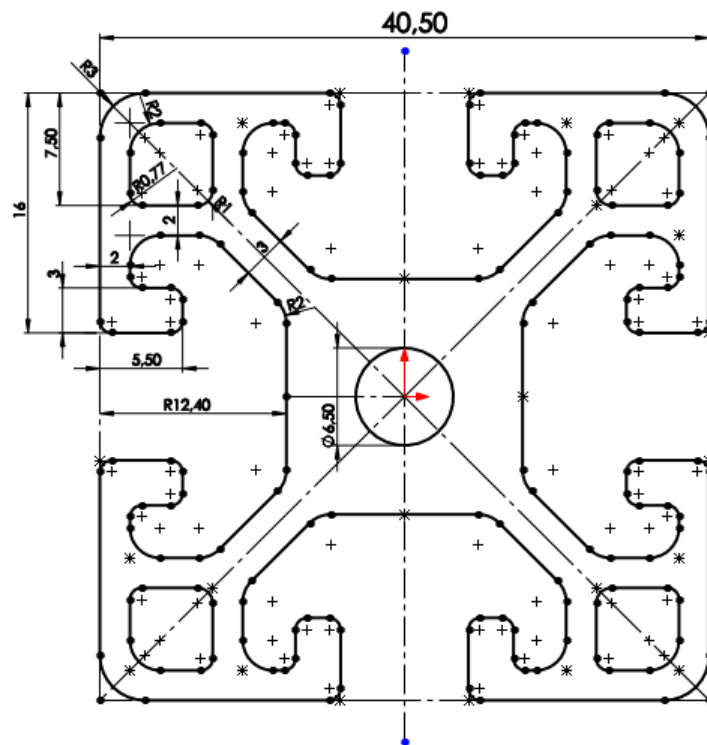


Figure 1.3.4 – A sketch with measures, obtained in Solidworks.

Another section size is also available, but is strictly dependent from the previous one, it is exactly the double along one side: obviously some shapes will be lose:

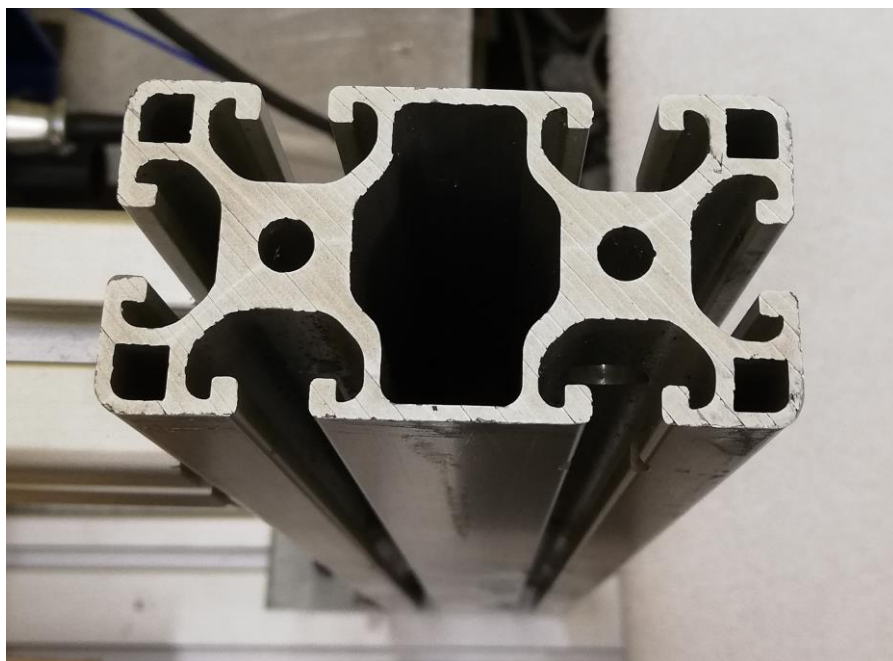


Figure 1.3.5 – CAD model of the ‘double’ profile.

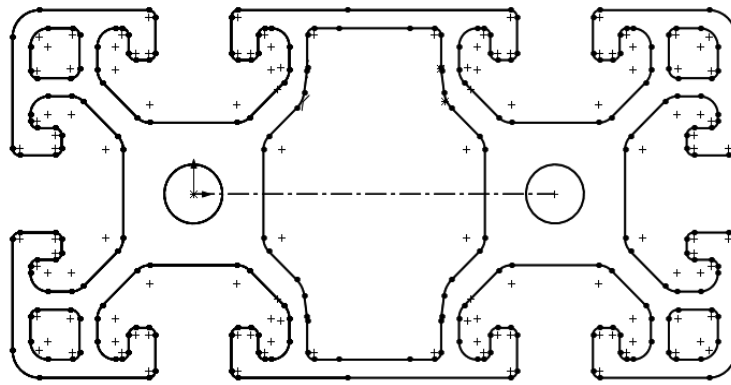


Figure 1.3.6 – Section sketch of the ‘double’ profile. For the quotas refer to Figure 1.2.4.

- A *piezoelectric load cell*, model PCB 208c02^[6]: can be mounted in axial direction thanks to the double female threading seat, but of a quite strange measure (10-32 of the Unified Thread Standard, some adapters will be necessary^[7]). It can measure up to 450 N circa (0.4448 kN) with a sensitivity of ($\pm 15\%$) 50 mV/lb (11241 mV/kN). The frequencies range goes from 0.001 Hz up to 36000 Hz. Thanks to his piezo-electric nature no amplifier o power supply will be necessary.

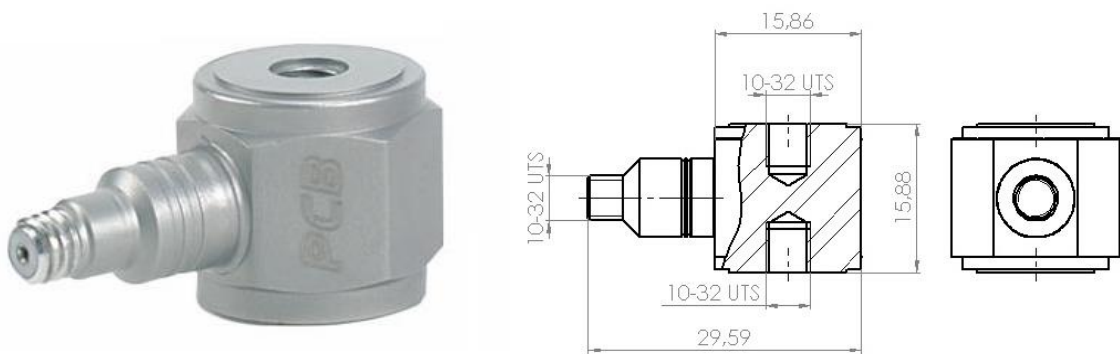


Figure 1.3.7 – A catalogue image of the load cell.

On the real image, the protruding thread on the left is where the electric wire will be connected. The top thread (10-32) is instead where the load is applied, an identical one is present at the bottom but is not visible. Both thread are visible in the sketch on the right, where there are also some measures. ^[6]

- Some *laser meters*: three different ones were available, but of the same brand. They differed in the distances they can measure. The smallest, for example, measures at an average distance of 5 cm (Keyence LK-H050), which means that if we measure a system that oscillates we cannot make its midpoint either 8 cm or even 3 cm. The other available meter sizes measure at average distances of 8 cm (Keyence LK-H080) or 15 cm (Keyence LK-H150). The existence of this three different size will make possible to place the meters in quite different positions. Obviously we would prefer the smallest one, because it is also the most accurate one, but if we would be in difficulties we can will also use some biggest one: a laser meter will always be characterized by a very high accuracy if compared with a traditional one. A pre-existing support plate will be used also for this experiment. The plate is directly mountable on the frame uprights described in previous point, and will permit some other regulations.



Figure 1.3.8 – A catalogue photo of the laser meter Keyence LK-H050^[5].

Looking at Figure 1.3.8 it will be possible to see how the laser is emitted by the upper blue pad in the normal direction. The reflected signal is captured by the lower pad (diagonal direction). It will be important that nothing exists between these two pads and the measuring surface.



Figure 1.3.9 – Available laser meter with the support plate mounted on the upright frame.

- Data acquisition system: good data acquisition hardware is available, such as the Siemens Scadas Simcenter, the proprietary laser controller, and a normal personal computer where all the data flow is channelled. The program for managing the acquisition is always from Siemens: LMS Testlab (vers. 2017), used with a pre-set suitable for characterizing structures.



Figure 1.3.10 – Siemens LMS SCADAS Mobile.



Figure 1.3.11 – Keyence laser controllers.

1.4 Basic ideas

The dynamic procedure partially described in the chapter 1.2 will be necessary. As said an axial load or displacement will be applied to the element, while an acquisition system will produce the data.

To produce the axial displacement will be sufficient to fix a part of the damper and to excite the other one through the shaker, as shown in Figure 1.4.1:

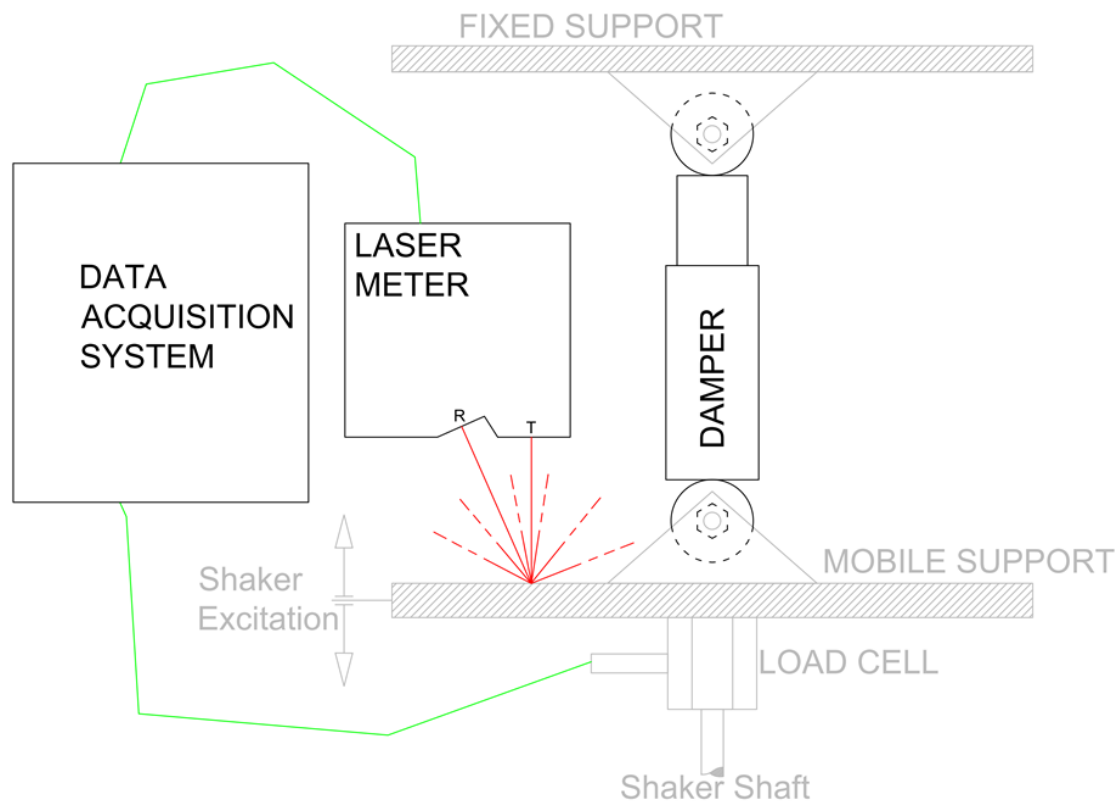


Figure 1.4.1 – Scheme of the damper experiment.

Looking at Figure 1.4.1 it is possible to notice that a configuration where the fixed part is upward, while the excitation comes from the low side, would like to be chose. The shock absorber will be fixed to the plates of the two supports (fixed and mobile) using common brackets available at any hardware store.

The load cell will be mounted under the mobile support and so between this plate and the shaker: it will measure the force that the shaker supply to the system. This force is obviously even equal to the response of the damper.

The laser, insisting on the upper plane of the plate and by being mounted on the fixed part, can measure the displacement, the velocity or the acceleration of the plate itself. In Figure 1.4.1 is also possible to see a schematic representation of the reflection of the laser on the surface, but the measurement will occur only in one of the infinite possible directions (T=transmitter, R=receiver).

No simple analytic formula will be available to calculate the value of 'c', viscous coefficient, but an algorithm will be necessary. It has to analyse the acquired data tables and to take out realistic values for the coefficients.

It will be of particular importance to minimize the influence of fixed frame vibrations on the measurements. From previous experiments has result that it is not convenient to connect the upper support part (where the damper is fixed) with the other fixed part, i.e. where the shaker is fixed. The best configuration would be, instead, the one where the two components are fixed both to the ground, which can be seen as an inertial reference system that does not suffer the effects of the shaker. If it is not possible to drill the floor to fix the various systems (as in this case), is possible to try keeping it all in place by using very stiff connection for the frame and trying to decouple the shaker vibrational effect by interposing a rubber strip between the table and the shaker support stirrup. As it will be possible to see in chapter 2 also in this second case the two system has to be maintained uncoupled, but will be unavoidable a certain coupling because the table on which the whole system will be mounted, even if it is quite massive (composed only by iron top and aluminium bars for the frame) is characterized by a certain resonance frequency that is of about ~ 7 Hz, a value that is, unfortunately, in the middle of the interest range.

1.5 The vehicle

As said our objective is to characterize the damper and the wheel of a RC car model, that in this case is:



Figure 1.5.1 – Top view of the Losi 5ive-T 2.0.^[2]



Figure 1.5.2 – View of Losi 5ive-T 2.0.^[2]

Since the experimental setup is designed before the purchase of the vehicle and the manufacturer does not provide technical details about the individual components, the only thing that could have been done is to deduce the various measures from the photos provided by catalogue. Knowing the scale factor of the car and the maximum dimensions it is possible to obtain an estimate of the measurements.

The rear suspension is sketched in the following picture, but is even quite similar to the front one:

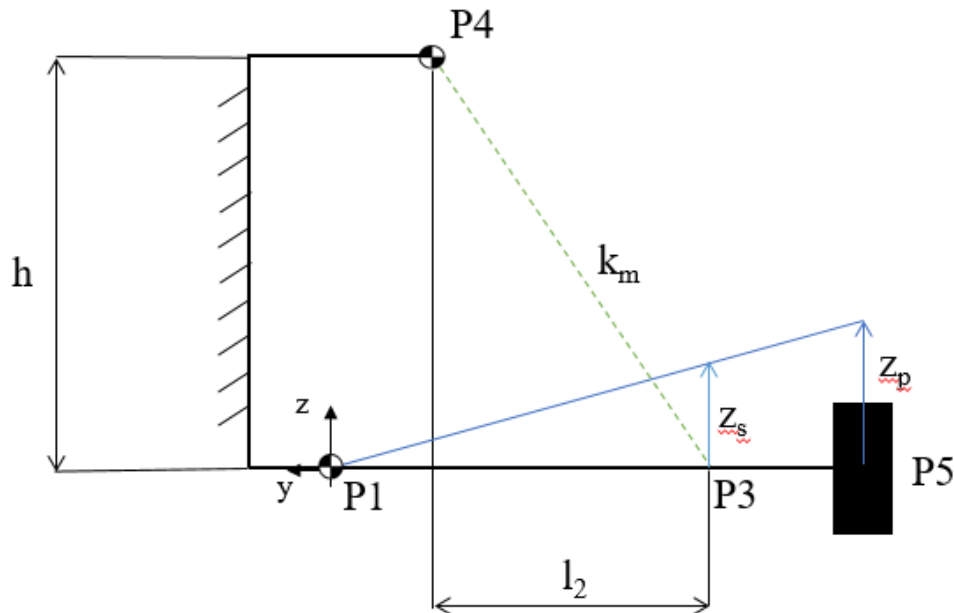


Figure 1.5.3 – Front view of Losi 5ive-T 2.0 suspension.^[2]

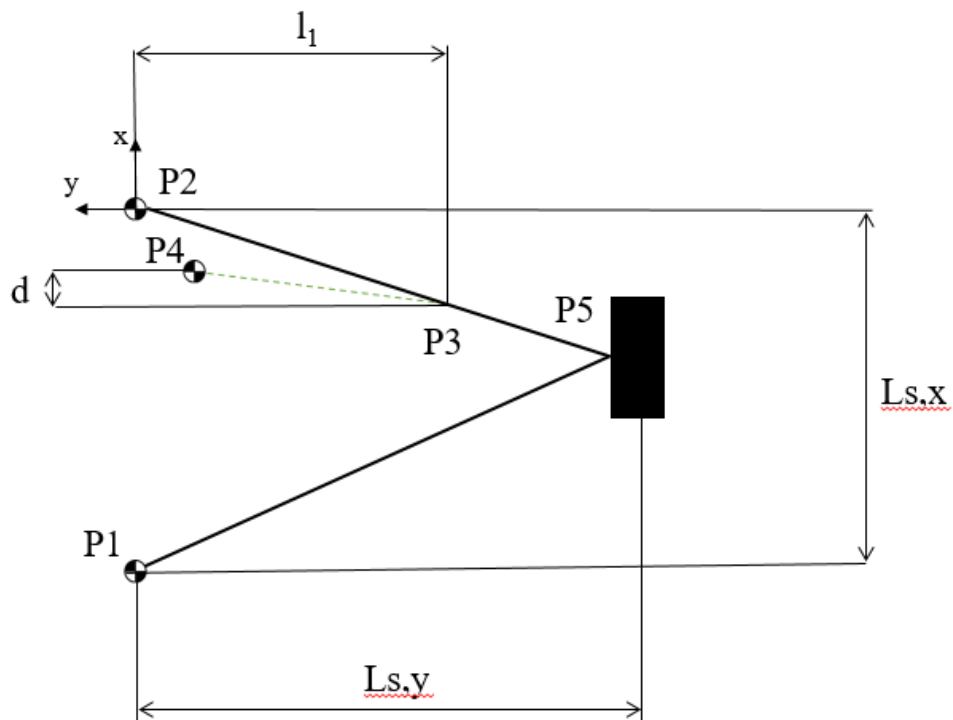


Figure 1.5.4 – Top view of Losi 5ive-T 2.0 suspension.^[2]

The following hardpoint are defined:

- P1 and P2 represents the points of attachment of the arm to the frame;
- P3 is the point of attachment of the spring to the element;
- P4 is the point of attachment of the spring to the frame;
- P5 is the point of attachment of the wheel to the suspension.

The following distances are measured using Figure 1.5.3 and Figure 1.5.4 as reference.

Table 1.5.1 – Front suspension lengths.^[2]

Symbol	Front suspension	Rear suspension	Description
$L_{s,x}$ [mm]	100	104	P1-P2 distance
$L_{s,y}$ [mm]	154	125	P1-P5 y-projection
l_1 [mm]	77	87	P2-P3 y-projection
l_2 [mm]	70	65	Spring y-projection
d [mm]	20	30	Spring z-projection
h [mm]	153	153	Spring x-projection

No other information were available. It is now possible to deduce the lengths of the damper with simple trigonometric steps, if is considered that:

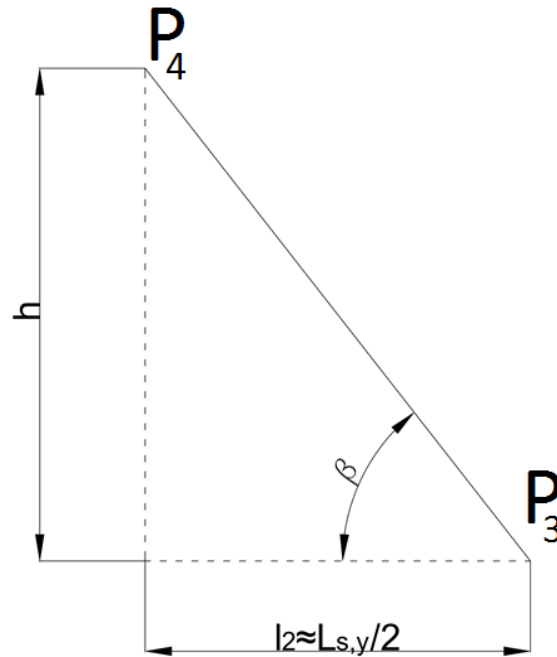


Figure 1.5.5 – The subsystem of Figure 1.5.3 for the trigonometric passage.

Simply writing the two projection equations along the two axes is possible to find $P_{3,4,y}$:

$$P_{3,4,y} \cos \beta = l_2 \quad (1.5.1)$$

$$P_{3,4,y} \sin \beta = h \quad (1.5.2)$$

Accepting the approximation:

$$l_2 \cong \frac{L_{s,y}}{2} \quad (1.5.3)$$

Is possible to write the solvable system of two equations and two unknowns:

$$\begin{cases} 2 P_{3,4,y} \cos \beta = L_{s,y} \\ P_{3,4,y} \sin \beta = h \end{cases} \quad (1.5.4)$$

That in explicit form become:

$$\begin{cases} \beta = \arctan \frac{2h}{L_{s,y}} \\ P_{3,4,y} = \frac{h}{\sin \beta} \end{cases} \quad (1.5.5)$$

Must take into account the little projection along x direction, so for passing to $P_{3,4,y}$ to $P_{3,4}$ is also necessary to apply Pythagorean theorem:

$$P_{3,4} = \sqrt{P_{3,4,y}^2 + d^2} \quad (1.5.6)$$

Therefore ultimately, by solving the system:

$$P_{3,4} = \sqrt{\left(\frac{h}{\sin \left(\arctan \frac{2h}{L_{s,y}} \right)} \right)^2 + d^2} \quad (1.5.7)$$

By numerical substitution is possible to obtain, referring to rear suspensions:

- $\beta \cong 63.3^\circ$
- $P_{3,4} \cong 172 \text{ mm}$

The system that will be designed has to absolutely able to adapt itself to such excursion by simple regulation of the piece of frame which has support the upper supports

This estimation proved to be absolutely accurate once it was possible to physically measure the piece. It was found that:

- $P_{3,4,real} = 165 \text{ mm}$

That means that the error with the used method was only of $\sim 4\%$.



Figure 1.5.6 – Real photo of the vehicle.



Figure 1.5.7 – Detail of suspension system.

2. Construction of experimental setups

2.1 Elementary CAD components

Is now possible to proceed to the realization of the firsts, elementary, components, the ones who are already available. It is pretty much important to take high, as much as possible, the level of detail in terms of dimensions, protruding parts, cable connections.

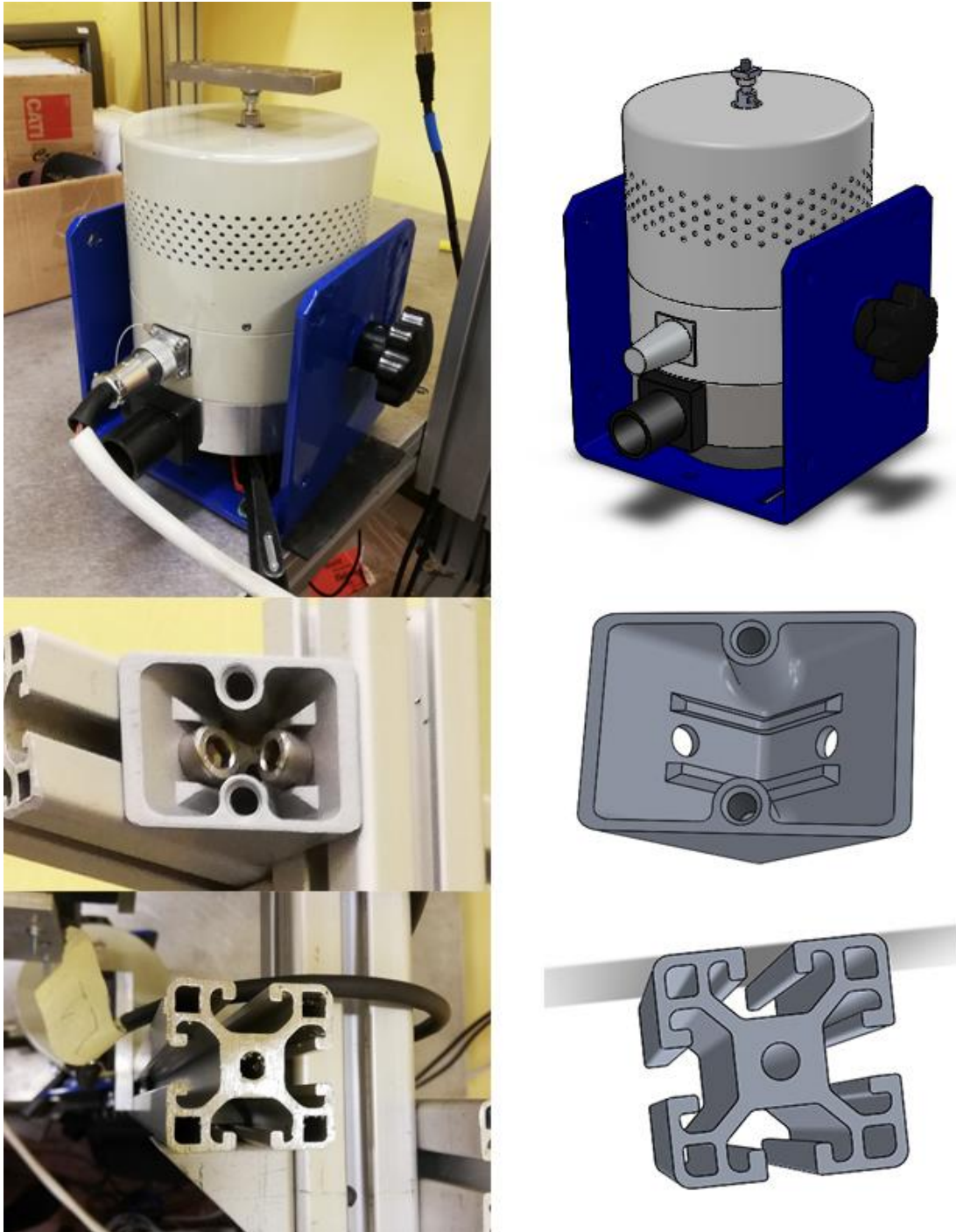


Figure 2.1.1 – Solidworks CAD models and comparison with photos of the shaker (it is already an 'assembly'), above; of an angular element for fixing the frame, in the centre; of a piece of frame, at the bottom.

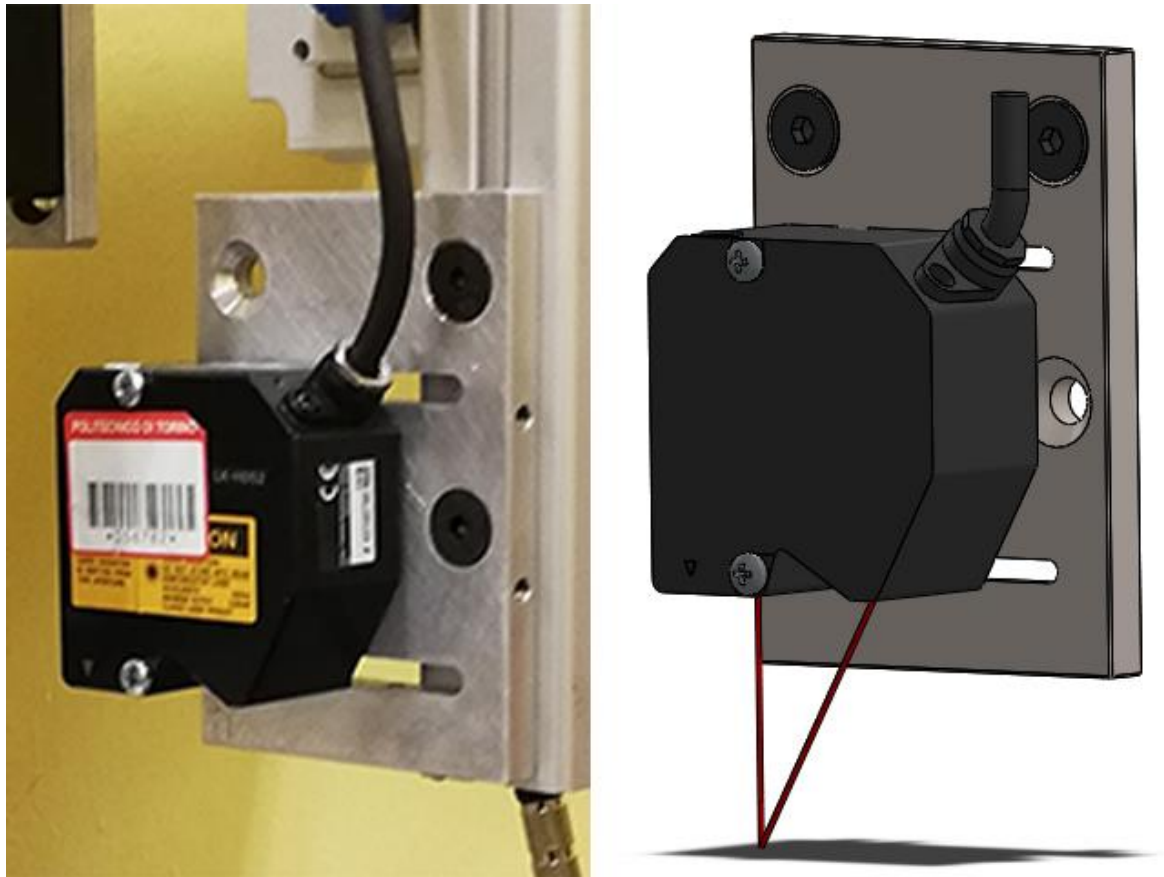


Figure 2.1.2 – Solidworks CAD model and comparison with photo of the laser meter. The direction of the laser and his reflection in the main direction has been represented too, at the standard distance, in order to evaluate the possible interactions with other objects.

The bar elements has been obtained as a simple extrusion of the profile already shown in Figure 1.2.3 and obviously it is possible to obtain various lengths: the only limitation concerns the maximum length, the original bar is 2 m, but this measurement is quite far from our maximum necessary size, which is shorter than 1 m.

For the shaker was been important to consider the two dofs it have, the first is obviously the relative movement between the shaft and the shaker case itself, the second is the angular position with respect of the main blue support. Two knobs on the sides block this angular position and so also this elements has to be represented even if they are not important for the experiment goal.

2.2 Setup design

2.2.1 Damper dimensions

First of all the dimensions of the shock absorber is needed to be known ^[2]. A first estimate was made in chapter 1.4. While once the vehicle was purchased it was possible to carry out a complete measurement and a CAD model.



Figure 2.2.1.1 – The real shock absorber.



Figure 2.2.1.2 – CAD model.

The shock absorber is only a part of the suspensions, that in the operative condition look like:

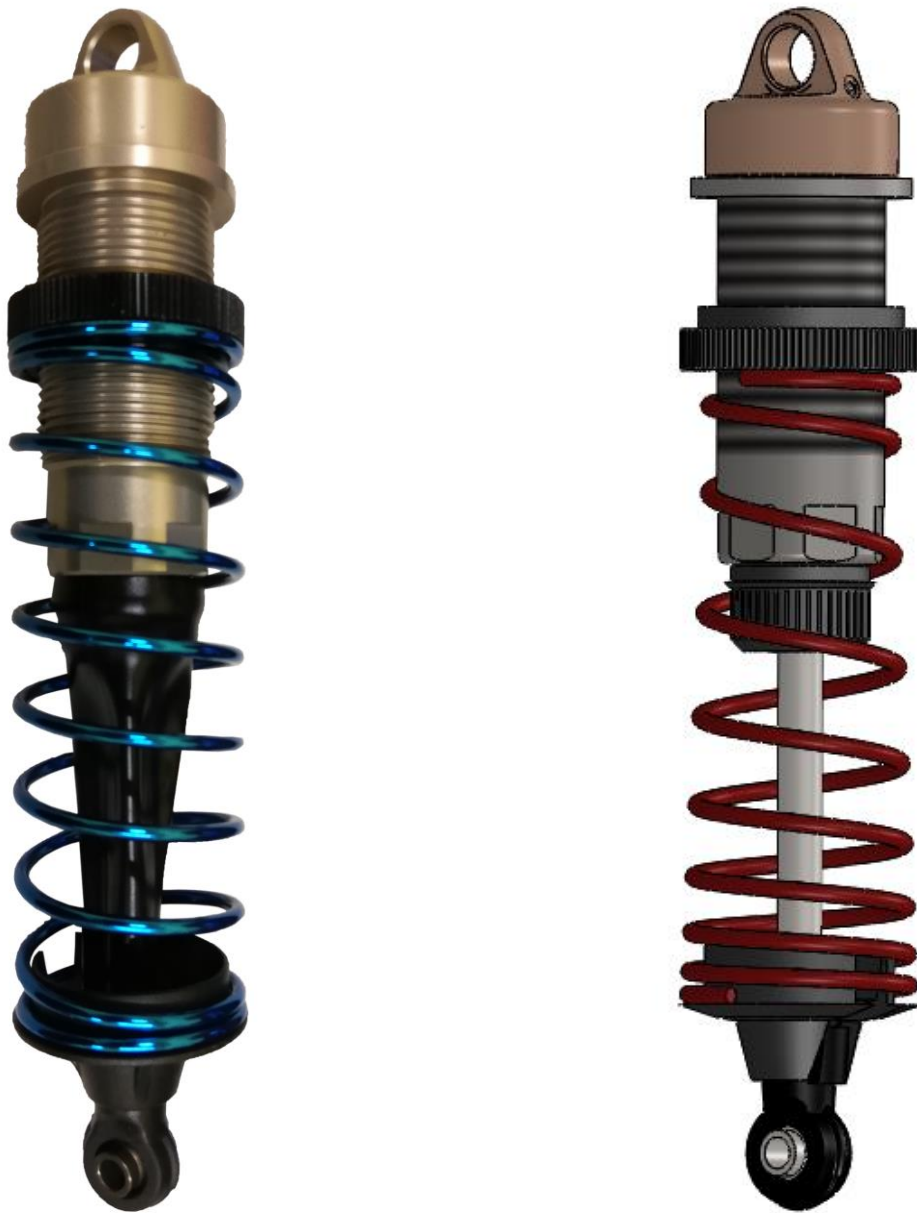


Figure 2.2.1.3 – Totally mounted suspension.

As it is possible to see the suspension has a pre-load system: this means that the height can be modified, for this reason the more logical things to do is to refer all the experiments to the nominal conditions, and to take all the measures when the suspension is mounted on the vehicle.

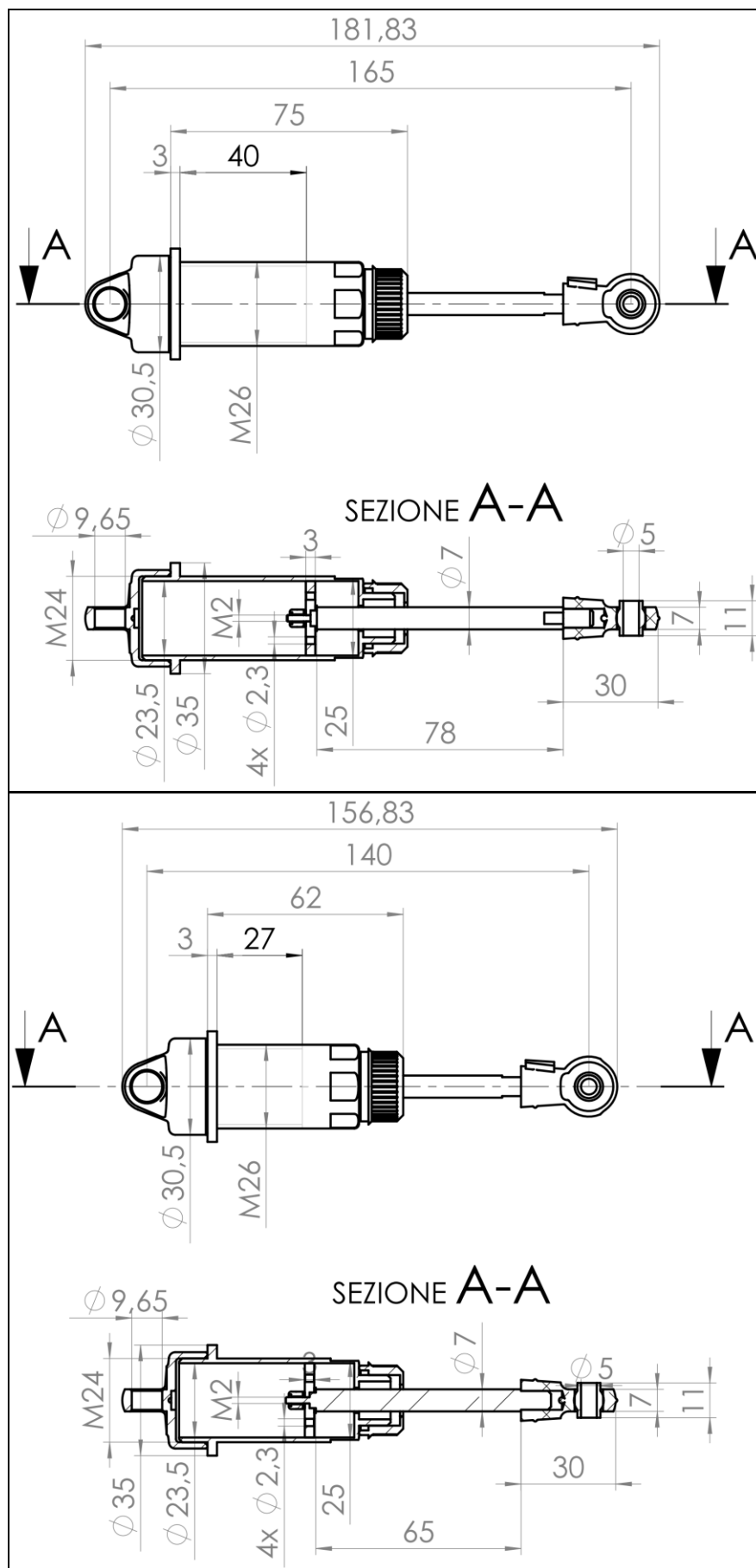
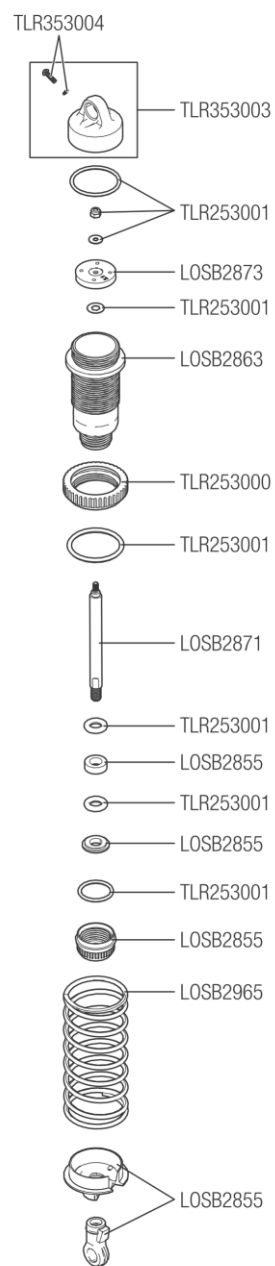


Figure 2.2.1.4 – Drawing of a rear (up) and front (down) damper with quotas

Front // Vorderseite //
Avant // Fronte



Rear // Rückseite //
Arrière // Retro

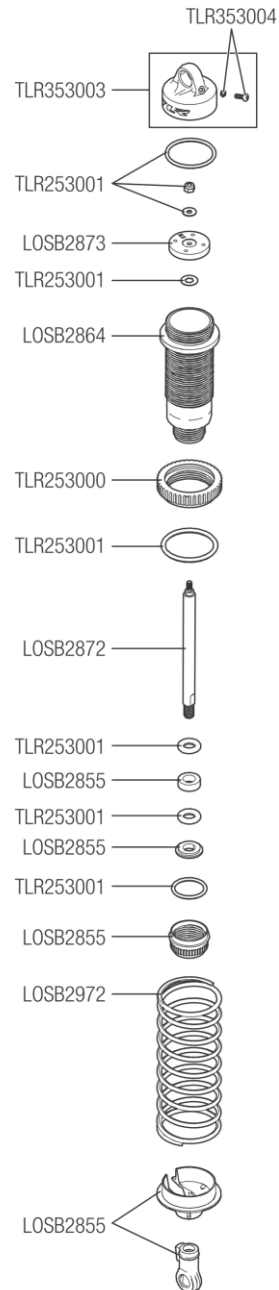


Figure 2.2.1.5 – Image from Losi 5ive-T 2.0 ^[2] use and maintenance manual.

One of the most important measure is the width of the fixing head (11 mm). This will be useful to found the correct supports configuration.

2.2.2 Upper frame

For the upper support a frame built of aluminium extruded bars was been designed. The frame had to be assembled by bolts and by angular elements, no welding was possible. Moreover the frame has to be as much as possible similar to itself for the different experiments (i.e. switching from a front damper to a rear one), this mean that an easy height regulation is needed.

The design idea is:

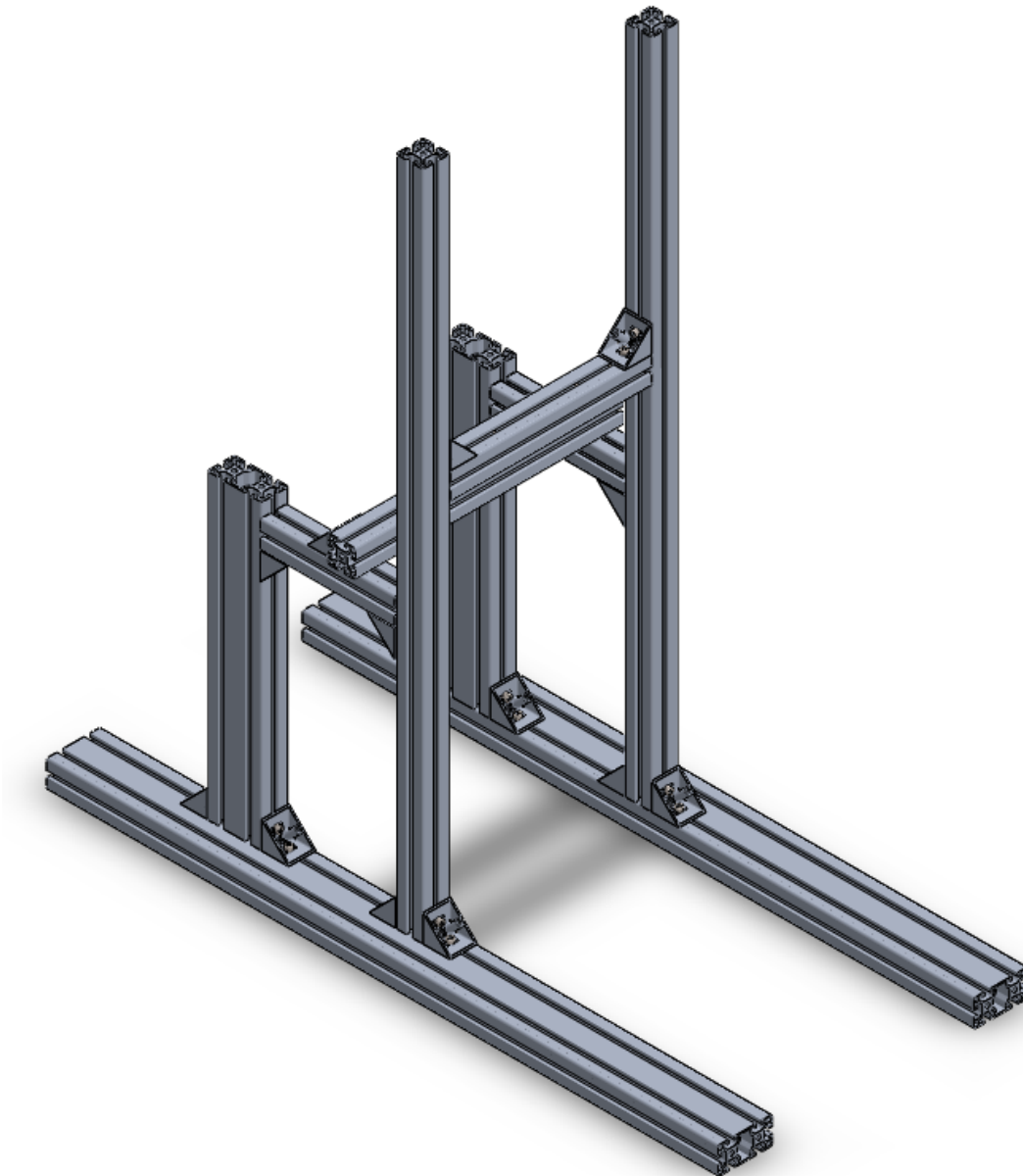


Figure 2.2.2.1 – Upper frame configuration.

As it is possible to observe in Figure 2.2.2.1 a 'bridge' configuration was designed. The central uprights support the central bar. The configuration provides that the central uprights are 'external' to the main upper bar, so that this last can move inside along vertical direction. Two additional uprights was added from one side in order to obtain an higher stiffness of the structure and to obtain some support space for laser meter fitting (see later).

2.2.3 Lower frame

For the lower frame a simply choose was made: adopt a long piece of iron which will be inserted between the shaker main support and the bottom of the shaker itself. This stirrup push the shaker against the experiment table through the use of simple M8 bolts. As said in the chapter 1.4 a rubber strip will be inserted between the shaker and the table.

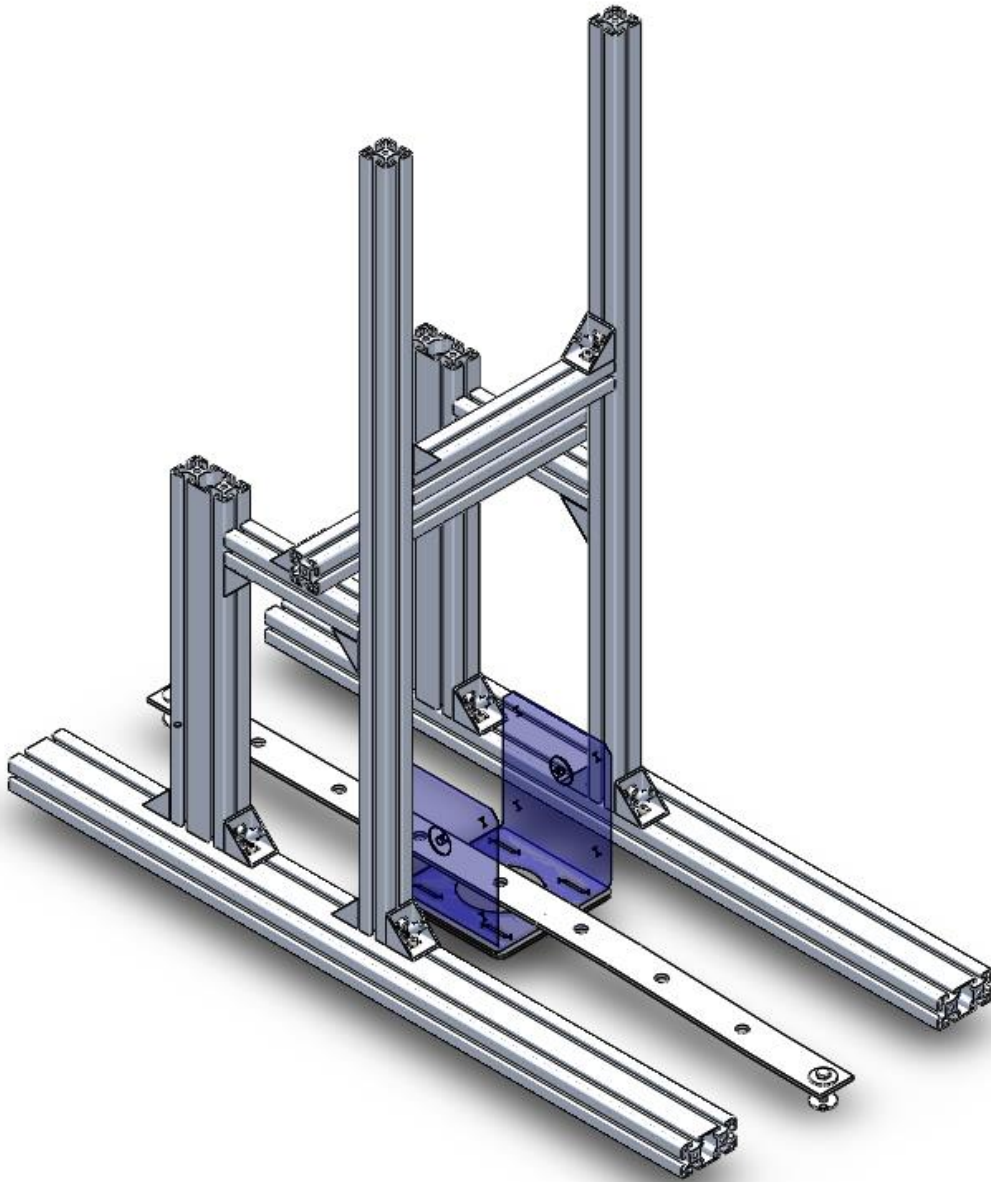


Figure 2.2.3.1 – Upper and lower frames configuration. The semi visible blue part is the shaker main stirrup, inserted between the rubber strip and the long stirrup bolted to the table.

This solutions looks necessary when considering that the table has no holes over the entire surface, but only somewhere: it is not a veroboard, and there is no possibilities to make other holes. The long stirrup is a simple piece of iron, 8 mm thick, that realize a certain deformation when bolted to the table, but that ensure very stiffly the shaker.

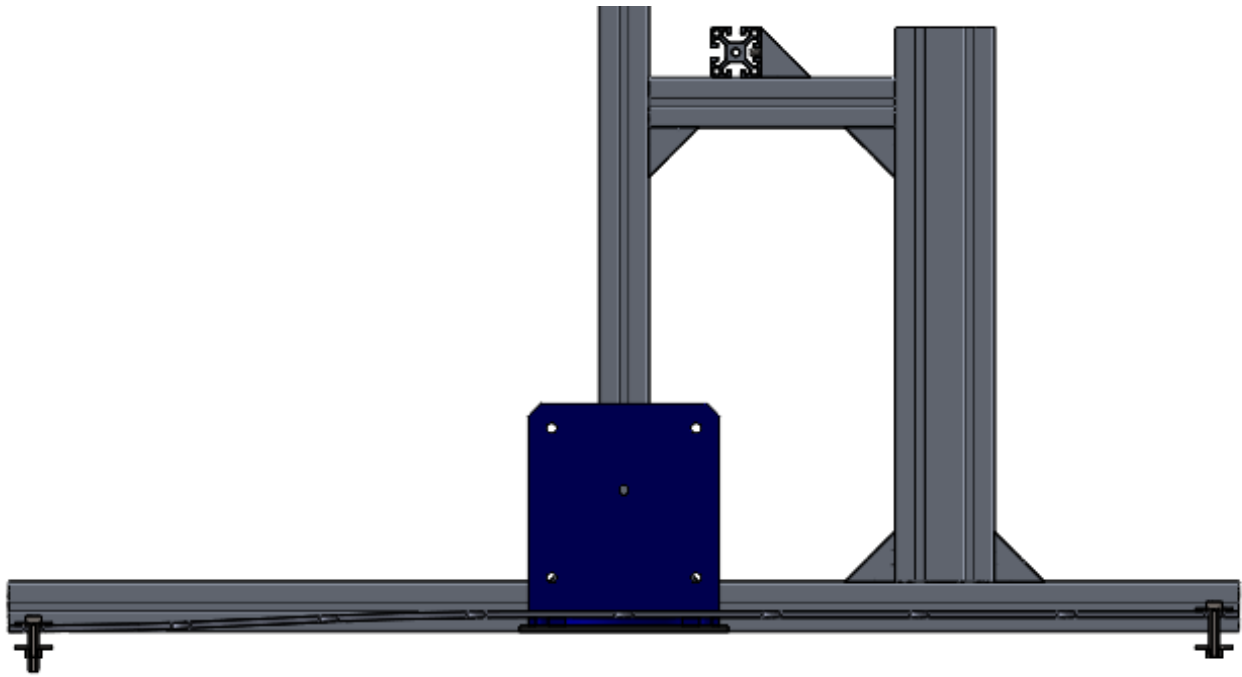


Figure 2.2.3.2 – Section side view of the frame. In the bottom the deformed long stirrup is visible.

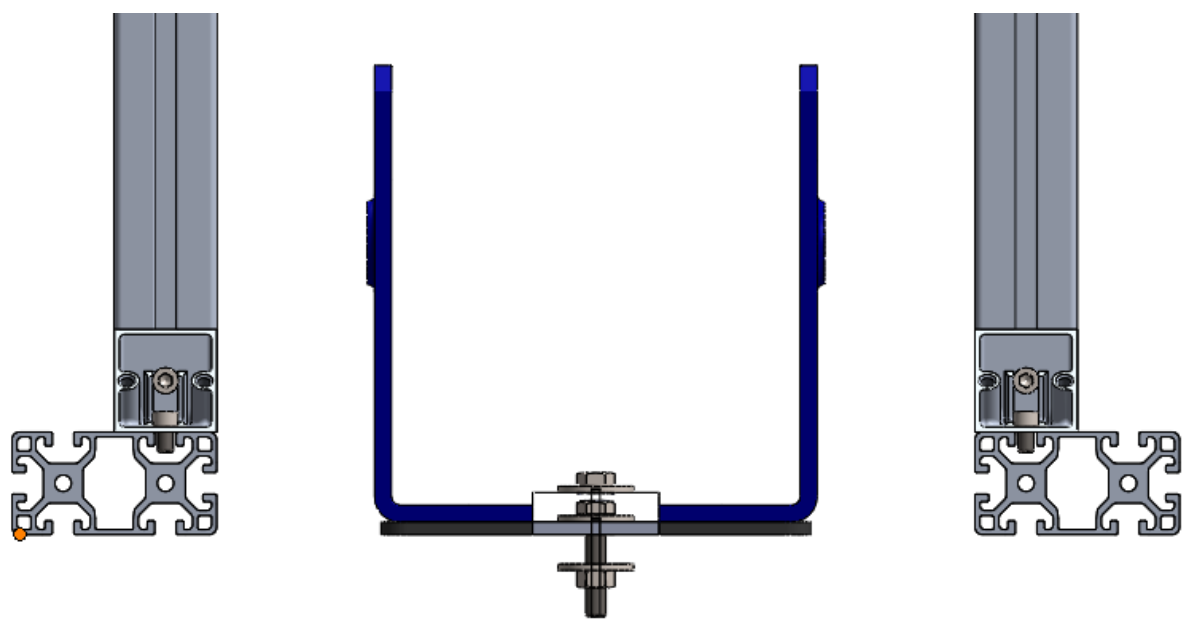


Figure 2.2.3.3 – Front view of the lower frame.

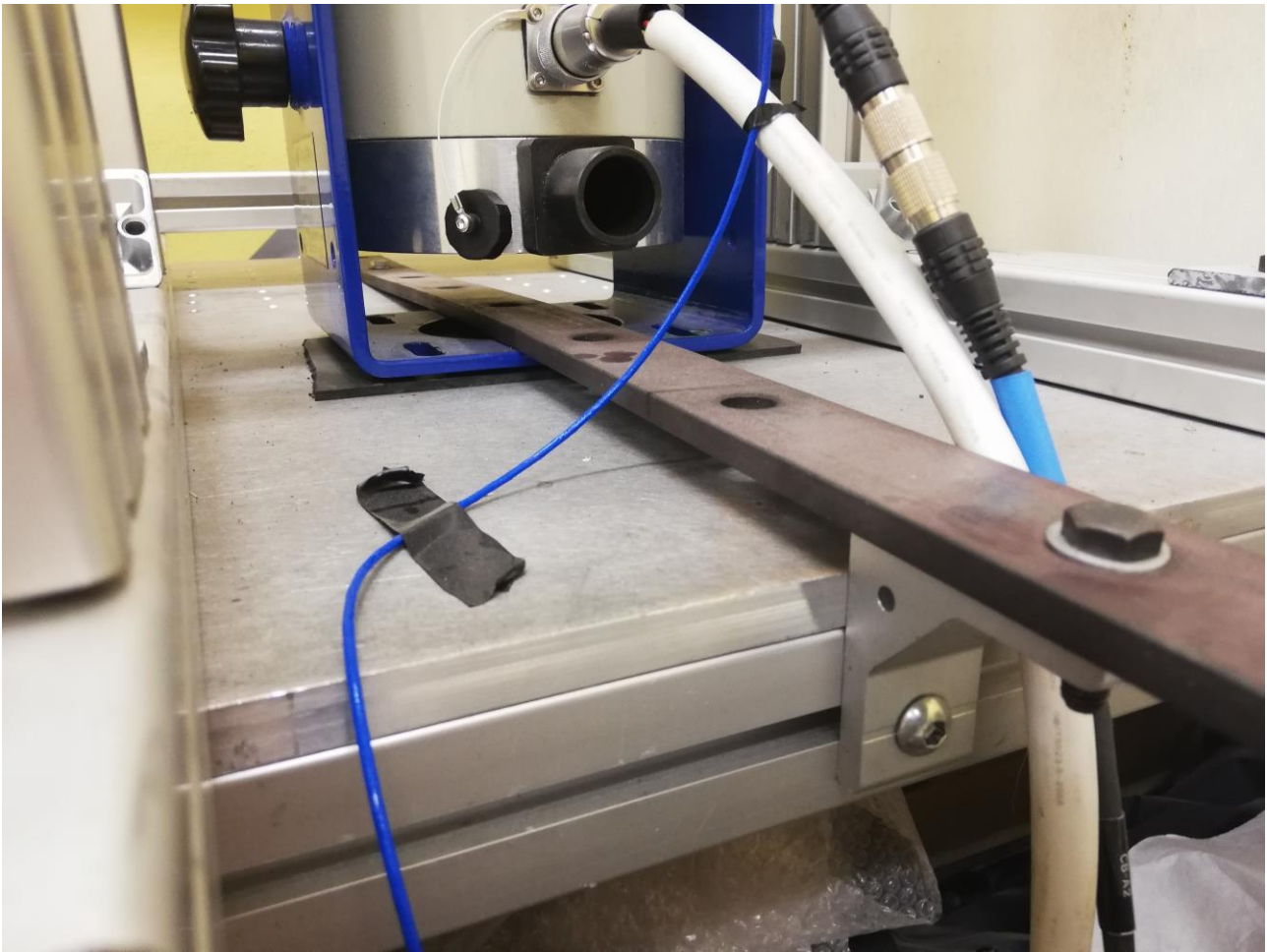


Figure 2.2.3.4 – Photo of the lower frame realization. In the back it is possible to see the holes in the table and the deformation of the iron strip.

2.2.4 Shaker position

The shaker has to be positioned in counter position with respect to the upper frame.

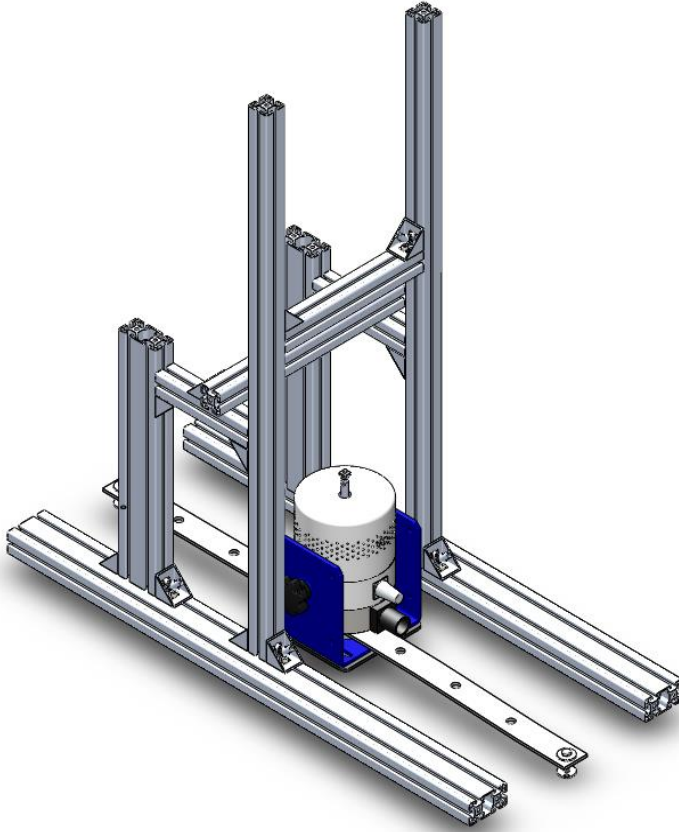


Figure 2.2.4.1 – Isometric view of the set.

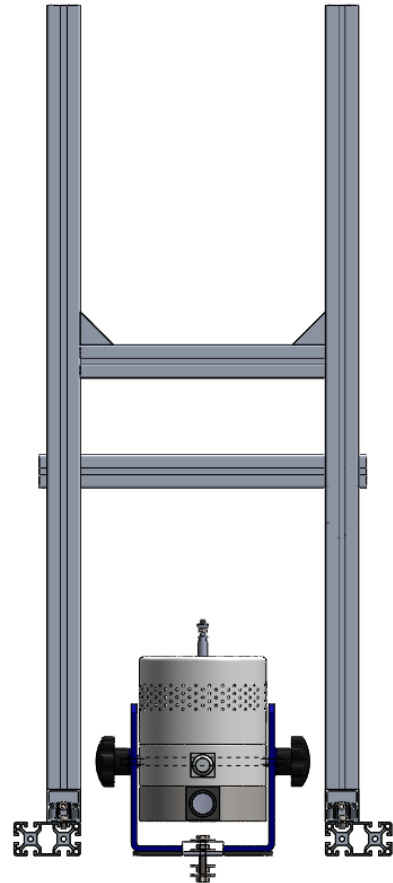


Figure 2.2.4.2 – Side view.

2.2.5 Lower plate

Here must be try to imagine a support that has to fit with the damper and also try to maintain the existing plate. Furthermore, trivial, try to lightly modify it in order to obtain all the functional characteristic required.

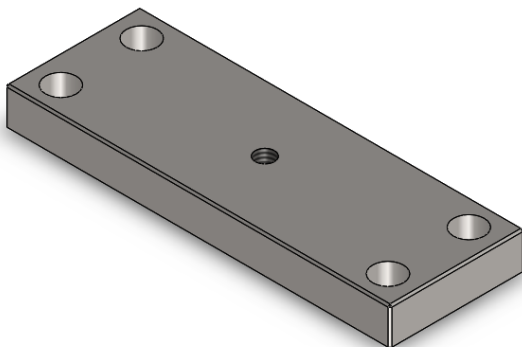


Figure 2.2.5.1 – Existing plate.

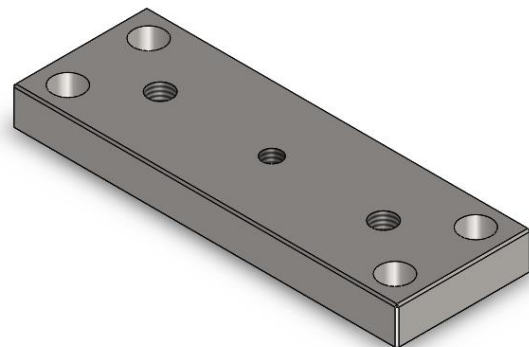


Figure 2.2.5.2 – Modified plate.

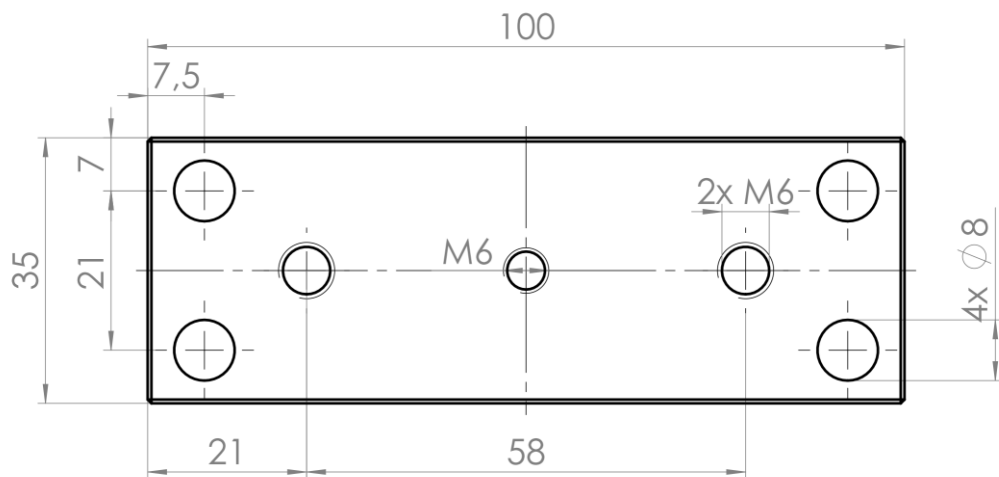


Figure 2.2.5.3 – Draft and section of the lower plate with quotas.

The central hole has function of connection to the shaker, while is unknown what were the four pre-existing holes function. As it possible to see in Figure 2.2.8 & 2.2.9 two more holes will be necessary, they will be useful to mount the supports.

The lower plate has then to be mounted on the shaker's shaft. Between the shaft and the plate the piezoelectric load cell has to be inserted. As already said in chapter 1.3 the cell has a quite strange thread standard, so two nipples^[7] will be necessary to convert from 10-32 to M6 standard, but since the nipples available are characterized by a male-male shape also a long M6 nut will be necessary, to convert from M6 male to M6 female and finally make possible to join the cell to the M6 male shaker's shaft.

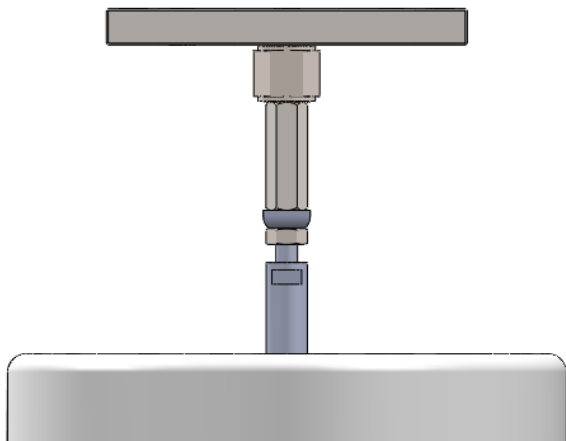


Figure 2.2.5.4 – The load cell connection.

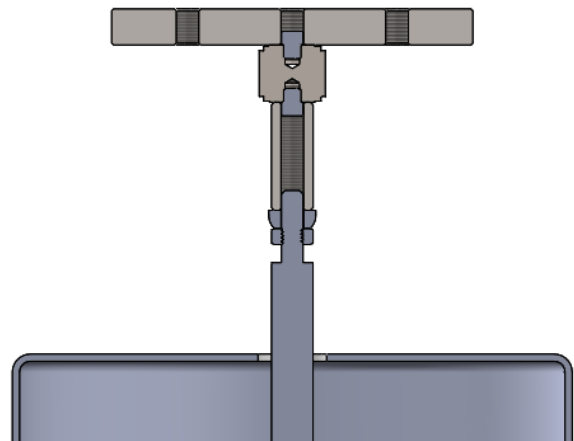


Figure 2.2.5.5 –Section view.

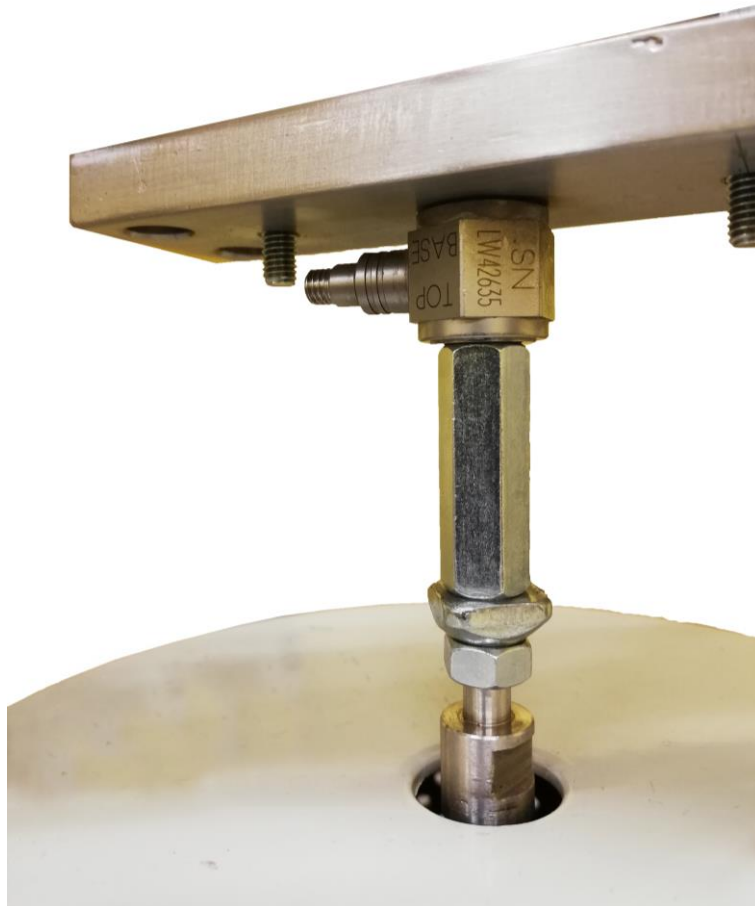


Figure 2.2.5.6 – Photo of the real load cell connection scheme.

2.2.6 Clamping systems

For the lower clamping the found system is to use a stirrup like:

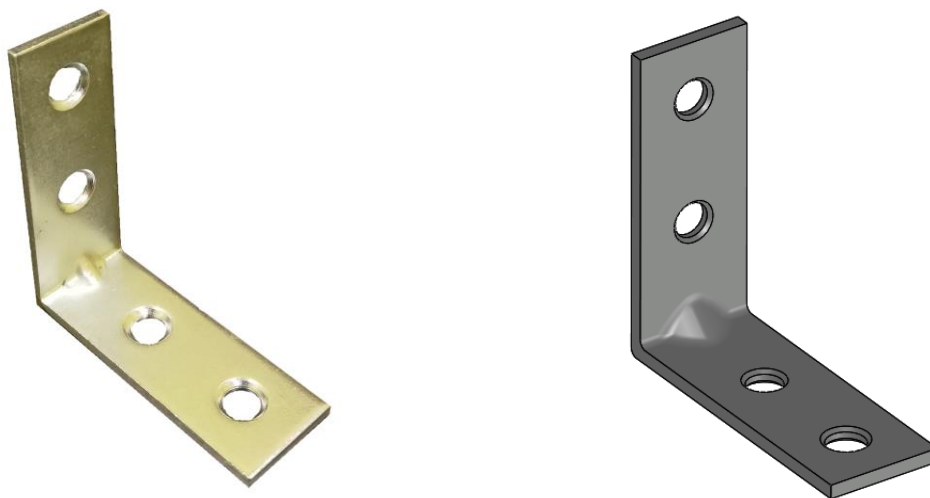


Figure 2.2.6.1 – The chosen damper support (photo and CAD model).

In order to allow easy adjustment a little modification will be done, passing from the two holes configuration to a slot on a side:

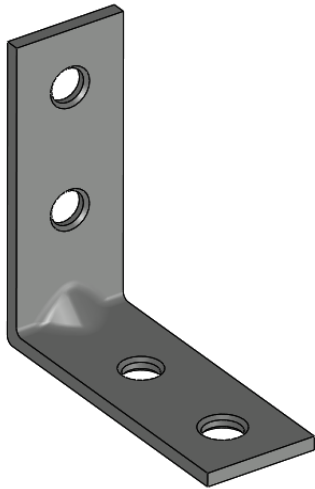


Figure 2.2.6.2 – Support as bought.

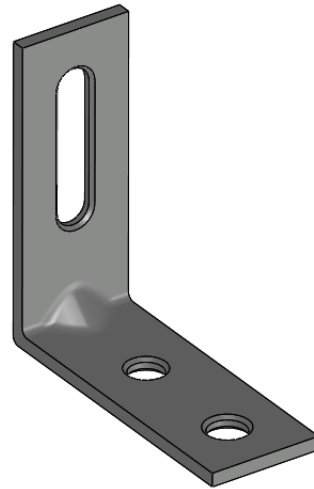


Figure 2.2.6.3 – Modified support.

The slot has to match with the two holes previously produced in the lower plate.

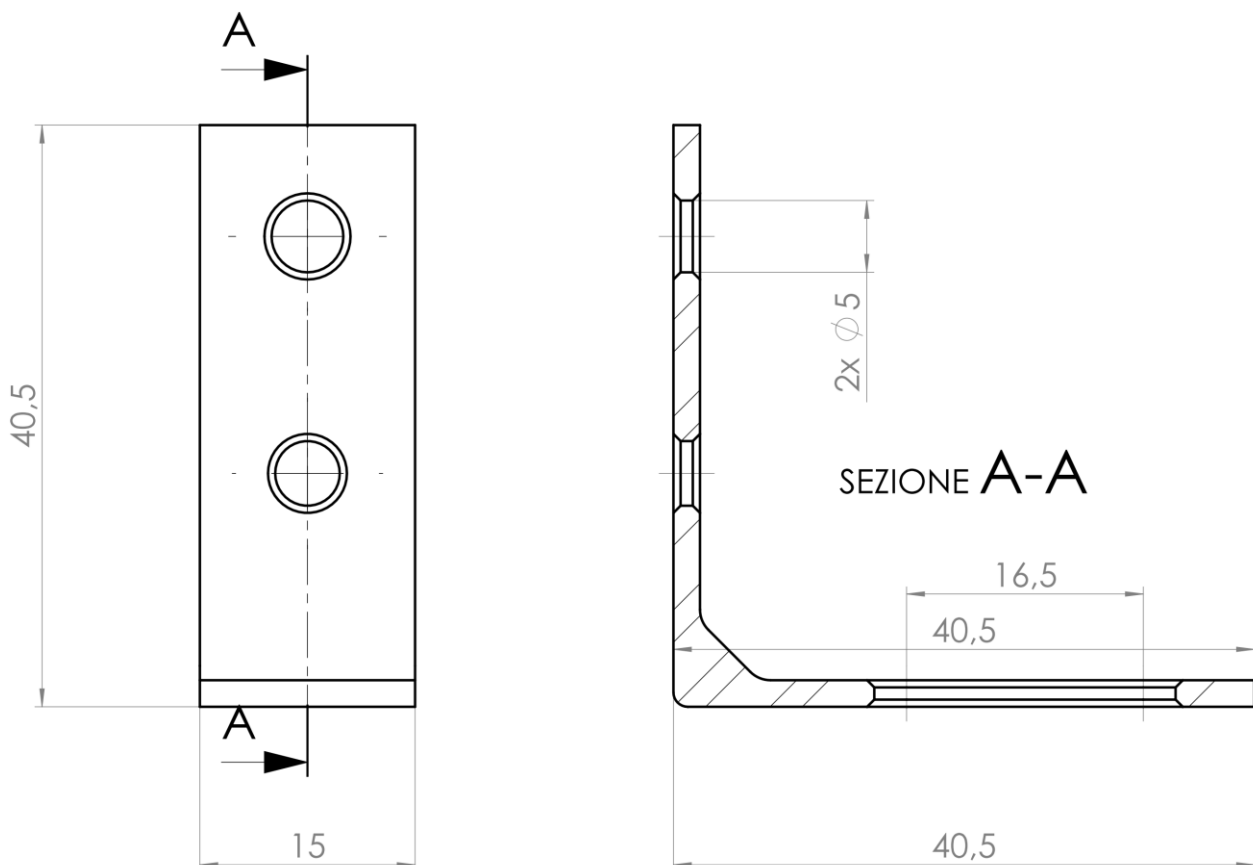


Figure 2.2.6.4 – Drawing with quotas of the chosen lower support.

This type of support is mountable to the lower plate through the slot in the base, while the pin passing by the two side (that will link these supports with the damper head) will be a simply M5

screw passing through one of the two holes to the other one and bolted with two M5 nuts for a major safety.

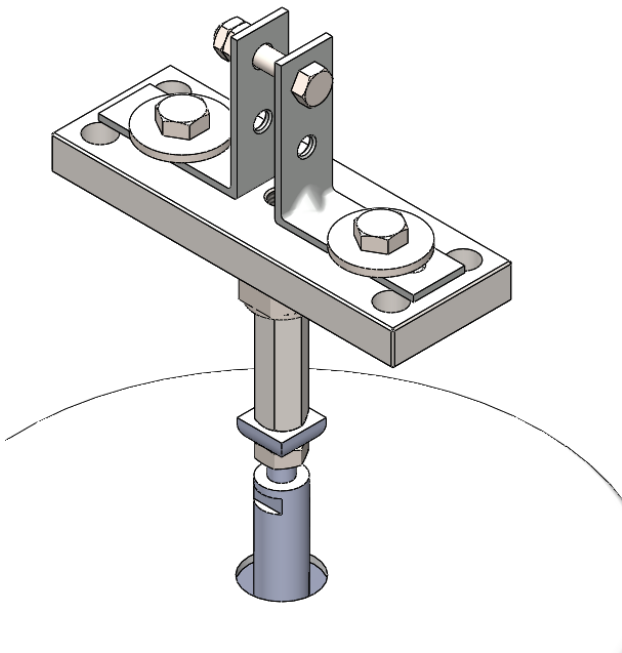


Figure 2.2.6.5 – Lower plate configuration.

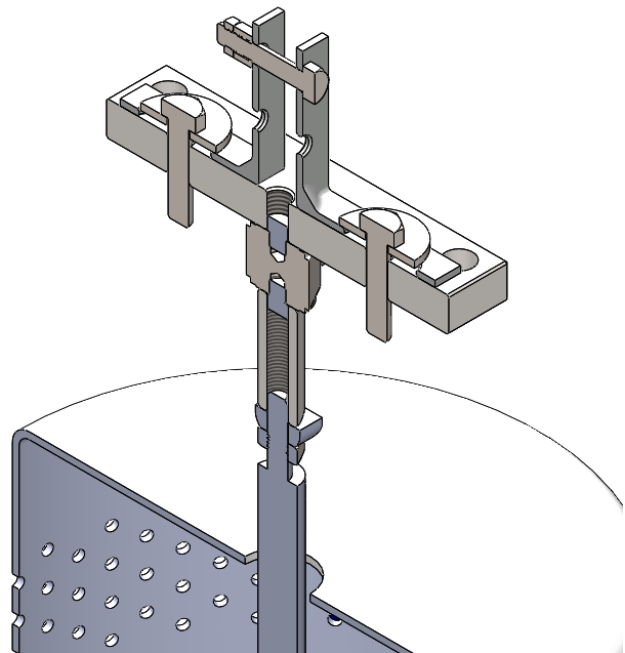


Figure 2.2.6.6 – Section view.

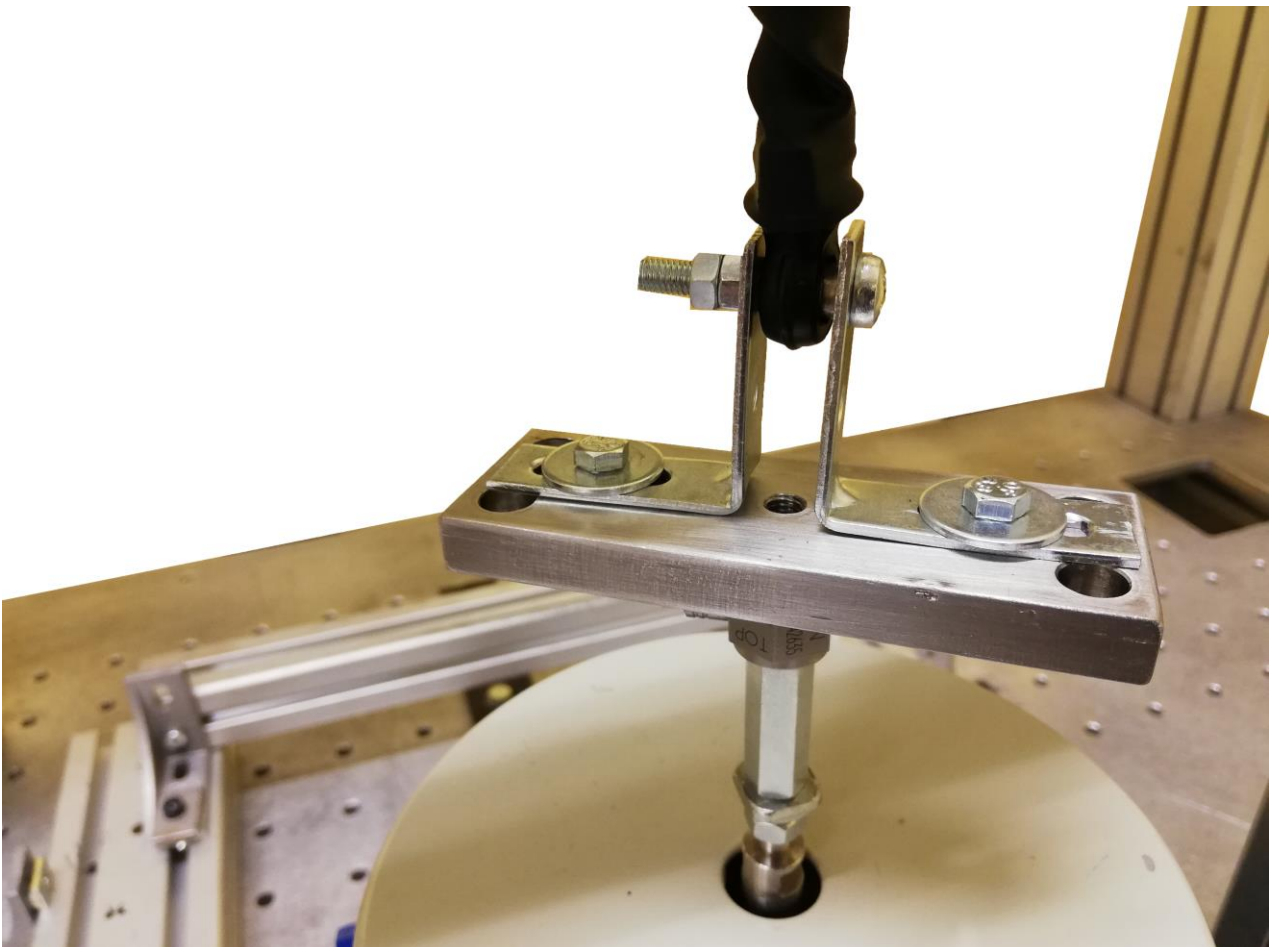


Figure 2.2.6.7 – Real photo of the lower clamping system. A damper is already mounted.

In the upper side a quite similar connection will be realized between the frame and the damper but a size adaptation has to be considered. In fact while the hole in the plastic head side has a 'simple' diameter of 5 mm, the one present in the metal cap side which close the oil cylinder (see Figure 2.2.1.4), has a quite strange diameter of 9.65 mm. This diameter becomes understandable if the mounting system on the vehicle is considered (Figure 1.4.7): an expansion bushing is interposed between this hole and the pin fixed at the vehicle, by tightening the M6 bolt this bushing (with original diameter 9 mm) is compressed in the axial direction and so expand itself in the radial direction, reaching more than 9.65 mm, and so realizing a flexible and resilient connection, with a certain grade of freedom.

For this reason it is necessary the realization of a dedicated shaft that has the exact diameter and that can then realize the connection with the frame:

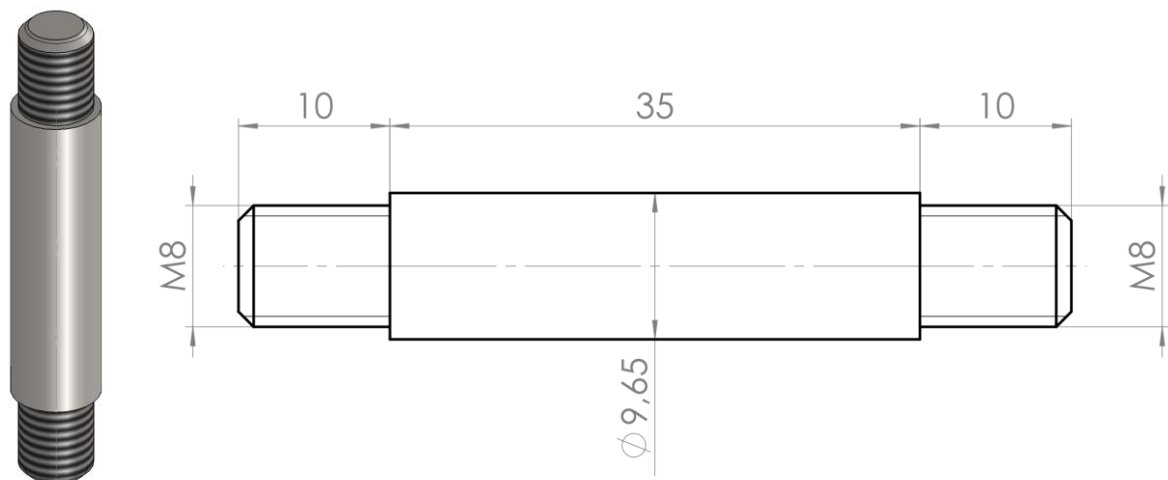


Figure 2.2.6.8 – Upper connection shaft, CAD (left) and drawing with quotas (right).

Associated to this shaft some supports with a 8 mm diameter holes will be necessary. As done for the stirrups of the lower connection the solution was found in a hardware store:

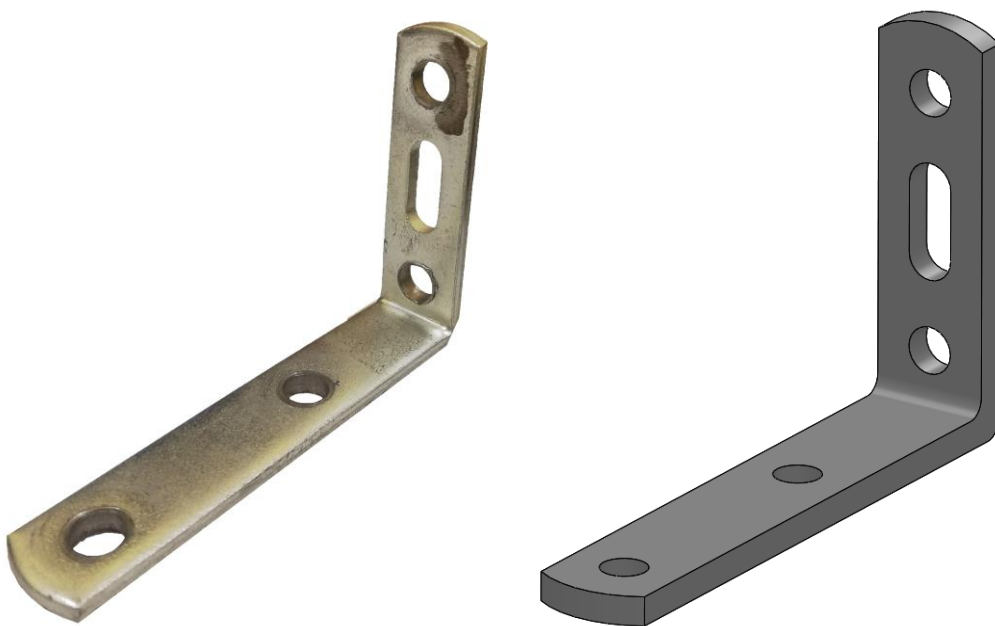


Figure 2.2.6.9 – Upper connection stirrup.

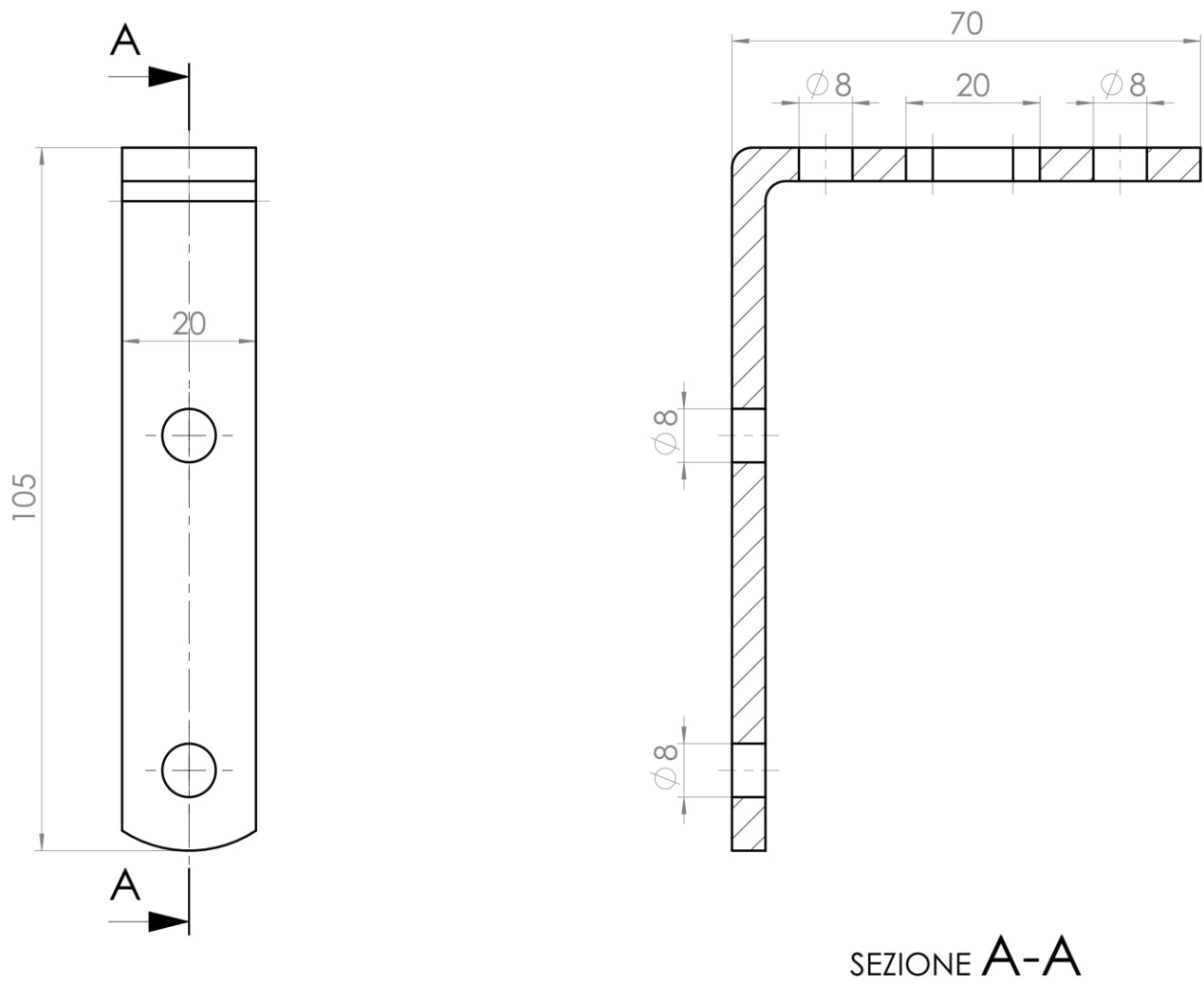


Figure 2.2.6.10 – Drawing with quotas of the chosen upper stirrup.



Figure 2.2.6.11 – Lower plate configuration.

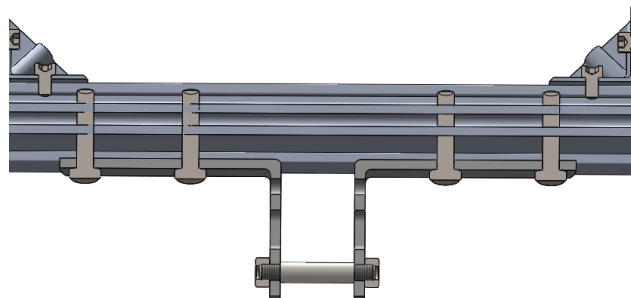


Figure 2.2.6.12 – Section view.

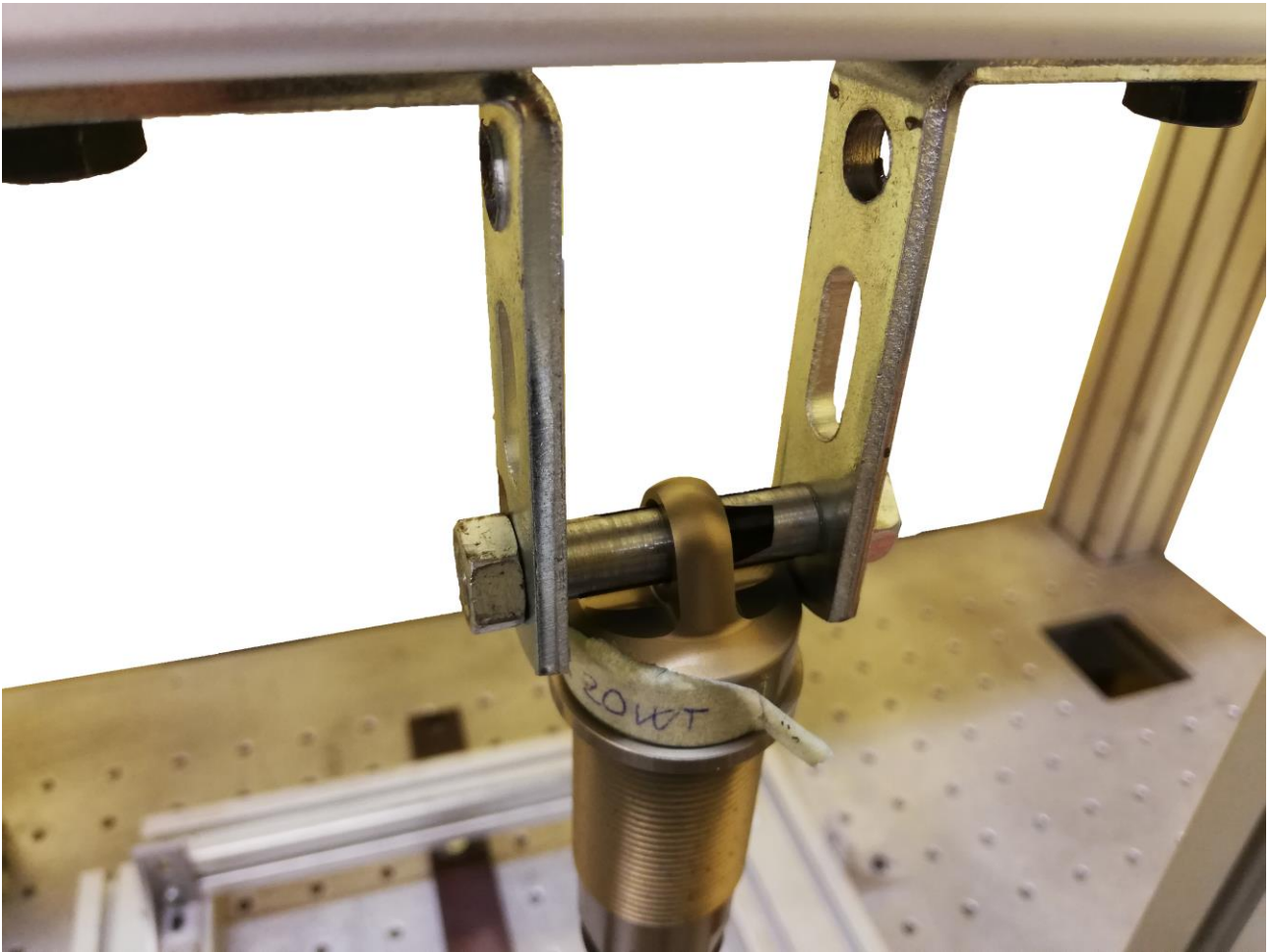


Figure 2.2.6.13 – Detailed photo of the upper clamping system. A damper is already mounted.

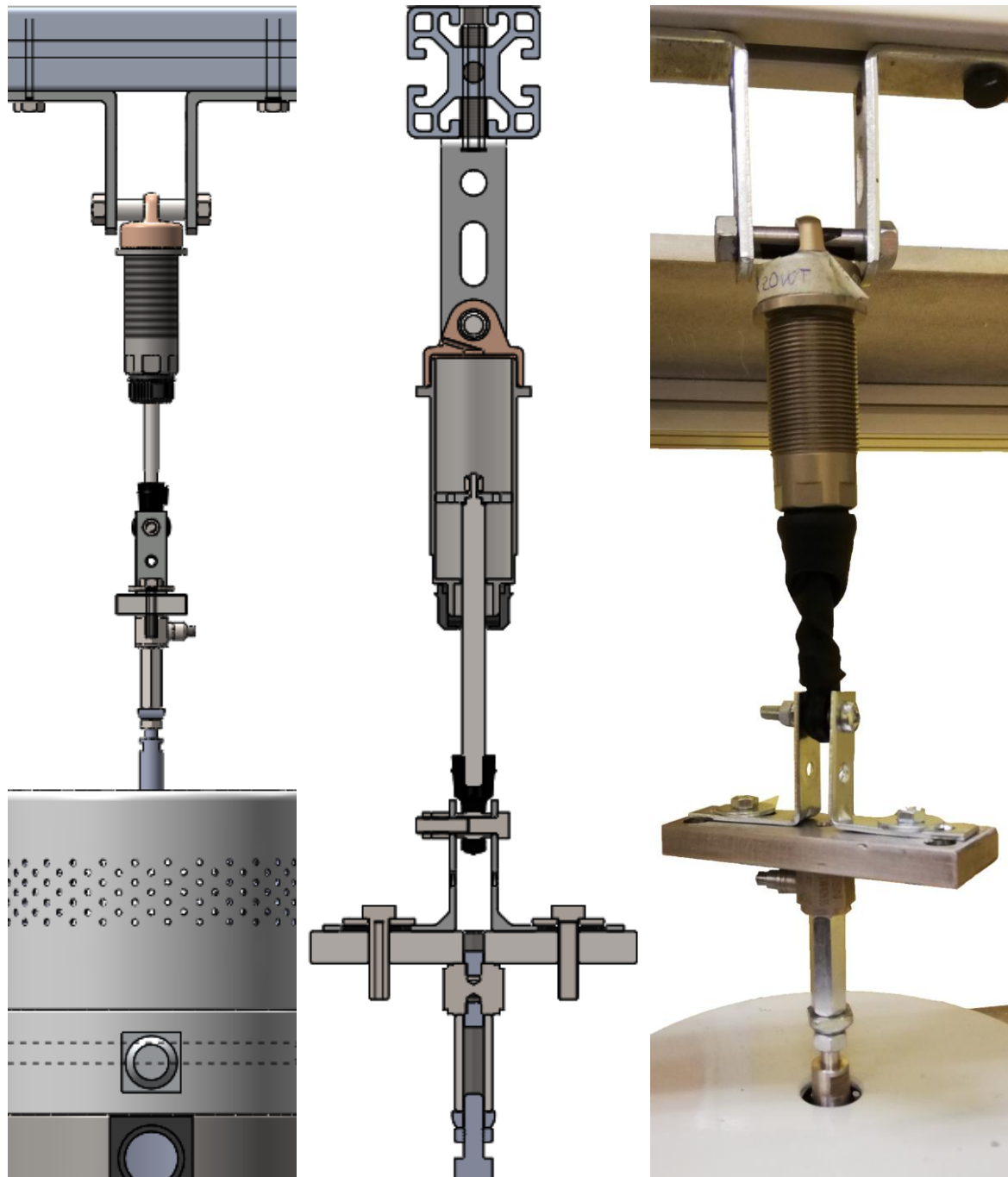


Figure 2.2.6.14 – Side view (left), section view (centre) and a real photo (right) of the entire damper clamping system.

2.2.7 Laser position

The last step is the laser positioning. As previously said (chapter 1.3) the laser meter will transmit a laser beam from a certain point and will read the reflection in a secondary point, pitched of a certain angle for trivial geometric reasons. So the main goal is to achieve a correct, solid, position for the laser that has to:

- Don't create interference between the various pieces.
- Have the correct medium distance from the measuring point.
- Don't have any objects or piece between the transmission point and the receiving one.
- Don't be subjected to vibrations (no 'flag' configurations).

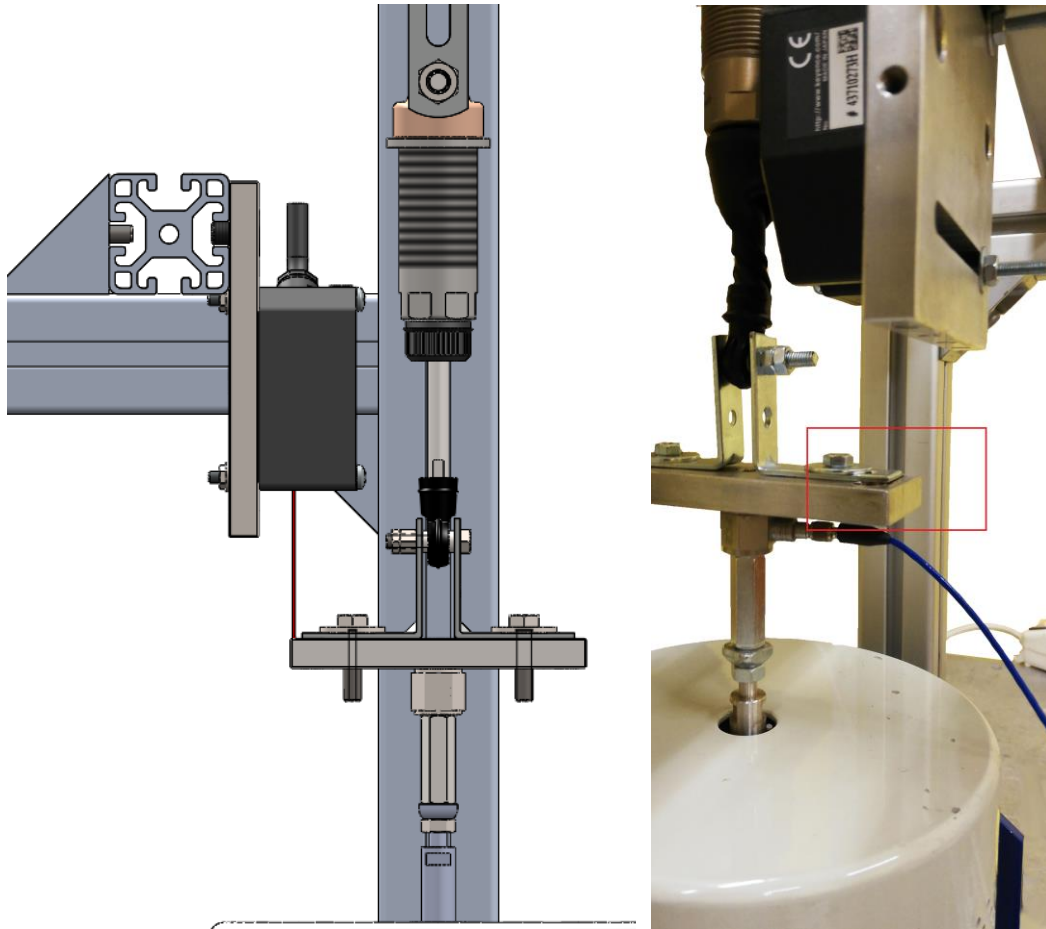


Figure 2.2.7.1 – Side view of the laser clamping system (left), a real photo (right). A zoom of the squared area is visible in Figure 2.2.7.3.

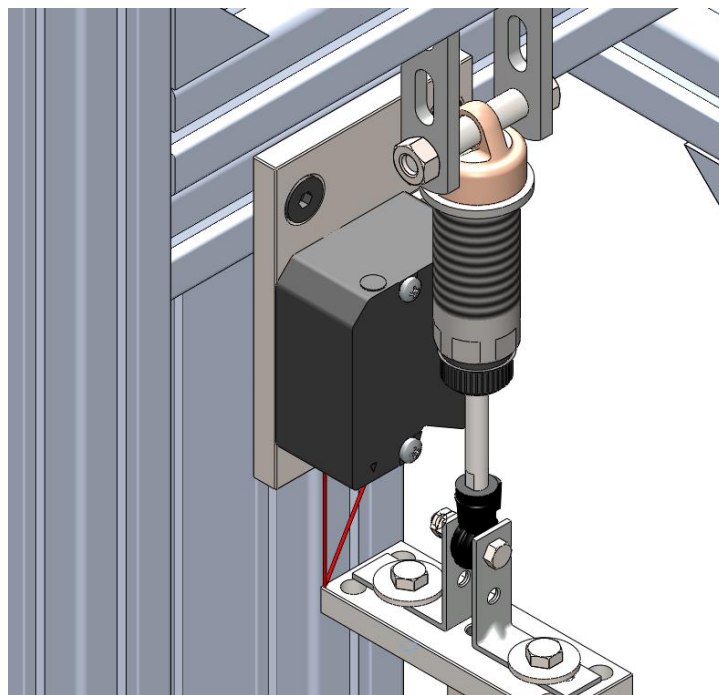


Figure 2.2.7.2 – Isometric view of the laser clamping system and reflection trajectory.

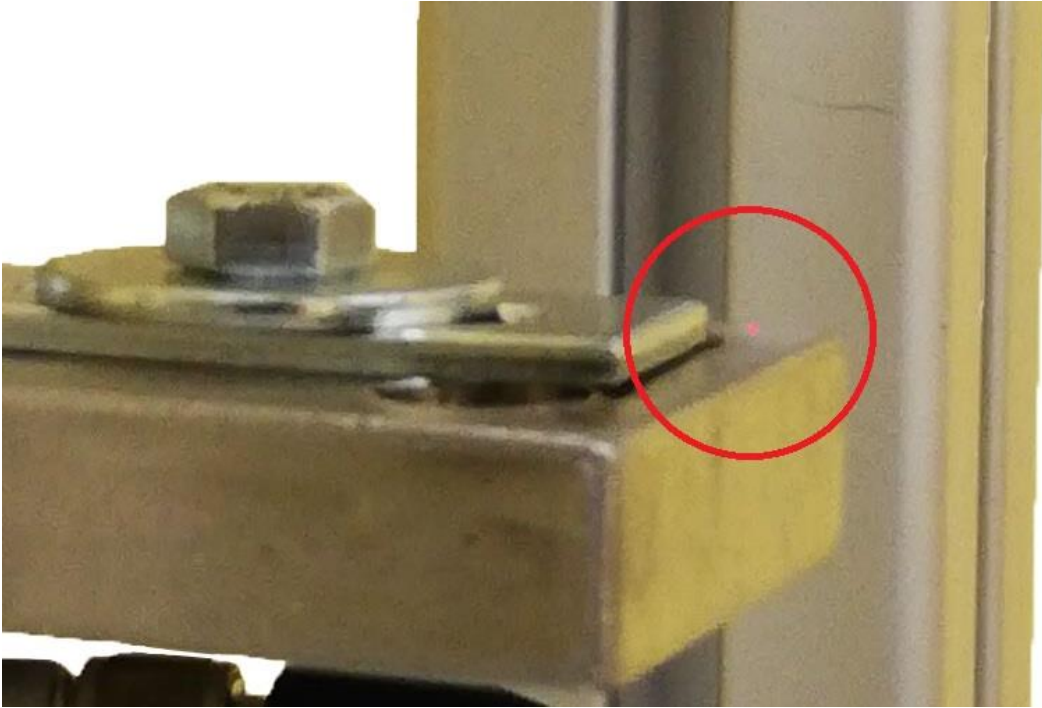


Figure 2.2.7.3 – In the circled area the point where the laser reflect is visible.

As it's possible to see in Figure 2.2.7.2 the laser beam reflects on the upper planar surface of the plate, that is the one moved by the shaker. The beam return to the laser meter without interfering with anything. The piece of frame on which is mounted is clamped to two upright by two angular elements, that makes the system very stiff. So all the points of the previous bulleted list is respected. This configuration is the result of a long series of attempts easily done only thanks to the use of CAD.

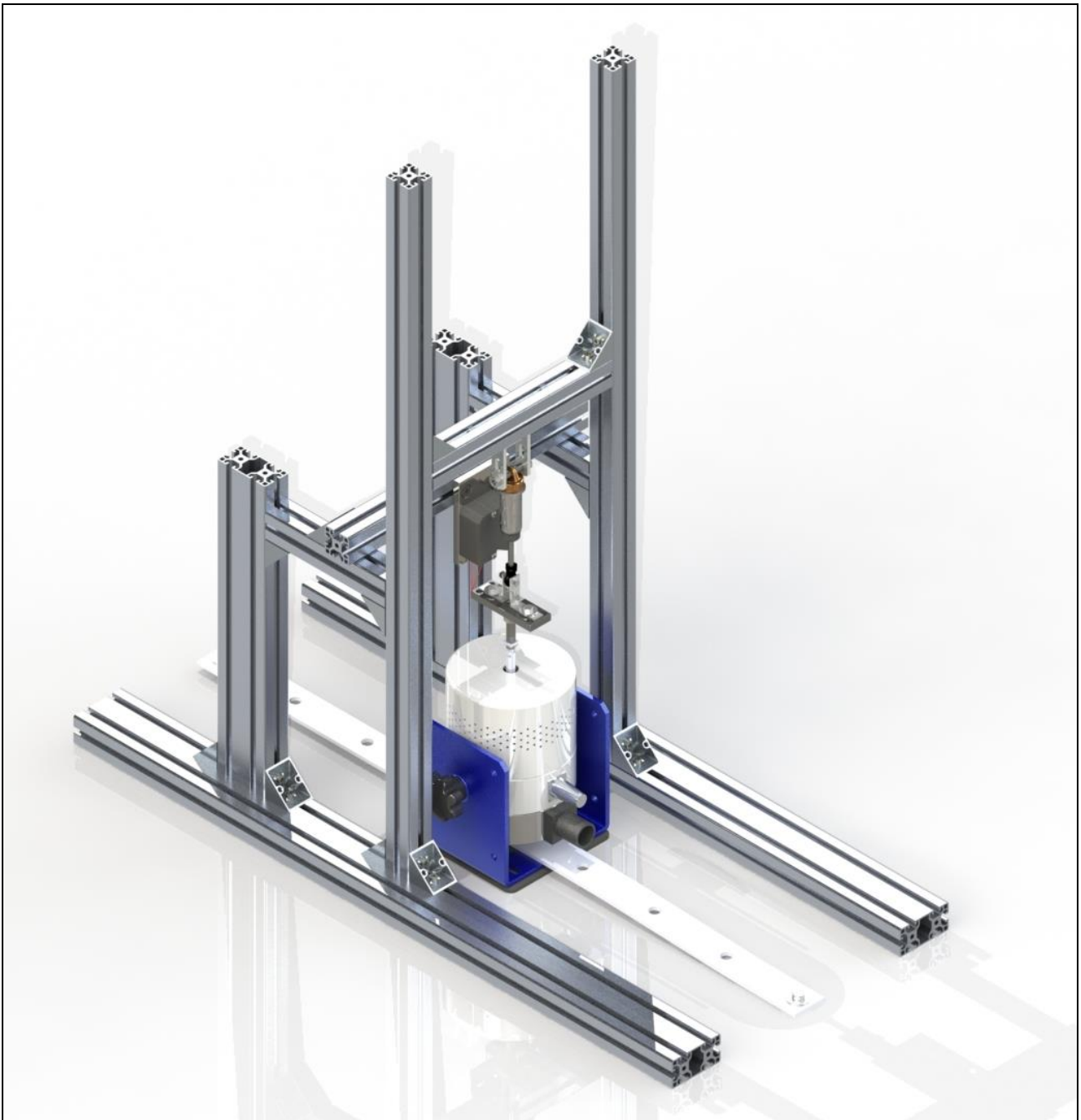


Figure 2.2.7.4 – Overall rendering of the damper experimental set.

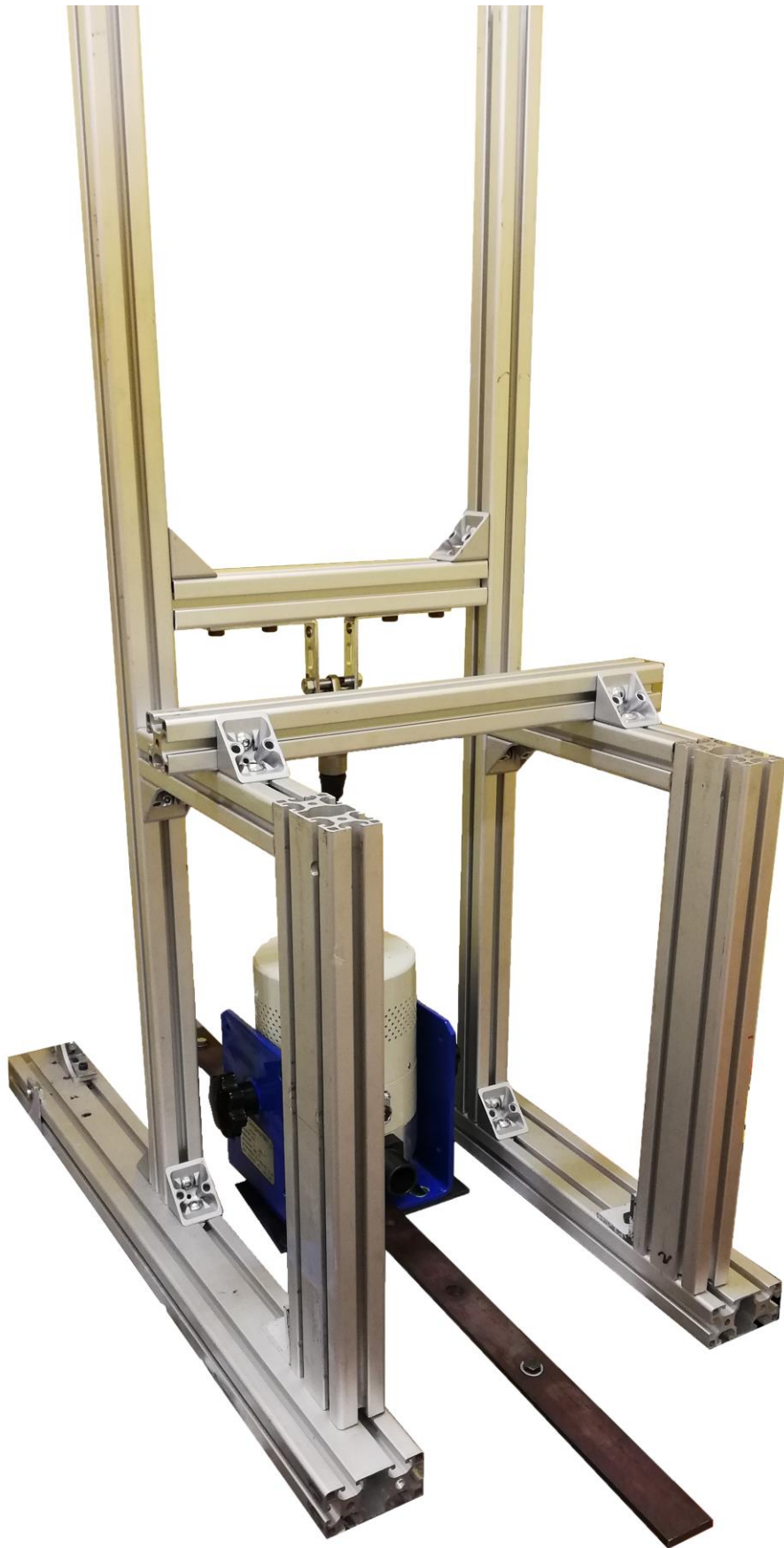


Figure 2.2.7.5 – Real photo of the experimental setup.



Figure 2.2.7.6 – Real photo of the test rig where also the laser meter is present and some cable connections.

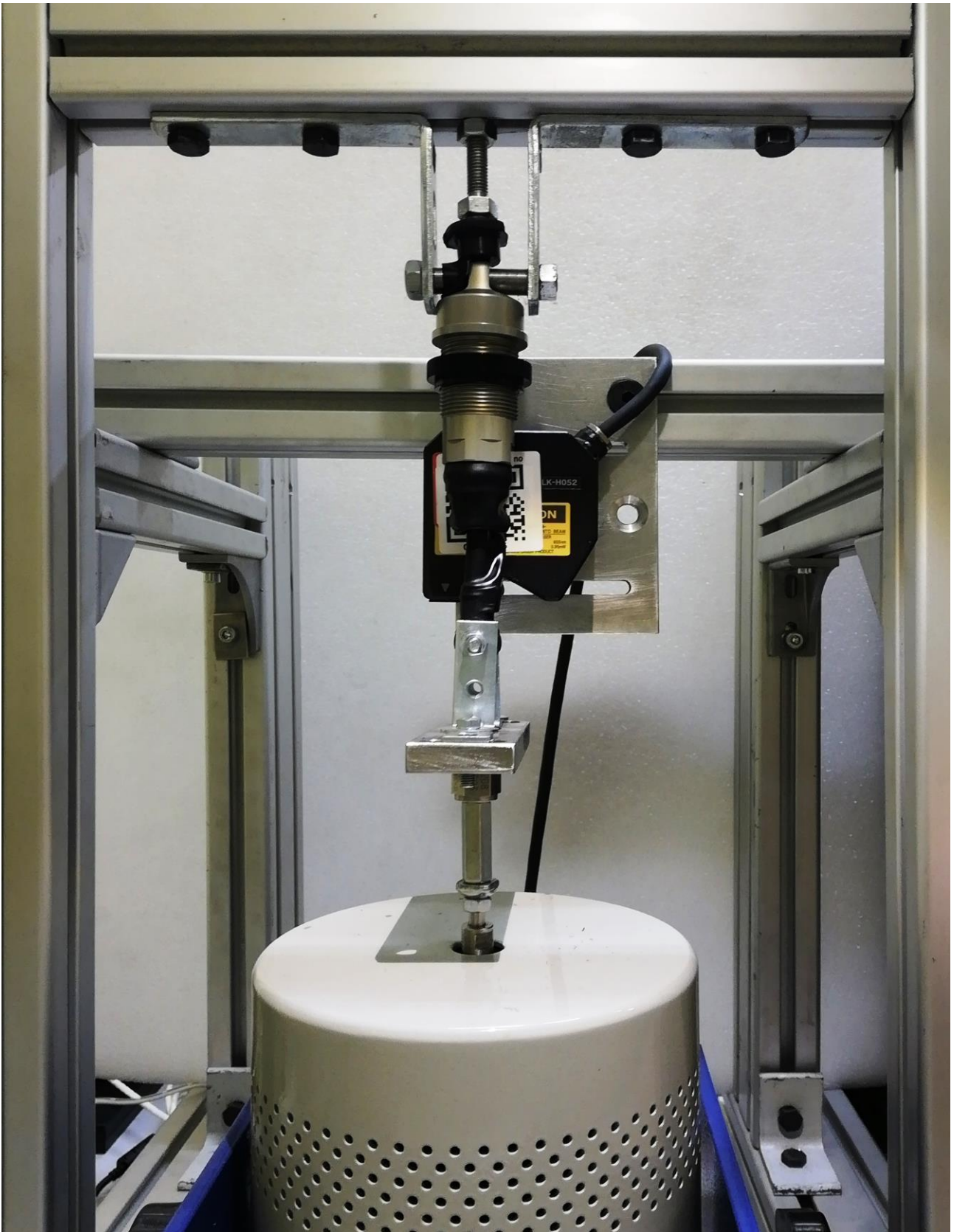


Figure 2.2.7.7 – Detailed photo of the test core, where shaker, damper, laser and load cell is present.

In the last steps a long M8 screw with plastic head was been added between the upper bar and the personalized shaft in order to minimize the residual gap and blocking definitively the damper cylinder along axial direction.



Figure 2.2.7.8 – The entire setup, on the left are also visible all the assembled dampers, on the right the data acquisition system (explained in chapter 4.1)

3. Simulation of data acquiring

In order to write the algorithm to deduce the required parameters from the experiments, and considering that until all the pieces and the car will be available and the experimental setup mounted there will could be no acquisition data, a program to simulate some experiments has to be write. For the same reason the data here used and the results here reported will have no physical sense and absolutely no correlations with our objects of study: here the only criteria to the choice is the possibility to observe the desired effect or result.

3.1 Single case

Considering the simplest dynamic equation that can describe a damper:

$$c \cdot \dot{x} = F(t) \quad (3.1.1)$$

Where:

- c [Ns/m] is the viscous coefficient;
- \dot{x} [m/s] is the velocity of the shaker's shaft;
- $F(t)$ [N] is the applied force;

It's possible to write the (3.1.1) just by considering that the inertial contribution of the damper is negligible (no ' $m \ddot{x}$ ' term) and also the stiffness one (no ' $k x$ '). For further information see chapter 4.2.4.

We should modify it by introducing some realistic noise for the various measured greatness, i.e. by considering, for example, the noise for the load cell:

$$c \cdot \dot{x} = F(t) + N(t) \quad (3.1.2)$$

Where $N(t)$ should be a random function, for example the Gaussian one.

So it's possible to try solve this equation by simply introducing some arbitrary value of c and obtaining by numerical procedure the solution for:

$$\dot{x} = \frac{F(t) + N(t)}{c} \quad (3.1.3)$$

Once obtained this solution tabled in time and with the shrewdness to have at the same time registered the force in his time history, we've complete our goals to have a $F_{tot}(t)$ to \dot{x} plot where:

$$F_{tot}(t) = F(t) + N(t) \quad (3.1.4)$$

With this solution is possible proceed to write the algorithm to obtain a value for ' c ', and then compare it with the arbitrary value inserted before to solve the (3.1.3) and evaluate how much good the algorithm is or how much bad the acquired data are. Obviously the data can be defined 'good' if show a certain dispersion, the already mentioned "cloud of points", while if, for example, they are perfectly aligned along a straight line it means that the data are too perfect and there will be no range to evaluate the algorithm. For the damping coefficient a certain difference from the linear value should be expected especially for the high velocity zones. From previous non reported

experiment has been results that the only introduction of a noise to the force function is not sufficient to obtain a well distributed solution that will appears too near to the ideal one. The solution was been to introduce another noise to the velocity in order to obtain a more realistic solution. So finally the solving equation will be:

$$\dot{x} = \frac{F(t) + N(t)}{c} + N_v(t) \quad (3.1.5)$$

where also the velocity noise $N_v(t)$ can be assumed as random Gaussian function. This noise will be proportional to the velocity itself, thanks to Simulink solver this will be easily possible.

So the schematic elementary solution that must be implement in Simulink would be:

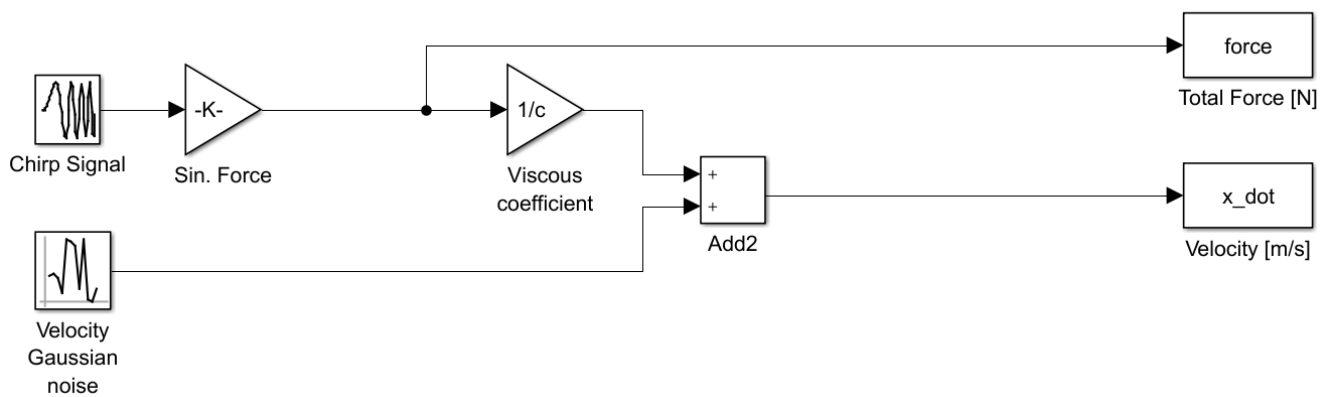


Figure 3.1.1 – Elementary Simulink scheme.

As is possible to see in Figure 3.1.1 the main force signal is generated as sinusoidal with the ‘chirp’ functional block. This block can generate a sinusoidal signal in a certain frequency range that is swept in a certain time. The exit signal from the ‘chirp’ function is in the range from 0 to 1, so it must be multiplied by a certain value: the maximum amplitude of the force. At the same time a ‘Gaussian Random Number’ functional block generate the noise for the velocity. Finally dividing the force signal by the arbitrary value of ‘c’ and by summing it with the value of random noise generated in a parallel line the velocity signal can be obtained and exported in the Matlab command window.

The complete scheme will be, instead:

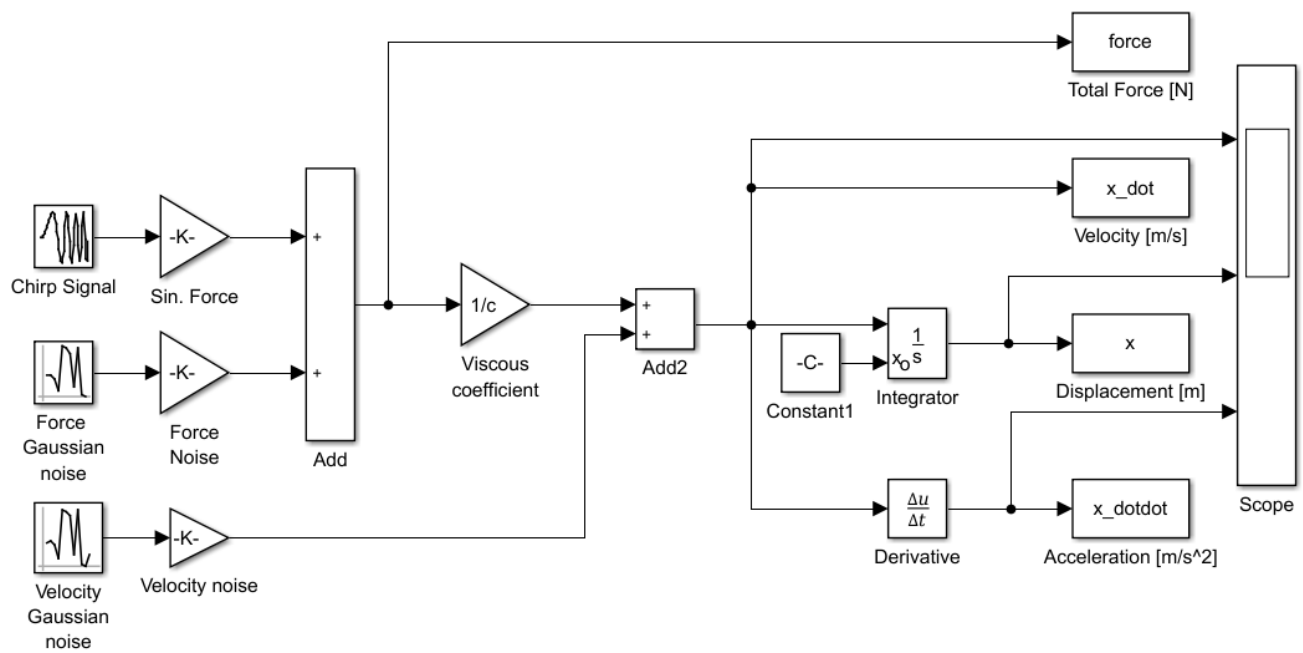


Figure 3.1.2 – Complete Simulink scheme.

In Figure 3.1.2 is possible to see that some other exports were introduced, in particular integrator and derivative functional blocks are been introduced in order to obtain also the displacement and the acceleration of the damper. Also a scope block is been introduced, to 'on line' monitor the data evolution, but a better visualization will be obtained later in the Matlab script.

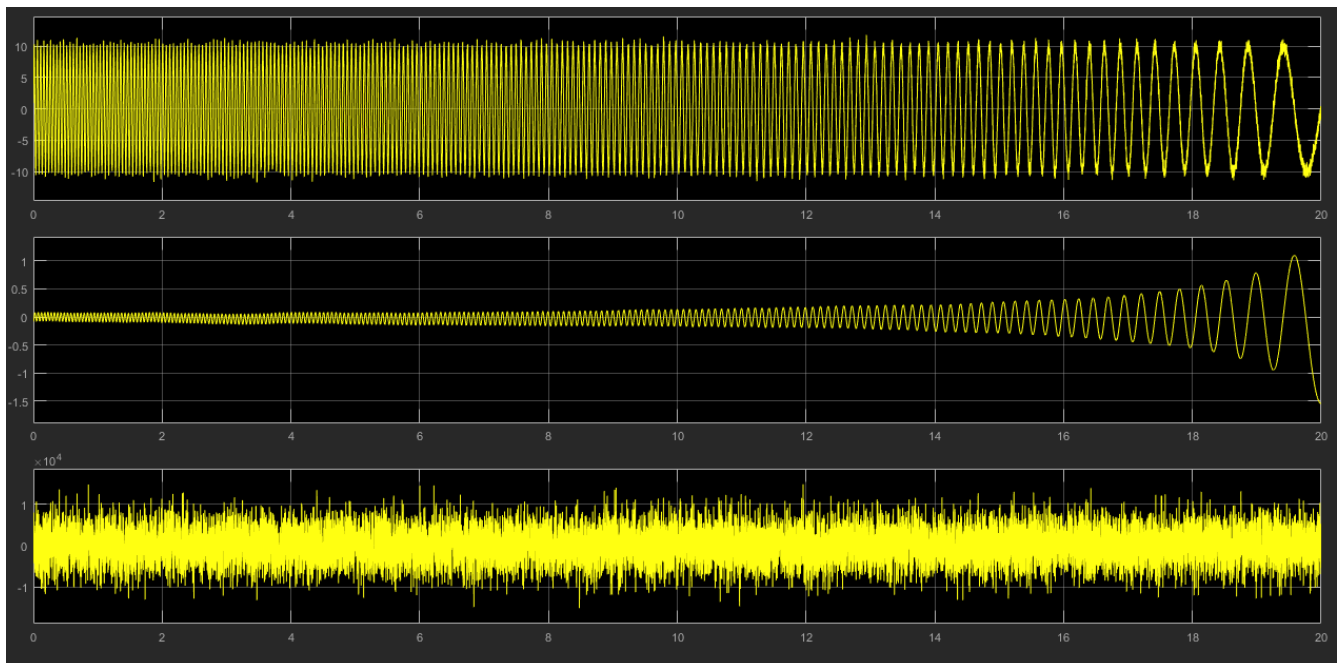


Figure 3.1.3 – Scope monitoring.

In order to obtain a correct answer in terms of displacement also the correct initial condition for the integrator block has to be calculated. If this condition will not be calculated and simply left at the default value of $x_0 = 0$ the answer will result centred at a certain offset value, because the system will respond, in the initial times, as if it is step-excited. In order to avoid other possible issue

another trick could be to set the initial frequency of the chirp block as the highest one, and the final as the smallest, especially when this lowest value is near to 0: a quasi-zero frequency force is pretty similar to a static one.

It is known that the initial velocity condition is of the form:

$$\dot{x}_0 = \omega_0 x_0 \quad (3.1.6)$$

Where:

- \dot{x}_0 [m/s] is the initial velocity;
- ω_0 [rad/s] is the initial frequency;
- x_0 [m] is the searched initial position;

At the initial instant the force is maximum, while the damping factor can be supposed to be quite similar to the arbitrary value, so is trivial:

$$\dot{x}_0 = \frac{F_{\max}}{c} \quad (3.1.7)$$

By substituting the (3.1.7) in the (3.1.6) and by writing the ω_0 [rad/s] in function of frequency [Hz] (adopted to be consistent with Simulink standard) is possible to obtain:

$$\frac{F_{\max}}{c} = f_0 2\pi x_0 \quad (3.1.8)$$

And finally:

$$x_0 = \frac{F_{\max}}{2\pi f_0 c} \quad (3.1.9)$$

The Simulink model is been totally automatized and implemented with a Matlab script where all the data can be simply modified and some useful graphs and exports can be implemented. The scripts are shown at the end of the thesis.

As will be possible to see the script also comprehend the linear regression algorithm through a simple line where the 'regress' function is implemented.

Executing this script the result will be something like:

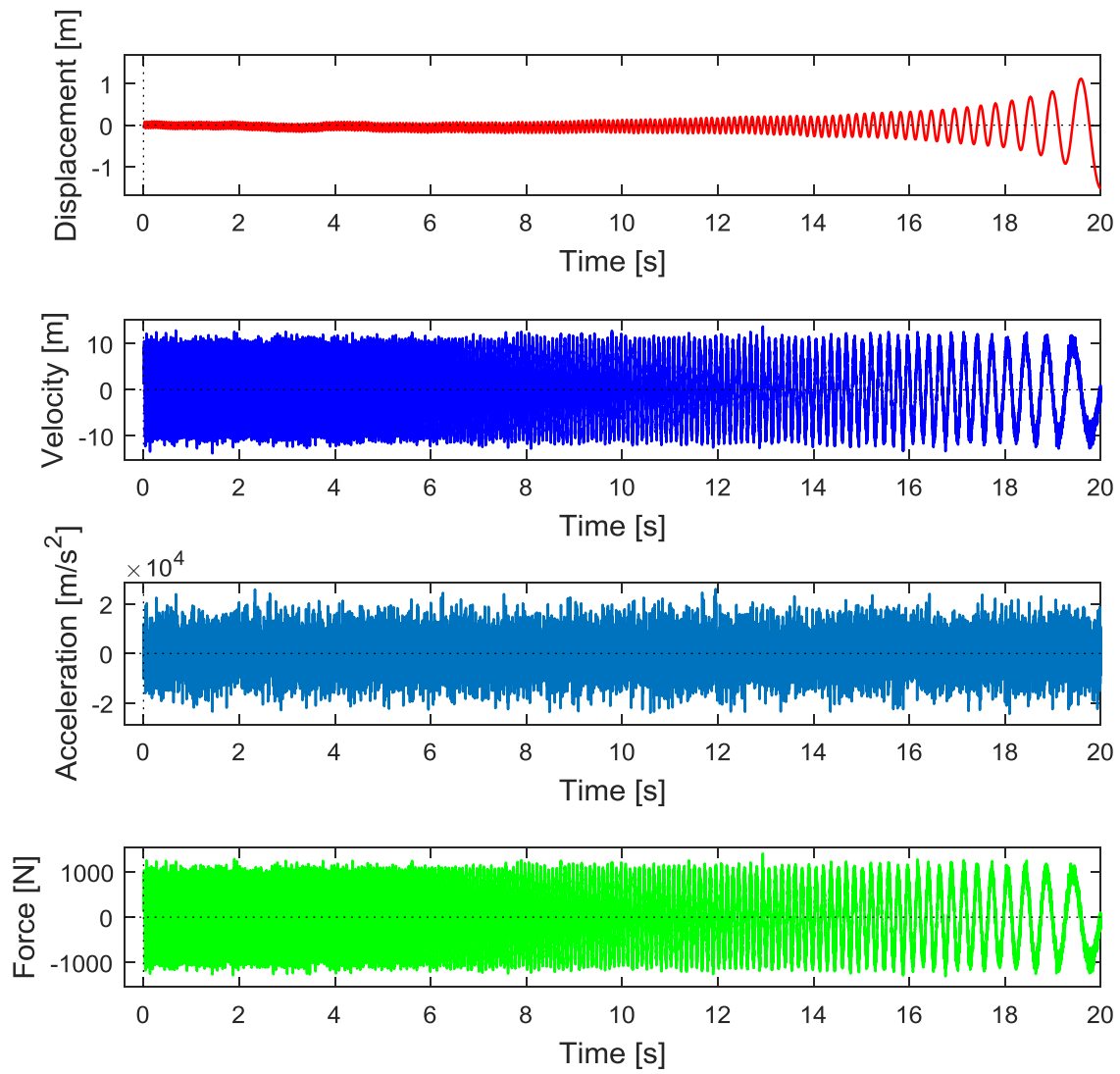


Figure 3.1.4 – Displacement, Velocity, Acceleration and Force plots.

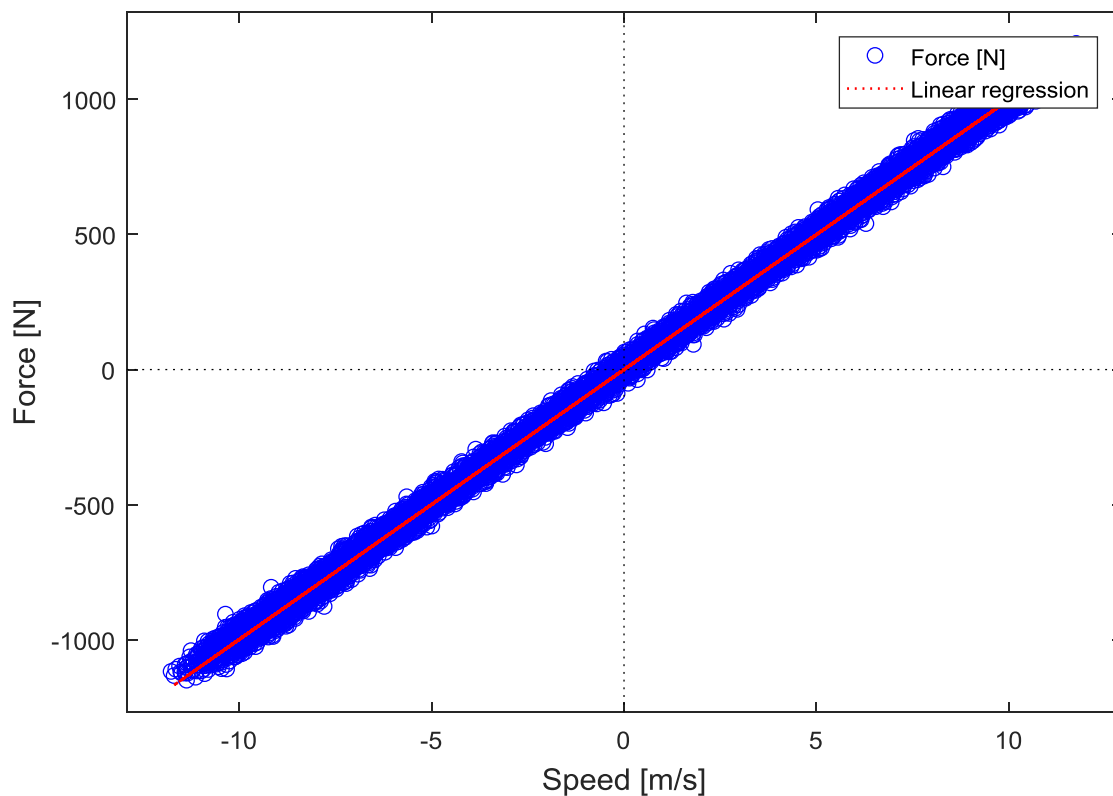


Figure 3.1.5 – The searched $F_{tot}(t)$ to \dot{x} plot, with already include the linear regression.

While the export in Matlab workspace will be:

```

Command Window

Signal simulation and acquired data analysis for damper experiment

Simulation time:          20 s
Sampling time:           0.001 s
Declared viscosity coefficient: 100 Ns/m
Viscosity coefficient:    99.878 Ns/m
Error:                   0.12198 %
  
```

Figure 3.1.6 – Matlab command window outputs.

So it is possible to said that the script return a well done simulation, the distribution of the points in the $F_{tot}(t)$ to \dot{x} plot is quite good, while the linear regression return a good approximation of the viscosity coefficient with an error that will be ever under few percentage points. The force-time plot show a realistic noise disturb.

3.2 State space and linear regression

In this refinement also the effect of the medium position of the damper will be considered. The simplest assumption that can be done is that there is a linear dependence by the position. In this case, to make a comparison, the (3.1.1) become:

$$(c_0 + c_1 x) \dot{x} = F(t) \quad (3.2.1)$$

Where:

- c_0 [Ns/m] is the constant viscous coefficient;
- c_1 [Ns/m²] is the multiplicative factor to take into account the state space effect;
- \dot{x} [m/s] is the velocity of the shaker's shaft;
- $F(t)$ [N] is the applied force;

Also in this case the introduction of the noises for the force and the velocity make the solution equation:

$$\dot{x} = \frac{F(t) + N(t)}{c_0 + c_1 x} + N_v(t) \quad (3.2.2)$$

So now the scheme shown in Figure 3.1.2 become:

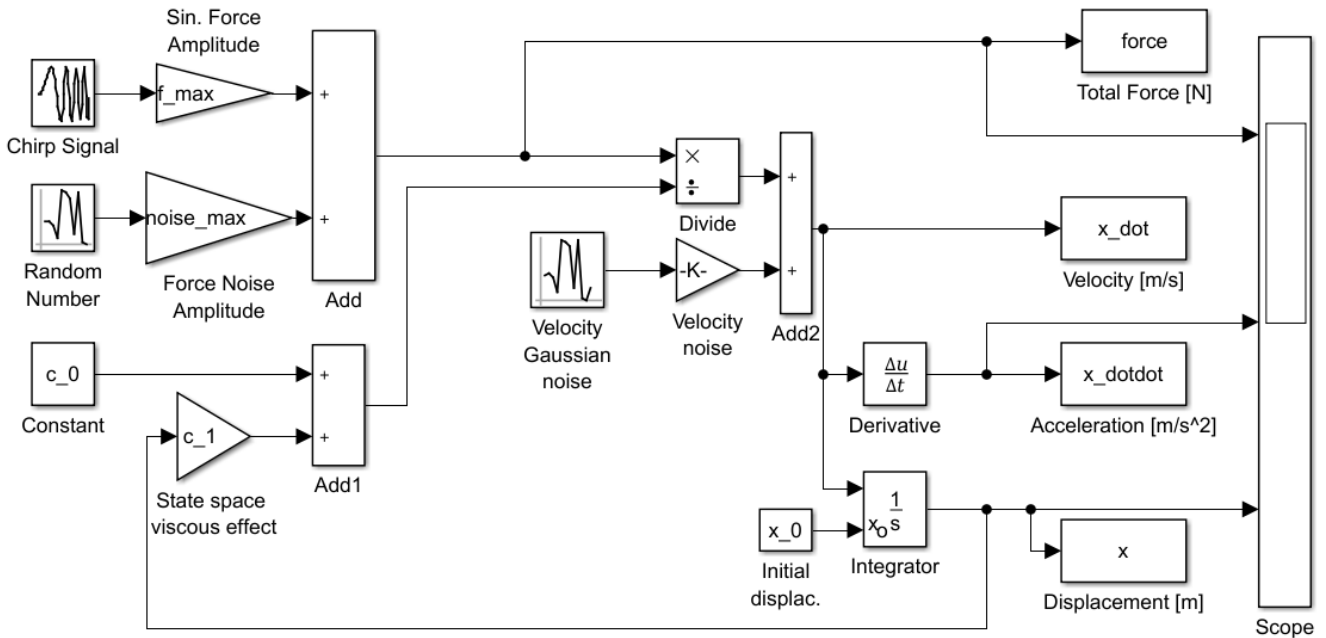


Figure 3.2.1 – Simulink scheme with state space effect.

As it is possible to see in Figure 3.2.1 another feedback signal is appeared: it bring the displacement (' x ') information that will be multiplied for the new gain factor c_1 to take into account the effect of the position on the viscosity.

At this point it will appear useless to make an evaluation of the whole cloud of point with the respect of an unique value of c . It will be more useful to consider the vector of viscous coefficients and to evaluate it properly. The (3.2.1) can be rewrite in the vector form:

$$\begin{bmatrix} \{1\} & \{x\} \end{bmatrix} \begin{Bmatrix} c_0 \\ c_1 \end{Bmatrix} \{\dot{x}\} = \{F_{tot}(t)\} \quad (3.2.3.a)$$

And by adopting compact notation:

$$\begin{bmatrix} \mathbf{1} & \mathbf{x} \end{bmatrix} \mathbf{c} \dot{\mathbf{x}} = \mathbf{F}_{tot} \quad (3.2.3.b)$$

So just by invert it^[8]:

$$\mathbf{c} = \begin{bmatrix} \mathbf{1} & \mathbf{x} \end{bmatrix}^{-1} \frac{\mathbf{F}_{tot}}{\dot{\mathbf{x}}} \quad (3.2.4)$$

Notice that $\frac{\mathbf{F}_{tot}}{\dot{\mathbf{x}}}$ will be a division point by point and that the inversion is in realities a pseudo-inverse.

Before continuing a verification of problem dimensions will be done to be sure of the congruence of what has been done. By considering the previous equation and by putting T equal to the number of time instants considered:

$$\mathbf{c} = \begin{bmatrix} \mathbf{1} & \mathbf{x} \end{bmatrix}^{-1} \frac{\mathbf{F}_{tot}}{\dot{\mathbf{x}}} \quad \begin{matrix} 2 \times 1 & 2 \times T & T \times 1 \\ & & \end{matrix}$$

So it become:

$$\mathbf{c} = \begin{bmatrix} \mathbf{1} & \mathbf{x} \end{bmatrix}^{-1} \frac{\mathbf{F}_{tot}}{\dot{\mathbf{x}}} \quad \begin{matrix} 2 \times 1 & 2 \times 1 \\ & \end{matrix}$$

And is therefore verified:

$$2 \times 1 = 2 \times 1$$

Another useful ideas could be to search the function that make the best approximation. The simplest idea is to search for a linear polynomial regression that will return the coefficients to write the force as:

$$F = B_0 + B_1 \cdot x + B_2 \cdot \dot{x} + B_3 \cdot x \cdot \dot{x} \quad (3.2.5)$$

The (3.1.2.5) coefficients (B_0 , B_1 , B_2 and B_3) can be simply found with the Matlab function `regress`.

Some others modification should be necessary to the Matlab script in order to obtain more useful graphs and exports. As usual the scripts are attached at the end of the thesis. In the script it will be called^[a] $\mathbf{A} = \begin{bmatrix} \mathbf{1} & \mathbf{x} \end{bmatrix}$.

The new plots will appear as:

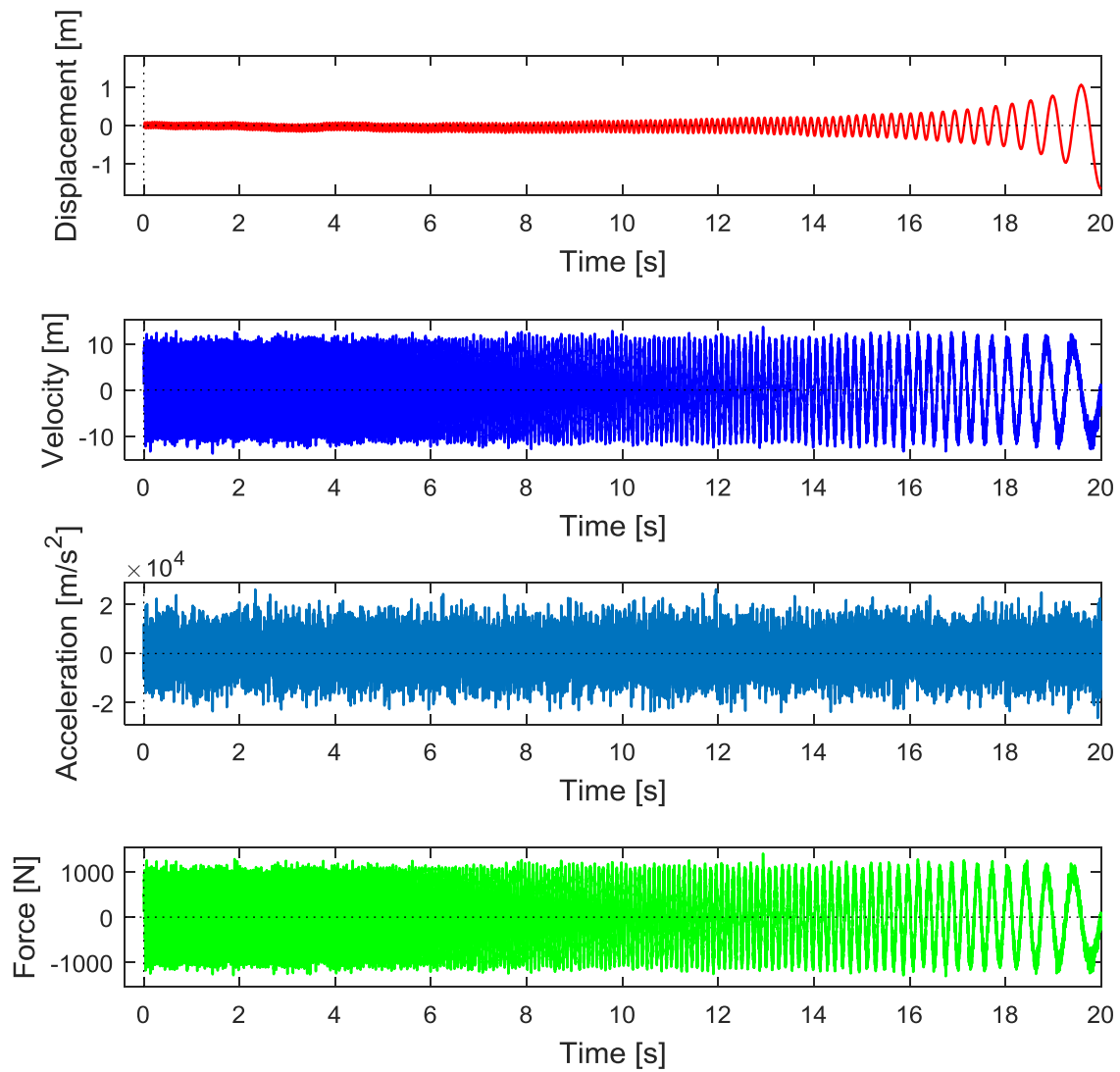


Figure 3.2.2 – Displacement, Velocity, Acceleration and Force plots.

While a simple two dimensional plot will not be any more sufficient to describe the evolution of the viscosity, a 3D one will be necessary:

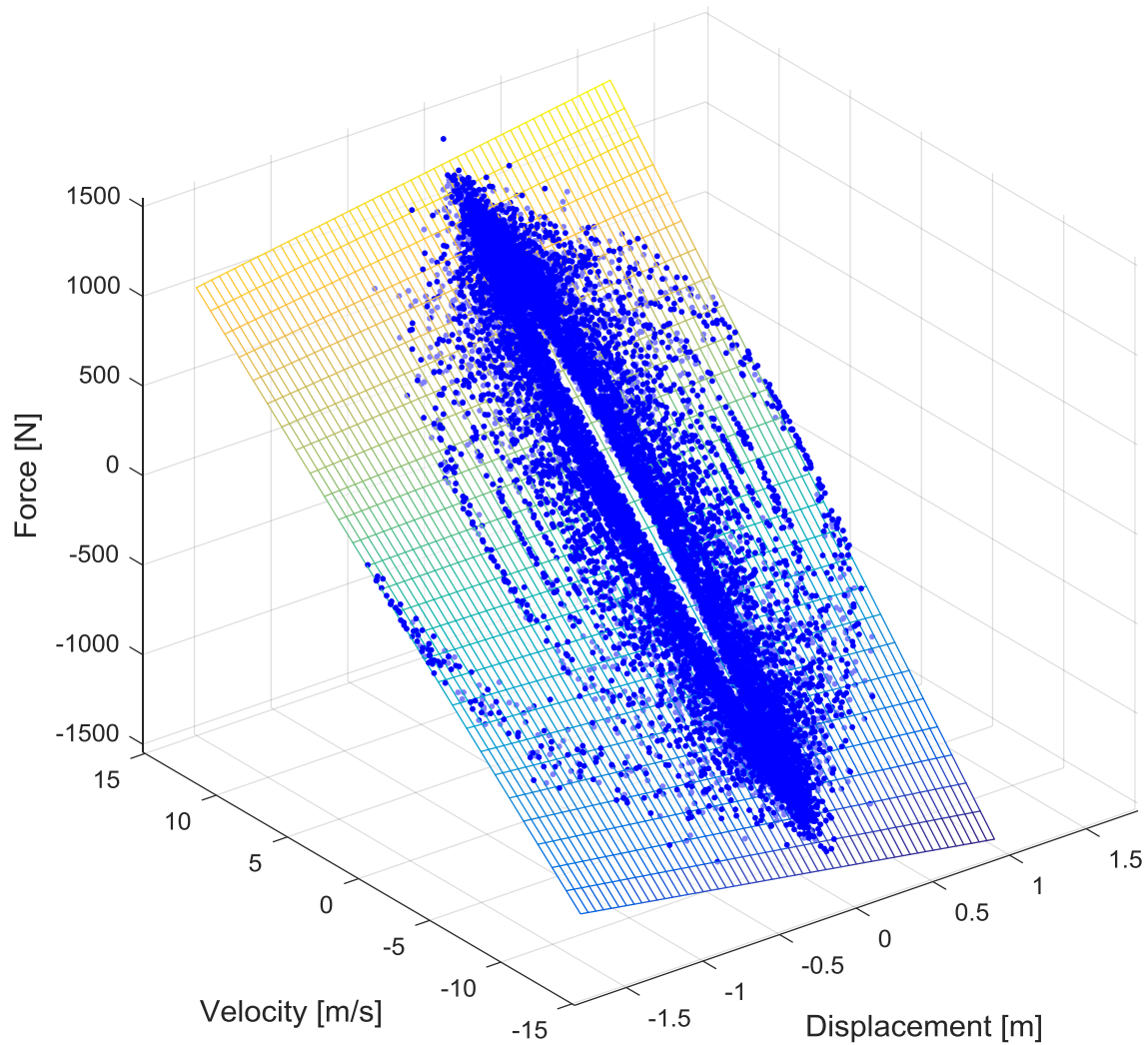


Figure 3.2.3 – 3D plot of the cloud of points and the surface coming out from linear regression.

As is possible to see in Figure 3.1.2.3 the data become more complex. The surface slice the cloud of points, is possible to appreciate this fact by the changing of colour of the points, the lightest blue dots signal are the points that are under the surface.

By watching the 3D plot from a side view normal to the Velocity-Force plane is possible to appreciate the changing of the slope of the surface:

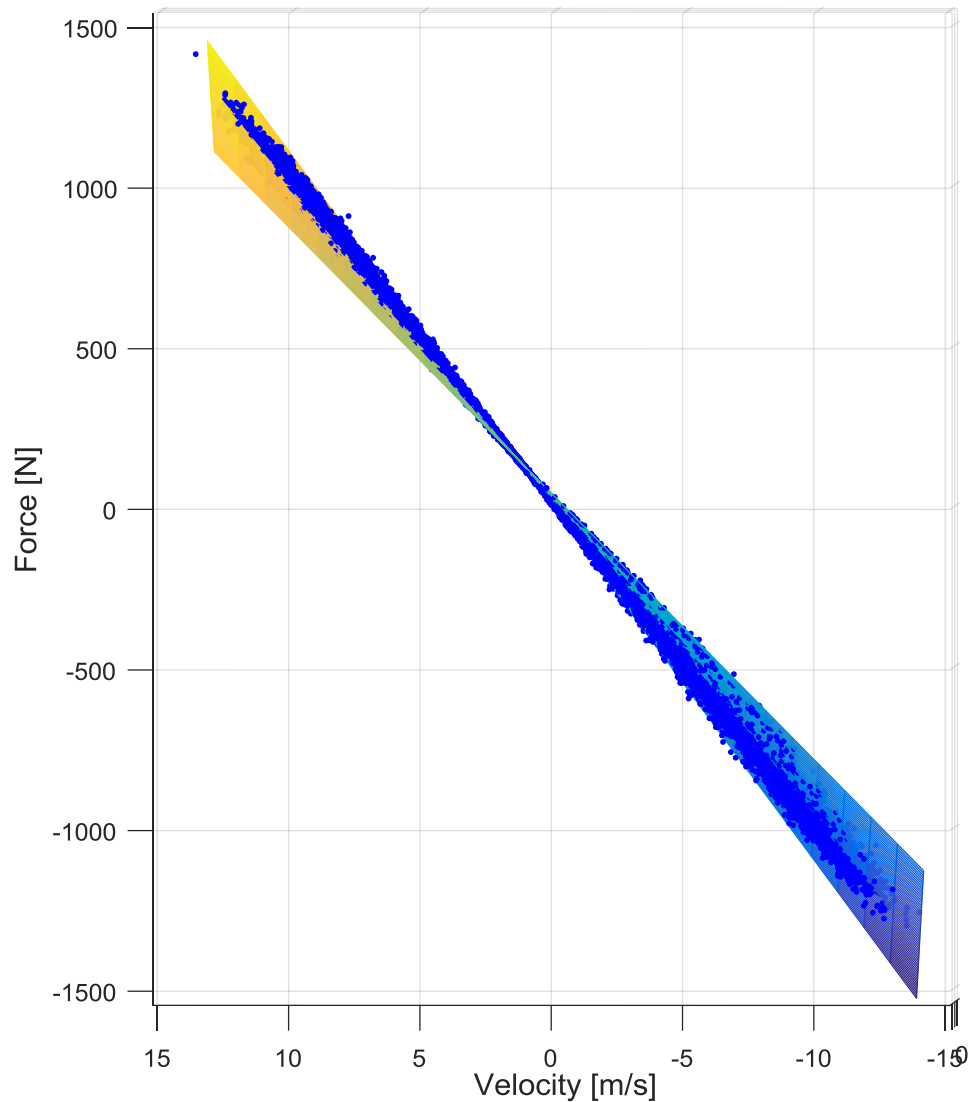


Figure 3.2.4 – Side view of the 3D plot

From the point of view shown in Figure 3.2.4 is more clear what's happening to the viscous coefficient. The slope of the surface with respect to the planes parallel to the $F_{tot}(t)$ - \dot{x} one, which represent the viscous coefficient, change at the various displacement considered. The fact that for positive displacement the viscous coefficient look increasing and for negative decreasing demonstrate a certain consistence with the positive multiplicative factor chosen. When the realistic data will be available a trial and error research for the correct multiplicative factor has to be done.

```
Command Window

Signal simulation and acquired data analysis for damper experiment
with medium displacement effect on viscous coefficient

Simulation time:      20 s
Sampling time:       0.001 s
Force amplitude:     1000 N
Force noise amplitude: 50 N

c_0 REGRESSION:
Declared viscosity coefficient: 100 Ns/m
Regression viscosity coefficient: 100.1211 Ns/m
Error on c_0:          0.12112 %

c_1 REGRESSION:
Declared state space viscous coefficient: 10 Ns/m^2
Regression state space viscous coefficient: 8.9714 Ns/m^2
Error on c_1:          10.2858 %

Polynomial linear regression coefficient: B0 = 0.0061924
                                           B1 = 0.11923
                                           B2 = 99.9935
                                           B3 = 9.9507
```

Figure 3.2.5 –Matlab command window outputs.

As shown in Figure 3.2.5 there is a larger number of useful export in this second case. With the chosen number of points per second a very good regression is resulted. In the last lines the regression coefficients are reported.

3.3 State space and polynomial regression

The natural step forward in writing the regression script is to hypothesize what would happen if the coefficient were not simply linearly dependent on the displacement, but could be represented by a polynomial function of generic degree n .

In this case the previous (3.1.1) and (3.2.1) will become:

$$(c_0 + c_1 \cdot x + c_1 \cdot x^2 + \dots + c_n \cdot x^n) \cdot \dot{x} = F(t) \quad (3.3.1)$$

And will be possible to search the solution in Simulink as:

$$\dot{x} = \frac{F(t) + N(t)}{c_0 + c_1 \cdot x + c_1 \cdot x^2 + \dots + c_n \cdot x^n} + N_v(t) \quad (3.3.2)$$

Where $N(t)$ and $N_v(t)$ are respectively the noise for the force signal and the noise for the velocity signal. From the Simulink scheme point of view no big differences will occur with respect to the one showed in Figure 3.2.1, the only one is the substitution of the gain factor for the displacement factor (x) with a polynomial functional block. This type of functional block will multiply the signal for the coefficients given through a vector in which the first member will be the coefficient of the highest exponent. For this reason the already declared \mathbf{c} vector has to be mirrored. To notice also that the grade of the problem, n , will not have to be mandatory also the grade of the regression and, nay, this discordance could be used to evaluate how much good the chosen grade of digression is. In this simulation will be obvious that the best approximation can only be obtained when the two chosen grade, the one of polynomial for the cloud of points generation and the one for the regression, will be the same: but there will be no sure data about the nature of the viscous coefficient variation when we will face with the real data.

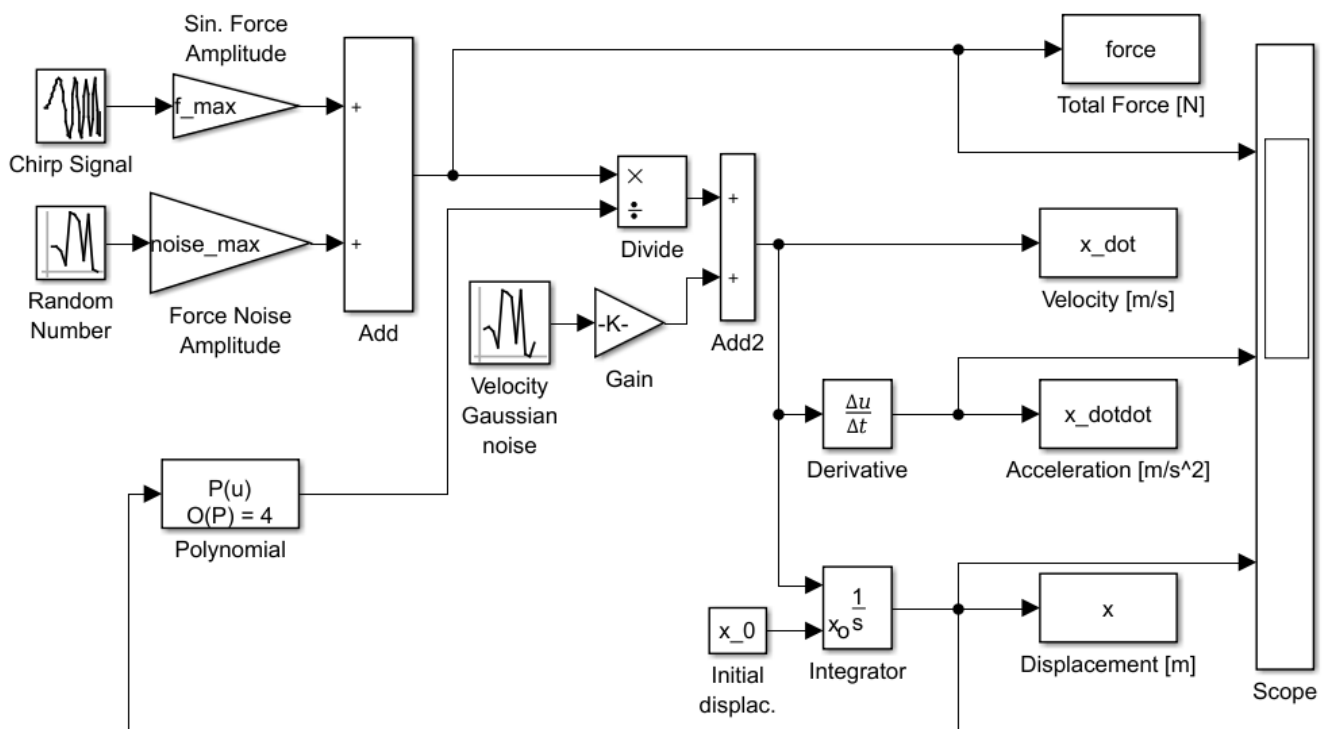


Figure 3.3.1 – Simulink scheme with state space effect and generic n-grade polinomial regression.

So once the data is been generated a regression procedure can be now implemented. By expand the (3.3.1) at the whole problem it become the vector equation:

$$\begin{bmatrix} \{1\} & \{x\} & \{x\}^2 & \dots & \{x\}^{n_r} \end{bmatrix} \begin{bmatrix} c_0 \\ c_1 \\ c_2 \\ \vdots \\ c_{n_r} \end{bmatrix} \{ \dot{x} \} = \{ F_{tot}(t) \} \quad (3.3.3.a)$$

To notice that, as said before, in general: $n_r \neq n$ with $n_r =$ grade of regression. And in compact form:

$$\begin{bmatrix} 1 & x & x^2 & \dots & x^n \end{bmatrix} \mathbf{c} \dot{\mathbf{x}} = \mathbf{F}_{tot} \quad (3.3.3.b)$$

By calling: $\mathbf{A} = \begin{bmatrix} 1 & x & x^2 & \dots & x^n \end{bmatrix}$ the resulting Vandermonde^[a] matrix it is possible to search the solution in Simulink as:

$$\mathbf{c}_r = [\mathbf{A}]^{-1} \frac{\mathbf{F}_{tot}}{\dot{\mathbf{x}}_{tot}} \quad (3.3.4)$$

Where \mathbf{F}_{tot} and $\dot{\mathbf{x}}_{tot}$ are the data acquired in Simulink which can be supposed to be similar to the data that will be acquired experimentally. The solution \mathbf{c}_r will be a vector of size $(n_r \times 1)$ that could be compare with the original \mathbf{c} coefficient-by-coefficient. Here is known that \mathbf{c} represent the correct solution, so it is easy to evaluate how much good the coefficients obtained by regression are. In order to get some other numbers also some evaluations of the error will be done. A first one will compare the two surfaces obtainable by the two series of coefficients, the first with the chosen coefficients of the vector \mathbf{c} (that could be considered as the ideal solution), and the second \mathbf{c}_r , the regression result. The surfaces will be compared in the points of the mesh to obtain a rapid result. The second comparison will be more accurate and will consider the difference between every point and the surface obtained by the regression coefficients. This second step will be more similar to what will be done in the real case, where the only available information is the cloud of points and is in the experience of the engineer the evaluation the correct grade of approximation to be chose.

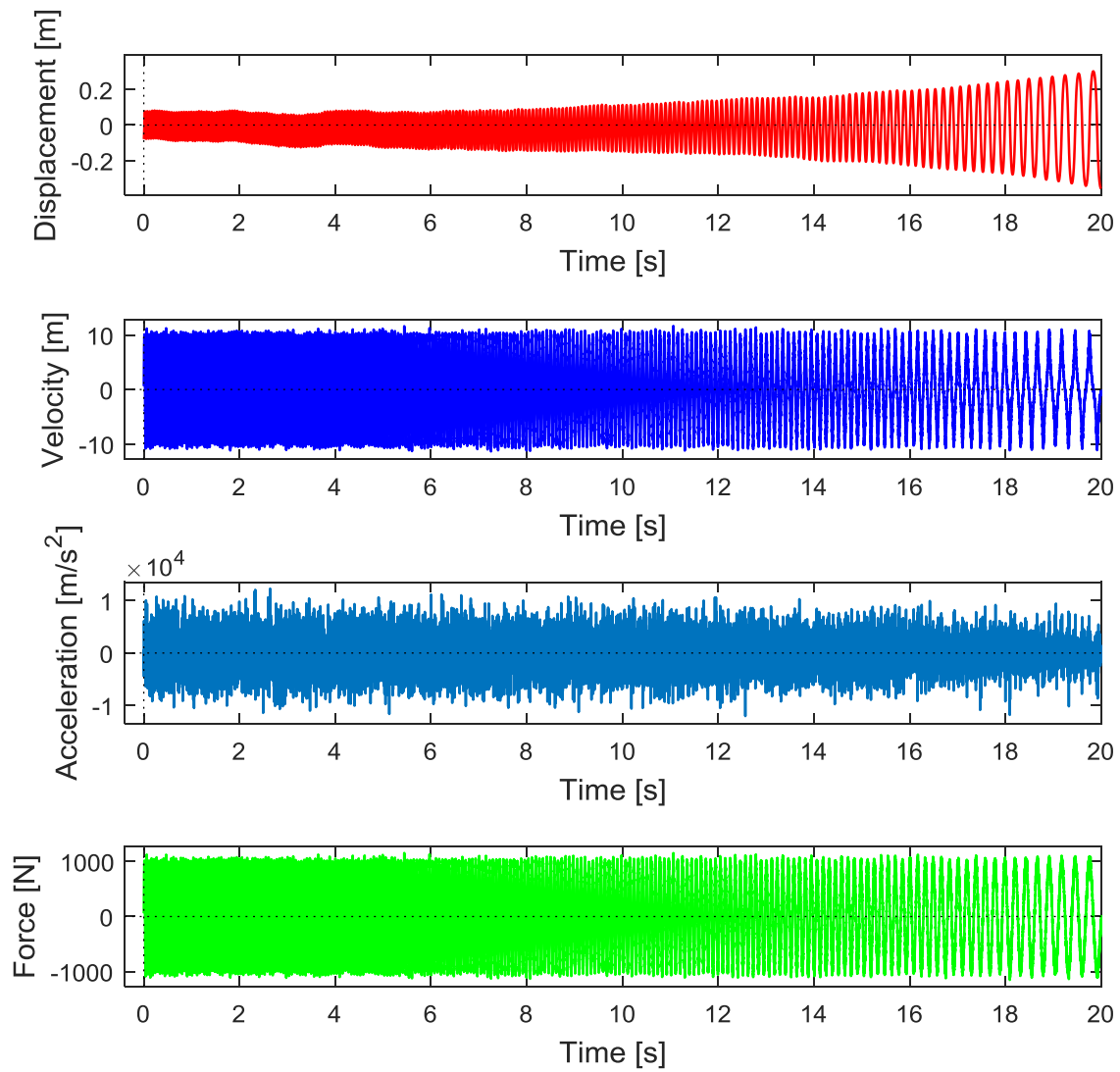


Figure 3.3.2 – Displacement, Velocity, Acceleration and Force plots.

In order to appreciate the values evolution when the regression grade change a comparison between four cases will follow. The grade of the exact solution will be always the same (4th) while the regression grade will be chosen as linear (1st), quadratic (2nd), cubic (3rd) and fourth grade (4th).

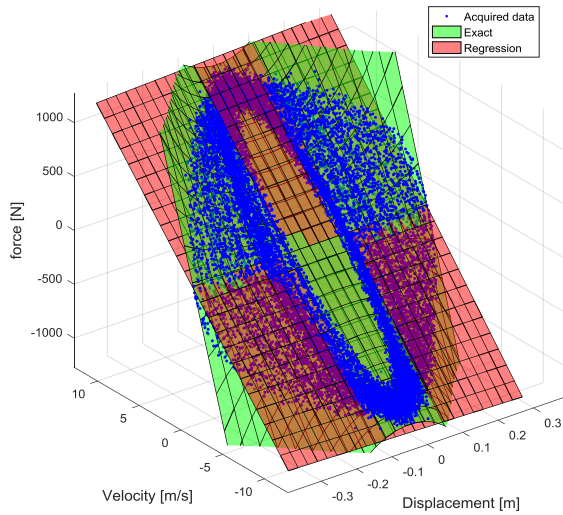


Figure 3.3.3 – Linear.

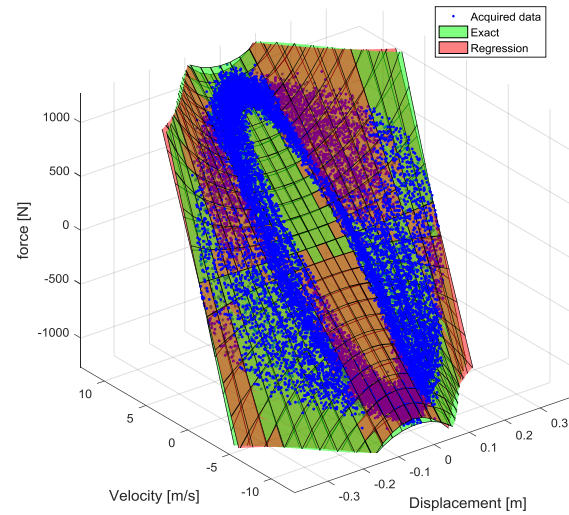


Figure 3.3.4 – Quadratic.

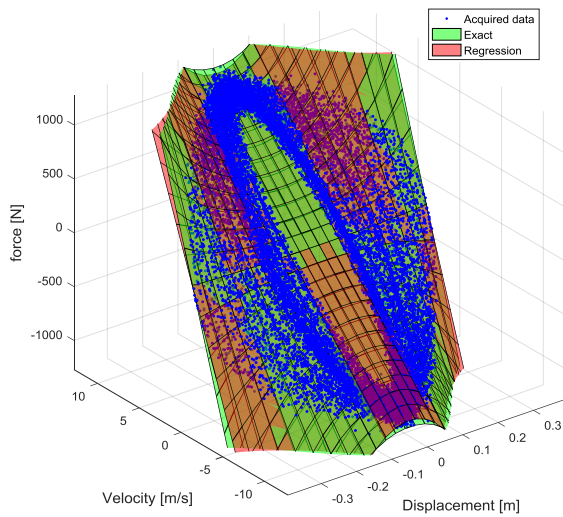


Figure 3.3.5 – Cubic.

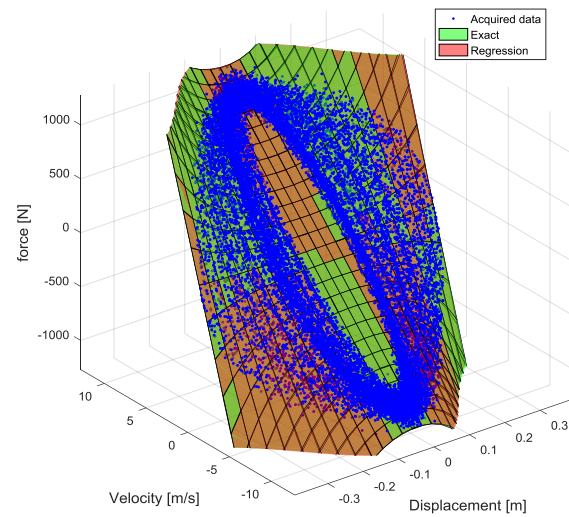


Figure 3.3.6 – Fourth grade.

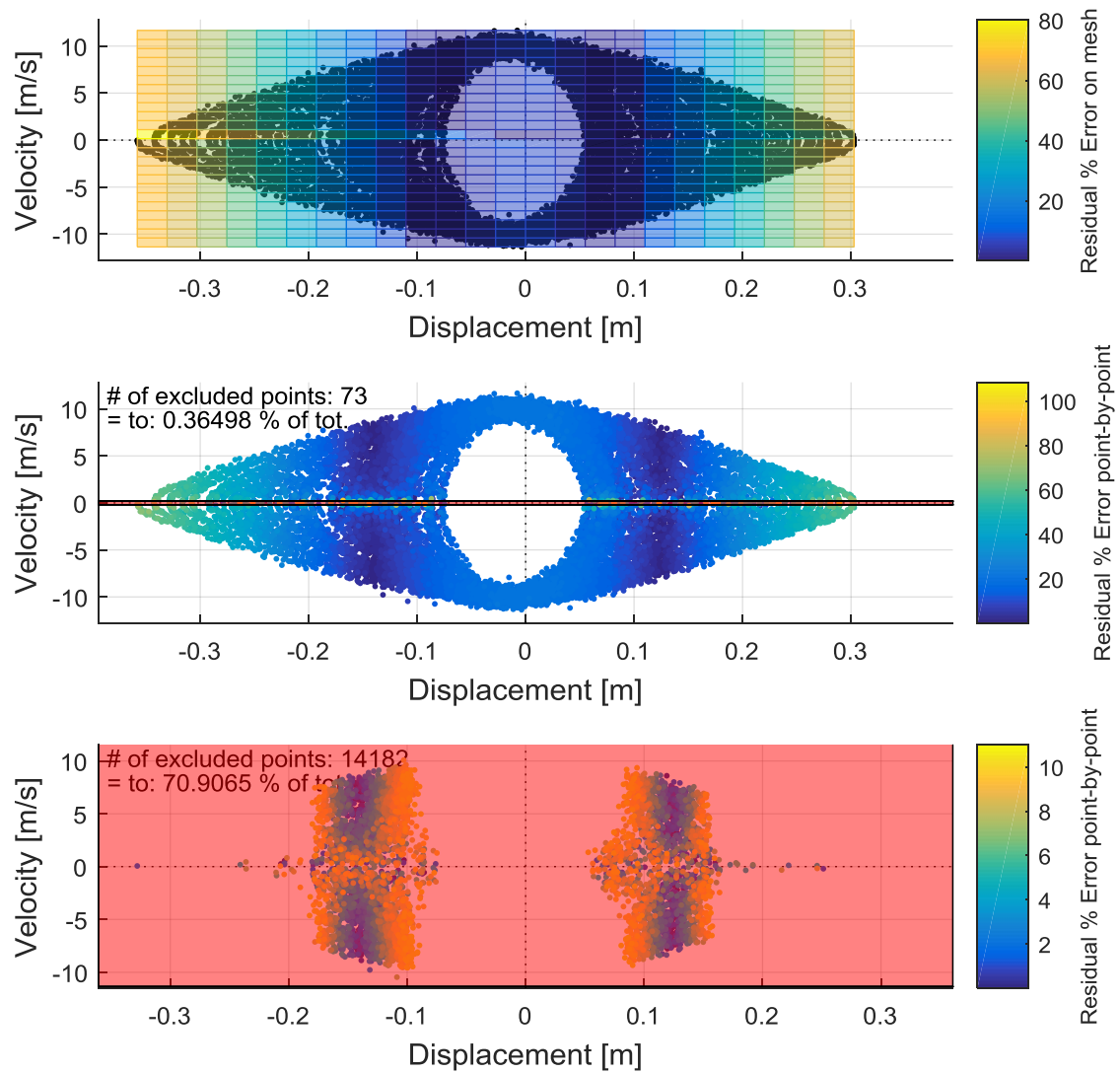


Figure 3.3.7 – Linear case: percentage error comparison between the mesh of the two surfaces (up), point-by-point with a scale 0-100 % (centre) and point-by-point with scale 0-10 % (down). The red zones is the exclusion one.

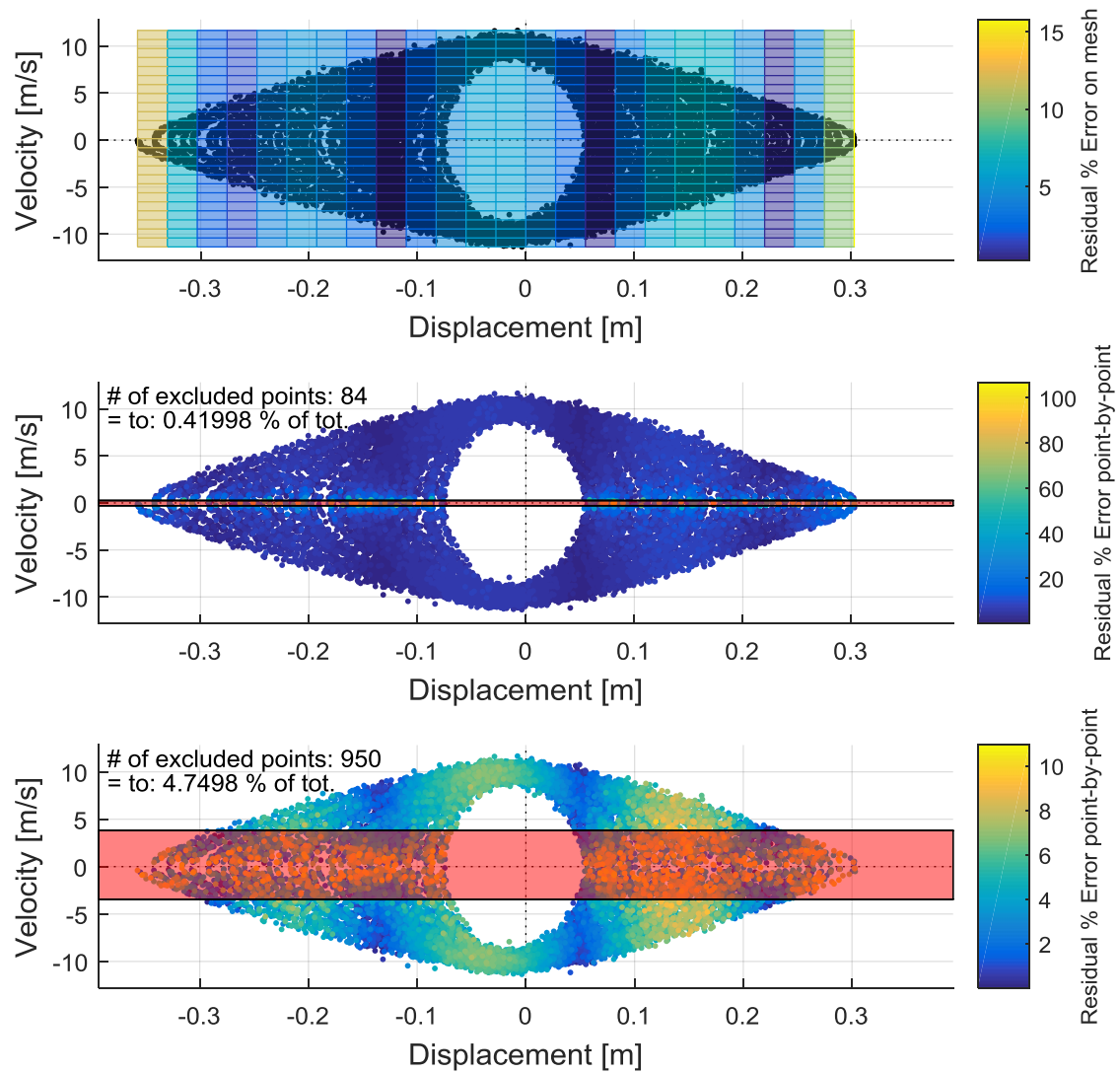


Figure 3.3.8 – Quadratic case: percentage error comparison between the mesh of the two surfaces (up), point-by-point with a scale 0-100 % (centre) and point-by-point with scale 0-10 % (down). The red zones is the exclusion one.

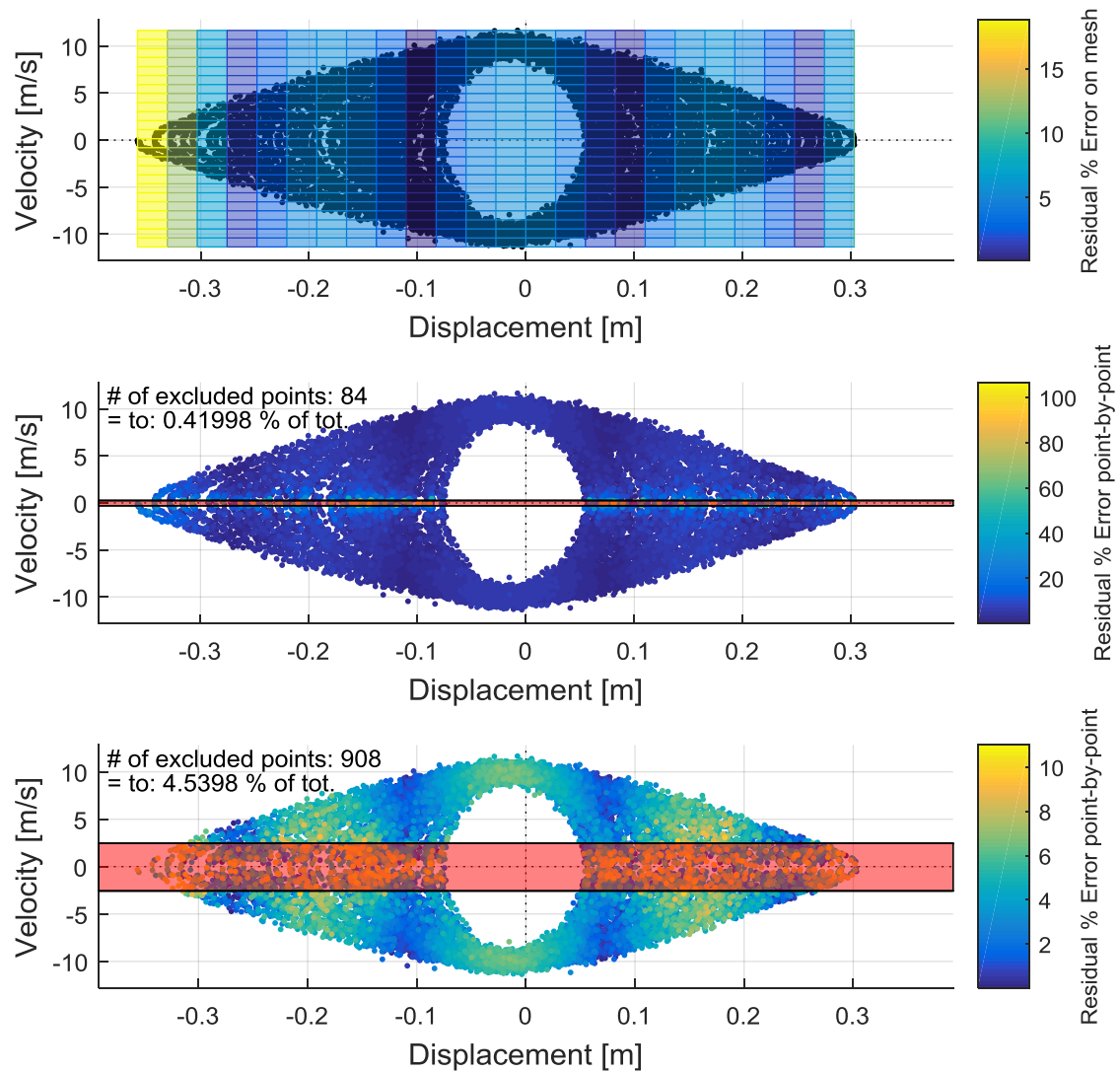


Figure 3.3.9 – Cubic case: percentage error comparison between the mesh of the two surfaces (up), point-by-point with a scale 0-100 % (centre) and point-by-point with scale 0-10 % (down). The red zones is the exclusion one.

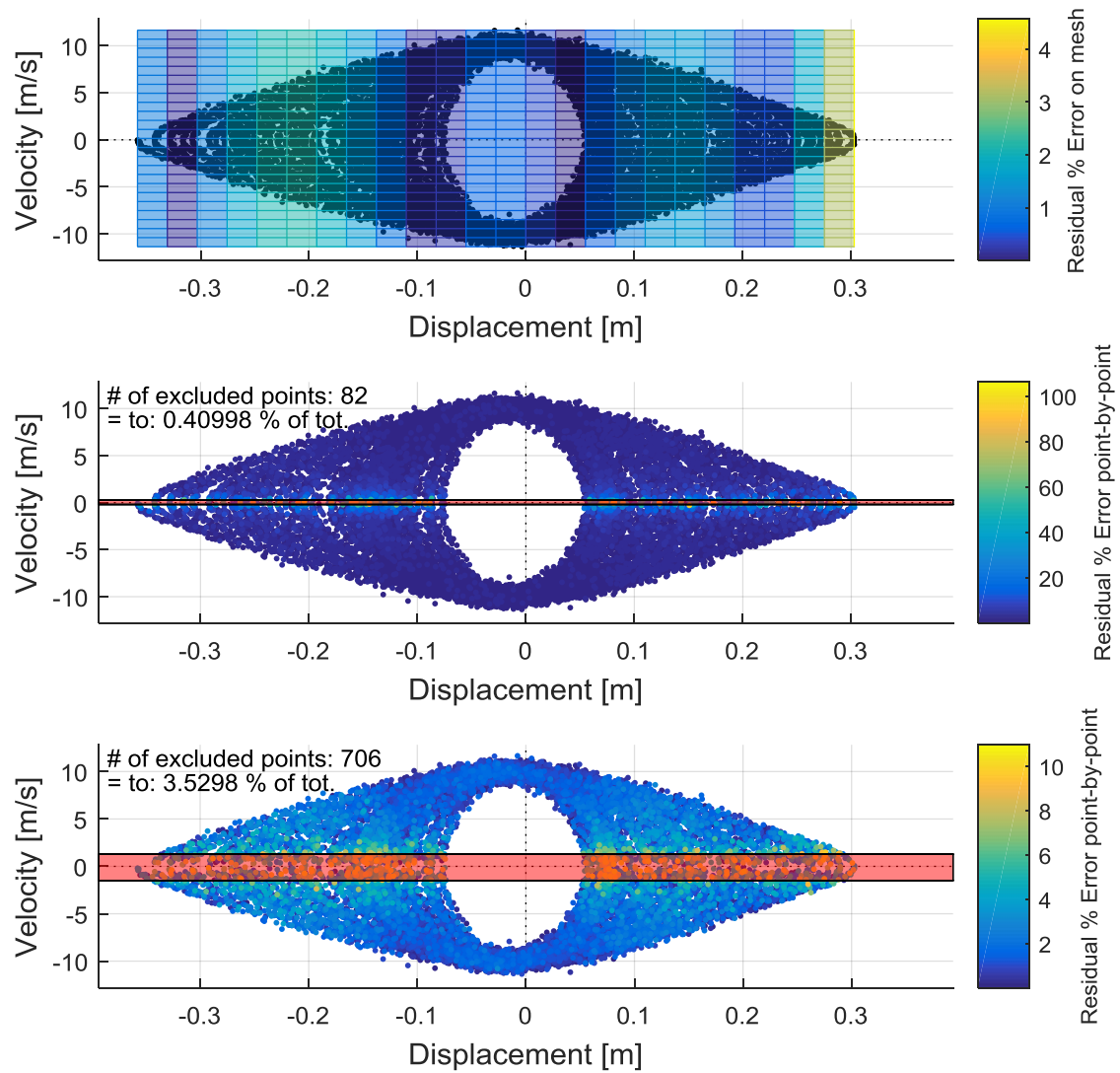


Figure 3.3.10 – Fourth grade case: percentage error comparison between the mesh of the two surfaces (up), point-by-point with a scale 0-100 % (centre) and point-by-point with scale 0-10 % (down). The red zones is the exclusion one.

The output in the Matlab command window be like:

```
Command Window

Signal simulation and acquired data analysis for damper experiment
with medium displacement effect on viscous coefficient

Simulation time:          20 s
Sampling time:           0.001 s
Force amplitude:         1000 N
Force noise amplitude:    50 N

Time for Simulink opening: 0.24875 s
Time for Simulink sim.:   3.7089 s
Total number of points:   20000

The exact function for state space variation is of grade: 4

-----
|          VISCOUS COEFFICIENTS REGRESSION          |
-----
| Visc. coeff. | Declared | Regression | %Error |
-----
|   c_0   | 100 Ns/m | 120 Ns/m   | 20 %   |
|   c_1   | 30 Ns/m  | 34 Ns/m^2  | 13 %   |
-----

Polynomial linear regression coefficient: B0 = -0.62368
                                           B1 = 15.477
                                           B2 = 106.4645
                                           B3 = 9.9302

Median on mesh % regr. error:          22.5214 %
Median point-by-point % regr. error: 15.3644 %

Number of point excluded in figure 3 subplot 2: 73 equal to 0.36498 % of the total
Number of point excluded in figure 3 subplot 3: 14182 equal to 70.9065 % of the total

Overall time:          9.2197 s
```

Figure 3.3.11 – Linear case outputs.

Command Window

Signal simulation and acquired data analysis for damper experiment
with medium displacement effect on viscous coefficient

Simulation time: 20 s
Sampling time: 0.001 s
Force amplitude: 1000 N
Force noise amplitude: 50 N

Time for Simulink opening: 0.2462 s
Time for Simulink sim.: 3.6481 s
Total number of points: 20000

The exact function for state space variation is of grade: 4

VISCOUS COEFFICIENTS REGRESSION				

Visc. coeff.	Declared		Regression	%Error

c_0	100 Ns/m		96 Ns/m	4 %
c_1	30 Ns/m		90 Ns/m^2	199 %
c_2	1000 Ns/m		1661 Ns/m^3	66 %

Median on mesh % regr. error: 4.2238 %
Median point-by-point % regr. error: 3.8381 %

Number of point excluded in figure 3 subplot 2: 84 equal to 0.41998 % of the total
Number of point excluded in figure 3 subplot 3: 950 equal to 4.7498 % of the total

Overall time: 8.9525 s

Figure 3.3.12 – Quadratic case outputs.

Command Window

Signal simulation and acquired data analysis for damper experiment
with medium displacement effect on viscous coefficient

Simulation time: 20 s
Sampling time: 0.001 s
Force amplitude: 1000 N
Force noise amplitude: 50 N

Time for Simulink opening: 0.25209 s
Time for Simulink sim.: 3.7629 s
Total number of points: 20000

The exact function for state space variation is of grade: 4

VISCIOUS COEFFICIENTS REGRESSION				
Visc. coeff.	Declared	Regression	%Error	
c_0	100 Ns/m	95 Ns/m	5 %	
c_1	30 Ns/m	55 Ns/m ²	83 %	
c_2	1000 Ns/m	1712 Ns/m ³	71 %	
c_3	1500 Ns/m	881 Ns/m ⁴	41 %	

Median on mesh % regr. error: 4.4868 %
Median point-by-point % regr. error: 3.514 %

Number of point excluded in figure 3 subplot 2: 84 equal to 0.41998 % of the total
Number of point excluded in figure 3 subplot 3: 908 equal to 4.5398 % of the total

Overall time: 9.2047 s

Figure 3.3.13 – Cubic case outputs.

```

Command Window

Signal simulation and acquired data analysis for damper experiment
with medium displacement effect on viscous coefficient

Simulation time:          20 s
Sampling time:           0.001 s
Force amplitude:          1000 N
Force noise amplitude:    50 N

Time for Simulink opening: 0.26794 s
Time for Simulink sim.:   3.7349 s
Total number of points:   20000

The exact function for state space variation is of grade: 4

-----
|          VISCOUS COEFFICIENTS REGRESSION          |
-----
| Visc. coeff. | Declared | Regression | %Error |
-----
|   c_0   | 100 Ns/m | 100 Ns/m   | 0 %    |
|   c_1   | 30 Ns/m  | 18 Ns/m^2  | 39 %   |
|   c_2   | 1000 Ns/m | 861 Ns/m^3 | 14 %   |
|   c_3   | 1500 Ns/m | 1939 Ns/m^4 | 29 %   |
|   c_4   | 10000 Ns/m | 12214 Ns/m^5 | 22 %   |
-----

Median on mesh % regr. error:      1.0311 %
Median point-by-point % regr. error: 0.8873 %

Number of point excluded in figure 3 subplot 2: 82 equal to 0.40998 % of the total
Number of point excluded in figure 3 subplot 3: 706 equal to 3.5298 % of the total

Overall time:                      8.9968 s

```

Figure 3.3.14 – Fourth grade case outputs.

Is now more clear that, generally, the higher the grade are the smaller the general error become. The highest value of error occur for the highest values of displacements. The residual error in the fourth grade case must be charged to the noise presence, in not reported experiment the error become zero when the noises are suspended. The algorithm works also for $n_r > n$, so when the real data will be managed, in the hypothesis that the viscous function can be expressed in a polynomial form, a solution for a rapid regression can be to put a very high value of polynomial grade and see what happens to the contribution of the n^{th} added term. The contribution can be evaluated as:

$$\text{contribution}_n = \text{median} \left(\frac{c_n \mathbf{x}^n}{\mathbf{F}} \right) \cdot 100 [\%] \quad (3.3.5)$$

So it will be possible to plot the n^{th} contribution with respect to the n^{th} grade. If a 20^{th} order regression is considered with respect to the same old 4^{th} grade exact solution the graph will result as:

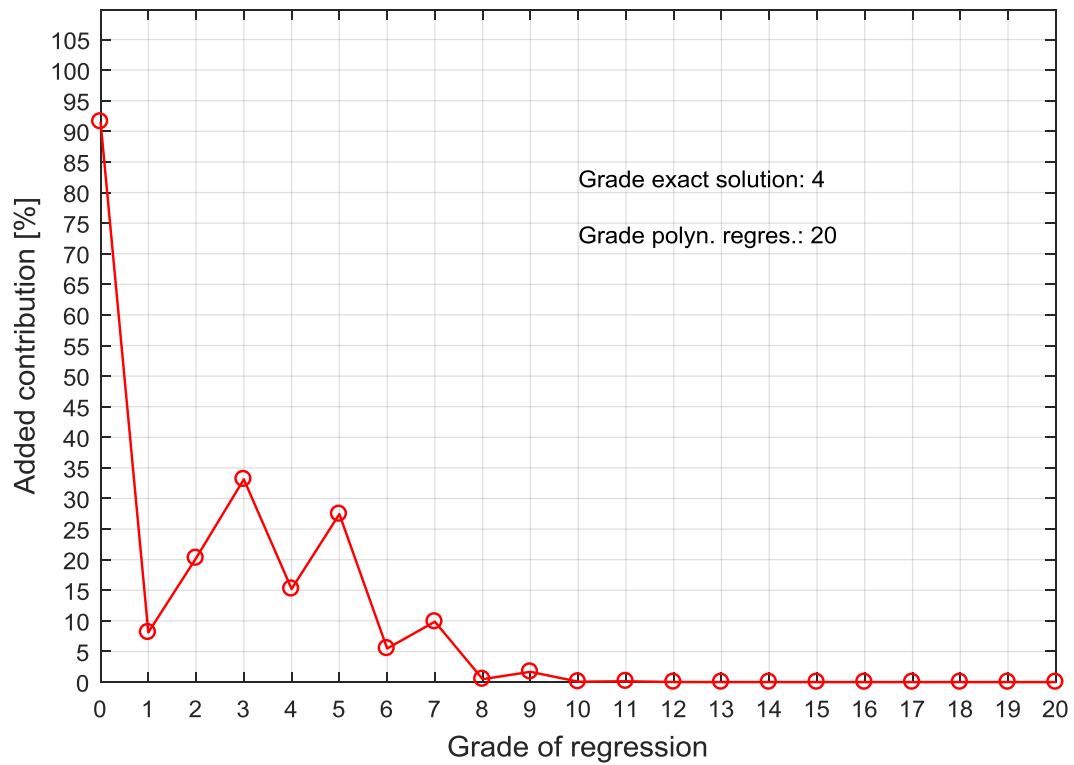


Figure 3.3.15 – Added contribution for a 20th order regression.

The graph in Figure 3.3.15 suggest, in the hypothesis that the exact grade is unknown, that it will be useless to consider anymore over the 10th grade. The procedure in realities become iterative, if a 10th grade regression is tried will result:

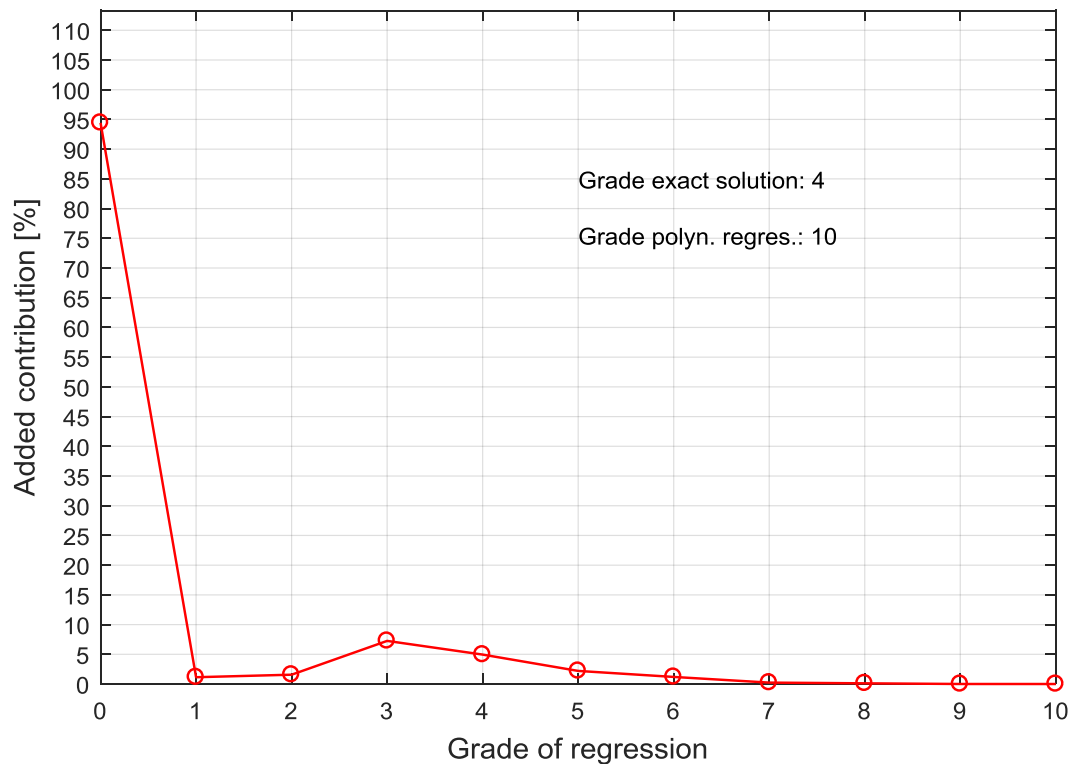


Figure 3.3.16 – Added contribution for a 10th order regression.

The solution suggest now to limit the regression to the 6th÷7th order. So by trying again:

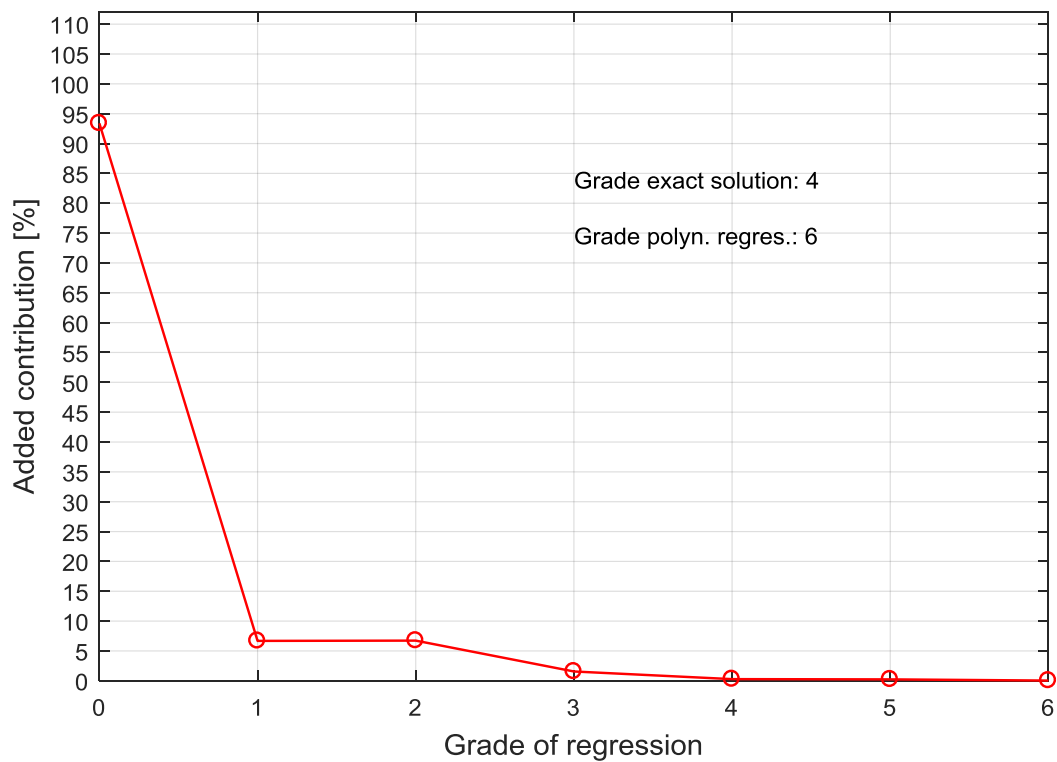


Figure 3.3.17 – Added contribution for a 6th order regression.

And finally the graph suggest a 4th grade regression, but how will be possible understood that the iteration is near to the true value? The answer appear more clear if a 4th grade regression is done:

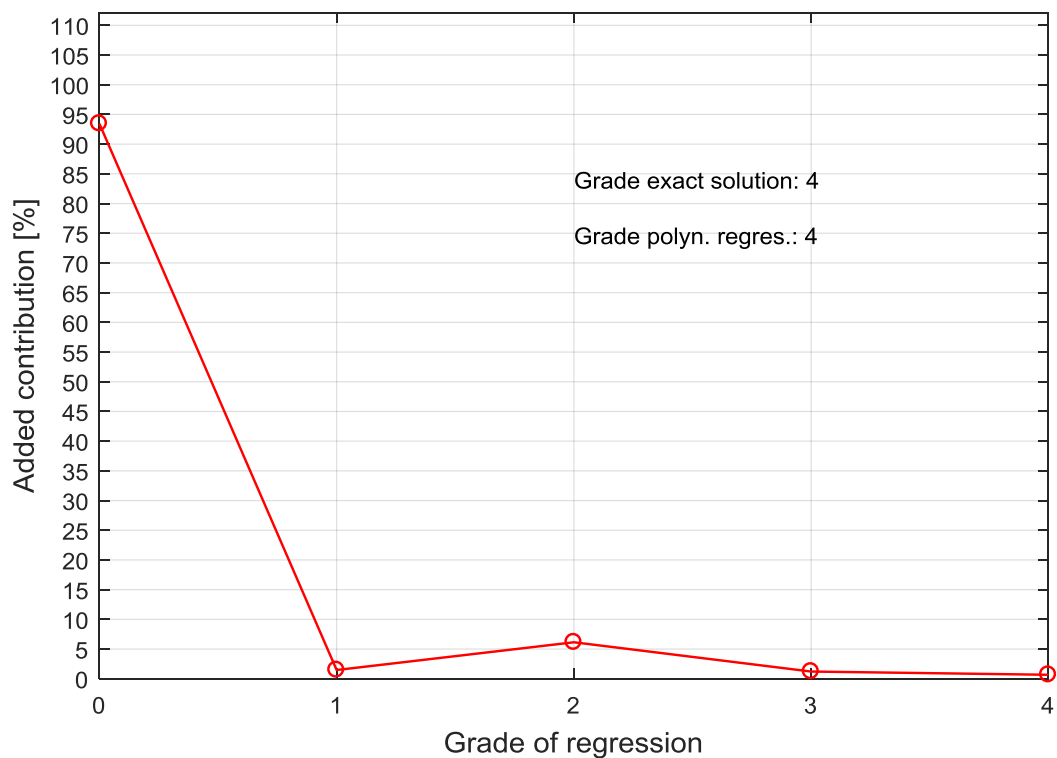


Figure 3.3.18 – Added contribution for a 4th order regression.

As it is possible to notice looking at Figure 3.3.18 the main difference from the previous iterative steps is that now the last considered grade is a non-zero value. In the other ones, instead, by lowering the regression grade the last non-zero value become increasingly lower:

Table 3.3.1 – Regression grade iteration.

Regression grade	Last non-zero grade
20 th	9 th
10 th	6 th
6 th	4 th
4 th	4 th

So it will be finally possible to say that if a coincidence between regression grade and last non-zero grade is reached the exact solution is found? Definitely no. This type of procedure can works only if is applied 'from above', indeed if we look what happens to the firsts 3 orders regressions:

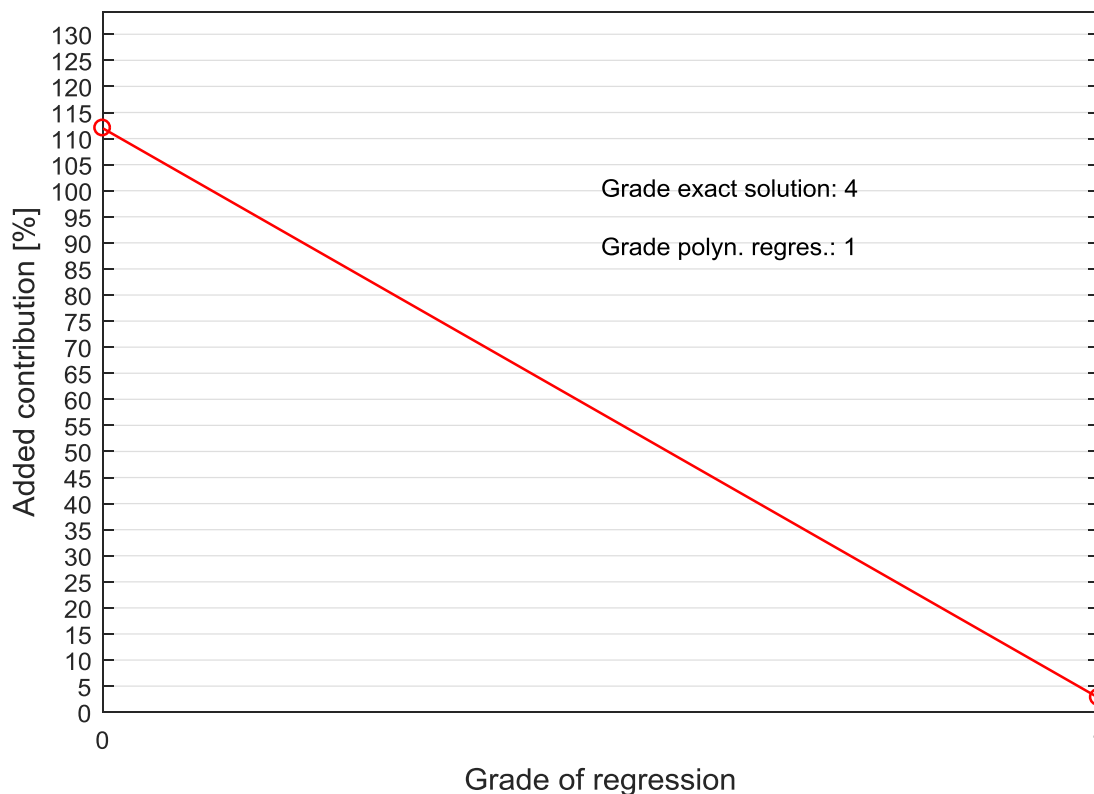


Figure 3.3.19 – Added contribution for a 1st order regression.

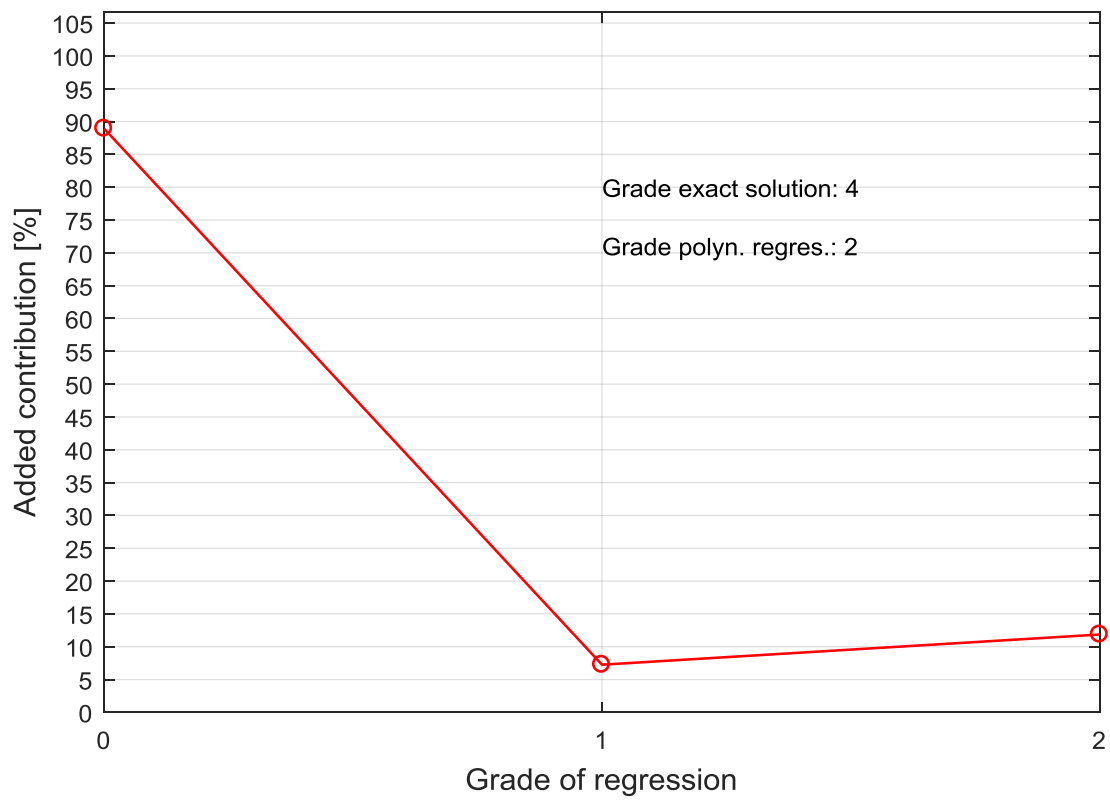


Figure 3.3.20 – Added contribution for a 2nd order regression.

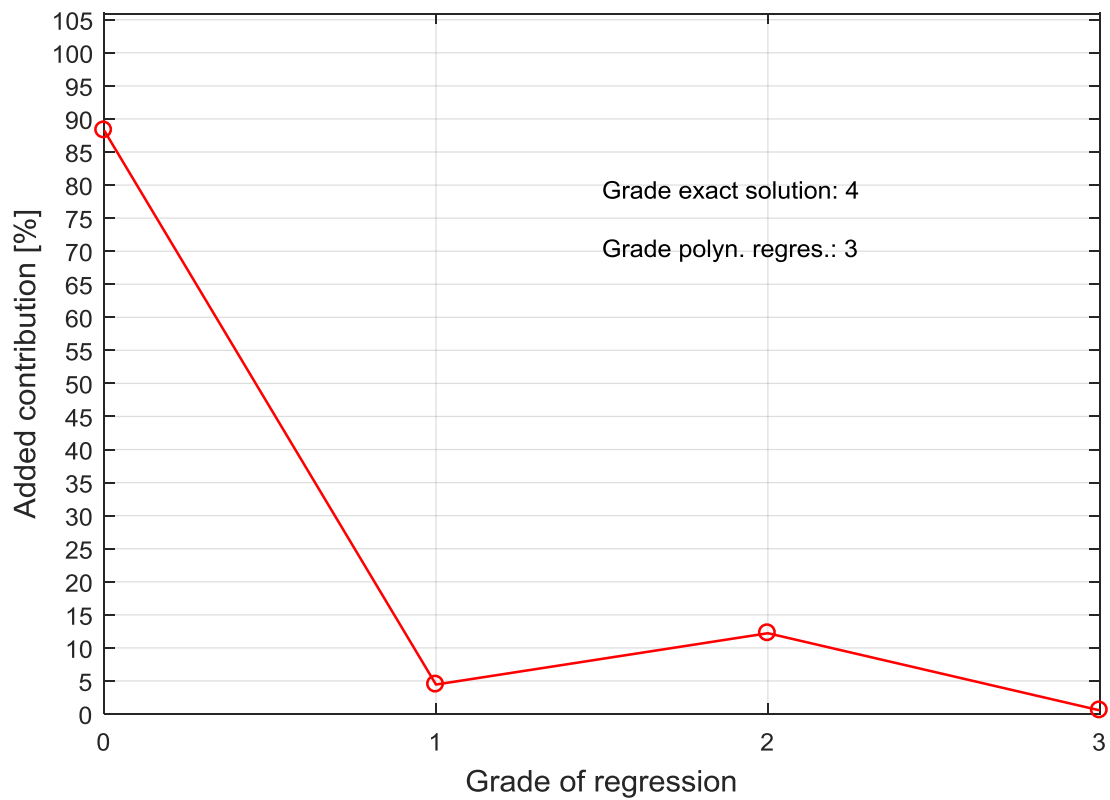


Figure 3.3.21 – Added contribution for a 3rd order regression.

In this 3 cases the same condition of the 4th order regression can be observed: the last grade is also the last non-zero value, so to judge if the polynomial regression is underestimated it will be possible to looking at 2 main criteria:

- Looking at the fitting in plots of the type shown in Figures 3.3.3 – 3.3.6: a sort of ‘manual’ estimation that could be very easy for a lower polynomial regression.
- Looking at the total amount of contributions: if summed this values has to return a value of about ~ 100 % unless the error due to measurement noise and the operation of media operated in the (3.3.5). So it will be possible to complete the previous table as follow:

Table 3.3.2 – Regression grade iteration.

Regression grade	Last non-zero grade	Total contribution
20 th	9 th	213.49 %
10 th	6 th	113.13 %
6 th	4 th	108.92 %
4 th	4 th	102.95 %
3 rd	3 rd	105.51 %
2 nd	2 nd	108.05 %
1 st	1 st	114.68 %

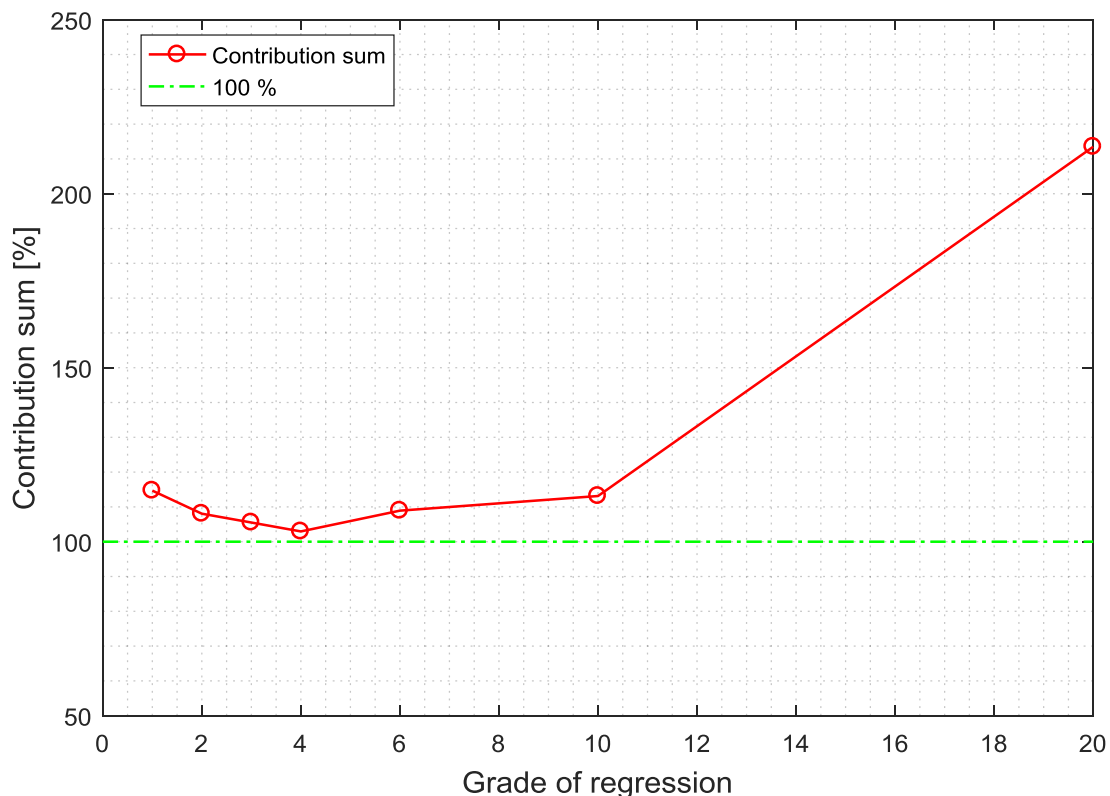


Figure 3.3.22 – Contribution sum for each regression grade.

Looking at Figure 3.3.22 looks definitively clear that this can be used as the parameters to check which grade of regression is the best one just by searching for the minimum, but also returns an idea of how much far are the other solutions from the objective one (100 %).

4. Real experiment

Once all the pieces were available was been possible to proceed with the assembly phases of the experimental setup (whose steps are been already shown in the chapter 2) and of the data acquisition system.

4.1 Data acquisition system

The acquisition system, as mentioned in paragraph 1.3, consists of:

- *Personal computer*: on it are installed the control programs for SCADAS and the laser meters.
- *Acquisition controller Siemens Simcenter SCADAS*: this component is the core of the control system. It can receive, process, and emit signals. It is continuously in communication with the Siemens control program “LMS Testlab (vers. 2017)”. The program permit to distinguish an input signal by treats it as a reference from another one that can be treat as a response. The reference can be used to produce an adequate output sinusoidal signal that is the one generating the excitation in the shaker (passing through the amplifier). In the first step this signal is generated on the base of a ‘System Identification’ in a certain frequency range, a procedure where the SCADAS emit random excitation signal and register the responses of the inputs. Later the data acquired from the real tests can be used to generate an output drive rise more and more precise, in order to respect as best as possible the parameter of the controlled signal (the reference one). Lastly the program can outputs the data directly in Matlab compatible format, helpful skill for the post processing.
- *Laser and laser controller Keyence*: very precise devices whose operating principle is based on interferometry. They require a dedicated control system that will be put in communication with the SCADAS (it will provide the reference signal) and with the PC where the proprietary program LK Navigator is present which allows to establish emission frequency, space, speed or acceleration range of interest. This is quite a limitation, this laser devices are very precise but cannot work on large ranges.
- *Shaker amplifier*: the output signal coming out from the SCADAS are characterized by very low voltage (from -10 VDC to +10 VDC) while the shaker need a voltage at least one magnitude order bigger. For this reason the signal is processed by the amplifier which only increase it of a value that can be decided by the user through a physical knob located in the front of the device. The shaker could receive signals of maximum 100 V: in fact the maximum settable gain on the amplifier is 10.
- *Piezoelectric load cell*: already well described in the chapter 1.3, is an electric passive device so it can be connected directly to the SCADAS don’t needing of any active supply system, the signal so generated is used as response.

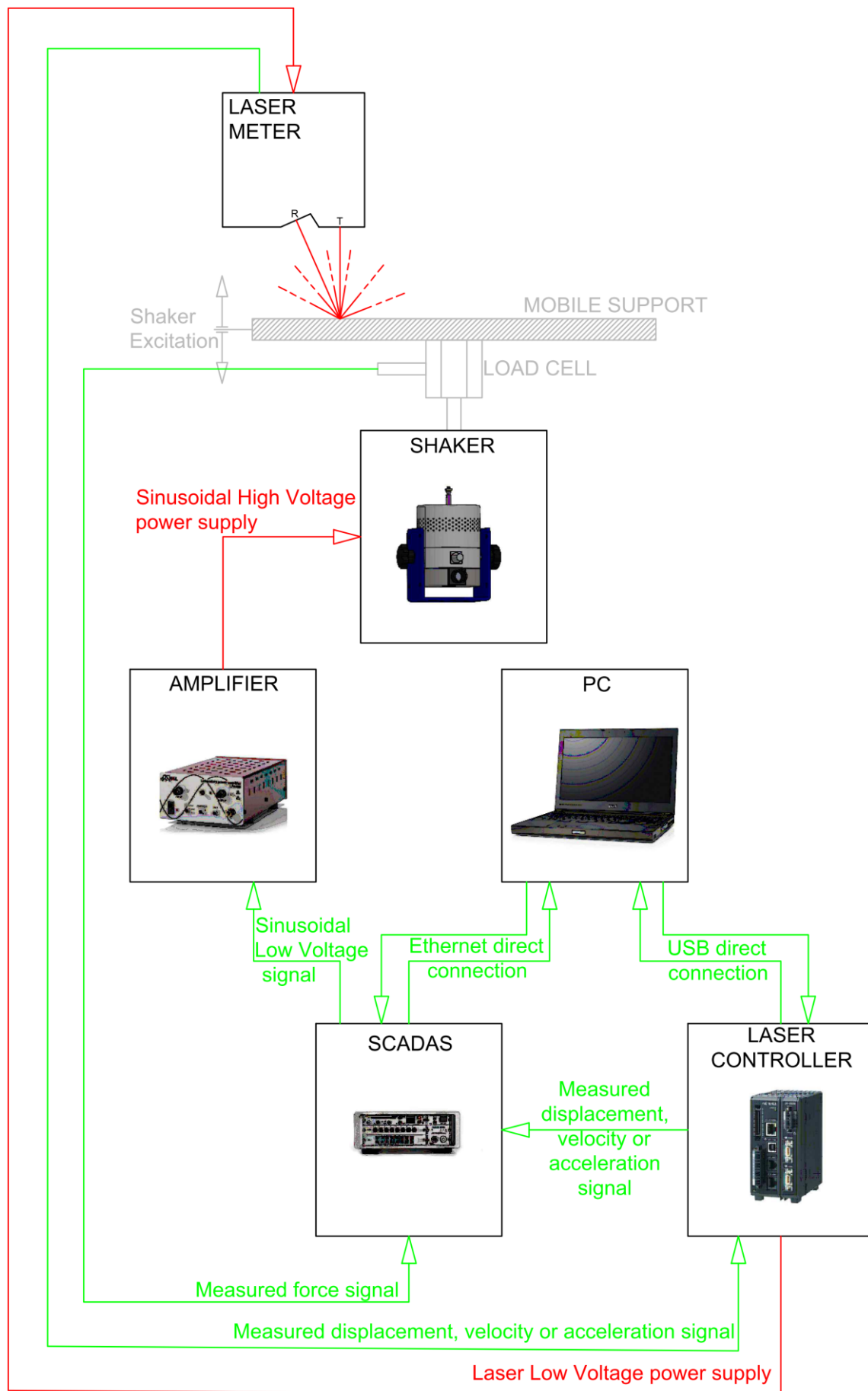


Figure 4.1.1 – Operating scheme and components of the control system.


4.2 Experiment procedure

4.2.1 Possible damper configurations

So it's been found a dimensional difference between the front shock absorber and the rear one. Moreover a large range of oil gradation has to be explored, in fact changing the oil is doing nothing but varying the damping parameter.

The manufacturer is able to provide oils characterized by 12 gradation:

Table 4.1 – Available oil gradation.

20	25	30	35	40	45	50	60	70	80	90	100
WT	WT	WT	WT	WT	WT	WT	WT	WT	WT	WT	WT
											




That means at least 24 shock absorber combination has to be assembled and tested, but in reality also 24 more become necessary when different setups has to be explored directly on the vehicle, where are necessary 4 damper for each oil gradation (total 48).



Figure 4.2.1.1 – The 12 different oils.

4.2.2 Damper assembly procedure

Table 4.2 – Step by step assembly procedure.

	<p>All the components are disposed on the table: the stem, the piston, the washers and nut for piston clamping, the cylinder, the rubber cap, the threaded ring, a series of seals, a ball joint, the sealing cap for gaskets and the plastic head. The only missing is the metallic cap for the cylinder closing.</p>
	<p>The piston is mounted on the stem, two washers of different dimensions are inserted respectively between the piston and the stem and between the piston and the nut that close the system.</p>
	<p>The O-ring is mounted in its specific location around the restricted part of the cylinder.</p>



The three rubber seals are inserted in the restricted part of the cylinder.



A particular plastic washer is positioned on the previous three rubber seals. The shape of this washer is specific for the compression of the seals when the system will be closed, as shown in the next steps.



The plastic cap is screwed up the restricted part of the cylinder. When it reach the end of his running push the plastic washer against the seal and compress also the O-ring ensuring pretty well the oil seal.



The threaded ring is screwed on the large part of the cylinder. It will be useful for spring pre-compression.



The piston-stem system is inserted in the cylinder one. Is now also possible to completely close the plastic cap. From this time on the oil seal is guarantee.



The plastic head is screwed up in the stem head. This plastic piece doesn't have a threaded hole, the metal head of the stem will get it by digging into virgin plastic with the right amount of force. An alternative can be to use a male threading tool to dig the first fillet round.



The rubber cap is mounted to cover the stem and to prevent other oil losses.



The spherical joint is inserted in the plastic head. A quite high force will be necessary.



The damper is mounted on a dedicated rotating support through the threaded ring.



The cylinder is filled of the oil for the specific configuration. The stem has to be totally out, so the piston totally inserted.



Before the cylinder closure the stem has to be totally inserted. In this configuration the piston become again visible.



The cap is mounted to close the cylinder. The screw for the air breather has to be totally opened. Once the cap is closed the stem has to be again pulled out but just for the half of the possible run. During this step a little quantity of oil can exit from the air breather: once it happens the screw can be tightened.



The damper is ready.

As said this series of operation was repeated 48 times. The average duration for the single assembly is 20 minutes, for a total duration of about 16 hours of assembly.



Figure 4.2.2.1 – 46 out of the 48 dampers.

4.2.3 Acquisition settings and procedure

In order to obtain a good repeatability and the possibility to compare the data between themselves a certain standard acquisition procedure has to be defined.

The LMS Testlab permit to choose a parameter to control as reference and the other as response. As already said the displacement is here assumed as reference, while the force as response. The program compute a drive profile to excite the shaker in two possible way:

1. On the basis of a 'System Identification': an output random signal is emitted and send to the shaker, and the response registered. Is possible to choose the frequency range of exploration. In this case is been chosen:

$$1 \text{ Hz} < \text{frequency range} < 20 \text{ Hz}$$

Chose on the basis of the range of interest for the vehicle characterization ($\sim 0 \div 15 \text{ Hz}$) and on the capability of the shaker to reach this values. As reported in chapter 1.3 the shaker has a nominal range of $5 \div 3000 \text{ Hz}$, so under 5 Hz it works out of nominal condition. It's been here pointed out that is not possible to go less than 1 Hz .

The program is able to deduce a profile in the considered frequency range of the response of the system. During this stage also the zeroing of the displacement signal is done. This profile is used, united to the sine signal settings, to compute a drive profile for the shaker. This procedure can be repeated a certain times, as larger this number is as precise the identification will be, but also the resolution and the bandwidth has a certain importance to obtain a good result. This step is the only thing possible to do as first, when no data on the damper is available.

2. On the basis of previous acquisitions data: the program refine the drive signal as function of the last data acquisition envelopes. The result obtained by this way is obviously more accurate. The iteration of n times can bring the test result near to the ideal profile. This procedure is done from the 2nd test on.

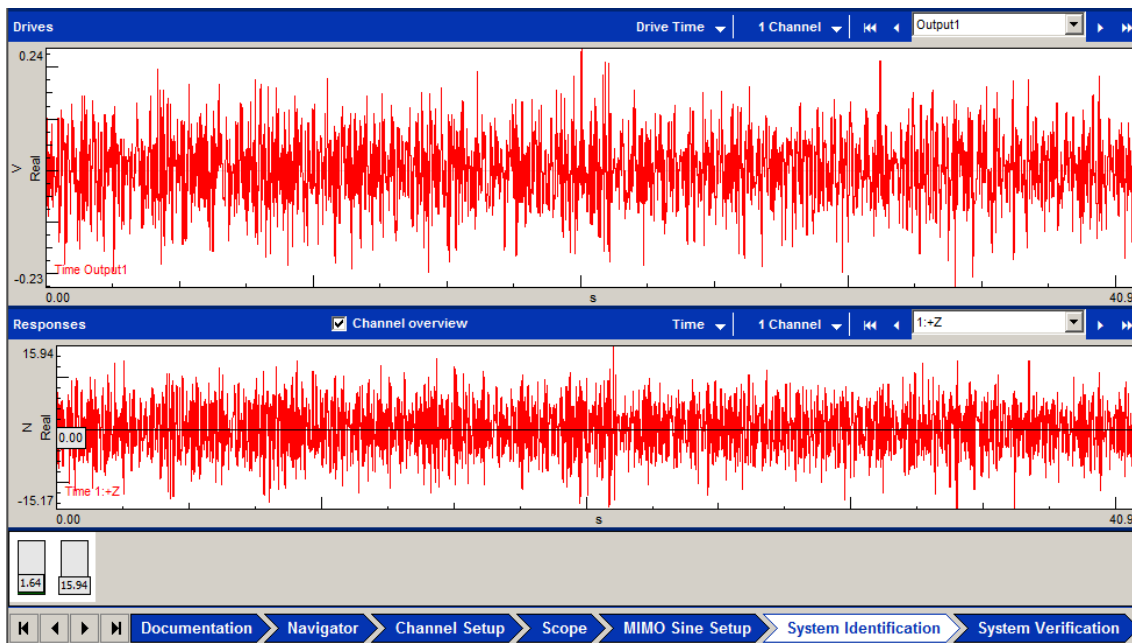


Figure 4.2.3.1 – System identification monitor: in the upper window 40 s of the random drive, in the lower the resulting registered response.

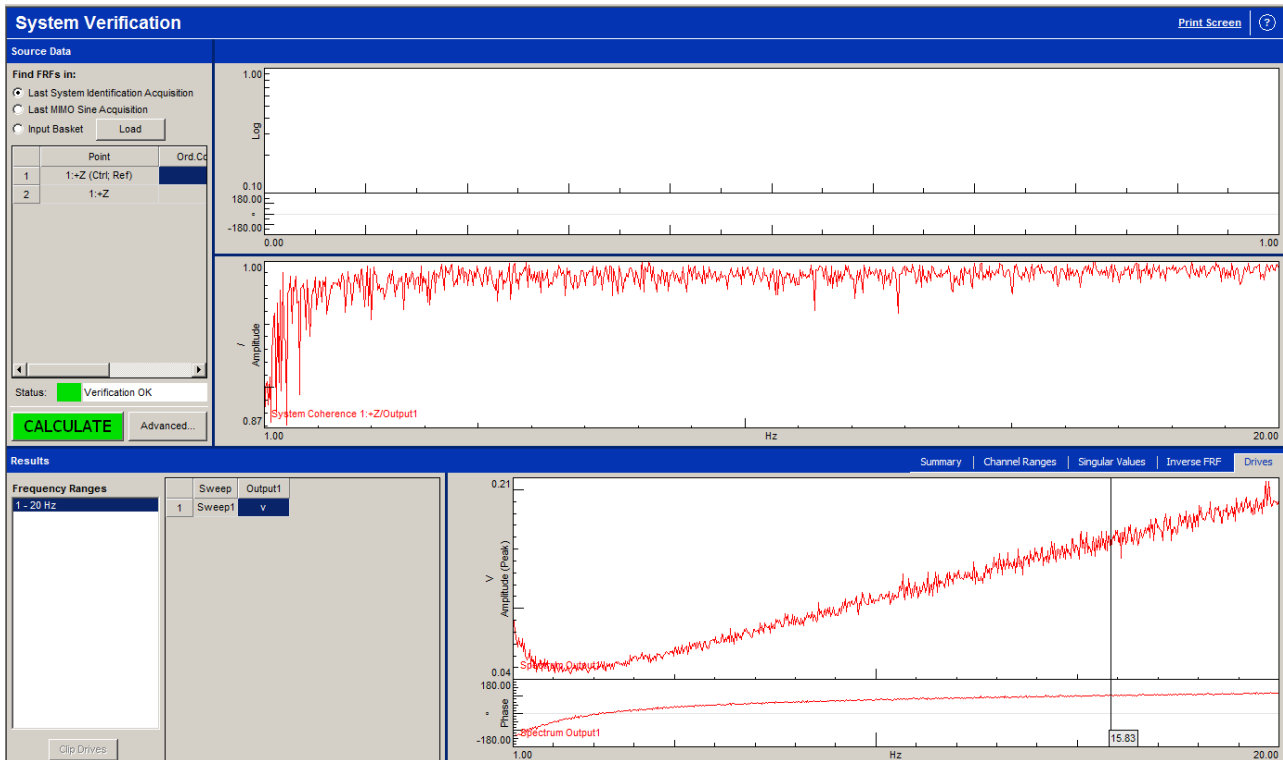


Figure 4.2.3.1 – LMS interface for drive calculation from system identification result.

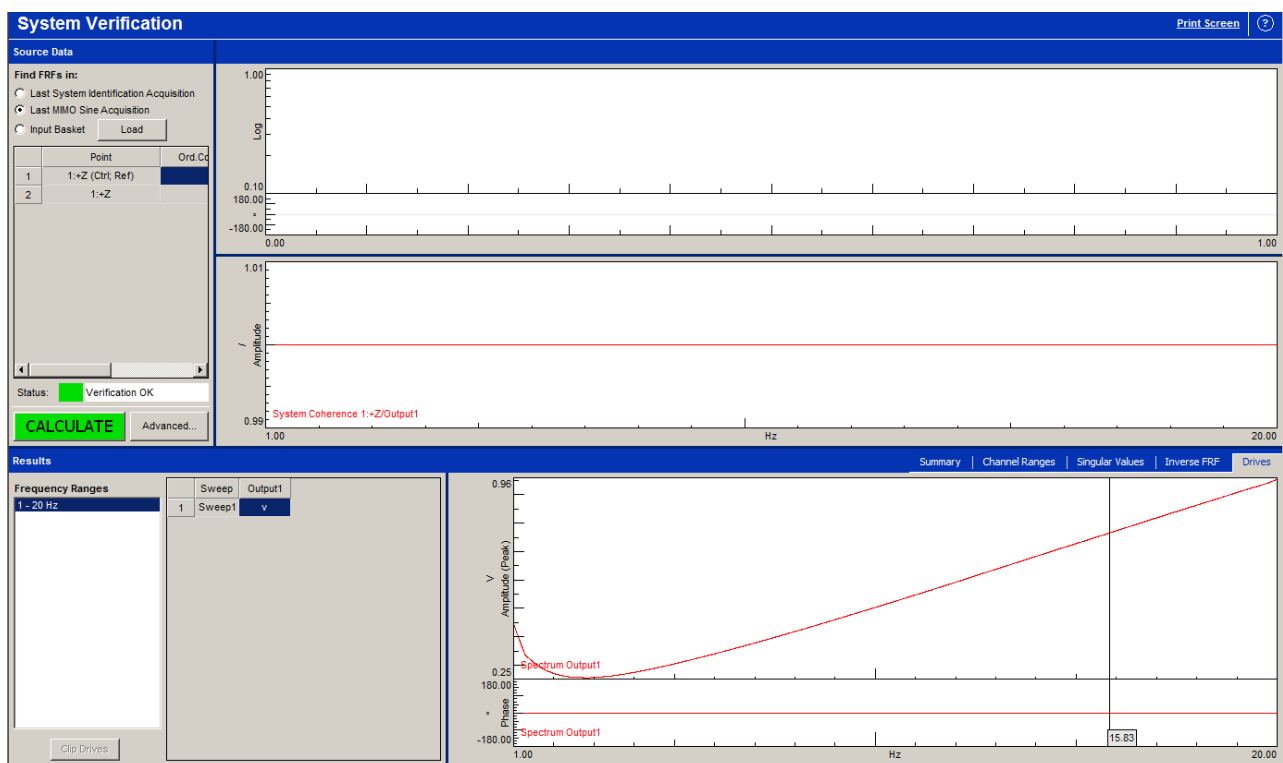


Figure 4.2.3.2 – LMS interface for drive calculation from previous acquisition.

Looking at Figure 4.2.3.1 is possible to see, in the upper side, the envelope mean result of the System Identification. In the lower zone the drive: envelope of the output signal for shaker

excitation. Is possible to notice how the first shape (Figure 4.2.3.1) is not so clean, especially if compared with the drive obtained from a previous acquisition and visible in Figure 4.2.3.2.

The program excite the system referring to the frequency, starting from the lowest value (1 Hz) and sweeping all the values until the highest chosen (20 Hz) with a certain growth rate (that the programs call ‘sweep rate’) expressed in Hz/s and that here is:

$$\text{sweep rate} = 0.2 \frac{\text{Hz}}{\text{s}}$$

This growth rate will determine the total time of the test run, obtainable as:

$$\text{runtime} = \frac{\text{frequency range}}{\text{sweep rate}} = \frac{20 - 1}{0.2} = 95 \text{ s} \quad (4.2.3.1)$$

At this time the system adds some time to ‘startup’ the system, a sort of transition phase in order to gradually move from the 0 Hz situation to the starting frequency (1 Hz) and therefore not stressing with any kind of impulse the system. For the same reason also a ‘shutdown’ time will be added.

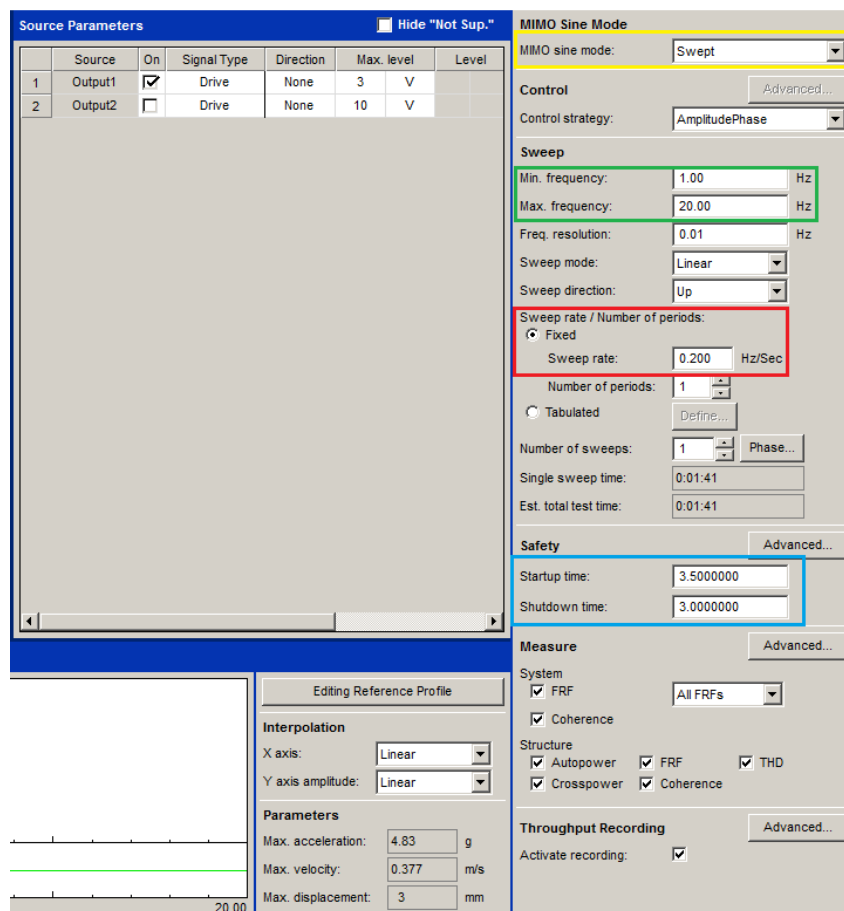


Figure 4.2.3.3 – Sine signal settings in LMS Testlab 2017.

Looking at Figure 4.2.3.3 all the characteristics of the sinusoidal signal are present. Circled in yellow the chosen mode of excitation: ‘swept’ means a linear variation of the frequency (the alternative was a step exploration). In green the parameter for the frequency range declaration, in red the sweep rate. In blue the startup and shutdown time as suggested by the program: under a threshold value the program don’t permit to run the test in order to avoid damages.

In the central zone also a ‘Editing Reference Profile’ button is present, this function will be explored later when the displacement amplitude must be declared.

From previous and not reported tests it seemed sufficient that the *standard procedure* provided:

1. 5 well refined system identifications. The final result of this 5 identification is automatically outputted as the mean value of they all.
2. 3 refining on the basis of the previous tests for each displacement amplitude value.
3. The 5th test, the 4th not considering the system identification, is considered as the good one.

At the first end of this procedure core the sinusoidal output signal can be switched to the successive displacement amplitude value. The chosen amplitude values to be considered are the following:

Table 4.3 – Displacement amplitude values.

0.5 mm	1 mm	1.5 mm	2 mm	2.5 mm	3 mm
--------	------	--------	------	--------	------

Note that by being an *amplitude* the total displacement made by the shaker will actually be twice this value. Moreover is important to notice that by switching from a certain amplitude to another one the system identification is not anymore necessary, it has to be re-done only when a new damper will be mounted in the test rig.

Once all the displacements are being explored (6 iterations), the damper can be changed with another one and the procedure can be repeated from the initial point.

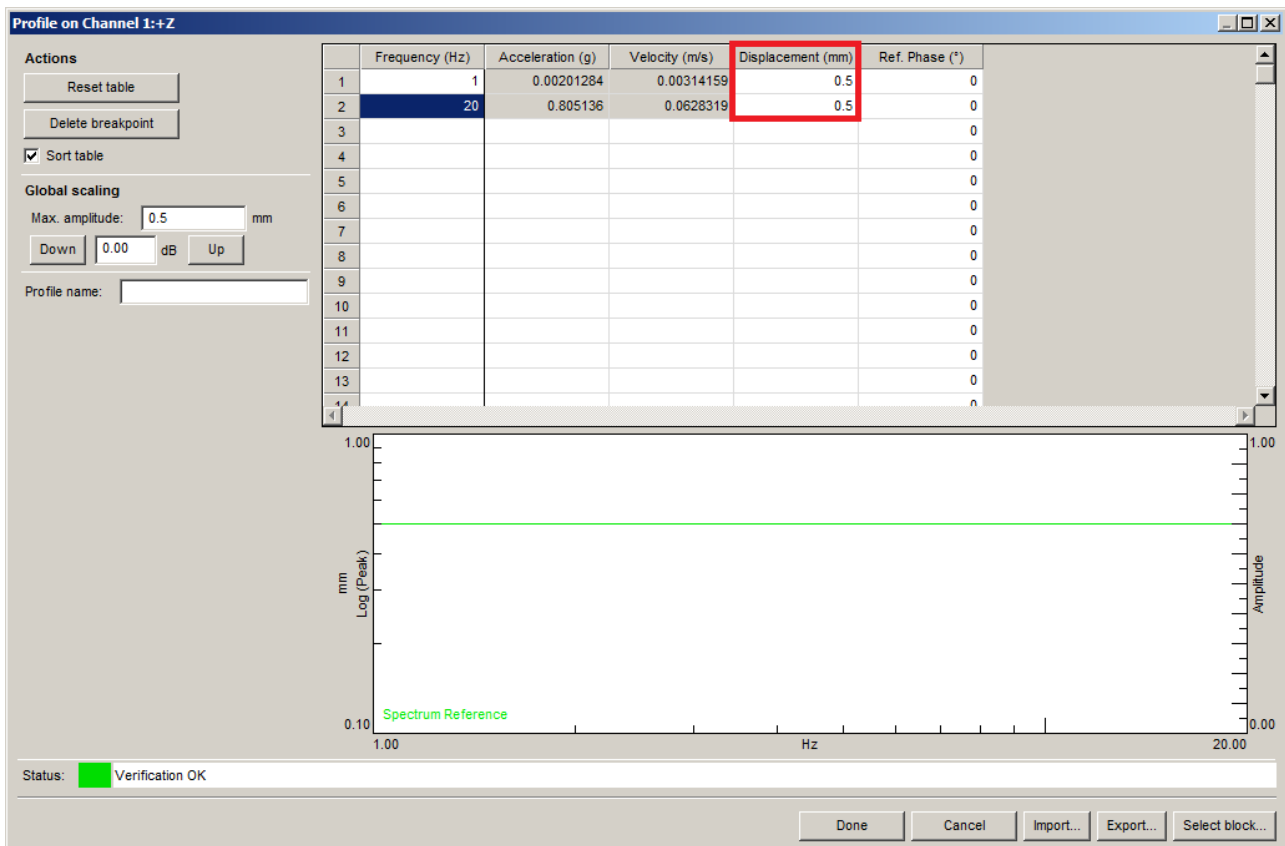


Figure 4.2.3.4 – The ‘Editing Reference Profile’ function where the displacement amplitude can be declared (red circle).

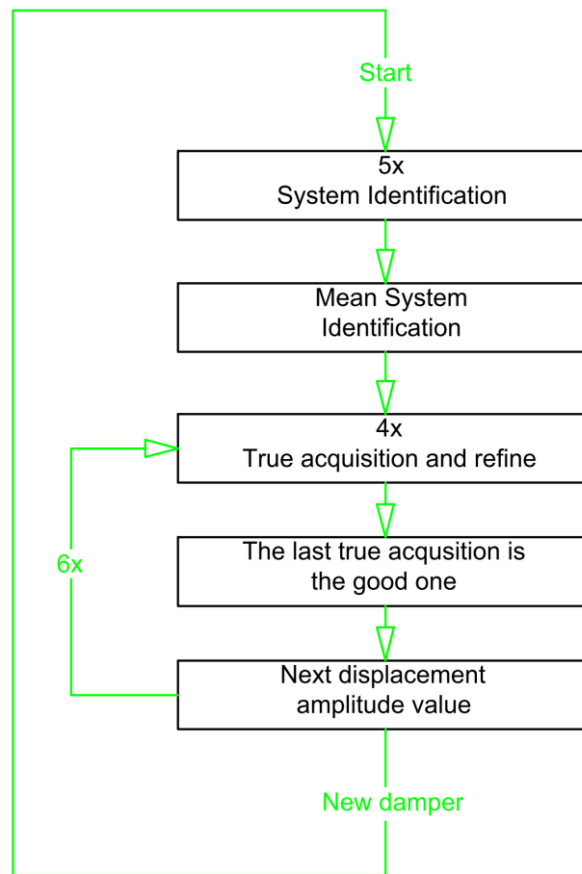


Figure 4.2.3.5 – Scheme of acquisition procedure.

This means, considering the 24 possible oil-damper configurations, if each of these has 6 possible amplitude values and each of them requires at least 4 iteration, that the total number of test do be done is equal to 576 and, considering moreover the 24 system identifications, the number reach 600 test run. The system identification procedure can take about 10 minutes, while a test run something about 2 minutes. The total time for the tests will therefore take about 35÷45 hours if the time required to mount the shock absorbers and adjust the system is also considered.

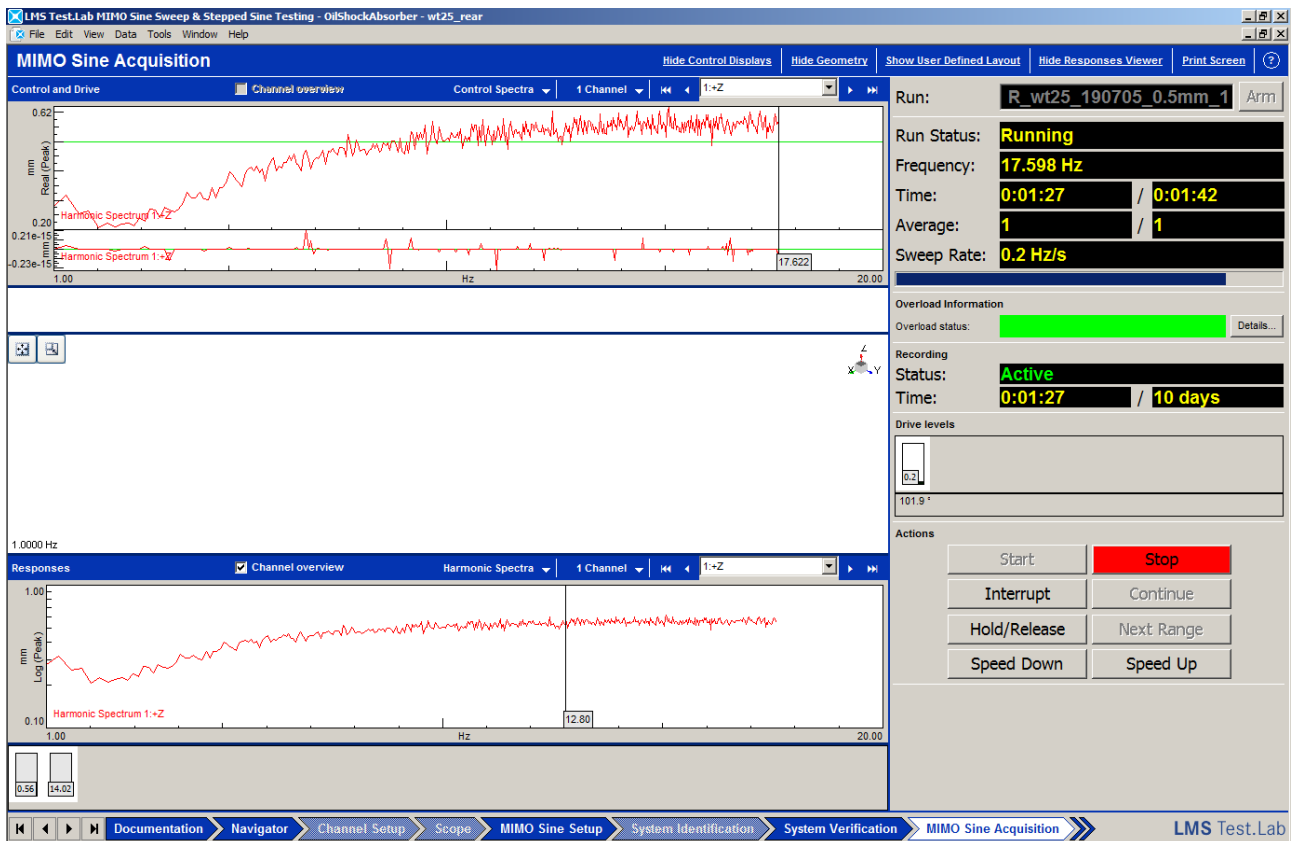


Figure 4.2.3.6 – LMS Testlab during an acquisition. On the upper window the reference data, on the lower the response.

The data acquired in Figure 4.2.3.6 are quite bad because it is a ‘first attempt’ obtained just after the system identification, in a good acquisition will look quite different the with the red line (real time data) that has to follow as well as possible the green on (reference parameter profile).

Once the tests on a damper ends it will be possible to export the acquired data directly in a Matlab format from the navigator tab of LMS Testlab. It’s been decided to export the so called ‘throughput’ data, which report 1600 Hz sampling data in time domain, and the envelopes of both response and reference (force and displacement).

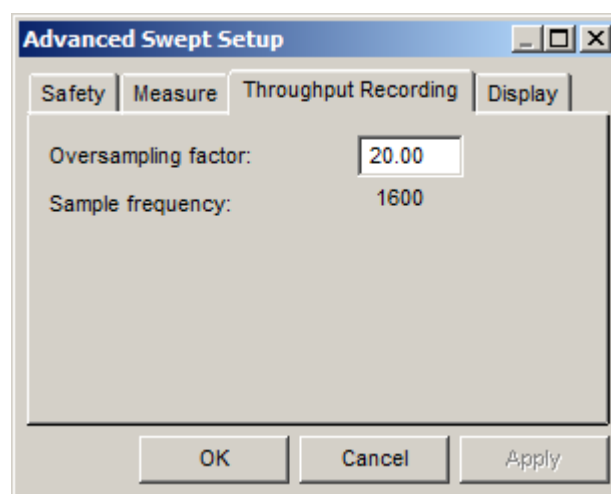


Figure 4.2.3.7 – LMS Testlab setting for throughput sampling.

4.3 Preliminary acquisition and model correction

4.3.1 First acquisition and comparison with the supposed models

Once the first oil shock absorber was ready and mounted on the test rig, it was possible to make a first acquisition (complete procedure) and compare the exported data with the shapes created in chapter 3.

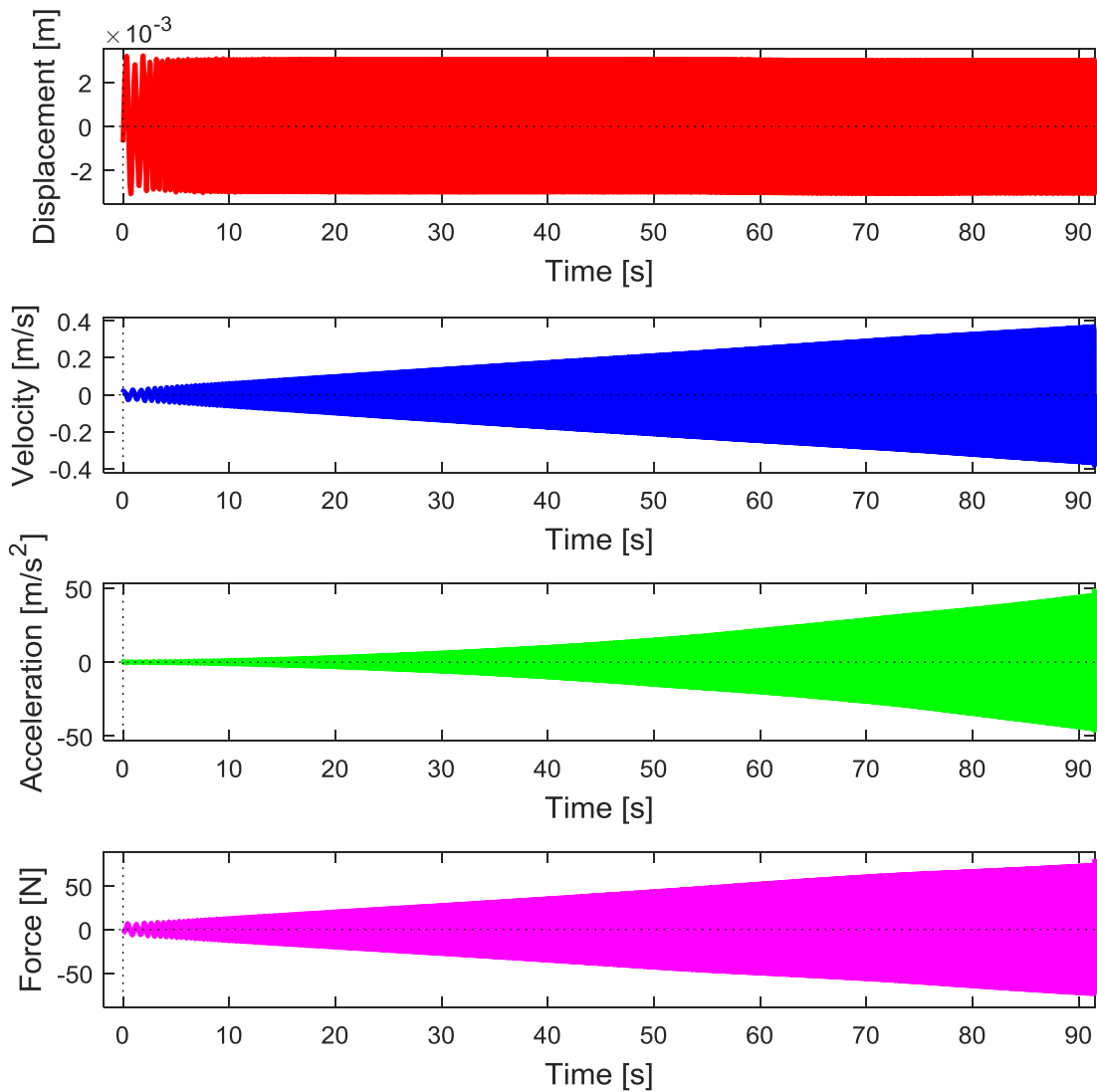


Figure 4.3.1.1 – An example of the acquisition data displayed in a Matlab graphs.

The signals shown in Figure 4.3.1.1 is already cleaned up of the transitory time intervals, while the velocity and acceleration signals are obtained directly in Matlab with a derivation operation. These signals looks consistent with each other: against a constant amplitude (but with increasing frequency), the speed increases linearly while the acceleration does it quadratically, as it's expected to be.

The trimming of the signals is visible in a graphs like:

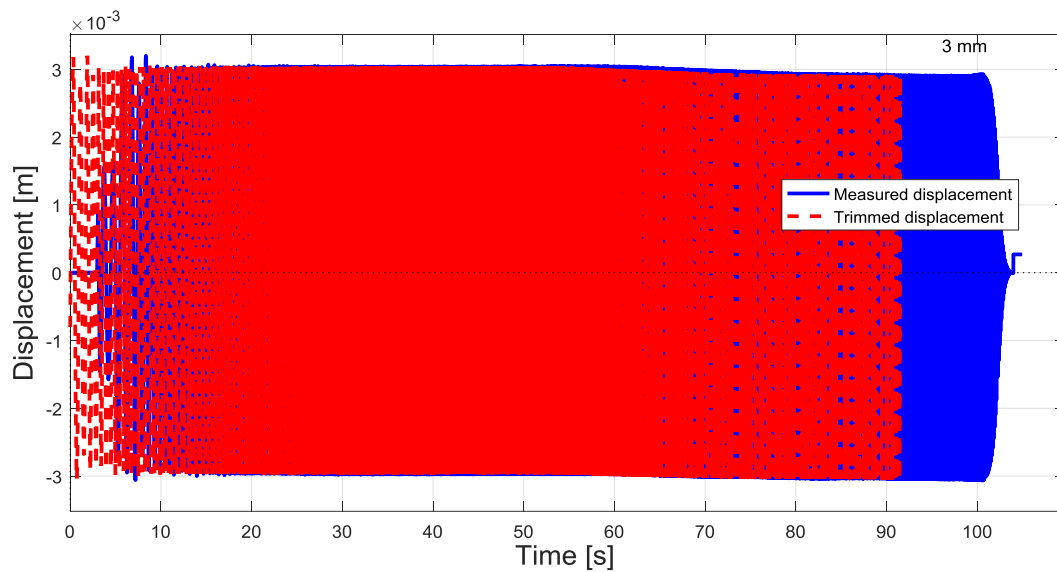


Figure 4.3.1.2 – An example of displacement signal trimming.

With a certain signal given in time it will be possible to deduce the envelope of it. Envelope signals are useful when comparison between signals become necessary and through them will be possible to make some consideration about the error (see, for example, Figure 4.2.5.3).

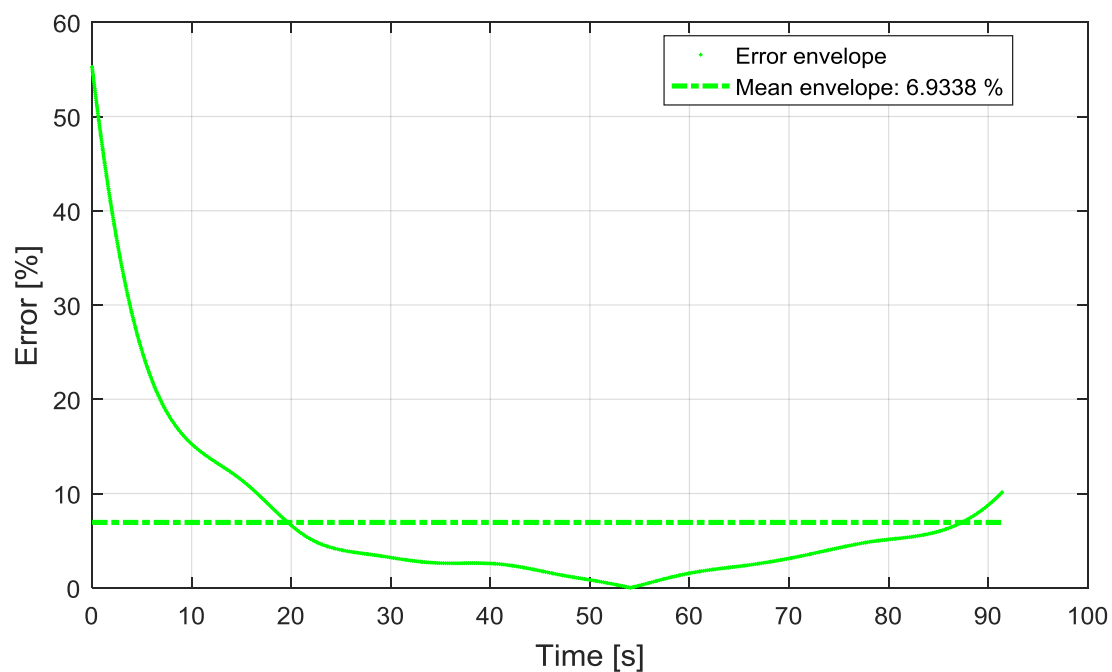


Figure 4.3.1.3 – An example of error evaluation between envelope signals.

Also a 3D plot can be obtained, as done in chapter 3:

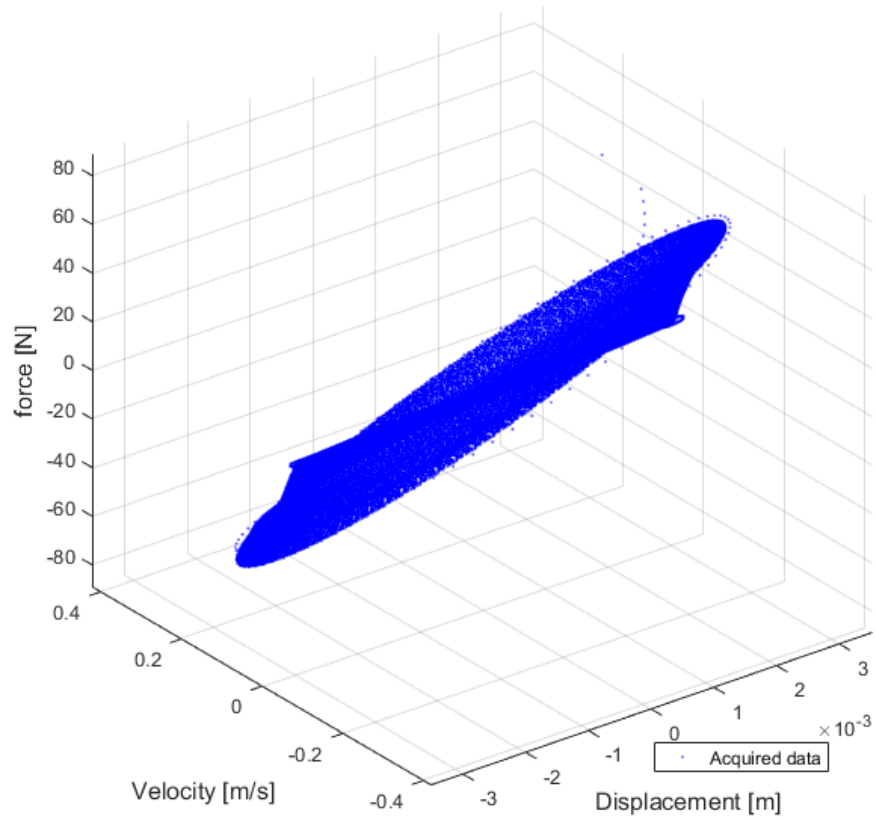


Figure 4.3.1.4 – 3D view of the obtained cloud of points in the state space.

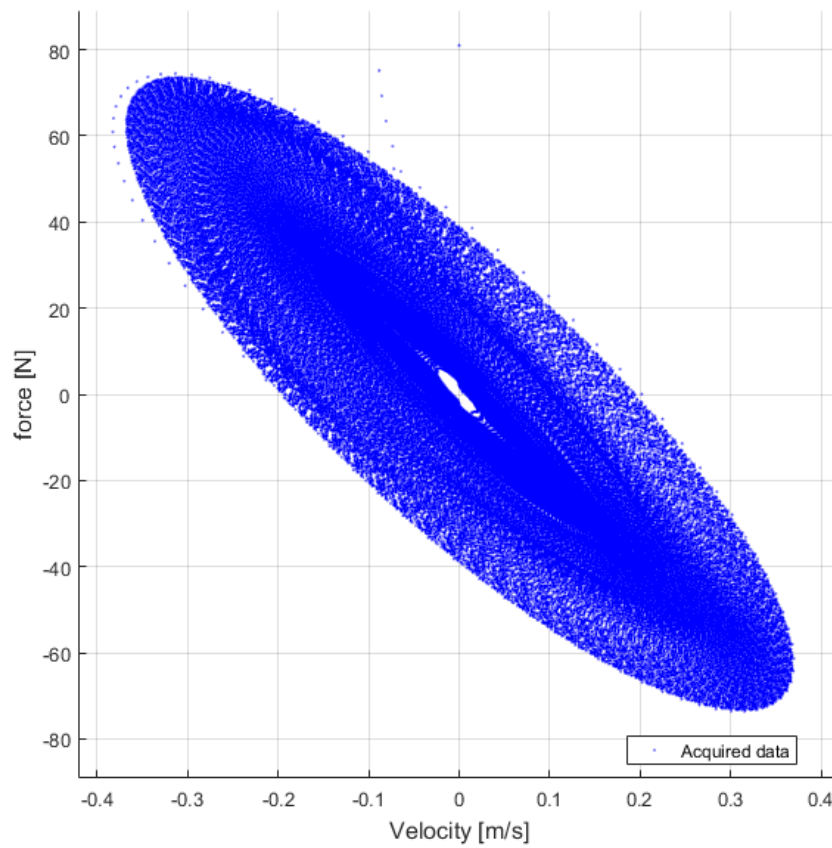


Figure 4.3.1.5 – Velocity-Force view of the obtained cloud of points in the state space.

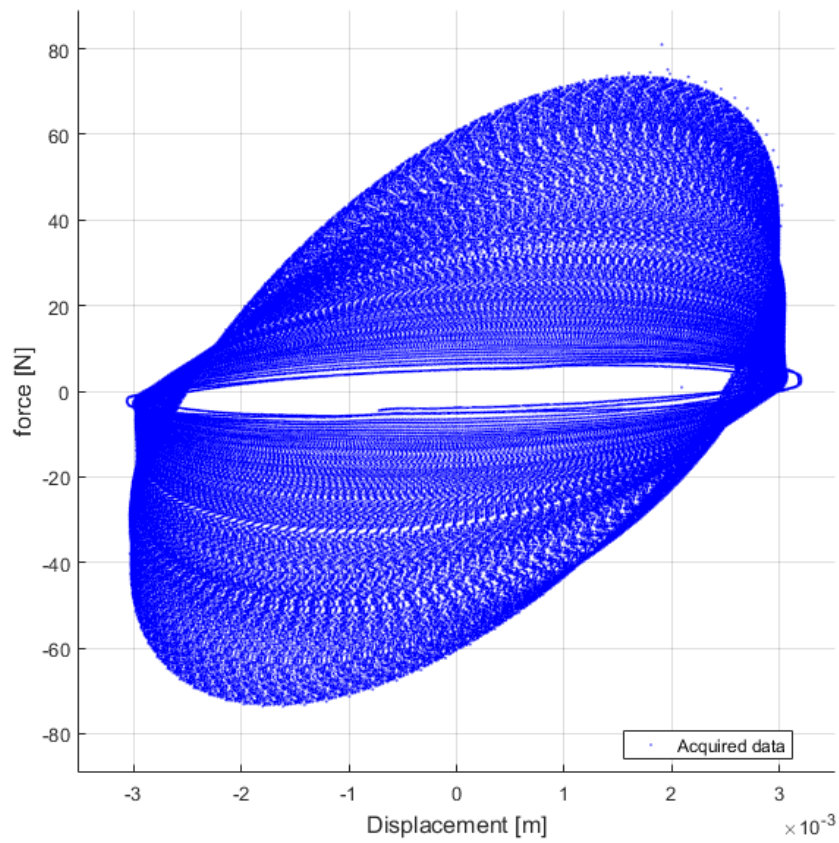


Figure 4.3.1.6 – Displacement-Force view of the obtained cloud of points in the state space.

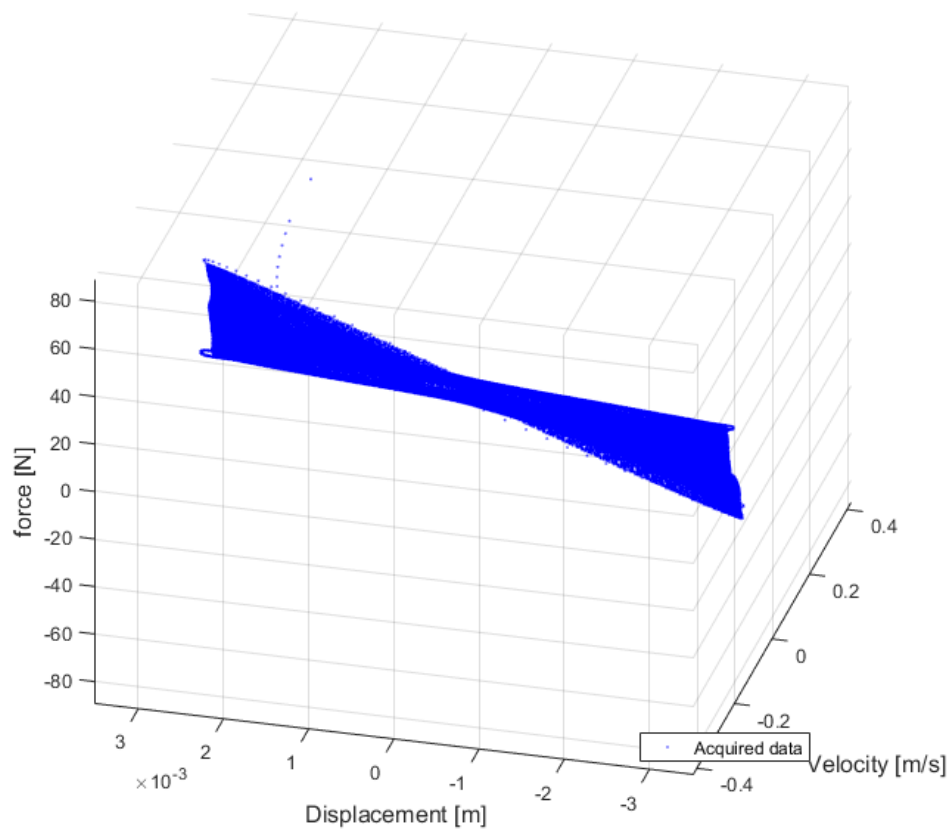


Figure 4.3.1.7 – Particular pitched view.

4.3.2 Model correction

Looking at Figure 4.3.1.7 is possible to notice that the solution is not unique for a given displacement and velocity. In some zones the shape bend over itself just as a Möbius surface^[b], it's possible to say that this is a not function in the considered domain. Shapes like this occur when some parameters are neglected in the model and in this particular case two heavy approximation have been done:

- Neglecting the mass of the system: this approximation was assumed in chapter 3.
- Neglecting the effect of the air gap: this technological aspect emerged when the assembly procedure has been addressed. The damper does not have a 'tank' system where to store the oil when the available volume in the cylinder change. It change when the stem is inserted cause of the stem volume itself. The oil is incompressible, so the air has to compensate this variable volume effect. So it is not possible to don't leave any air inside the cylinder, but otherwise is not possible to leave too much of it. It will be discovered that a right air quantity could be the one obtainable by closing the system when the stem is at the half of the run.

The probably presence of a 3rd and maybe also a 4th parameter of dependence will make definitively useless these 3D plots if not as an exercise in style. To make they representatively a not-existing 4D or 5D plots would be needed. For the evaluation of the possible good or bad quality of the assumed models will result more helpful to compare the acquired data and the regression in simple 2D graphs where the force is plotted with respect of the time.

The most interesting achievement is that the cloud's shape suggest a not displacement-dependant model (for the considered amplitude), while the last and most complete model supposed in the chapter 3 was, by recalling it:

$$(c_0 + c_1x + c_1x^2 + \dots + c_nx^n) \cdot \dot{x} = F(t) \quad (3.1.3.1)$$

(Refer to chapter 3 for the parameter explanation). The dependence by displacement was even polynomial.

Here the model look more velocity-dependant, so the first attempt is been to modify the model as:

$$c_1\dot{x} + c_2\dot{x}^2 + c_3\dot{x}^3 + \dots + c_n\dot{x}^n = F(t) \quad (4.3.2.1)$$

with a simply polynomial dependence by the velocity. But the mass contribution and the air effect are still neglected. So a more complex model has to be write:

$$m\ddot{x} + c_1\dot{x} + c_2\dot{x}^2 + c_3\dot{x}^3 + \dots + c_n\dot{x}^n + k_Ax_A = F(t) \quad (4.3.2.2)$$

Where:

- m [kg] is the involved mass, a constant;
- k_A [N/m] is the air stiffness that will be volume-dependant;
- x_A [m] is the displacement of the air-oil surface in the cylinder.

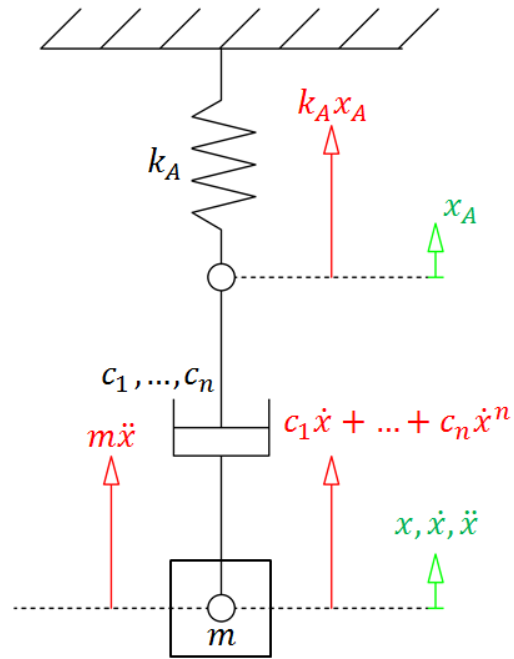


Figure 4.3.2.1 – New model scheme with force contribution and a new degree of freedom.

More accurate explanation about this model's contribution will follow.

4.3.3 Mass effect

If the inertial contribution want to be evaluate the moving parts mass involved has to be counted. Once this operation will be completed the result will be assumed as a constant. This involved a small approximation, all the oil mass will be considered as moved also if is known that it change with the displacement, but as it will possible to see the oil mass is greatness order smaller than the total, so it would not be useful to consider a variable mass model.

First of all the oil density has to be evaluate, since it was not declared by the manufacturer. A very important result is that the density seems don't change with the changing of oil viscosity, in fact from a first detection results, considering that an empty bottle weight is 16.9 g:

Table 4.4 – Oil bottle weight detection.

Oil bottle measured	Mass detected	Oil mass
WT 20	72.1 g	55.2 g
WT 50	72.1 g	55.2 g
WT 100	71.8 g	54.9 g

In fact on the bottle a weight of 2 Oz is declared, that corresponds to 56.7 g. The small variation of 0.3 g for WT 100 oil is considered as ordinary production error.

Once detected the oil weight is the same for all the gradation become possible an unique calculation for the density:

Table 4.5 – Oil density evaluation.

Total weight	72,1 g
Bottle weight	16,9 g
Oil weight	55,2 g
V_{bottle}	60726,2006 mm ³
Oil density	0,000908998 g/mm ³
	909,00 kg/m ³

The volume of the bottle was been assumed as:

$$V_{\text{bottle}} = \pi r^2 h \quad [\text{m}^3] \quad (4.3.3.1)$$

With $r = 33$ mm the internal radius and $h = 71$ mm the internal height.



Figure 4.3.3.1 – The oil bottle in a real photo (left), CAD model (centre) and drawing with useful quotas (right).

To finish the volume inside the damper cylinder has to be know so that through it the weight could be desumed by:

$$W_{oil,damper} = V_{oil,damper} \rho_{oil} \text{ [kg]} \quad (4.3.3.2)$$

Where ρ_{oil} is trivial the oil density evaluated in the previous steps. The $V_{oil,damper}$ is, instead, not the overall available volume inside the cylinder (that will be here called V_{cyl}), but the one occupied by the oil, so the remaining volume when also the one occupied by stem (V_{stem}) and by the piston (V_{pist}) are considered. So at the end will result:

$$V_{oil,damper} = V_{cyl} - V_{stem} - V_{pist} \text{ [m}^3\text{]} \quad (4.2.5.3)$$

Table 4.6 – Oil volume and weight evaluation.

Rear		Front	
V_{cyl}	28843,45 mm3	V_{cyl}	24506,09 mm3
V_{pist}	1301,21 mm3	V_{pist}	1301,21 mm3
V_{stem}	2559,22 mm3	V_{stem}	2174,37 mm3
$V_{oil,damper}$	24983,02 mm3	$V_{oil,damper}$	21030,51 mm3
Oil weight	22,71 g	Oil weight	19,12 g

As it is possible to notice a front-rear differentiation is necessary.

The oil is not the only mass contribution in the system but there are a lot of other moving components, in particular:

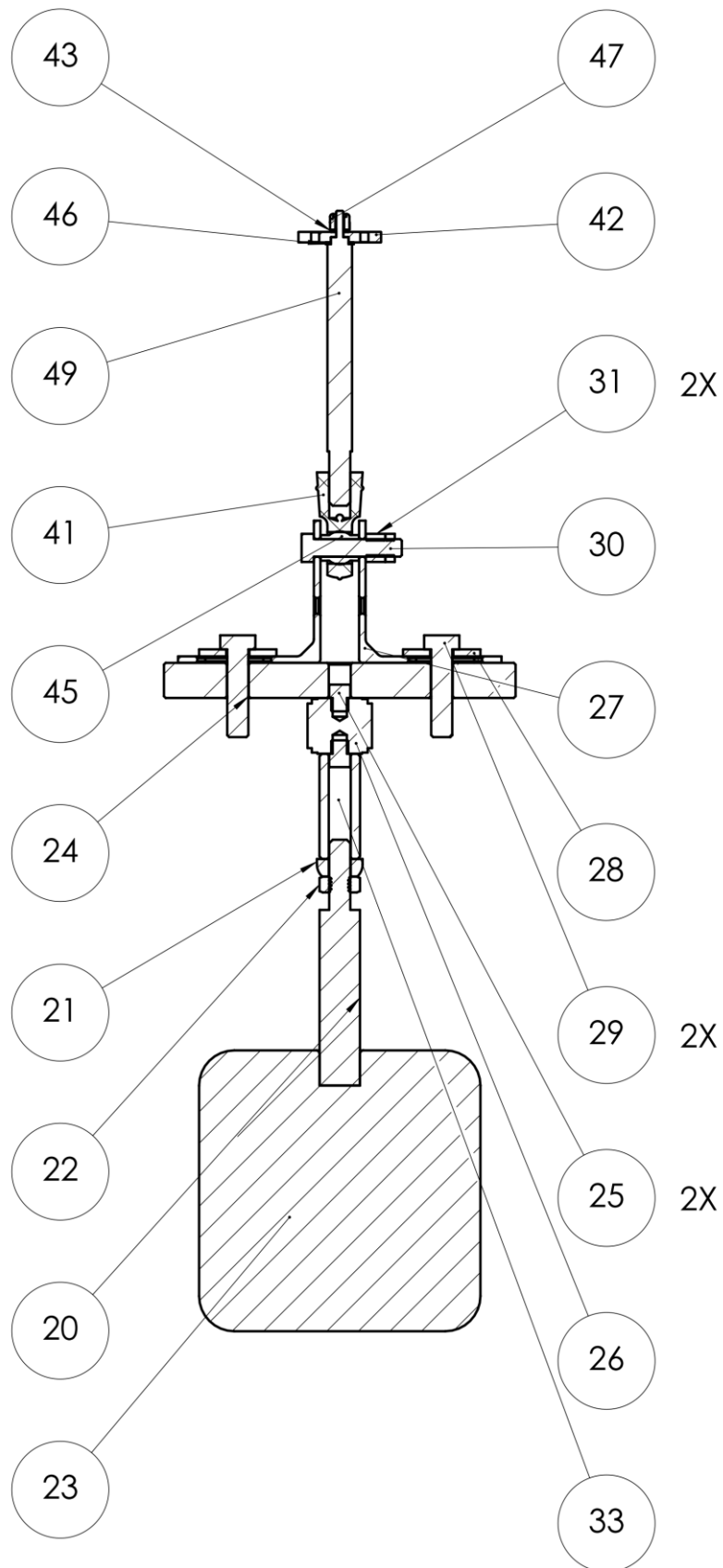


Figure 4.3.3.2 – Section view of the only-moving parts.

Table 4.8 – Weight of all the components.

Part number	Description	Rear	Front
		Mass [g]	Mass [g]
20-23	Inside shaker (with shaft)	450	450
22	M6 small nut	2,46	2,46
21	M6 squared nut	4,78	4,78
33	M6 long nut	13,02	13,02
26	Load cell	22,7	22,7
25	2x M6/10-32 adapter	2,76	2,76
24	Main stirrup	249,46	249,46
27	2x 'L' stirrup	29	29
29	2x M5 screw	7,6	7,6
28	2x M5 washer	6,4	6,4
31	2x M5 nut	2	2
45	M5 screw cross key	5,3	5,3
49-46-43-47	Stem (with washers and M2 bolt)	30	22,3
Not in drawing	Rubber cap	2,7	2,3
42	Piston	2,2	2,2
45	Spheric joint	2,4	2,4
Not in drawing	Oil	22,71	19,12
TOTAL		855,49 g	843,80 g
		0,8555 kg	0,8438 kg

As it is possible to notice the largest contribution becoming by the mass moved in the electromagnetic shaker (in Figure 4.3.3.2 a pure schematic representation is reported) and by the main stirrup, but all together the other components make up the ~20% of the weight that is important to not neglect.

In the following images a 'regression force' signal appears, is now not important to understand how it is obtained because the objective is only to show the effect of the mass introduction. In chapter 4.4.2 will be explained how the regression signal is obtain but the procedure is not so far from what already done in chapter 3.

From the point of view of results the mass has a great effect, as these graphs telling:

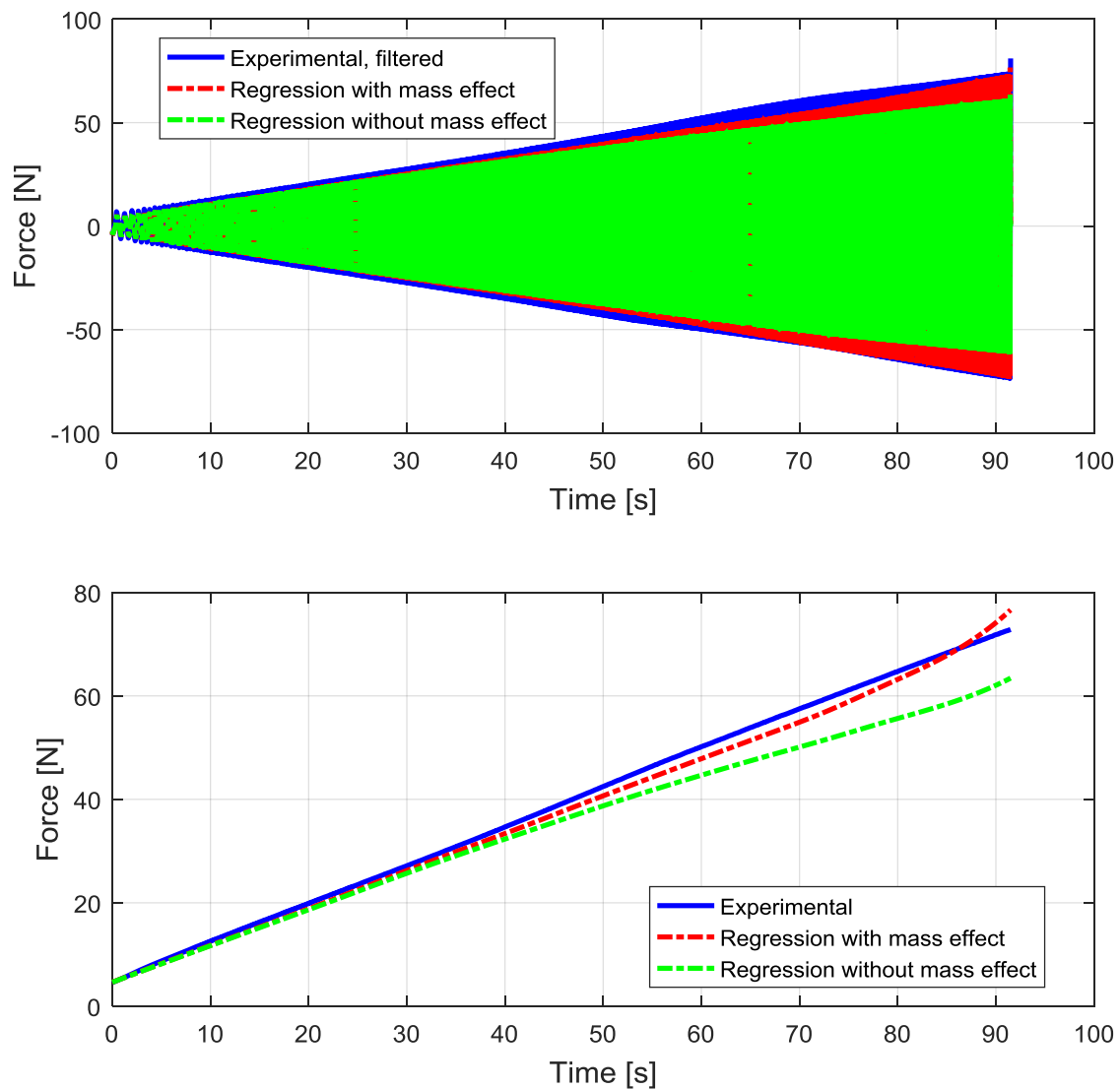


Figure 4.3.3.3 – History force-time point-by-point (up) and the corresponding envelopes (down).

Looking at Figure 4.3.3.3 is possible to notice how the mass has a larger effect for high values of time that, thinking at how the system is excited, suggest that this occur for the highest values of frequency and so also for the highest values of velocity and acceleration.

The same improvement effect can be see if the errors are evaluated:

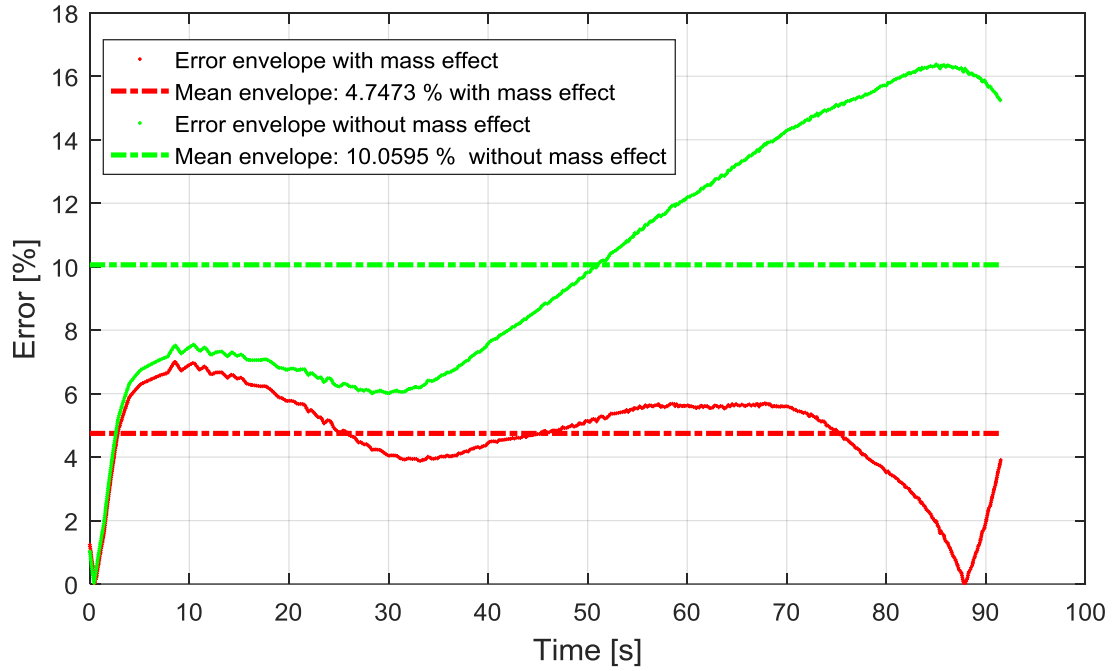


Figure 4.3.3.4 – Error comparison between the case with mass effect not considered (green) and when considered (red).

It's clear, looking at Figure 4.3.3.4 that the mass introduction has greatly reduced the error especially for the higher frequencies. Notice also that at a certain time the error reach a value near to zero and later start growing up again: it's sufficient to looking at Figure 4.3.3.3 (envelopes) to understand that this point is the same of the envelopes coincidence, indeed the error is always evaluated as:

$$error = \frac{|force_{restoring} - force_{regression}|}{force_{restoring}} \cdot 100 \quad [\%] \quad (4.3.3.3)$$

It is implied that all signals are envelopes.

4.3.4 Air effect

As mentioned in chapter 4.3.2 an air gap effect has to be explored. When the damper assembly procedure was known the impossibility to avoid air inside the cylinder was discovered. On the contrary this trapped air has an important technological function: compensate the volume variation due to the stem introduction into the cylinder chamber.

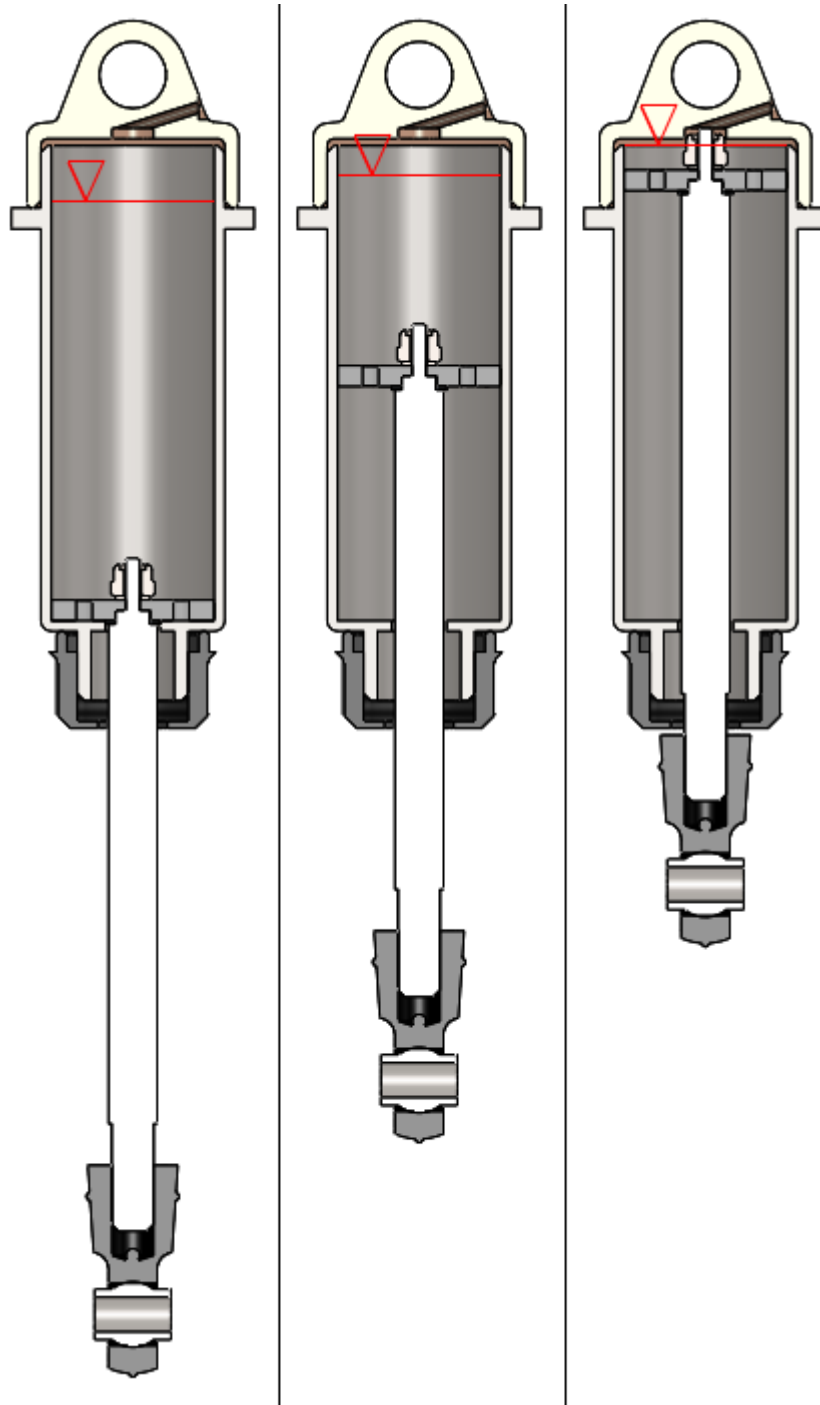


Figure 4.3.4.1 – Three possible position of the stem and schematic representation of the oil-air surface.

Looking at Figure 4.3.4.1 the problem become more clear: when the system is closed at the end of the assembly procedure (central figure) the stem is at the half of the possible run. A certain air quantity is inside the cylinder: at this time the screw is bolted in the breathing hole and no air or oil can anymore entry or exit. On the left the situation with the stem totally out of the cylinder: in this situation the air volume is at his maximum value and so the pressure is lower than the nominal condition (~ 1 atm) and the air entrapped must be enough to not make an impossible negative pressure because if this value of pressure is reached the stem will not be able to end his run and will result blocked. On the right the opposite situation with the stem totally inserted: in this case the air volume is at his minimum so the pressure goes to higher values, also in this case the air has to be enough because if the pressure goes to too high values the stem will not again be able to end his run. In both cases the air pressure effect is to carry the piston back to his equilibrium position. Also a maximum air quantity threshold will exist: if a too large volume of air is entrapped, when the ‘totally inserted stem’ situation will occur, the piston will not be any more immersed in oil and the damping effect will disappear for some trice, with catastrophic consequences when it re-impact with the oil surface.

What is researched here is the effect of the air as a spring which act in series with the damping returned by the oil. From an analytic point of view the force due to the air stiffness can be written as:

$$F_{air} = k_A (x - x_a) \quad [\text{N}] \quad (4.3.4.1)$$

Where:

- k_A [N/m] is the air stiffness;
- x [m] is the displacement of the piston (the same of the stem);
- x_a [m] is the displacement of the air-oil surface.
-

While there is obviously a relation between the position of the stem and the position of the air surface, which determine also the air volume. This relation is convenient because the position of the stem is exactly the same position that is measured by the laser.

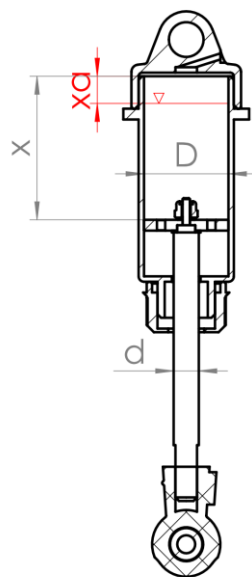


Figure 4.3.4.2 – Reference scheme for displacements and diameters.

It's not so difficult to understand that air volume reduce himself of the same quantity of stem volume that entry in the cylinder. Equating the two volume variations is possible to obtain a direct relations between x and x_A :

$$\Delta V_{stem} = \Delta V_{air} \quad [\text{m}^3] \quad (4.3.4.2)$$

Exploring it:

$$\pi \left(\frac{d_{stem}}{2} \right)^2 \cdot \Delta x = \pi \left(\frac{d_{cylinder}}{2} \right)^2 \cdot \Delta x_A \quad [\text{m}^3]$$

$$\Delta x_A = \frac{\pi}{\pi} \frac{4}{4} \left(\frac{d_{stem}}{d_{cylinder}} \right)^2 \cdot \Delta x \quad [\text{m}]$$

$$\Delta x_A = \left(\frac{d_{stem}}{d_{cylinder}} \right)^2 \cdot \Delta x \quad [\text{m}]$$

And finally, referring to the same reference system (same x_0) and with $x_0=0$ is possible to write:

$$x_0 - x_A = \left(\frac{d_{stem}}{d_{cylinder}} \right)^2 \cdot (x_0 - x) \quad [\text{m}]$$

$$x_A = \left(\frac{d_{stem}}{d_{cylinder}} \right)^2 \cdot x \quad [\text{m}] \quad (4.2.6.3)$$

The (4.3.4.3) highlight how the relations between x_A and x is simply linear and that the proportional factor only depend on geometric parameters (diameters of the stem and of the cylinder). But pay attention: the (4.2.6.3) only express the relation between the modulus of the oscillation, in fact the air gap displacement will be characterized by a certain phase delay with respect to the displacement due to the inertia of the air to change his temperature condition. So by passing to a vector notation will result more correct to rewrite the (4.2.6.3) as:

$$\{x_{0A}\} = \left(\frac{d_{stem}}{d_{cylinder}} \right)^2 \cdot \{x_0\} \quad [\text{m}] \quad (4.2.6.4)$$

While the direct relation between $\{x_A\}$ and $\{x_0\}$ has to be written as:

$$\{x_A\} = \{x_{0A}\} \cdot \text{sen} \left(\{\omega t\} - \frac{\pi}{2} - \{\phi\} \right) \quad [\text{m}] \quad (4.2.6.5)$$

And substituting the (4.2.6.4) in the (4.2.6.5):

$$\{x_A\} = \left(\frac{d_{stem}}{d_{cylinder}} \right)^2 \cdot \{x_0\} \cdot \text{sen} \left(\{\omega t\} - \frac{\pi}{2} - \{\varphi\} \right) \quad [\text{m}] \quad (4.2.6.6)$$

Where:

- $\{x_0\}$ [m]: stem displacement amplitude vector, envelope of the measured position in time by the laser.
- $\{\omega\}$ [rad/s]: frequency of excitation.
- $\{\varphi\}$ [rad]: phase angle.

The phase angle $\{\varphi\}$ is the same that characterize the force $\{F\}$, so it can simply be assumed as:

$$\{\varphi\} = \arctan \frac{\text{Im}(\{F\})}{\text{Re}(\{F\})} \quad [\text{rad}] \quad (4.2.6.7)$$

While the frequency in [rad/s] is simply deducible from the correspondent values in [Hz], $\{f\}$, as:

$$\{\omega\} = 2\pi \cdot \{f\} \quad [\text{rad}] \quad (4.2.6.8)$$

So by substituting the (4.2.6.7) and the (4.2.6.8) in the (4.2.6.6) the definitive analytic relation between $\{x_A\}$ and $\{x_0\}$ can be obtained as:

$$\{x_A\} = \left(\frac{d_{stem}}{d_{cylinder}} \right)^2 \cdot \{x_0\} \cdot \text{sen} \left(2\pi \cdot \{f\} - \frac{\pi}{2} - \arctan \frac{\text{Im}(\{F\})}{\text{Re}(\{F\})} \right) \quad [\text{m}] \quad (4.2.6.9)$$

And as it is possible to see depends only on parameters known or measured during the test.

Also an analytic solution for k_A could be explored but first it is necessary to highlight a big problem: the *temperature dependence* of k_A . During the test the temperature will change his value so a continuous monitoring will be necessary, with non-negligible technological complications: the temperature sensor would be inside the damper, and this is already a big problem if the total number of dampers is considered (for each of them at least one hole should be made with the subsequent sealing problem), but even considering the temperature sensor installed, who could guarantee that the revealed temperature is the one of the air and not the one of the oil? Or who could guarantee the temperature sensor is not affected by the temperature of the metallic parts of cylinder? For all this reasons it's been decided to neglect this analytic approach and to deduce the air stiffness exactly in the same way the other parameters (damping ones) will be: to do it is always needed the (4.2.6.9).

How important is the considered air effect when associated with the characteristic displacements of this problem? In reality it is very small, at least negligible, as is possible to see looking at:

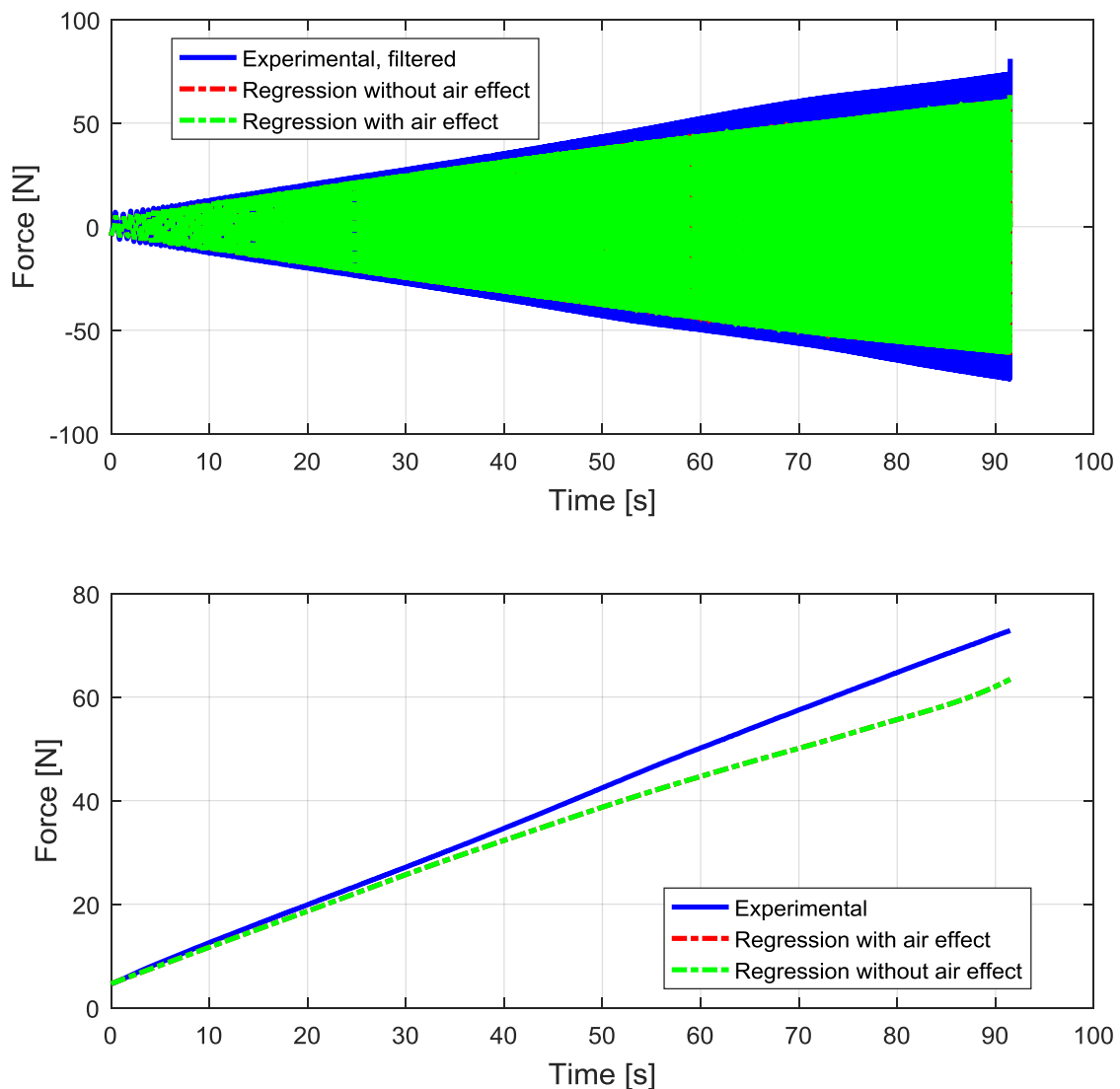


Figure 4.3.4.3 – History force-time point-by-point (up) and the corresponding envelopes (down).

Looking at Figure 4.2.6.3 is not possible to see the difference between the trail of the two cases, to see it is necessary to widely zoom-in the figure. To have a numeric evaluation is possible to see how the error behaves:

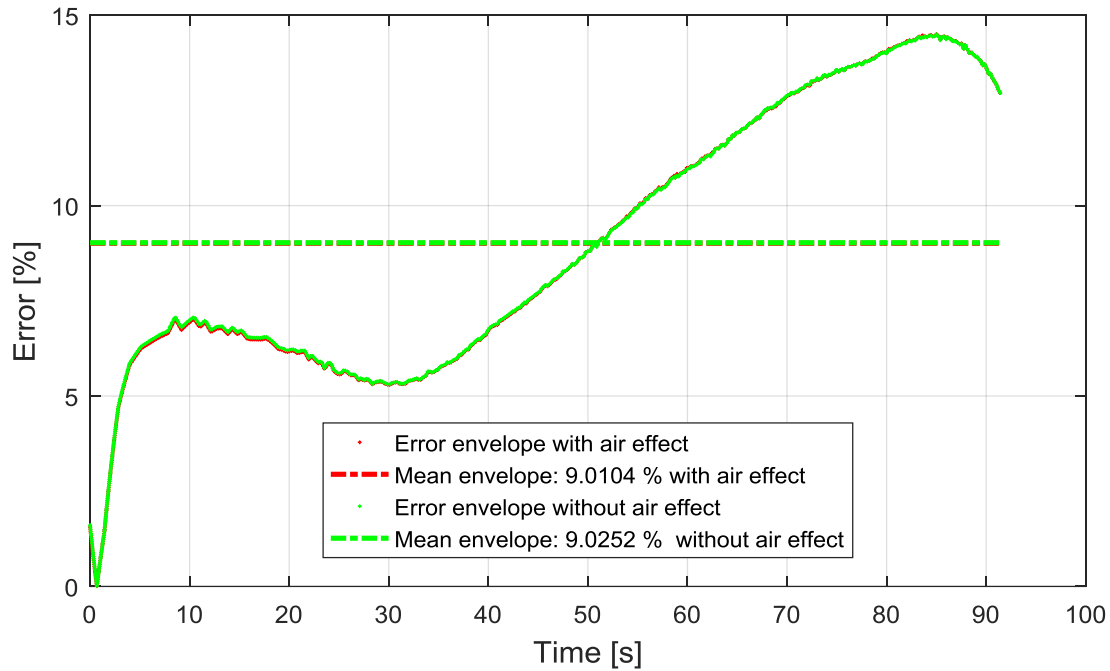


Figure 4.3.4.4 – Error comparison between the case with air effect not considered (green) and when considered (red).

Reading in the legend of Figure 4.2.6.4 become clear that the realized improvement by considering the air effect is really small, in percentage terms it is two greatness order smaller than the error. This means that remembering the two approximation done and firstly explained in chapter 4.2.4 only the mass effect has a relevant weight in terms of force: this is due to the small displacement realized in the operative condition analyzed, moreover also by operating simply manual test on the damper look clear that the effect of the air become tangible only in the final parts of the stem run, while near the equilibrium point and for almost an half length of the available run this effect is too small to be felt: maybe it is even smaller than the static friction force.

This is also visible if the obtained regression value for k_A is considered:

$$k_A \cong 30 \frac{\text{N}}{\text{m}}$$

Also by taking the maximum displacement realized (3 mm) the resulting air-oil surface displacement is, recalling the (4.2.6.4):

$$x_{0A} = \left(\frac{d_{stem}}{d_{cylinder}} \right)^2 \cdot x_0 = \left(\frac{7}{23.5} \right)^2 \cdot 3 \cong 0.266 \text{ mm}$$

And so the maximum force contribution result:

$$F_{k_A} = k_A x_{0A} = 30 \cdot 0.266 \cdot 10^{-3} = 0.00798 \text{ N}$$

When the force range of interest is resulting to be from 20 N to 100 N. For this reasons the air effect will be not considered anymore. But also considering a very high air stiffness value (under the hypothesis the regression one is underestimate) as:

$$k_A \cong 2000 \frac{\text{N}}{\text{m}}$$

The resulting maximum force contribution will be of the equally negligible value of:

$$F_{k_A} \cong 0.5 \text{ N}$$

4.4 Postprocessing and results

4.4.1 Signal filtering

As often happens the original acquisition signals are affected by a certain quantity of noise. This noise could seem small and negligible but, especially when the data has to be used as basis for derivative greatnesses, as happens in this particular case, produce larger and larger error each time the data is some way processed.

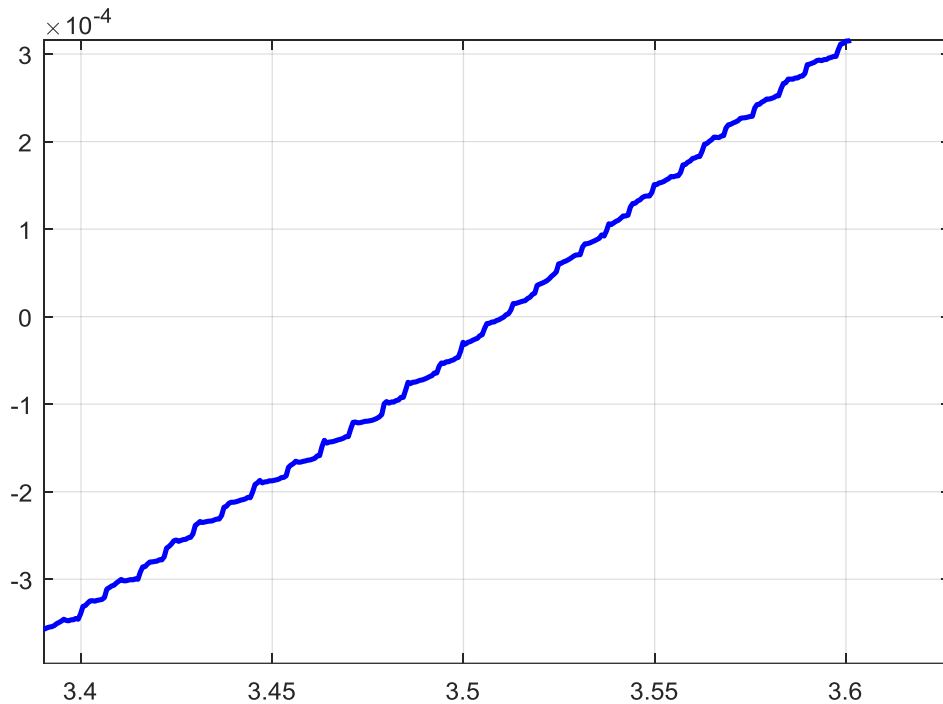


Figure 4.4.1.1 – A zoomed view of one side of sinusoidal displacement signal. Noise crests are visible.

But the worst effect is visible when the original signal with noise (the displacement) is visualized in the same interval with his first derivative (velocity) and the second one (acceleration), remembering that \dot{x} and \ddot{x} are both used in the chosen model:

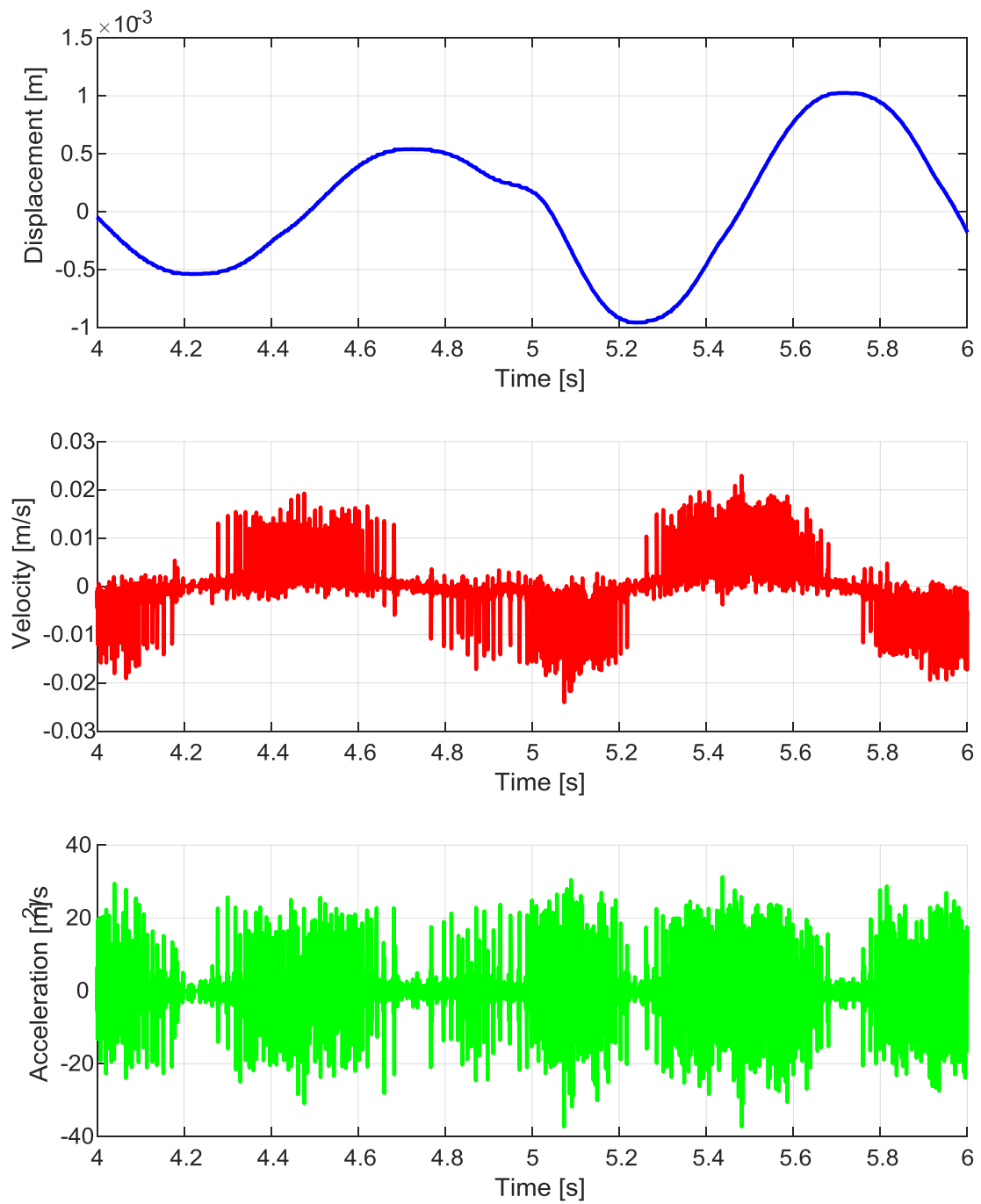


Figure 4.4.1.2 – Noised displacement, velocity and acceleration in a restricted time interval. The noise effect increase with successive derivations.

The noise entities can be also evaluated looking at an FFT diagram:

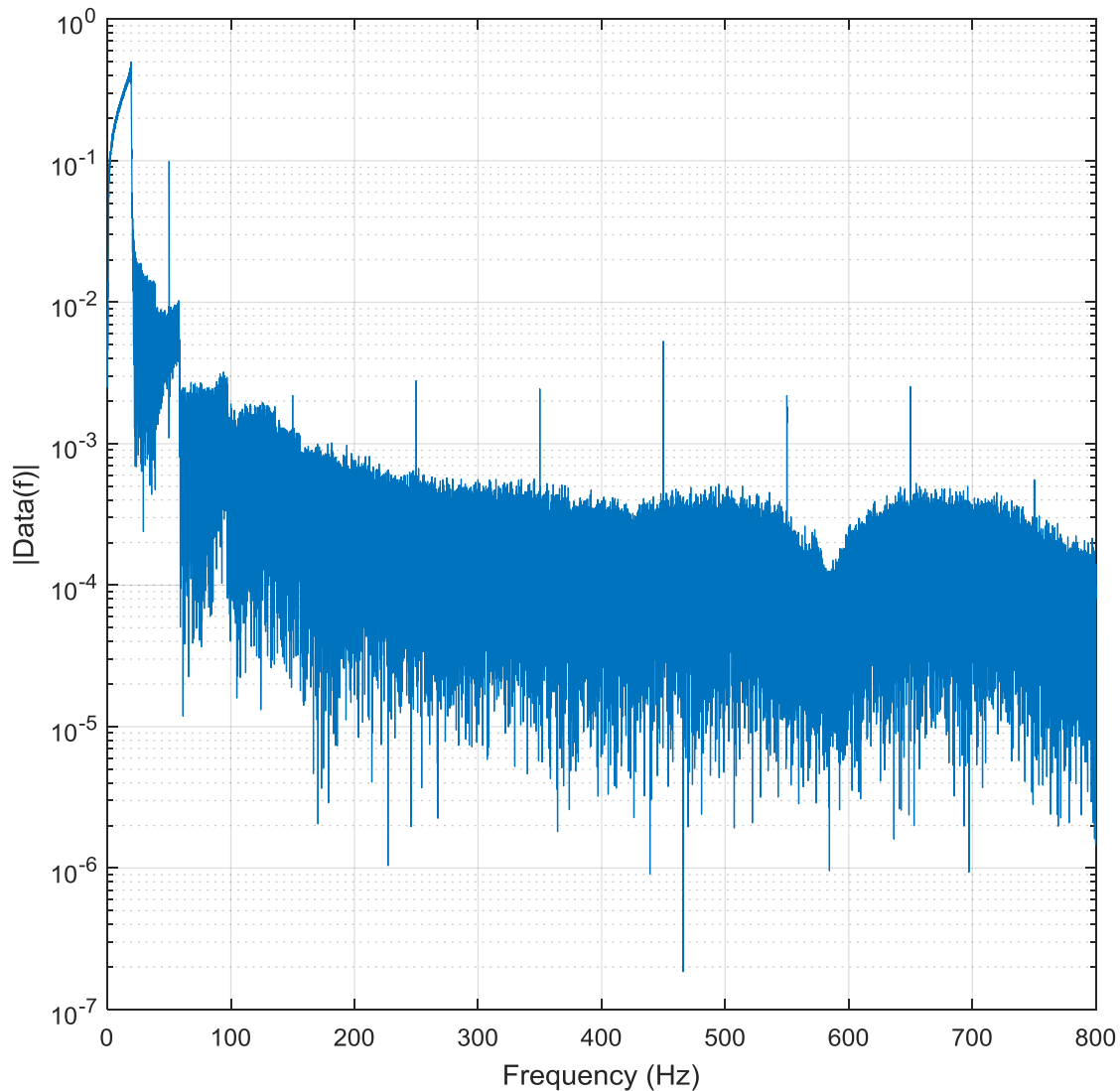


Figure 4.4.1.3 – FFT diagram for the original acquisition data.

Looking at Figure 4.3.1.3 is possible to see that in the range 0-20 Hz a quite regular function is present and it is expected to be like this, because this is the characteristic exciting range of the test. The problem are the other peaks (8 of it are immediately visible), the first and most important is visible at 50 Hz (electricity network frequency) and is almost to understand that everything over 30÷40 Hz does nothing but dirty the signal and is of no interest.

The solution is to build a *lowpass filter* which has to silence all the frequencies above a certain chosen threshold. This threshold value can be choice with reasonable goodness in the frequency interval so describe:

$$\max(\text{excitation range}) < \text{threshold} < \text{electricity network frequency}$$

That means:

$$20 \text{ Hz} < \text{threshold} < 50 \text{ Hz}$$

And it's been here chosen:

$$\text{threshold} = 30 \text{ Hz}$$

Remember: this operation is possible due only thanks to the 1600 Hz sampling rate chosen, chapter 4.2.3. If the original signal is not well sampled there is a the real risk of subsampling the result.

Matlab is equipped with a large number of instrument to build an efficient filter, in this particular case is possible to see the designed filter in a diagram like:

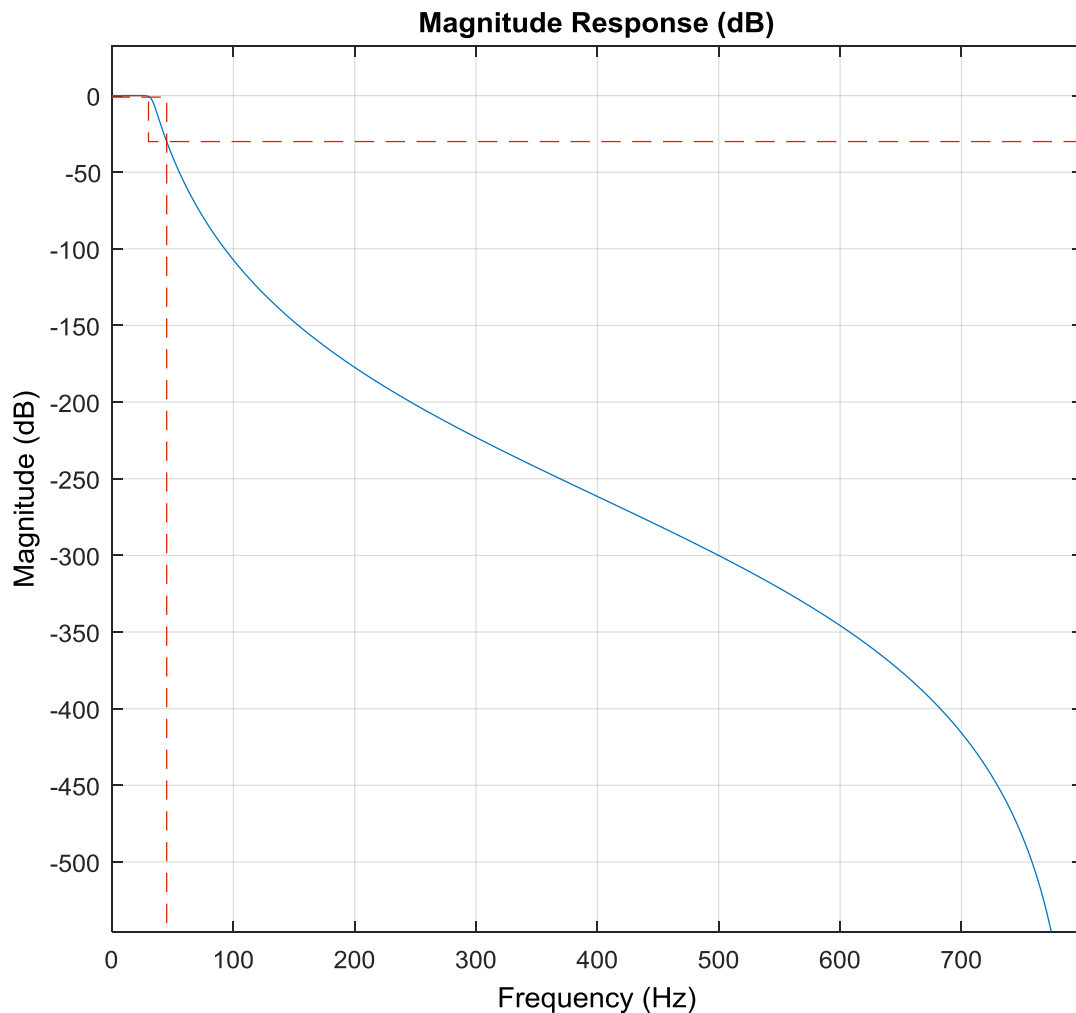


Figure 4.4.1.4 – Filter visualization.

Looking at Figure 4.4.1.4 the filter is visualized, the blue line indicate how much the signal is attenuated at the correspondent frequency. The magnitude is a value given in dB.

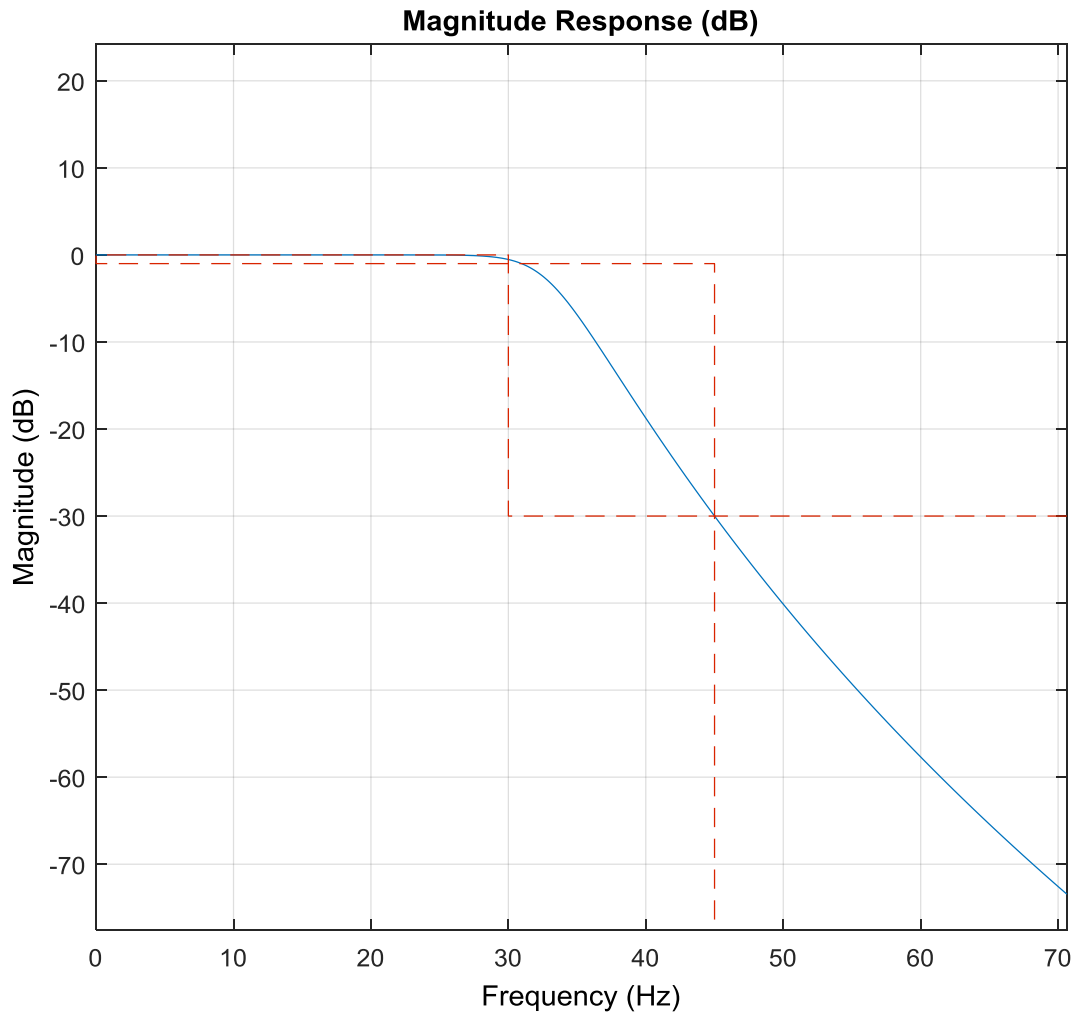


Figure 4.4.1.5 – Zoom in on Figure 4.4.1.4 in the interesting range.

The red dotted lines highlight the frequency interval where the attenuation begin (30 Hz) and the frequency where to refer the given decay value (45 Hz). So this diagram has to be read as “start silencing from 30 Hz onwards so that at 45 Hz at least a 30 dB decay was made”. Indeed is possible to notice that before the 30 Hz line a 0 dB decay is imposed. By this method at the previous annoying frequency of 50 Hz a 40 dB decay is imposed.

To evaluate if this chosen decay value is good enough will be sufficient to compare the previous noised signal with the filtered one:

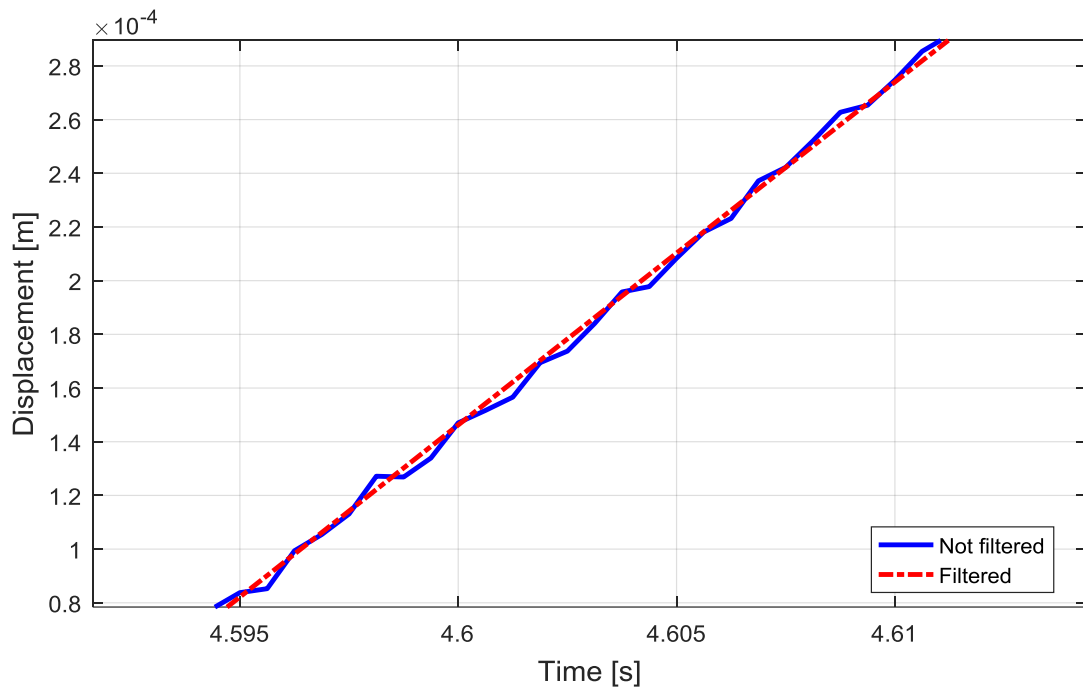


Figure 4.4.1.6 – Filtering effect on the displacement signal.

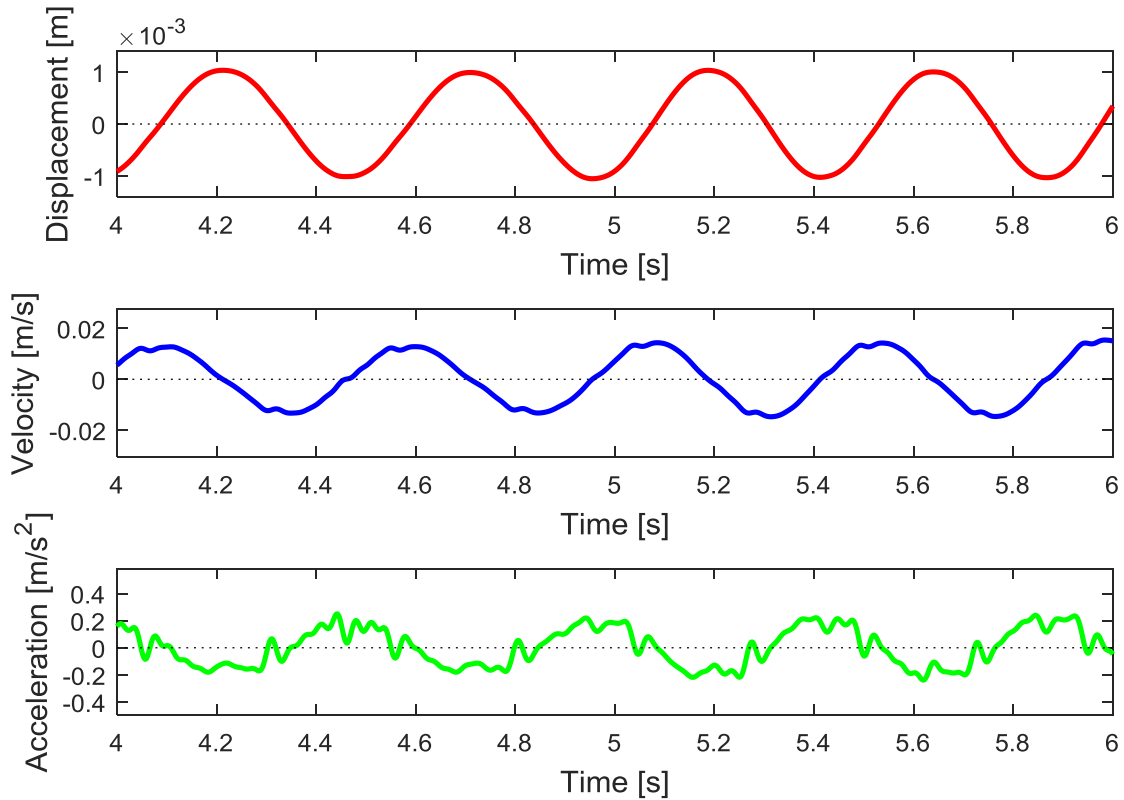


Figure 4.4.1.7 – Filtering have been a large impact on the quality of derivative signals.

4.4.2 Regression

As mentioned in chapter 4.3.2 the most complete model should have to be:

$$m\ddot{x} + c_1\dot{x} + c_2\dot{x}^2 + c_3\dot{x}^3 + \dots + c_n\dot{x}^n + k_A x_A = F(t) \quad (4.3.2.2)$$

But as established in chapter 4.2.6 the air effect can be neglected and so the model reduce to:

$$m\ddot{x} + c_1\dot{x} + c_2\dot{x}^2 + c_3\dot{x}^3 + \dots + c_n\dot{x}^n = F(t) \quad (4.4.2.1)$$

And by passing to a vector notation:

$$m\{\ddot{x}\} + c_1\{\dot{x}\} + c_2\{\dot{x}\}^2 + c_3\{\dot{x}\}^3 + \dots + c_n\{\dot{x}\}^n = \{F(t)\} \quad (4.4.2.2)$$

Or in a more convenient notation:

$$m\ddot{\mathbf{x}} + c_1\dot{\mathbf{x}} + c_2\dot{\mathbf{x}}^2 + c_3\dot{\mathbf{x}}^3 + \dots + c_n\dot{\mathbf{x}}^n = \mathbf{F}(\mathbf{t}) \quad (4.4.2.3)$$

In order to proceed to the regression the (4.4.2.3) has to be rewritten as:

$$\mathbf{F}_{\text{res}}(\mathbf{t}) - m\ddot{\mathbf{x}} = c_1\dot{\mathbf{x}} + c_2\dot{\mathbf{x}}^2 + c_3\dot{\mathbf{x}}^3 + \dots + c_n\dot{\mathbf{x}}^n \quad (4.4.2.4)$$

Where is implicit that the passage from the generic $\mathbf{F}(\mathbf{t})$ to the *restoring force* $\mathbf{F}_{\text{res}}(\mathbf{t})$ resulting from the test run is been done. Obviously also the $\dot{\mathbf{x}}$ and $\ddot{\mathbf{x}}$ is assumed to be the experimental ones, while the mass m has to be considered (as well explained in chapter 4.3.3) differently between the front damper case to the rear one. Once the restoring force is been purged by the inertial contribution will be possible to proceed to the regression for the damping parameters by writing:

$$\mathbf{F}_{\text{res}}(\mathbf{t}) - m\ddot{\mathbf{x}} = \begin{bmatrix} \dot{\mathbf{x}} & \dot{\mathbf{x}}^2 & \dot{\mathbf{x}}^3 & \dots & \dot{\mathbf{x}}^n \end{bmatrix} \begin{Bmatrix} c_1 \\ c_2 \\ c_3 \\ \vdots \\ c_n \end{Bmatrix} \quad (4.4.2.5)$$

And by calling:

- $\begin{bmatrix} \dot{\mathbf{x}} & \dot{\mathbf{x}}^2 & \dot{\mathbf{x}}^3 & \dots & \dot{\mathbf{x}}^n \end{bmatrix} = \mathbf{A}$
- $\begin{bmatrix} c_1 & c_2 & c_3 & \dots & c_n \end{bmatrix}^T = \mathbf{C}$

Is possible to rewrite it as:

$$\mathbf{A} \cdot \mathbf{C} = \mathbf{F}_{\text{res}}(\mathbf{t}) - m\ddot{\mathbf{x}} \quad (4.4.2.6)$$

Finally^[8] is possible to deduce an expression for \mathbf{C} as:

$$\mathbf{C} = \mathbf{A}^{-1}(\mathbf{F}_{\text{res}}(\mathbf{t}) - m\ddot{\mathbf{x}}) \quad (4.4.2.7)$$

Once the vector of damping factors is been obtained is possible to rebuild the *regression force* as:

$$\mathbf{F}_{\text{regression}}(\mathbf{t}) = m\ddot{\mathbf{x}} + c_1\dot{\mathbf{x}} + c_2\dot{\mathbf{x}}^2 + c_3\dot{\mathbf{x}}^3 + \dots + c_n\dot{\mathbf{x}}^n \quad (4.4.2.8)$$

by obviously using as $\dot{\mathbf{x}}$ and $\ddot{\mathbf{x}}$ the experimental ones in order to compare the restoring force to the regression one.

The difference between the two shapes is visible in a point-by-point graphs or also in an envelopes one:

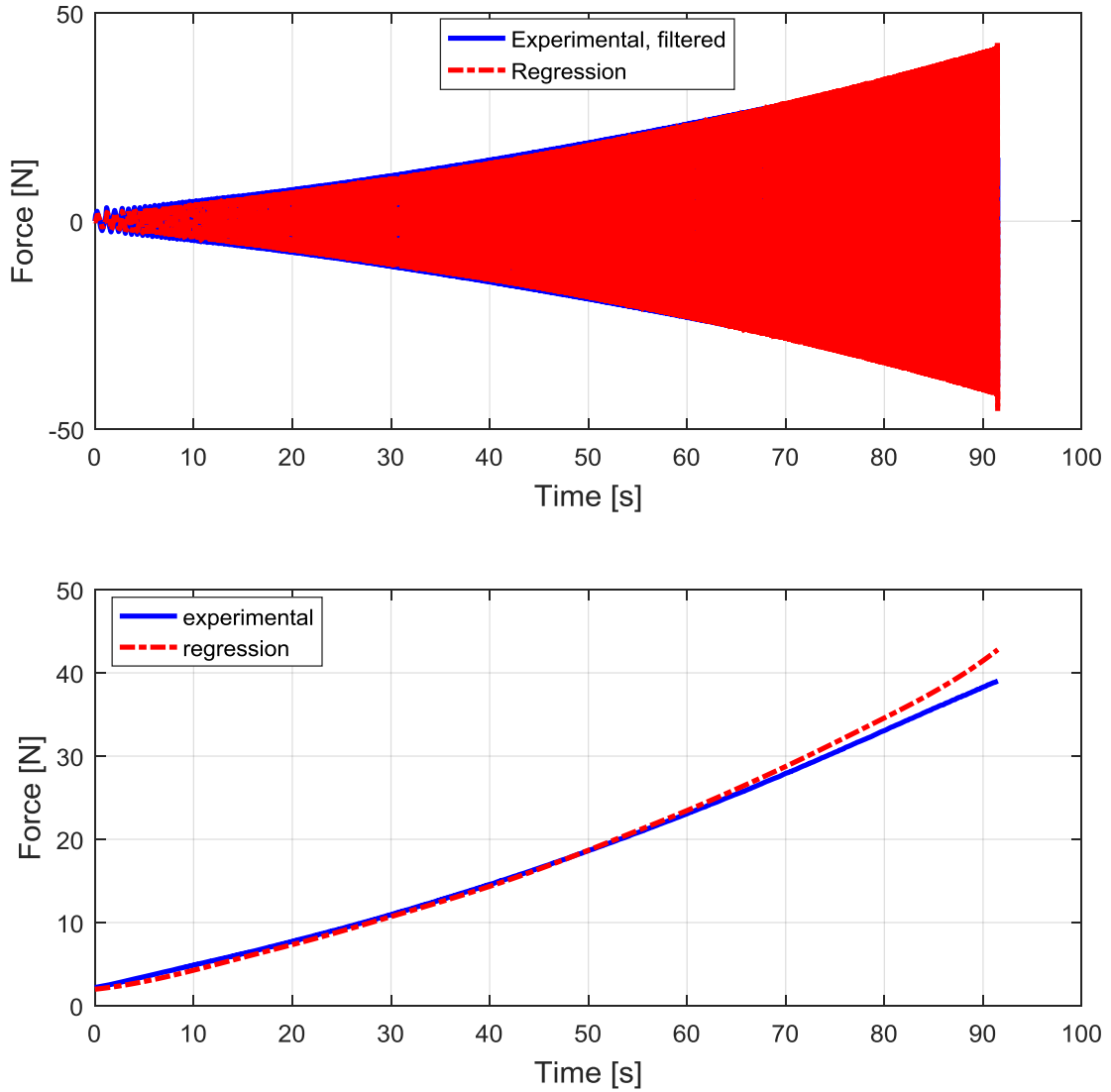


Figure 4.4.2.1 – Point-by-point comparison (up) and envelopes one (down).

Is also possible to visualize the correctness of the envelopes by superposing them to the correspondent force trace:

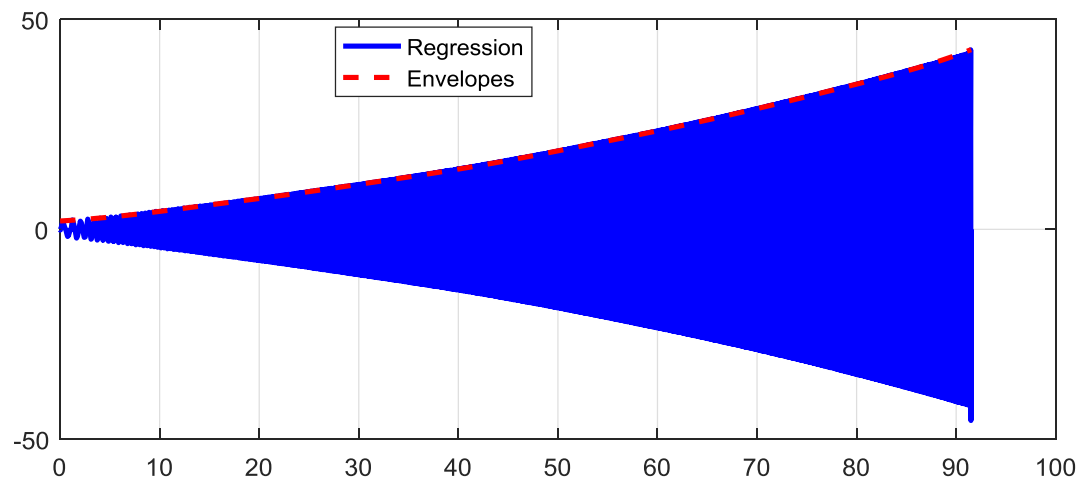
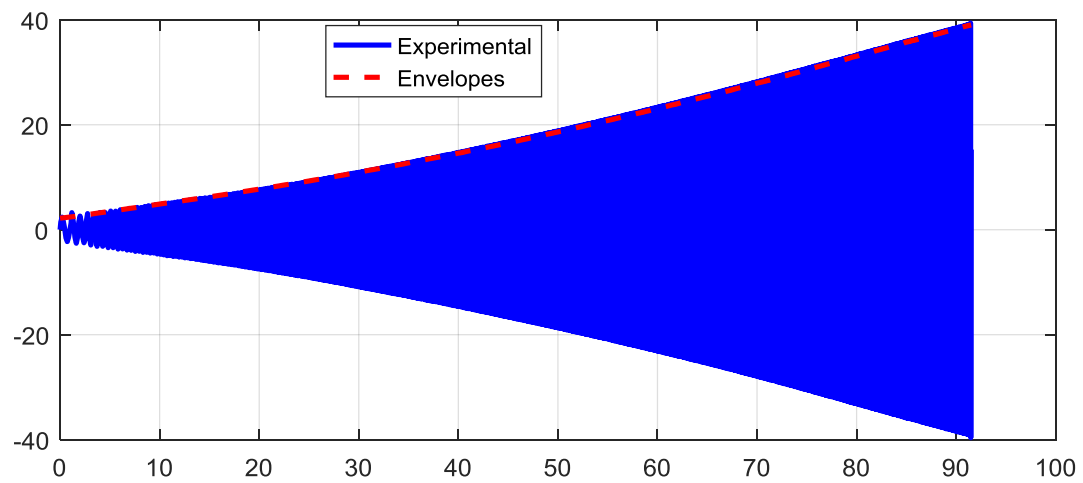


Figure 4.4.2.2 – Superposition of the envelopes with the forces generating themselves.

On the base of the envelopes the error can be estimated and visualized in a graph as:

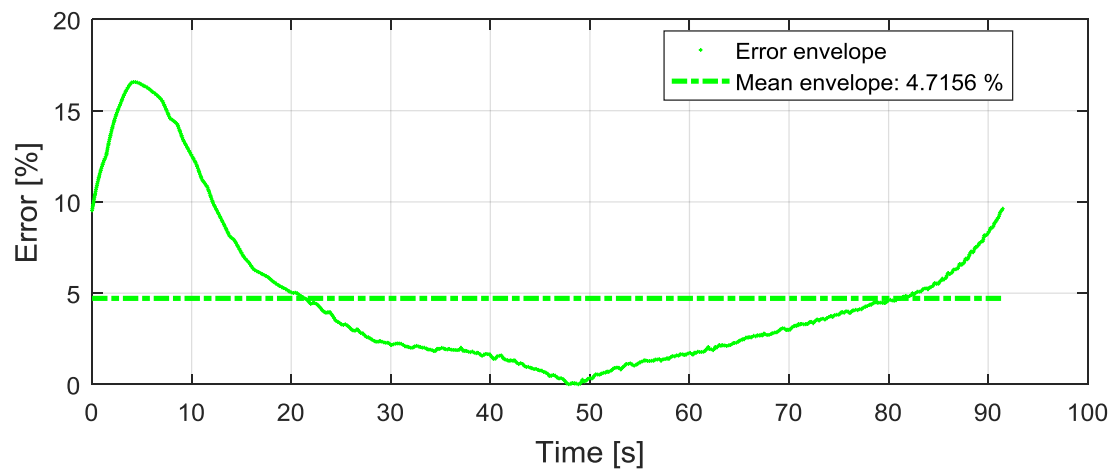


Figure 4.4.2.3 – The error evaluated on the envelopes.

In order to check that the original signals was been well trimmed is possible to plot something like:

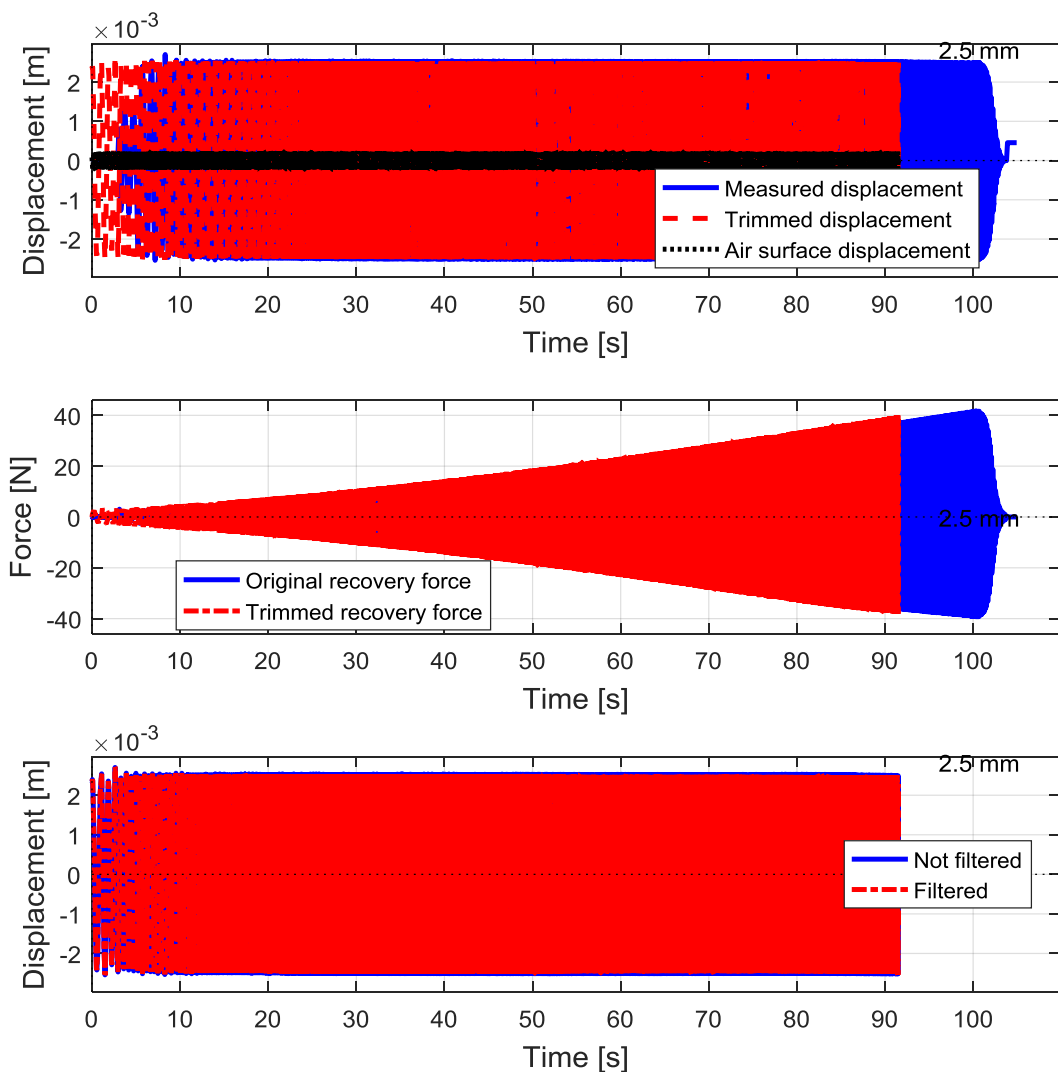


Figure 4.4.2.4 – Original and trimmed signals comparisons.

Also an export in the Matlab command window is been implemented and it report the results as:

```

Command Window

-----

Coefficient regression WT25 0.5mm:
c_1: -353.7322 N/ ((m/s)^1)
Fmax_c_1: 22.3305 N
c_3: 48446.2176 N/ ((m/s)^3)
Fmax_c_3: 12.188 N

Max % error envelope: 63.5612 %
Mean % error envelope: 10.6601 %
-----

```

Figure 4.4.2.5 – Export in Matlab command window.

Looking at both Figure 4.4.2.1 & 4.4.2.3 and at the export on Matlab command window (Figure 4.4.2.5) an evaluation on the grade of regression can be done by looking at what is the contribution in terms of force simply considering the maximum reported in the rows next to the considered coefficient.

For example looking at Figure 4.4.2.5 a 3rd order regression is been done and the value of the maximum force generated by this last order (12.188 N) is still comparable with the first one (22.3305 N) that will always be the biggest in magnitude.

But why is the 2nd order contribution missing in the export? It's been discovered that the even parameters (2nd, 4th, 6th, etc.) given a contribution negligible, while the odds (1st, 3rd, 5th, etc.) not. Is not very clear why this is an odd function, but it is necessary to take note of it and act accordingly, neglecting the contribution of the even coefficients, therefore the definitive model has become:

$$m\ddot{x} + c_1\dot{x} + c_3\dot{x}^3 + c_5\dot{x}^5 + \dots + c_{n,odd}\dot{x}^{n,odd} = F(t) \quad (4.4.2.9)$$

While the regression behaves as:

$$F_{\text{regression}}(t) = m\ddot{x} + c_1\dot{x} + c_3\dot{x}^3 + c_5\dot{x}^5 + \dots + c_{n,odd}\dot{x}^{n,odd} \quad (4.4.2.10)$$

In particular from previous and not reported test it's been found that is useless to go up to:

$$n_{odd,max} = 3$$

And that also this second coefficient (c_3) become zero for the highest values of displacement amplitude but has to be considered for the smaller values.

This results are referable only to a given WT grade and a given displacement. By fixing the WT grade and exploring the 6 possible displacements (0.5, 1, 1.5, 2, 2.5, 3 mm) is possible to obtain a graph where all the values of c_1 and c_3 for each displacement amplitude

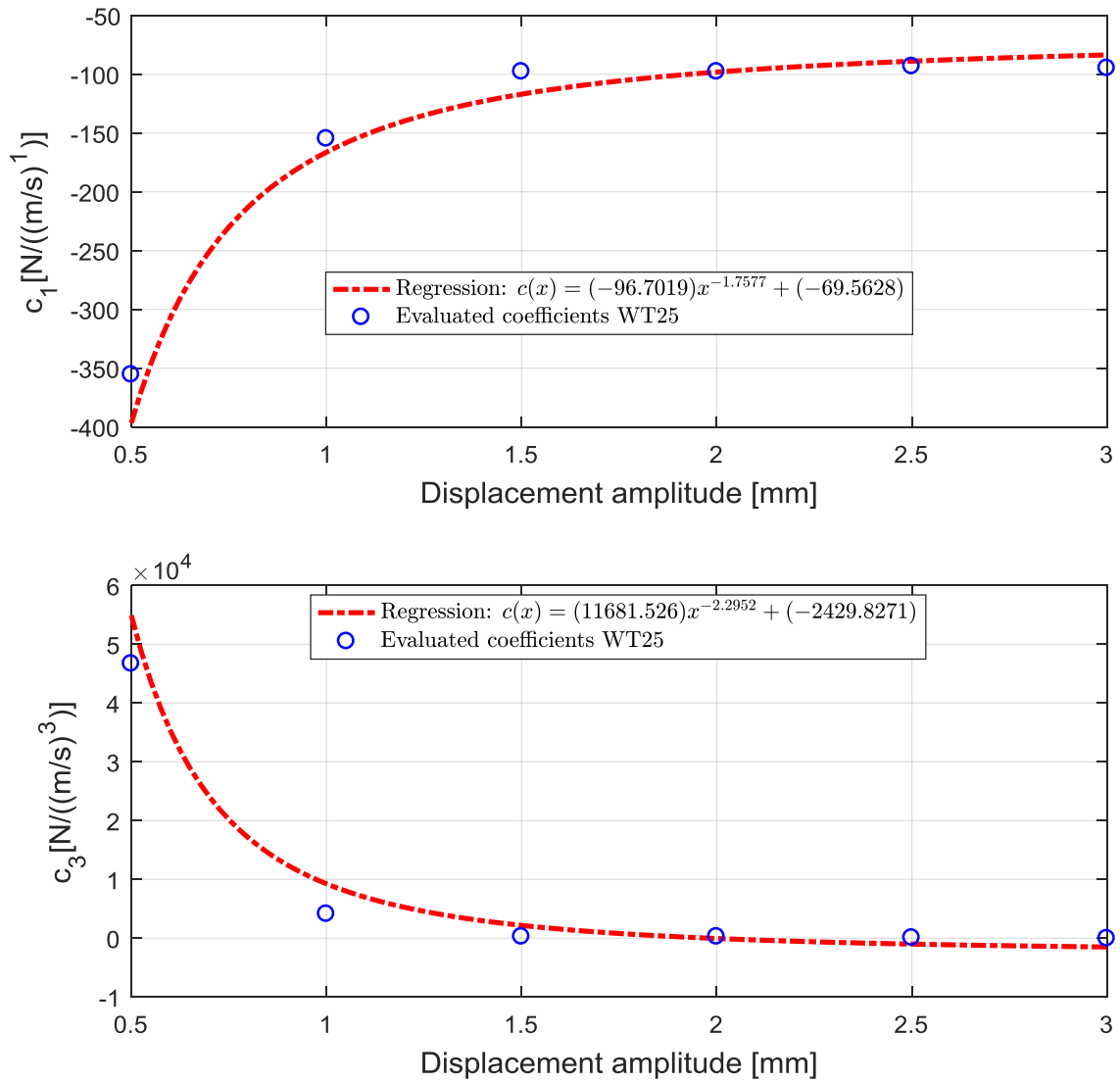


Figure 4.4.2.6 – Regression for a given WT grade and all the displacement amplitudes explored.

Looking at Figure 4.4.2.6 is possible to notice how the first coefficient tends to stabilize, in this case, as the displacement amplitude increase, around a value of:

$$c_1 \rightarrow 90 \frac{\text{N}}{\text{m/s}}$$

While the second coefficient tends to:

$$c_3 \rightarrow 0 \frac{\text{N}}{(\text{m/s})^3}$$

But has some significant numerical values until 2 mm.

The chosen regression method is the ‘power regression’ that is the one which seems best, and is of the form:

$$c_i(x_0) = a_i x^{b_i} + d_i \quad (4.4.2.11)$$

Where x_0 is the displacement amplitude (and not the pure displacement $x(t)$).

The values of the coefficients are automatically obtained in Matlab with a `fit` function and are possible to be read directly in the plot’s legend (Figure 4.4.2.6). Notice that the 3rd coefficient (d) is also representative of the asymptotic value of the function and so, if in a possible simplified model the transition behaviour of the parameter would be neglected, could seem sufficient to say:

$$c_i(x_0) \cong c_i = d_i \quad \forall x \quad (4.4.2.12)$$

4.4.3 Overall damper regression

If what showed in chapter 4.4.2 is repeated exploring all the values of the oil viscosity grade will be possible to have an overall vision of the damping characteristic for a certain shock absorber, that could be a front model or a rear one. The result will look like:

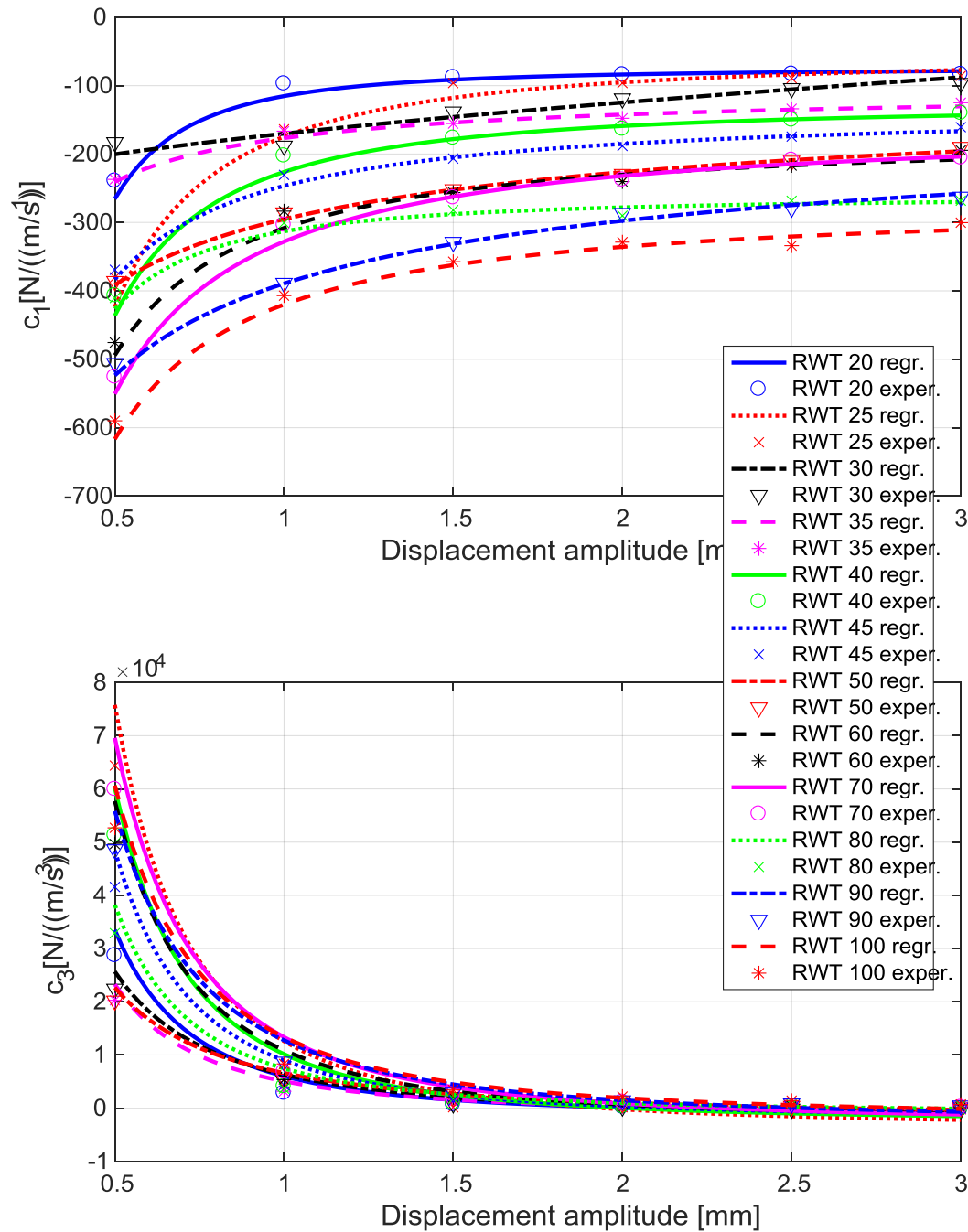


Figure 4.4.3.1 – Overall power regression for a rear damper.

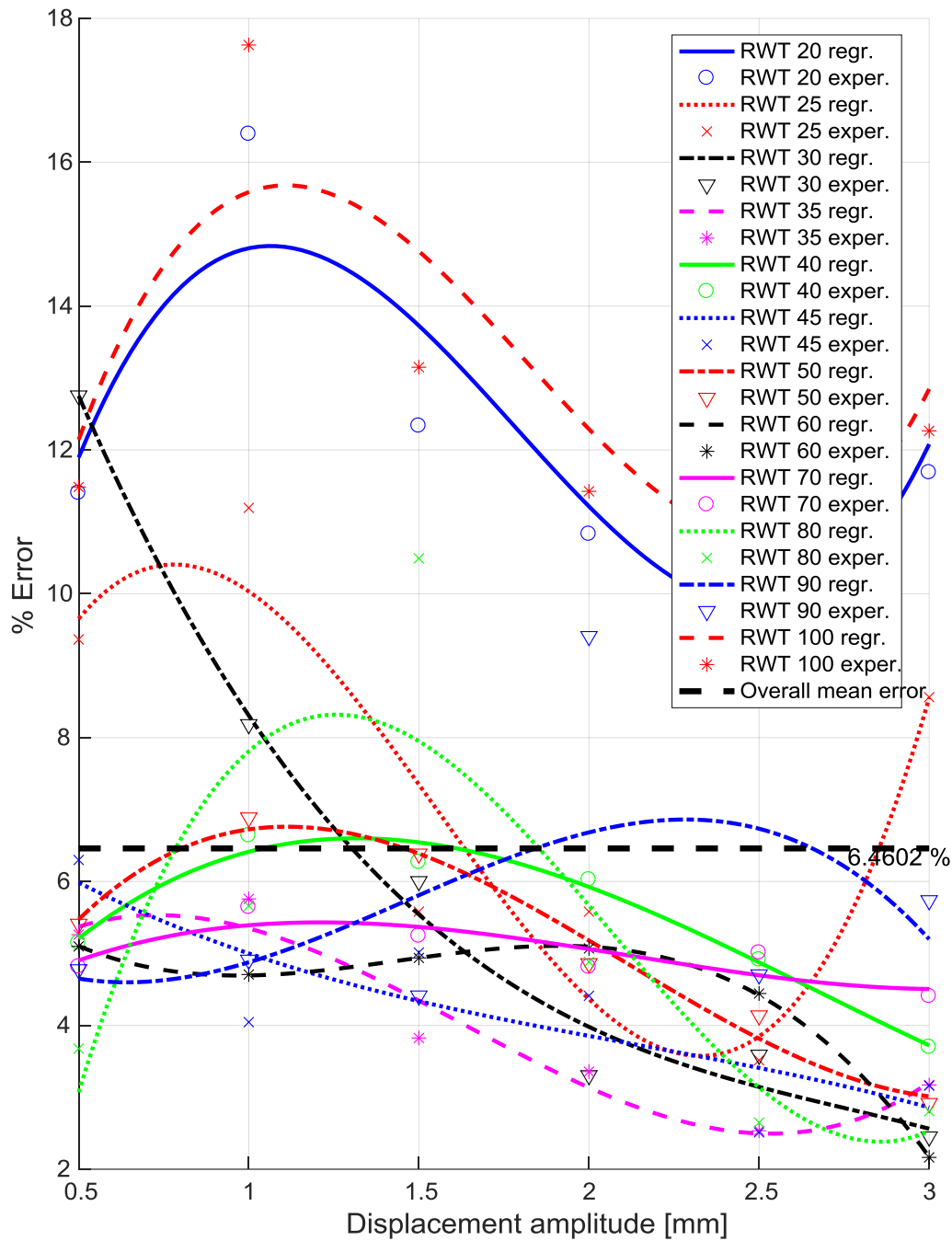


Figure 4.4.3.2 – Error analysis for a rear damper (RWT). The overall mean value line is also visible.

Looking at Figure 4.4.3.1 will be possible to see the good consistence of the obtained results. Highest values of c_1 are been obtained for the highest values of oil viscosity and vice versa, exactly as expected. The same happens for c_3 paying attention to the sign. All the trend lines between the maximum and the minimum are arranged in ascending order for the largest part of the displacement amplitude interval. A large number of trend line show the same shape. Notice that also if the oil

identification grade pass from 20WT to 100WT (5 times growth) the asymptote for c_1 has been growth of only 3 times in the range. The error (Figure 4.4.3.2) don't show significant trends with respect to the oil viscous grade. The solution can be seen also in a numerical table form:

Table 4.9 – Regression coefficients for a rear damper.

Oil viscous grade	C₁			C₃		
	a₁	b₁	c₁	a₃	b₃	c₃
WT20	-18,12	-2,31	-79,24	3992,94	-2,43	-394,06
WT25	-86,84	-3,59	-83,84	6939,16	-4,11	-235,43
WT30	-133,91	-1,14	-55,85	6717,61	-2,96	-513,49
WT35	14,19	1,25	-178,38	4651,94	-1,79	-781,77
WT40	-377,67	-0,16	176,67	5406,00	-2,56	-443,13
WT45	330,77	0,18	-561,03	5975,96	-2,15	-642,48
WT50	250,27	0,29	-533,90	7078,97	-1,98	-679,87
WT60	42,24	1,00	-321,58	6954,92	-1,96	-683,1
WT70	-585,45	-0,19	279,95	8802,99	-1,89	-999,16
WT80	5,13	1,75	-298,39	4961,61	-1,23	-747,21
WT90	-182,75	-1,17	-212,52	10069,16	-2,39	-222,31
WT100	-130,73	-1,21	-278,76	9552,27	-1,93	-191,32

Remembering that the adopted regression model is:

$$c_i(x) = a_i x^{b_i} + d_i \quad (4.4.3.11)$$

And x is the displacement amplitude and not the absolute instantaneous displacement.

The results look similar for a front damper:

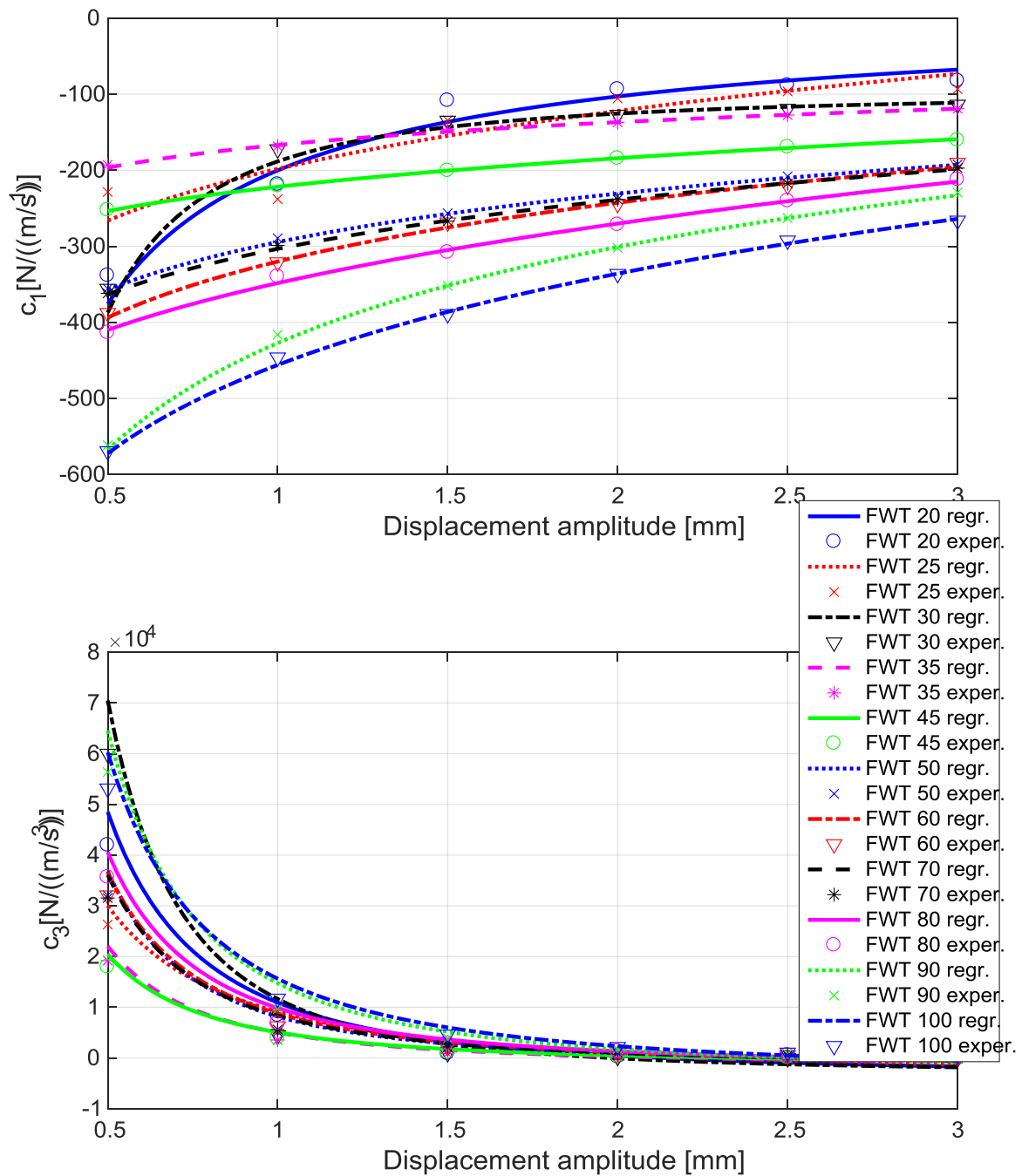


Figure 4.4.3.3 – Overall regression for a front damper.

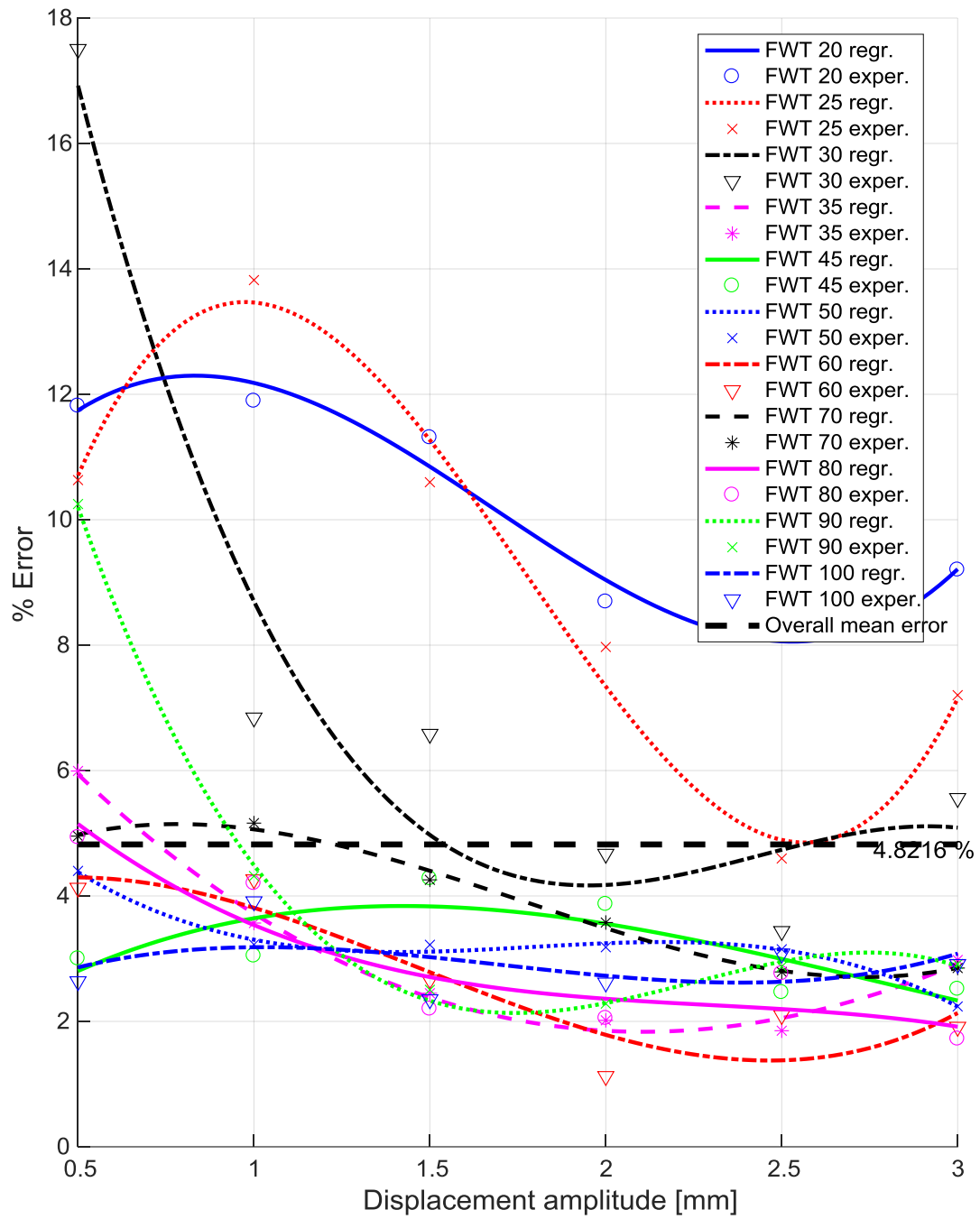


Figure 4.4.3.4 – Error analysis for a front damper (FWT). The overall mean value line is also visible.

Also in this case the solution can be seen from a numerical point of view:

Table 4.10 – Regression coefficients for a front damper.

Oil viscous grade	C₁			C₃		
	a₁	b₁	c₁	a₃	b₃	c₃
WT20	-217,79	-0,85	17,63	14545,79	-1,84	-3610,93
WT25	629,59	0,16	-827,81	13567,08	-1,34	-4434,16
WT30	-91,90	-1,66	-96,44	14605,99	-2,33	-2969,03
WT35	7016,46	0,01	-7183,27	6577,80	-1,84	-1555,83
WT45	209,81	0,24	-431,54	6500,55	-1,75	-1436,64
WT50	3333,11	0,03	-3627,52	9655,65	-1,99	-1479,10
WT60	1554,51	0,07	-1874,50	10644,83	-1,85	-1867,72
WT70	838,53	0,11	-1141,79	9961,37	-1,92	-1609,36
WT80	290,72	0,34	-639,06	11808,01	-1,85	-1948,32
WT90	-1267,05	-0,15	839,88	17618,70	-1,94	-2874,22
WT100	3775,96	0,05	-4231,88	18926,96	-1,75	-3303,15

4.4.4 Front–rear comparison

The results showed in chapter 4.4.3 are characteristic of a rear damper or a front one. What happens if the dampers are compared to each other? In order to visualize a better comparison only a 1st grade order regression will be done and not anymore a 3rd (relative ratios don't change):

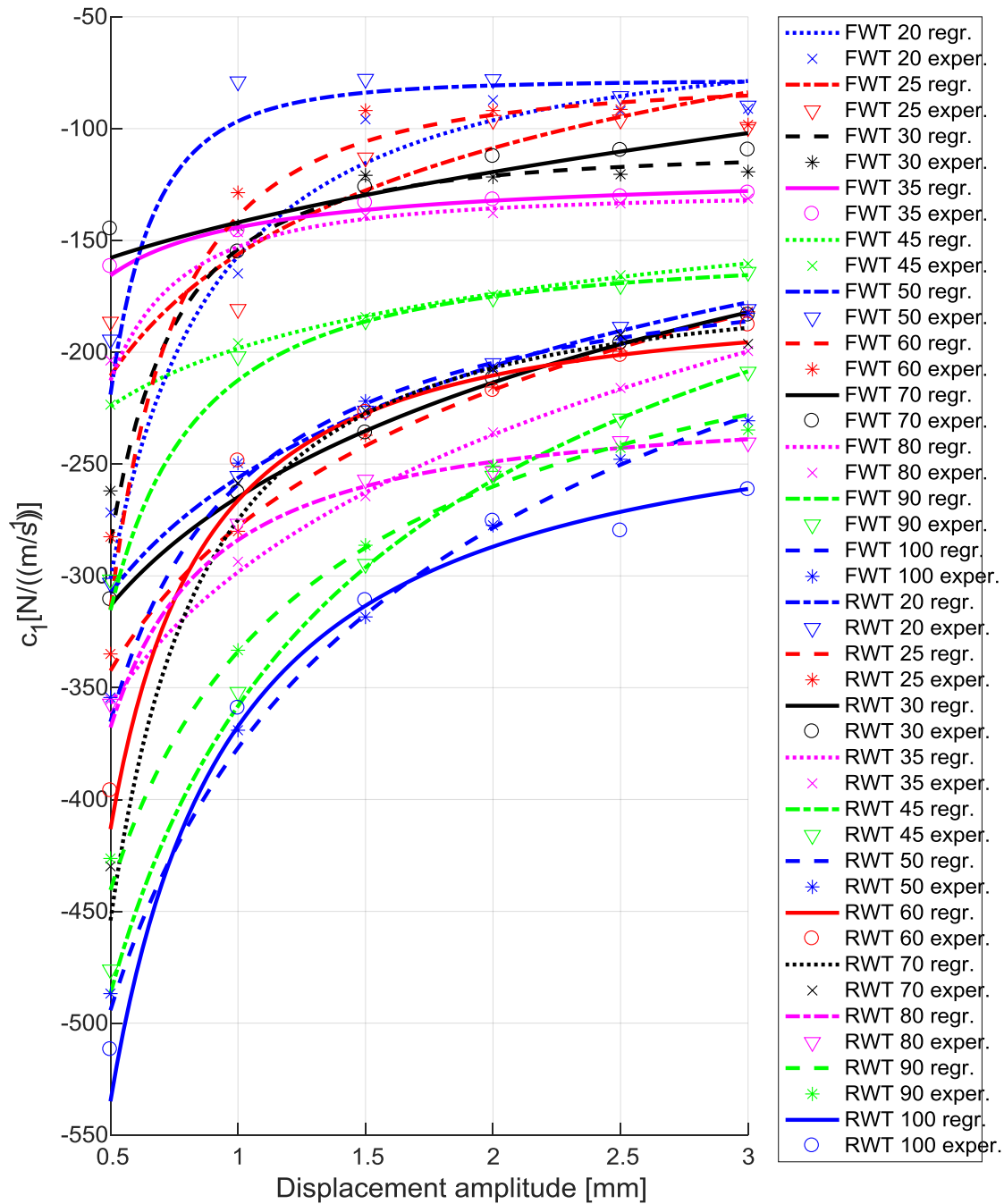


Figure 4.4.4.1 – General comparison between a rear damper (RWT) and a front one (FWT).

The obtained Figure is not so clear, so by plotting just 3 values of oil grade: WT20, WT50 and WT100:

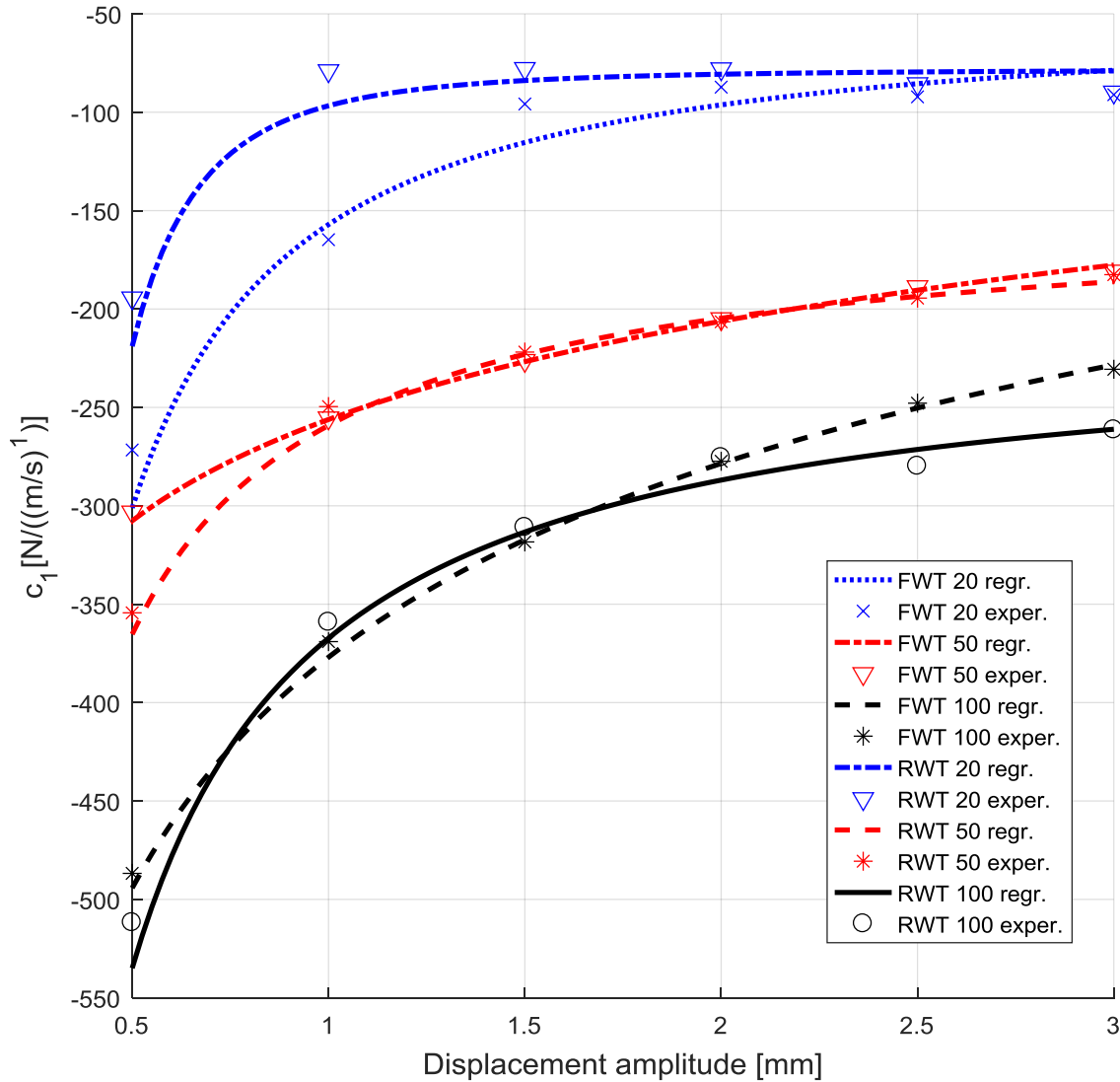


Figure 4.4.4.2 – Comparison between front/rear for 3 oil gradation.

Looking at Figure 4.4.4.2 is possible to notice that some difference will occur between a front damper and a rear one. These differences may be more or less important, for example the comparison on the WT20 is very bad compared to the one on the other two. What are these differences due to? The front shock absorber is smaller, the amount of oil is smaller, the stem is shorter, consequently the amount of trapped air is certainly different, also although the geometric difference between front and rear is anywhere of 13 mm, the position of work is changed by 20 mm, which means that the front works, in nominal conditions, in a 'higher' position.

4.4.5 Temperature effect

During the assembly and disassembly phases of the shock absorber from the test rig, it emerged that at the end of the test cycle the shock absorber had a decidedly high temperature. Not surprisingly, the damper is nothing more than an energy sink. The natural consequence of this finding was to investigate about the effect of this temperature change. The suspicion is that the previously obtained damping trends are mainly due to the rise in temperature, and therefore that in reality the model could be not anymore:

$$c_i = c_i(x_0) \quad (4.4.5.1)$$

But that may be more representative to indicate it as:

$$c_i = c_i(x_0, T) \quad (4.4.5.2)$$

Where T is the temperature.

To evaluate the heat effect a preliminary verification has been done, at the end of the test cycle for one shock absorber it's been decided to repeat by sweeping the displacement amplitudes for the highest one to the smaller. In this backward case the damper start from a high temperature situation and goes toward a cold one. This comparison was been the first to be done because it is also the fastest. It's been obtained:

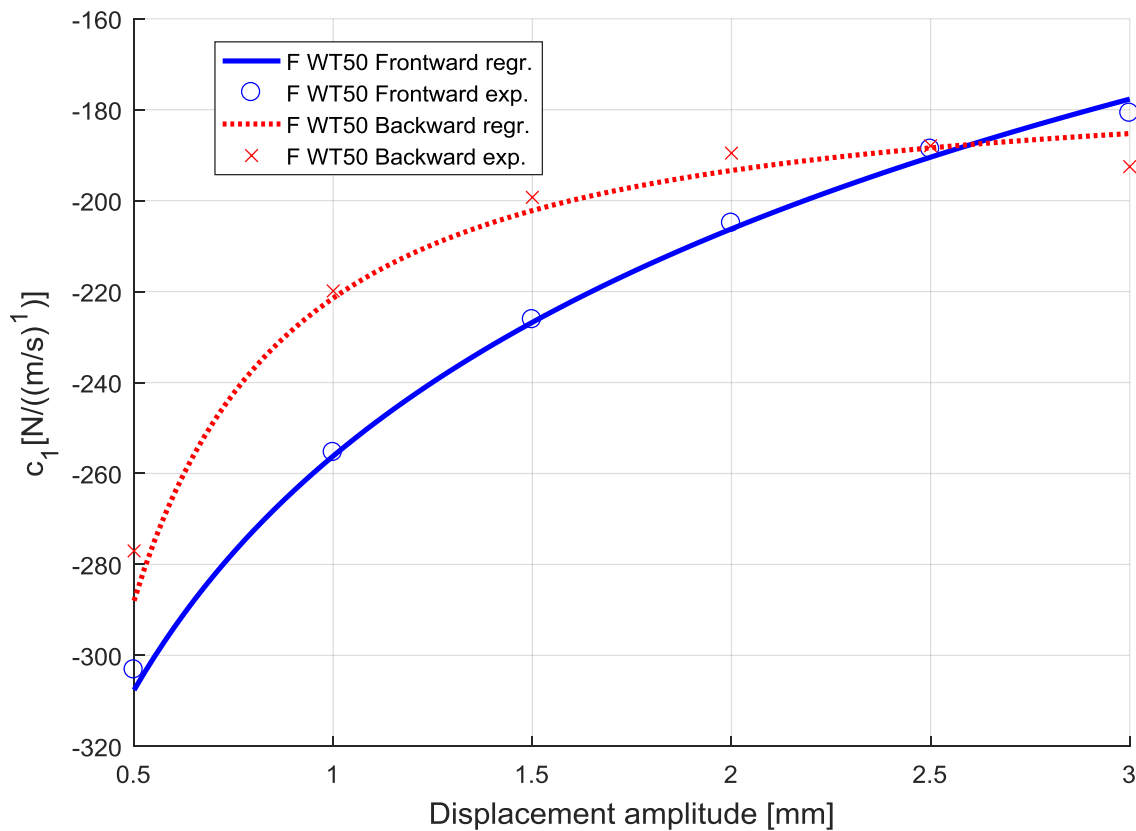


Figure 4.4.5.1 – Frontward/backward cycles comparison.

Looking at Figure 4.4.5.1 appears immediately clear that a temperature effect exists and does not seem to be so negligible. Once stated this dependence was been possible done test which requires a very long time where, differently by what happened in the previous case, a certain time interval will occur between one test and another so that the shock absorber recovers the temperature of the environment. This time interval is been fixed at 20 minutes, this means that for a complete test cycle more than 8 hours will be necessary for just a damper. This 3rd type of test is been called 'Constant temperature'. By plotting the result on the previous comparison:

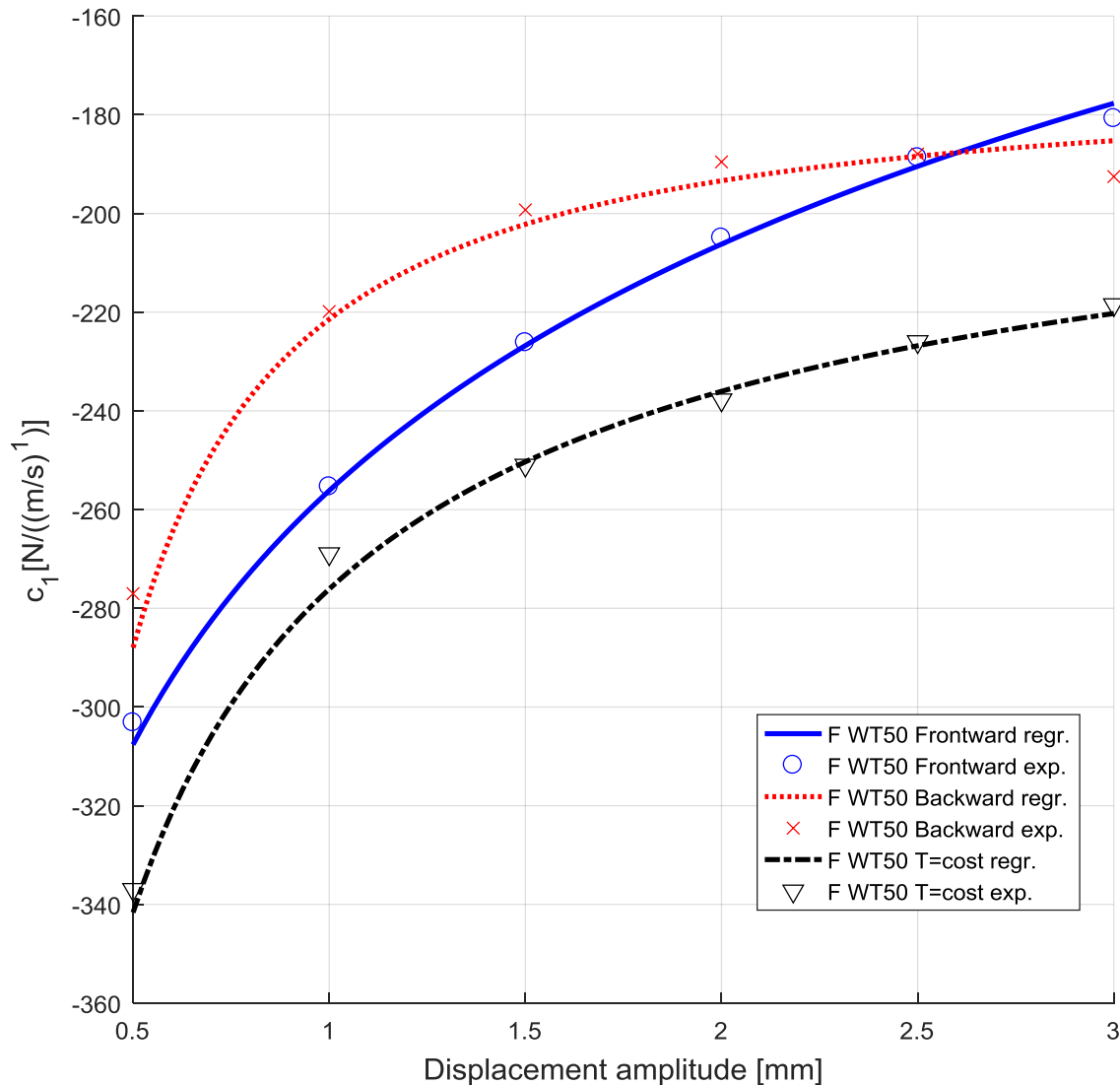


Figure 4.4.5.2 – Frontward/backward/T=cost cycles comparison.

Obviously a 3rd, different, trend line, was been obtained. This result is totally coherent with the physics nature of the oil: the viscous coefficient rise for low temperature values, while drops for increasing temperature. But the most important result of this comparison may be that the shape doesn't change so much, maintaining the power regression law as the optimal one. This statement avoid the previous suspicious that the decreasing trend was mainly due to the temperature effect, while seems that heat only act scaling the problem of a certain mean value, that in the analysed case (WT50) was something near ~20%. Obviously the time ratio (8hrs vs. 1.5hrs) has not allowed to repeat all the tests with the constant temperature procedure, which will probably be the subject of future projects.

4.4.6 Friction effect

As known will always exist a friction contribution, also in this case where all the parts are immersed in the oil and well lubricated, there is a certain contribution due to the presence of the seals between the stem and the cylinder and also due to the natural friction between the piston and the cylinder walls, where there is no seals and so mutual rubbing is allowed. The presence of this type of contribution in this particular case is visible especially at the lower frequencies, initial times of the test run, where the shape of the restoring force, that should be pseudo-sinusoidal, looks instead like:

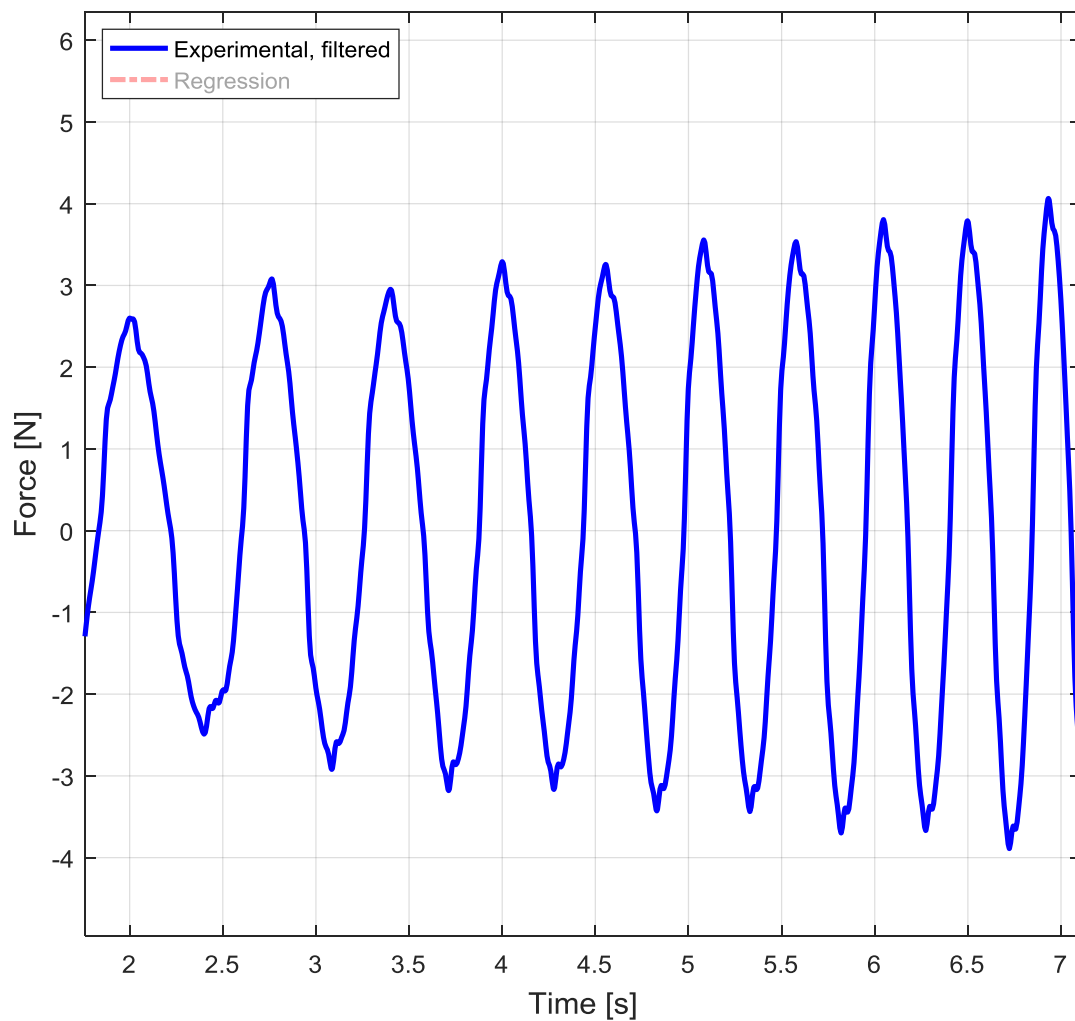


Figure 4.4.6.1 – Restoring force at low frequencies.

The problem is the shape at the tops of the signal, by zooming on one of it:

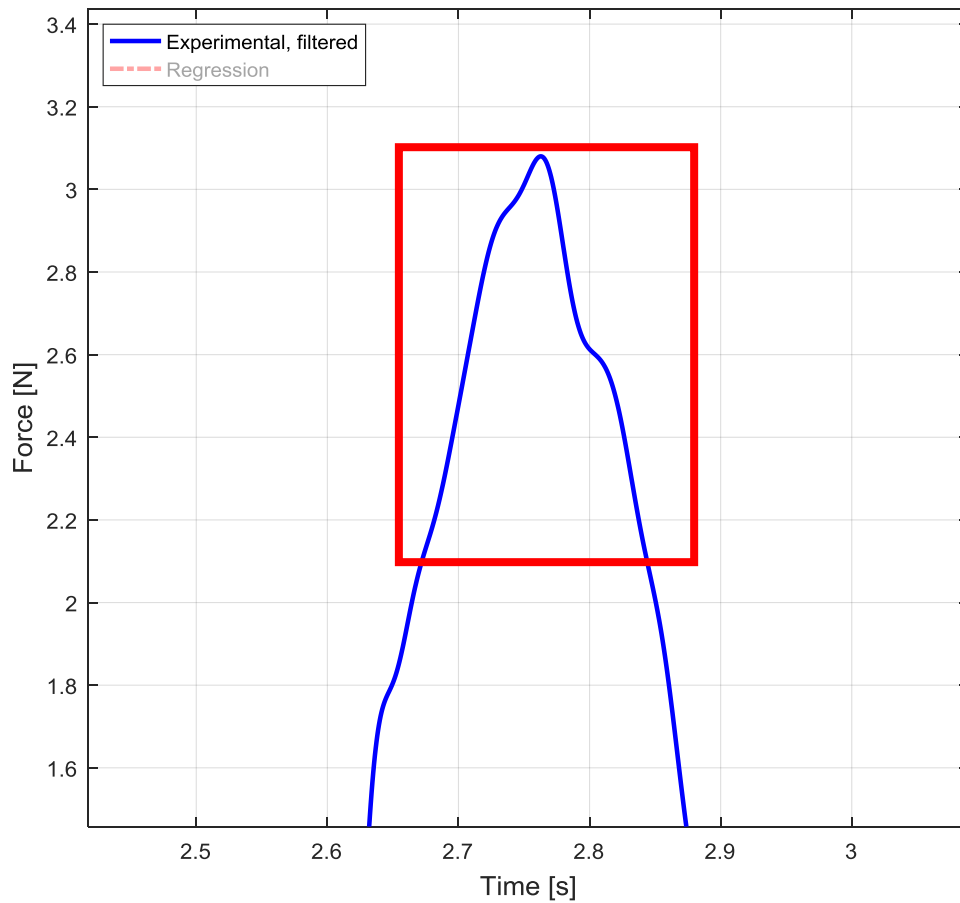


Figure 4.4.6.2 – Zoom in of the friction effect on the restoring force.

As known, looking at the red square in Figure 4.4.6.2, a ‘maximum force’ instant is observed, that moment correspond to a minimum velocity one, because it also mean maximum displacement: it is the moment when the stem is at the maximum amplitude and the shaker has to apply the maximum force to make the system restart in the opposite direction.

This effect, fortunately, disappear for medium and high frequencies, where will be not anymore possible to observe the same:

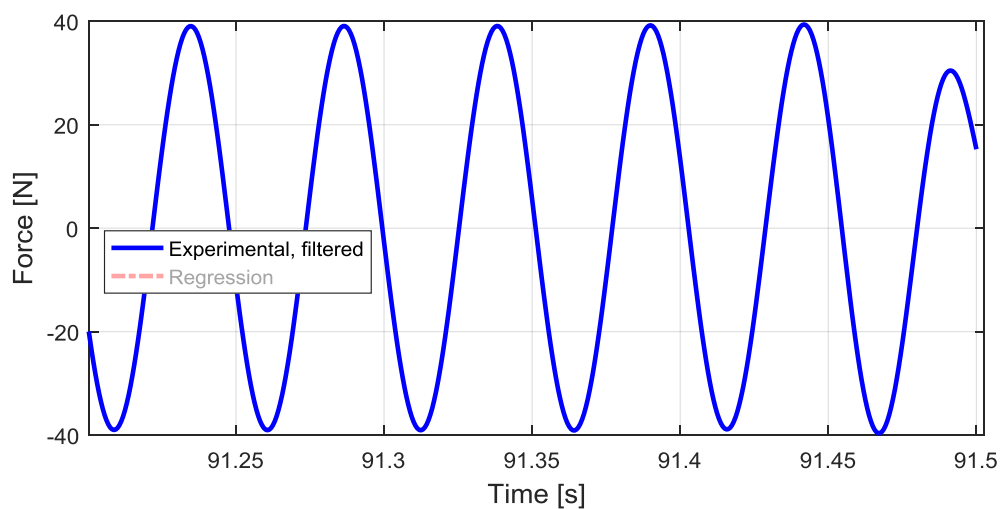


Figure 4.4.6.3 – Restoring force for the highest frequencies, friction effect has disappear.

But why, looking for example at Figure 4.4.6.2, the force behave like this? Why this step-shape? The answer is the physical behaviour of the friction if the transition from the static to the dynamic one is considered:

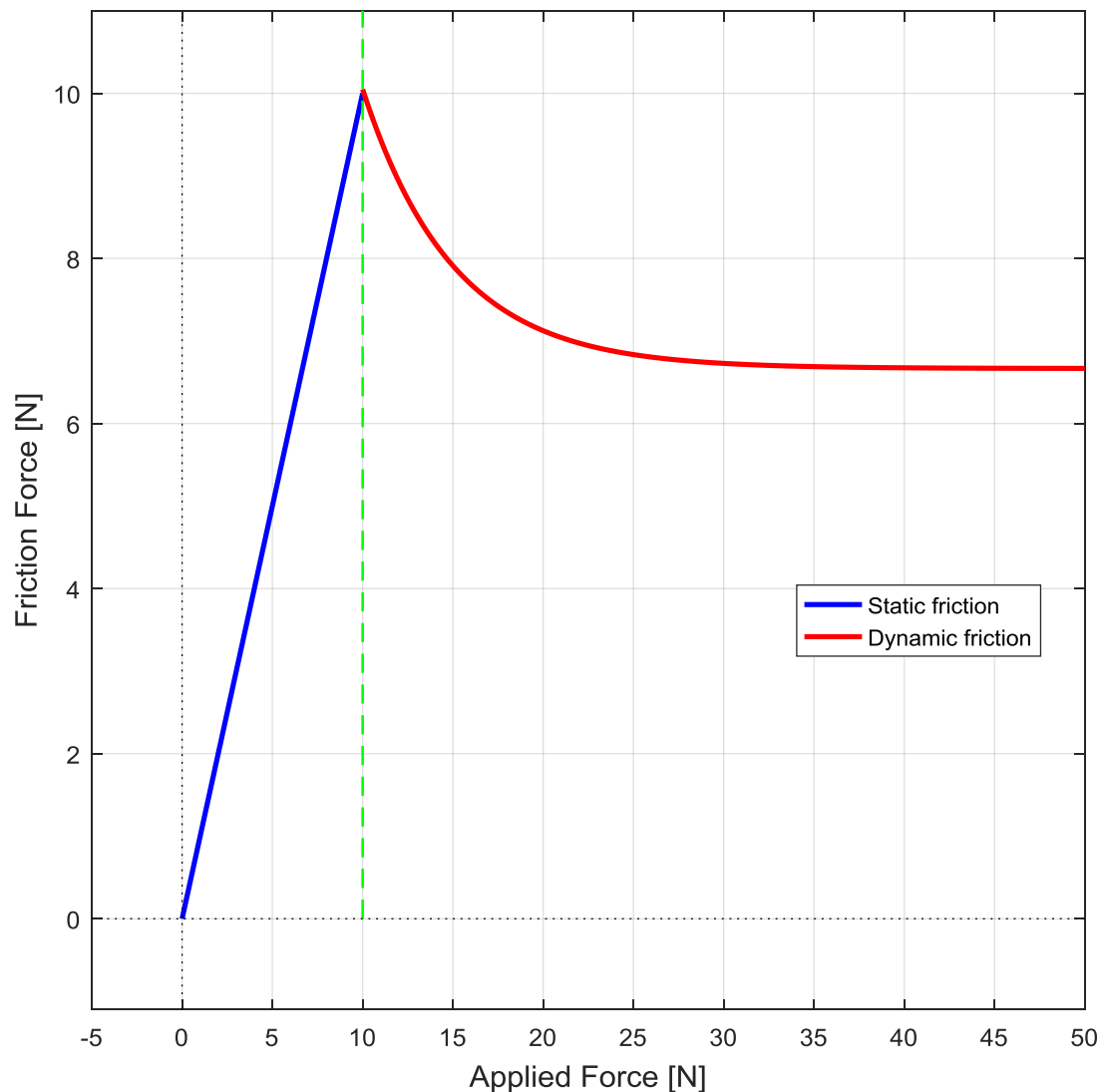


Figure 4.4.6.4 – Coulomb friction trend.

In Figure 4.4.6.4 a friction force is been plotted with respect of an applied force which try to move a body to another one. In the first range there is no relative movement and the friction is of the static type, the pitch of the line is the friction coefficient. At a certain point the first subtle movements begin and the response force start to drop down, the friction model become for successive force more and more dynamic up to an asymptotic value of force. Between this two phases a drop-mixed zone is present.

So the phenomenon can also be seen with respect to the velocity:

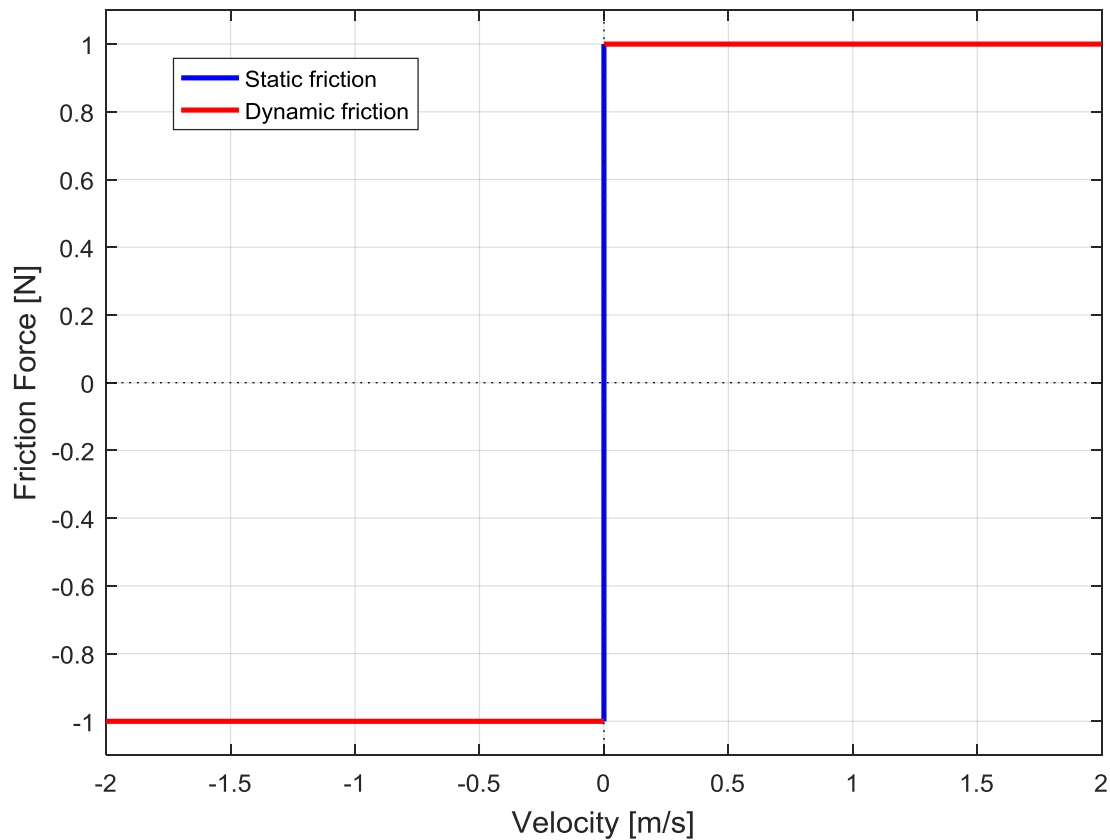


Figure 4.4.6.5 – Coulomb friction trend with respect to velocity.

For nonzero velocity the friction behaves as dynamic, while at zero velocity a certain range of response force is possible and it is proportional to the applied force. This behaviour totally justify the step-shape of the restoring force obtained, when the stem slow down the friction begin to feel the static component, at zero speed is totally static, while in the exit phase the dynamic friction transition is visible in the horizontal stretch. The hypothesis which justify the absence of this effect for the higher frequencies is that the larger values of velocities reached reduce so much the static friction time interval that, at least, it become invisible and the effect intangible.

The obtained result has to be considered in the regression algorithm? A perfect refine procedure should be include it but as show the effect is limited to the lower frequency only and to purified the signal of this contribution a test-by-test manual measurement will be necessary. The measure has to quantify a mean value of force between the top of the sinusoid to the horizontal stretch:

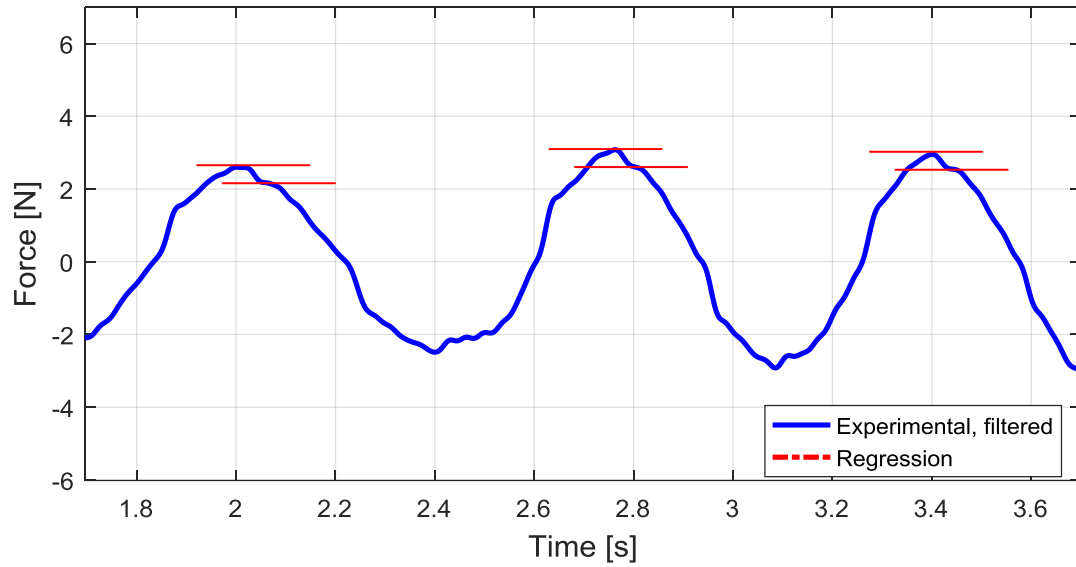


Figure 4.4.6.6 – $\Delta F_{friction}$ measurement.

Once measured could be possible to purify the signal similarly to what was been done for the inertia contribution, with a formula like:

$$F_{purified} = F_{restoring} - \frac{\Delta F_{friction}}{2} \text{sign}(\dot{x}) \quad (4.4.6.1)$$

As it is possible to understand the procedure is not so difficult but it is time onerous because the measurement showed in Figure 4.4.6.6 cannot be implemented as automatic reading in the algorithm, moreover the error obtained without considering this effect is already good.

Is very nice to see how the step-effect is also partially visible in the 3D plot:

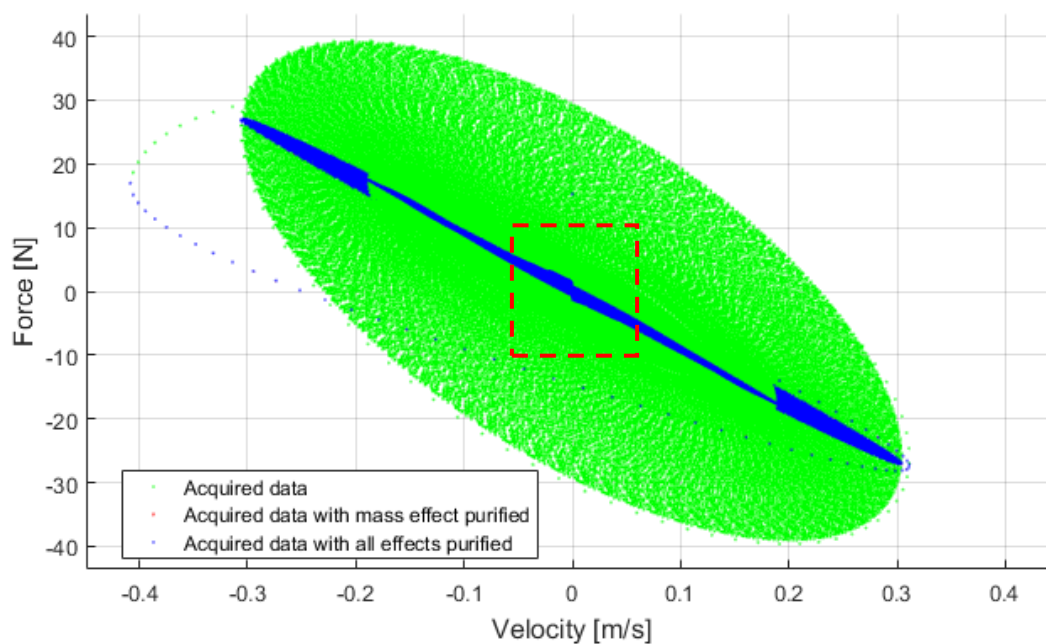


Figure 4.4.6.7 – Step friction effect from a side view of the 3D plot.

The effect become soonely more clear if the force is purified of the mass effect, as it is possible to notice by looking at the central part of Figure 4.4.6.7.

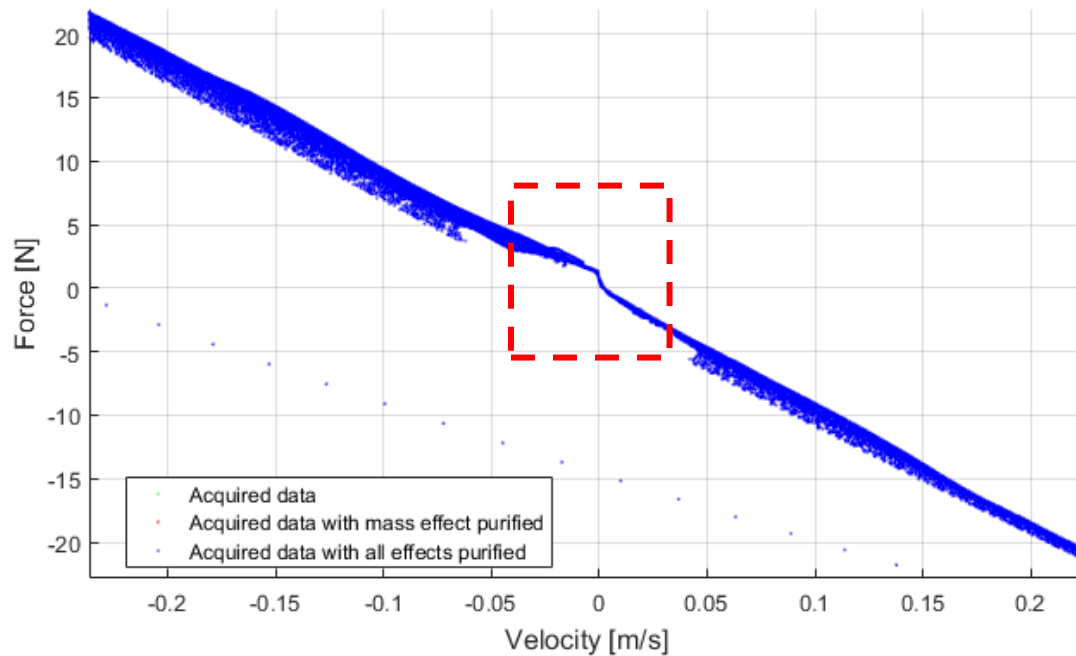


Figure 4.4.6.8 – Highlighted step friction effect on the cloud of points.

From this point of view il also possible to notice that the “not function” effect (mentioned in chapter 4.3.2) is thus largely reduced and also the negative values of c_1 obtained in the previous chapters (4.4.2 & 4.4.3) become definitively clear.

4.4.7 Compression or extension effect

A final control can be done to evaluate a possible difference between the compression behaviour and the extension one. In real automotive dampers the force generated during the extension phase is higher than the compression one: this result is obtained by a smart shape of the nozzles in the piston, which are asymmetric. In the studied case, instead, a first geometric evaluation suggest that the nozzles are perfectly symmetric with respect to the middle plane of the piston. If this is true the force signal should result perfectly centred on the time axis, to visualize if this is true the upper and lower peak envelopes will be plotted both on the positive side:

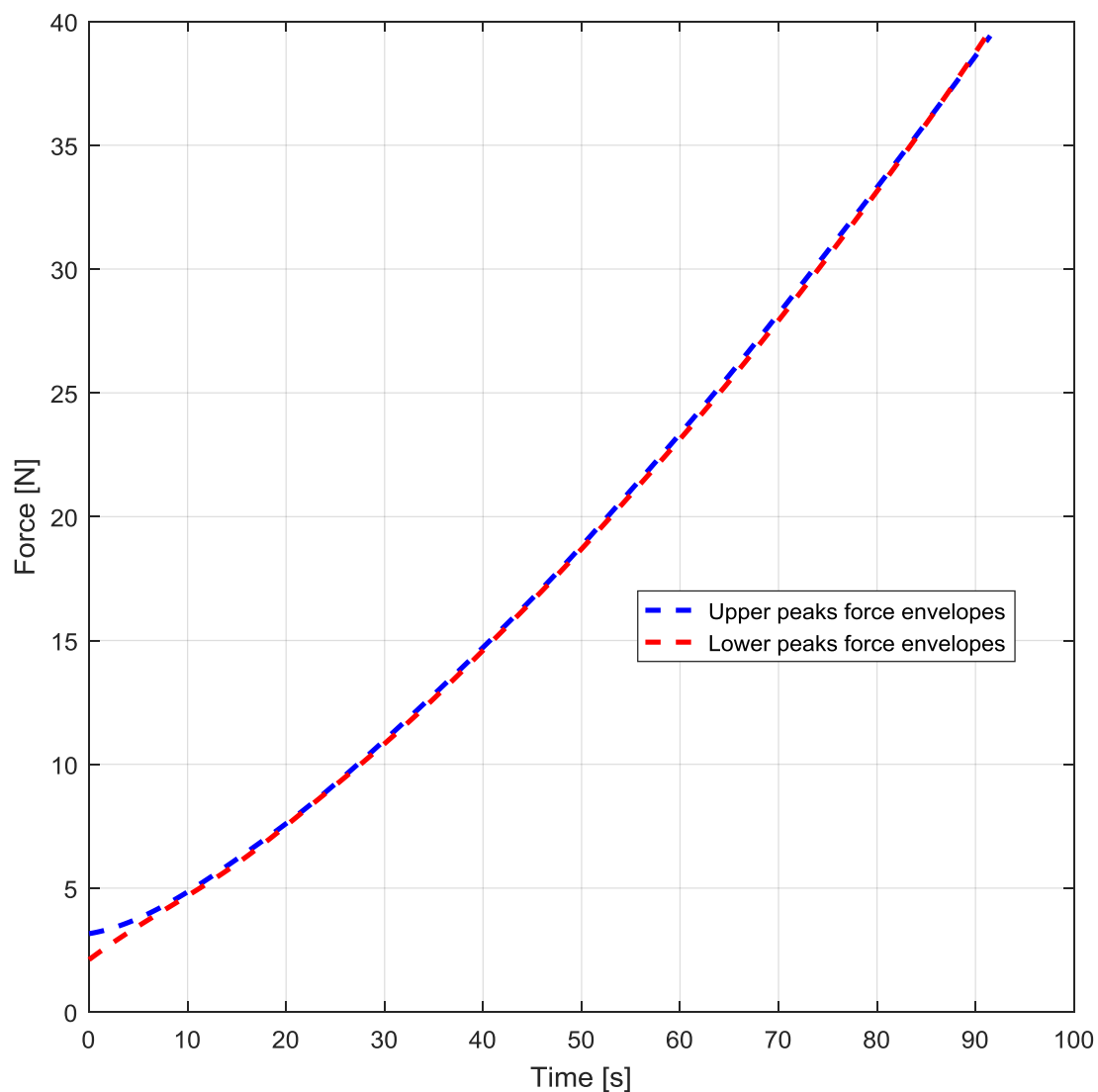


Figure 4.4.7.1 – Upper-lower peaks envelopes comparison.

As expected the two envelopes coincides for the largest part of the test run, with exclusion of the initial time steps where, as explained in the chapter 4.4.6, friction effects play an important role making the acquisition less reliable as representative of the viscous behaviour.

Conclusions

The designed experiment has created reliable results as they are consistent with each other and characterized by excellent repeatability. Through these tests it has been possible to observe many phenomena that have made everything interesting since it is not easy, for example, to obtain an experimental Mobius surface. Even if indirectly it was possible to observe also the behaviours of inertia, of the frictions, of the air as a spring and, lastly and would seem more important of all, the one of the temperature whose effect has certainly heavily influenced the result. The problem is that it is not possible to establish a priori which temperature conditions will occur during the normal use of the vehicle: surely the fact that the vehicle is normally in motion will generate a heat dissipation effect, but it could also be that the rhythms and the displacements imposed by the track are never sufficient to heat the shock absorber as much as it happened during these tests: in this case all the thermic considerations would be useless and tests has to be repeated as done for the 'constant temperature' one. Therefore, anyway, to obtain results that fully adhere to the studied vehicle case, some starting data must be added and, in particular, those of a thermal nature. It would also be useful to know the characteristic range of excursion for the vehicle, here arbitrarily imposed up to only 3 mm but which could perhaps be very different from this one. Therefore the empirical model here formulated can be further improved by characterizing it also on the basis of the temperature and of the correct range of displacement amplitudes. But like any other empirical model, even if it is very refined, it will always be characterized by an implicit incompleteness and poor aptitude to justify the physics of the problem. In fact, it should be noted that in the thesis laws concerning fluids are never mentioned, for example the ones describing the relationship between viscosity and temperature or between viscosity and deformation speed.

The results here obtained are however an important starting point for future refinements of the model, as well as having certified that the chosen vehicle constitutes a good basis on which to work, enjoying the sought-after repeatability, consistency, adjustability and implicit scalability that a model in scale involves.

From a purely personal point of view the accumulated experience has compensated the educational gap in the experimental field which unfortunately characterise the course of studies. Becoming familiar with the instrumentation and experimental procedures, as well as with the approach to analysing the results, will surely prove to be usable in the not so distant future.

Appendix

- [a] *Vandermonde Matrix*^[3]: in linear algebra, a Vandermonde matrix, is a matrix with the terms of a geometric progression in each row, i.e., an $m \times n$ matrix:

$$\begin{bmatrix} 1 & a_1 & a_1^2 & \dots & a_1^{n-1} \\ 1 & a_2 & a_2^2 & \dots & a_2^{n-1} \\ 1 & a_3 & a_3^2 & \dots & a_3^{n-1} \\ \vdots & \vdots & \vdots & \ddots & \vdots \\ 1 & a_m & a_m^2 & \dots & a_m^{n-1} \end{bmatrix} \quad (5.1)$$

Or:

$$V_{i,j} = a_i^{j-1} \quad (5.2)$$

- [b] *Möbius surface*^[4]: is a surface with only one side (when embedded in three-dimensional Euclidean space) and only one boundary. The Möbius strip has the mathematical property of being unorientable.

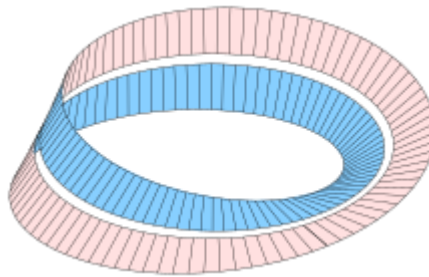


Figure 5 – Möbius strip.

Reference

- [1] Bonisoli, Prandina, Marcuccio, Esposito, Brino, Manca, Scapolan, Lisitano, Dimauro, Lomuscio, Venturini: *LUPOS - Lumped Parameters Open Source FEM code* - Tutorial – © v.2019-03-16, pp 146-154.
- [2] Vella, Lisitano, Bonisoli, Vigliani: *Analysis of a scaled rc vehicle*, Report, Facoltà di Ingegneria Meccanica Politecnico di Torino, 2019-03-20, pp 19-21.
- [3] https://en.wikipedia.org/wiki/Vandermonde_matrix available in 2019-07-08
- [4] https://en.wikipedia.org/wiki/M%C3%B6bius_strip available in 2019-07-08
- [5] <https://www.keyence.it/products/measure/laser-1d/lk-g5000/models/lk-h050/index.jsp> available in 2019-05-03
- [6] <http://www.pcb.com/products/model/208c02> available in 2019-05-03
- [7] <https://www.johnmorrisgroup.com/AU/Product/9880/Metric-mtg-stud,-10-32-to-M6-x-075-x-0300-long,-BeCu,-no-shoulder> available in 2019-05-03
- [8] G. Genta, *Vibration Dynamics and Control*, Springer, Turin, 1997, pp. 175-176